

Copyright

by

Srikanth Tadepalli

2009

The Dissertation Committee for Srikanth Tadepalli
certifies that this is the approved version of the following dissertation:

Advances in Empirical Similitude Method

Committee:

Kristin L. Wood, Supervisor

David L. Bourell

Matthew I. Campbell

Richard H. Crawford

Björn Engquist

Advances in Empirical Similitude Method

by

Srikanth Tadepalli, MSE, B.Tech

Dissertation

Presented to the Faculty of the Graduate School of

The University of Texas at Austin

in Partial Fulfillment

of the Requirements

for the Degree of

Doctor of Philosophy

The University of Texas at Austin

May 2009

Dedicated to
My Parents

Acknowledgments

It has been a long and arduous journey completing research but motivation to forge ahead lay in the joy of creating something innovative and giving life to a piece of work that was non-existent not so long ago. Much of the credit must go to Dr. Kristin L. Wood, my supervisor, for his patience and guidance over the last few years. You have my sincere gratitude for innumerable deep and insightful discussions we have had that has resulted in this treatise. More importantly I thank you for the development of my personality as a thinker, designer and researcher. I am particularly grateful for extensive learning I have had associating analytical work with practical examples and physical reality.

Dr. Richard H. Crawford, Dr. Matthew I. Campbell, Dr. David L. Bourell and Dr. Björn Engquist have been a source of continued support and assistance throughout the project work. Thank you all for your expert supervision and scientific direction.

A word of gratitude is due, to past and current members of LFF and MADLab and many other well-wishers that I have had the privilege of acquaintance. There are too many to list here, but I do appreciate help extended by all of you over the last few years with codes, debugs, designs and presentations. I wish you all the success in your future endeavors.

A special word of appreciation to Dr. Richard H. Crawford and Dr. Glenn Y. Masada for mentoring and tutoring me for the qualifiers.

Above all, I am deeply indebted to my parents and brother who have stood by me all these years and have been a constant source of inspiration and strength. Never has there been a wane in my admiration for their support and encouragement.

I cannot thank National Science Foundation enough, for their trust and enthusiasm in funding the Empirical Similitude Method project. My earnest thanks for financial assistance provided and intellectual benefits of conferences.

SRIKANTH TADEPALLI

The University of Texas at Austin

May 2009

Abstract

Advances in Empirical Similitude Method

Publication No. _____

Srikanth Tadepalli, Ph.D.
The University of Texas at Austin, 2009

Supervisor: Kristin L. Wood

Dimensional Analysis is a technique that has allowed engineering evaluation of complex objects by scaling analysis results of representative simpler models. The original premise of the procedure stems from the idea of developing non-dimensional parameters to relate physical events and underlying analytical basis. Extending the process to incorporate non-linear and time variant behavior has led to development of a novel process of similitude called the Empirical Similitude Method (ESM) where experimental data of test specimen is combined to produce the required prediction values.

Using the original motivation and hypothesis of ESM, this research

has expanded the experimental similitude process by using adapted matrix representations and continuous functional mapping of test results. This new approach has provided more rigorous mathematical definitions for similarity and prediction estimations based on an innovative error minimization algorithm. Shape factors are also introduced and integrated into ESM to obtain comprehensive evaluation of specimen choices.

A detailed overview is provided summarizing methods, principles and laws of traditional similitude (TSM) and systems that satisfy extension into ESM. Applicability of ESM in different systems is described based on the limitations of TSM in the evaluation of complex structures. Several examples and ideas spanning aerodynamic, thermal, mechanical and electro-magnetic domains are illustrated to complement inherent technical analysis. For example, the new ESM procedure is shown to be considerably more accurate than earlier methods in predicting the values of drag coefficient of an airfoil. A final foray into the regime of “design evaluation by similarity” is made to elucidate applicability and efficiency of developed techniques in practical systems and products. A thorough methodology is also presented highlighting pertinent procedures and processes in usage of this method.

Contents

Acknowledgments	v
Abstract	vii
List of Tables	xiii
List of Figures	xvii
Chapter 1 Introduction	1
1.1 Units and Dimensions	2
1.2 Models and Prototypes	8
1.3 Scales in Similitude	9
1.4 Applications of Similitude	10
1.5 Similitude with Experimental Prototypes - The Empirical Similitude Method	11
1.6 Objectives and Hypothesis of Research	13
1.7 Dissertation Layout	14
Chapter 2 Background	16
2.1 Dimensional and Similarity Analysis	16
2.2 Buckingham π Theorem-Traditional Similitude Method (TSM)	20
2.3 Buckling of Columns	22
2.4 Principles and Rules of Buckingham π theorem	27
2.5 Backpack Buckle	37

2.6	Other Methods of TSM	43
2.7	A Simple Pendulum	46
2.8	Summary	49
Chapter 3 Advances in Traditional Similitude Method		51
3.1	Similarity Methods in Design	52
3.2	Water-Rocket: Analysis of a Dynamic System	53
3.3	Modified Analysis	59
3.4	Numerical and Experimental Analysis	67
3.5	System Dynamics	75
3.6	Nodes and Graphs	78
3.7	Development of the Graph	79
3.8	Summary	97
Chapter 4 Development of Empirical Similitude Method (ESM)		99
4.1	Limitations of TSM	99
4.2	Motivation for ESM	111
4.3	Method and Systems in ESM	115
4.4	Principles of ESM	118
4.5	Quantifying Similarity and Distortion in ESM	120
4.6	Summary	124
Chapter 5 Linear Methods		125
5.1	Test for Linearity-Statistical Procedures	126
5.2	Linear ESM Methods	129
5.2.1	Diagonal Matrix Method	130
5.2.2	Pseudo-Inverse Method	132
5.2.3	Circulant Matrix Method	134
5.2.4	Compensation Matrix Method	136
5.2.5	Hankel Matrix Method	137
5.2.6	Comparison of Methods	140
5.2.7	Toeplitz Matrix-Conjugate Gradient Method	141

5.3	USB Clip-Deflection Analysis	145
5.4	Transformer-Magnetic Flux Analysis	154
5.5	Summary	159
Chapter 6 Non-Linear Methods		161
6.1	Test for Non-Linearity-Statistical Procedures	161
6.2	Non-Linear ESM Methods	163
6.2.1	Polynomial Methods	164
6.2.1.1	Bilinear Method	164
6.2.1.2	Polynomial Method	168
6.2.1.3	Adaptive Polynomial Method	172
6.2.1.4	Spline Fit Method	182
6.2.2	Regression Methods	186
6.2.2.1	Adaptive Exponential Regression Method	186
6.2.2.2	Adaptive Power Regression Method	189
6.2.3	Trigonometric Methods	192
6.2.4	Comparison of Methods	196
6.3	Skillet-Temperature Analysis	198
6.4	Airfoil-Coefficient of Drag Analysis	206
6.5	Summary	217
Chapter 7 Error Estimations		218
7.1	Error Definitions	218
7.1.1	Intermediate Error Estimation in Adaptive and Trigonometric ESM	220
7.2	Selection of Method in ESM	222
7.3	Summary	226
Chapter 8 Shape Factors		228
8.1	Motivation for Shape Factor Study	228
8.2	Applications of Shape Factors in Engineering	230
8.3	Integration of Shape Factors in ESM	242

8.4	Keyboard Spring-Deflection Analysis	243
8.5	Interconnect-Deflection Analysis	251
8.6	Summary	261
Chapter 9 Experimental Verification		262
9.1	Welding Experiment-Temperature Analysis	262
9.2	Summary	268
Chapter 10 Results and Conclusions		269
10.1	Research Contributions	269
10.2	Future Work	270
10.3	Summary	272
Appendix A Conjugate Gradient Method		273
Appendix B Transformer-Magnetic Flux Analysis		275
Appendix C Airfoil-Coefficient of Drag Analysis		280
Appendix D Keyboard Spring-Deflection Analysis		288
Appendix E Interconnect-Deflection Analysis		292
Appendix F Welding Experiment-Temperature Analysis		294
Appendix G Test Equipment and Process		297
Bibliography		300
Vita		311

List of Tables

1.1	Fundamental dimensions	3
1.2	Units and dimensions	4
2.1	Dimensional matrix for column buckling	24
2.2	Echelon matrix for column buckling	25
2.3	A typical dimensional-echelon matrix	32
2.4	Dimensional matrix for clip deflection	39
2.5	Refined dimensional matrix for clip deflection	40
2.6	Echelon matrix for clip deflection	41
2.7	Dimensional matrix for Taylor's method	48
2.8	Reduced matrix for Taylor's method	48
2.9	Final matrix for Taylor's method	48
3.1	Output and system variables for the water-rocket	55
3.2	System variables for the water-rocket	55
3.3	System variables and constants for the water-rocket	55
3.4	System variables and constants for the water-rocket	56
3.5	Combined matrix for the water-rocket	57
3.6	Combined matrix for fluid thrust	60
3.7	Combined matrix for resistance	61
3.8	Combined matrix for Bernoulli's equation	64
3.9	Combined matrix for isentropic expansion	65
3.10	Combined matrix for continuity	66

3.11	Input parameters and values for the algorithm	69
3.12	Estimated values of constants using the algorithm	70
3.13	Input conditions to experimental setup of the water-rocket	72
3.14	Results from traditional simulation	72
3.15	Results from DA simulation	72
3.16	Experimental values from the water-rocket setup	73
3.17	Error margins comparing traditional and DA solutions	73
4.1	Combined matrix for barometric formula	100
4.2	Similarity and distortion measures	124
5.1	Spearman's test for X_{ms} and X_{ps}	128
5.2	Spearman's test for X_{ms} and X_m	129
5.3	Comparison of linear methods	140
5.4	Improvements over earlier linear methods - I	145
5.5	Improvements over earlier linear methods - II	145
5.6	ESM representation of the clip	147
5.7	Test data from representative geometries of the clip	148
5.8	Distortion, similarity measure and condition number for all linear methods	151
5.9	Predicted values for clip deflection	152
5.10	Error values for clip deflection	153
5.11	ESM representation of the transformer system	157
5.12	Test data from representative geometries of the transformer system	157
5.13	Predicted values for transformer flux measurement	158
5.14	Error values for transformer flux measurement	159
6.1	Spearman's test for X_{ms} and X_{ps}	162
6.2	Spearman's test for X_{ms} and X_m	163
6.3	Comparison of non-linear methods - I	198
6.4	Comparison of non-linear methods - II	198

6.5	Comparison of non-linear methods - III	198
6.6	ESM representation of the skillet	200
6.7	Measurement data for skillet experiment	201
6.8	Predicted temperature values for skillet	207
6.9	Error values in temperature prediction for skillet	209
6.10	ESM representation of the airfoil system	211
6.11	Test data from representative geometries of the airfoil system .	212
6.12	Predicted values for airfoil drag	213
6.13	Error values for airfoil drag	216
7.1	Error norms used in ESM	220
7.2	Error estimation in all linear methods and, bilinear, polynomial, regression and spline fit non-linear methods	223
7.3	Illustration of error estimation in all linear methods and, bi- linear, polynomial, regression and spline fit non-linear methods using the Magnetic Flux example	223
7.4	Error estimation in adaptive polynomial and trigonometric meth- ods	224
7.5	Illustration of error estimation in adaptive polynomial and trigono- metric methods using the Skillet example	224
7.6	Prediction error estimation in all methods	225
7.7	Illustration of prediction error estimation in all methods using the Magnetic Flux example	225
8.1	Engineering shape factors and their usage	241
8.2	Geometric data of a keyboard spring	245
8.3	ESM representation of the keyboard spring	246
8.4	Specimen shape factors for keyboard spring experiment	246
8.5	Material data for keyboard spring experiment	247
8.6	Measurement data for keyboard spring experiment - Model and Product	247
8.7	Measurement data for keyboard spring experiment - All specimen	248

8.8	Predicted values for keyboard spring - scaled	249
8.9	Error values for keyboard spring - scaled	250
8.10	Geometric data of an interconnect	254
8.11	ESM representation of the interconnect	254
8.12	Specimen shape factors for interconnect experiment	254
8.13	Material data for interconnect experiment	254
8.14	Measurement data for interconnect experiment - Model and Product	255
8.15	Measurement data for interconnect experiment - All specimen	255
8.16	Predicted values for interconnect - scaled	256
8.17	Error values for interconnect - scaled	257
8.18	Guidelines for using shape factors in ESM	259
9.1	ESM representation of the welding system	264
9.2	Welding parameters	264
9.3	Measurement data for welding experiment	265
9.4	Predicted values for welding temperature measurement	266
9.5	Error values for welding temperature measurement	266

List of Figures

1.1	Modeling aircraft wing behavior as an airfoil - similitude . . .	2
1.2	A simple mass - spring - damper mechanism	4
1.3	Heat conduction through a block	7
1.4	A wind tunnel test for dynamic similitude	11
1.5	The ESM process - Adapted from [Cho, 1999]	12
1.6	The ESM process - Genesis and current status	13
2.1	Similar figures	17
2.2	Similar geometries	17
2.3	Geometric similarity between two beams	18
2.4	Buckling of a <i>fixed-fixed</i> column	23
2.5	A simple backpack clip	37
2.6	Clip geometry	38
2.7	Configuration of the clip	38
2.8	Flow chart for applying Buckingham π theorem	43
2.9	A simple pendulum	46
3.1	A basic water-rocket assembly	53
3.2	Optimal values using Excel solver	68
3.3	Experimental setup for water rocket - Adapted from [Otto et al., 2001]	71
3.4	Comparison of different solutions	73
3.5	Error trends from different solutions	74

3.6	Comparison of numerical and experimental solutions for varying pressure levels	74
3.7	Conventional TSM analysis	76
3.8	Modified TSM analysis	77
3.9	A simple flow graph	79
3.10	Multiple domain flow graph	80
3.11	Graph for a known relationship - finite edge weight	81
3.12	Graph for an unknown relationship - infinite edge weight	82
3.13	Flow graph for thrust	87
3.14	Flow graph for drag	89
3.15	Flow graph for inertial effects	90
3.16	Flow graph for translational dynamics	91
3.17	Control volume for the water-rocket	92
3.18	Flow graph for Bernoulli's equation	94
3.19	Flow graph for isentropic expansion	95
3.20	Flow graph for continuity	96
3.21	Flow chart for graphical dimensional analysis	98
4.1	Distortions in engineering systems	104
4.2	Detailed primary distortions	105
4.3	Detailed secondary and tertiary distortions	106
4.4	Dissimilarity in material response	107
4.5	Product with multiple materials - The CPU of a computer	108
4.6	Different approaches of system modeling	113
4.7	ESM process	115
4.8	Unique mapping between two distinct geometries	118
4.9	Simplified representation of a piston	119
5.1	USB Clip	146
5.2	USB Clip - Solid model	146
5.3	USB Clip - Half section	147
5.4	USB Clip - Specimen	148

5.5	Linearity of test data from representative geometries of the clip	149
5.6	Prediction plot for clip deflection	153
5.7	Error plot for clip deflection	154
5.8	Transformer layout and operation	155
5.9	ESM quartet for the transformer system [Adapted from Gysel selinck et al., 2001]	156
5.10	Prediction plot for transformer flux measurement	159
5.11	Error plot for transformer flux measurement	160
6.1	Adaptive polynomial method	182
6.2	Effect of higher order continuity	183
6.3	Position continuity	188
6.4	Adaptivity of the developed methods	197
6.5	Skillet geometry	200
6.6	Skillet specimen geometry	200
6.7	Prediction plot for skillet temperature - Bilinear and Polynomial ESM	207
6.8	Prediction plot for skillet temperature - Adaptive polynomial and Spline fit ESM	208
6.9	Prediction plot for skillet temperature - Regression methods ESM	208
6.10	Prediction plot for skillet temperature - Trigonometric ESM .	209
6.11	Error plot in temperature prediction for skillet	210
6.12	ESM quartet for the airfoil system [Adapted from Selig et al., 1995]	211
6.13	Prediction plot for airfoil drag - Bilinear and Polynomial ESM	214
6.14	Prediction plot for airfoil drag - Adaptive polynomial and Spline fit ESM	214
6.15	Prediction plot for airfoil drag - Regression methods ESM . .	215
6.16	Prediction plot for airfoil drag - Trigonometric ESM	215
6.17	Error plot for airfoil drag	217
7.1	Selection of method in ESM	227

8.1	Spline shaft representation using circular and elliptical cross-sections	230
8.2	Regular square vs. I cross-section	232
8.3	Shape factor distribution in an ellipse without thickness - Bending and Buckling modes	235
8.4	Shape factor distribution in an ellipse with thickness - Twisting mode	235
8.5	View factors in radiative heat transfer	238
8.6	A typical keyboard spring	244
8.7	Force input and motion in a keyboard spring	244
8.8	Dimensions of a keyboard spring	244
8.9	Specimen choices for keyboard spring	245
8.10	Errors due to shape factors for keyboard spring - scaled	250
8.11	A typical interconnect geometry	252
8.12	Stress element and deformed stress element of the interconnect neck region	252
8.13	Specimen choices for interconnect	253
8.14	Errors due to shape factors for interconnect experiment - scaled	258
8.15	Shape factor integration in ESM	260
9.1	Geometries for the weld experiment	263
9.2	Temperature measurement locations in the weld experiment	264
9.3	Prediction plot for welding temperature measurement	267
9.4	Error plot for welding temperature measurement	267
G.1	Welding experiment - Physical prototypes	297
G.2	Welding experiment - Thermocouples affixed and system integrated into the welding station	298
G.3	Welding experiment - Finished weld joint	298
G.4	Welding experiment - Welding station	299

Chapter 1

Introduction

“Every science begins as philosophy and ends as art.” - Will Durant

Design studies often involve selection and implementation of geometry and material choices such that an optimal combination produces desired functional result in the most efficient manner. Several different approaches have been employed to identify and model geometric and material parameters including classic closed-form analysis [Otto et al., 2001], bond graph analysis [Karnopp et al., 2006], FEM techniques [Becker et al., 1981] and design methodology functional modeling methods [Otto et al., 2001]. An important method in the same league, involves the technique of dimensional analysis, which is a tool used to develop scaling factors¹ between several influencing variables² using a structured and methodical approach. A unique feature of this method is the use of parameters (π groups) that are dimensionless. These parameters combine all pertinent variables in the analysis to produce a simplified dimension free quantity thus making mathematical management simple and effective.

Similitude (property of similar structures) and similarity methods (techniques employing similar structures for analysis) have evolved from the idea of

¹Scaling factors can be interpreted as the ratio of a parameter in different modes, regimes or conditions.

²Influencing variables are parameters of a system that actually affect its response.

dimensional analysis where a complex object is represented by a simpler and more manageable system. Complexity of an object can be attributed to its size, cost constraints (manufacturing and maintenance), modeling difficulty, material choices, and inputs to the object or measurement intricacy. A classic example of such modeling is where the full span of a wing of an airplane is replaced by a simpler and usually smaller airfoil for testing (see Figure 1.1).

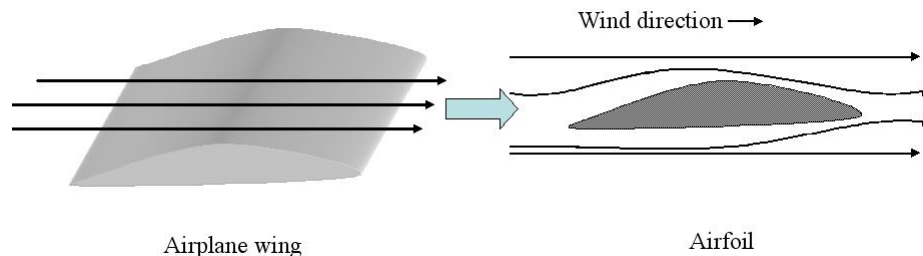


Figure 1.1: Modeling aircraft wing behavior as an airfoil - similitude

Similitude as a science has incorporated benefits of these scaled models and put them into technical analysis for quantitative mapping of experimental results. The basis of similitude thus arises from the hypothesis that simpler scaled models can be experimented with to determine the response of associated complex designs with reasonable effort and desired error bounds. Much of this effort thus lies in judicious selection of the model to represent the actual system. Such a selection encompasses decisions relating to scaling consistency such that the similarity in material, geometric and parametric features is maintained. Expanding on the concept of dimensional analysis, the next section introduces the very basic definitions of units and dimensions and discusses how several individual dimensions can be systematically combined to derive more complex parametric forms that are widely used in engineering.

1.1 Units and Dimensions

Units and dimensions form the basis of all engineering metrics and provide numerical and dimensional character to a parameter of interest. While

units are comparable and transformable between different systems³ and scales, dimensions are generally unique and provide individual combination of fundamental dimensions. Table 1.1 lists fundamental engineering dimensions while Table 1.2 provides units and dimensions for some of the common engineering parameters in most frequently used unit systems. All parameters irrespective of their domain thus share a common relationship. They have units (none in the case of mathematical constants such as π and e) and dimensions. The force applied on a body has units of *Newtons* (SI system) and dimensions of $[MLT^{-2}]$. It is simple to notice that force being the product of mass and acceleration, generates the required dimensional form. Theoretically, dimensions can be assigned to just about every parameter known to science, and the study of such dimensions as applied to engineering problems is called dimensional analysis.

Table 1.1: Fundamental dimensions

Fundamental Dimension	Parameter
M	Mass
L	Length
T	Time
θ	Temperature
i	Current
L	Luminous Intensity
σ	Solid Angle

Any engineering variable will have a dimension set with a combination of the fundamental dimensions with different values of exponents. Consider a simple example that illustrates robustness of dimensional analysis. Let an input force be applied to a spring to cause deflection from its position of static equilibrium. Further, assume that this force is caused by suspending a mass m (see Figure 1.2). The objective of this example is to illustrate dimensional equivalence and establish the dimensions of the characteristic parameters of the system. From Newton's third law, we know,

³The common systems of units include SI, MKS, CGS, FPS and IPS.

Table 1.2: Units and dimensions

Parameter	Domain	Units					Dimensions
		SI	MKS	CGS	FPS	IPS	
Length	Any	m	m	cm	ft	in	L
Mass	Any	kg	kg	gram	lb	lb	M
Time	Any	sec	sec	sec	sec	sec	T
Temperature	Thermal	K	°C	°C	°F	°F	θ
Pressure	Hydraulic	Pa	N/m ²	bar	psf	psi	$[ML^{-1}T^{-2}]$
Force	Mechanical	N	kg m/s ²	dyne	lbf	lbf	$[MLT^{-2}]$
Velocity	Mechanical	m/s	m/s	cm/s	ft/s	in/s	$[LT^{-1}]$
Current	Electrical	A	A	Bi	A	A	$[i]$
Power	Any	W	J/s	erg/s	hp	in-lb/s	$[ML^2T^{-3}]$

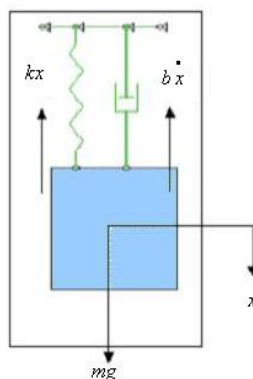


Figure 1.2: A simple mass - spring - damper mechanism

$$F_{spring} = mg \quad (1.1)$$

where F_{spring} is the parameter being ascertained. Further, simple dynamics suggests that for steady analysis, only the deflection length and a spring characteristic parameter should affect the value of F_{spring} . There are no other variables that affect the system. Using dimensional analysis,

$$F_{spring} = [M^1 L^1 T^{-2}] = [M^1 L^0 T^0][M^0 L^1 T^{-2}] \quad (1.2)$$

Since deflection length is one of the output variables,

$$[M^1L^1T^{-2}] = A[M^0L^1T^0] \quad (1.3)$$

and hence the constant A needs to have dimensions $[M^1L^0T^{-2}]$ which is the well known spring constant. If the spring had a dashpot attached in series, then for transient dynamic equilibrium,

$$A\ddot{x} + B\dot{x} + Cx = mg \quad (1.4)$$

$$A[M^0L^1T^{-2}] + B[M^0L^1T^{-1}] + C[M^0L^1T^0] = [M^1L^1T^{-2}] \quad (1.5)$$

i.e., the sum of the spring force (dependent on deflection), the resistance due to the dashpot (dependent on deflection rate change) and the inertial force (dependent on rate of deflection rate change). Hence for homogeneity in dimensions, *i.e.*, dimensional equivalence on either side of the equation, we need to have,

$$[M^aL^bT^c]_A[M^0L^1T^{-2}] = [M^1L^1T^{-2}] \quad (1.6)$$

$$[M^aL^bT^c]_B[M^0L^1T^{-1}] = [M^1L^1T^{-2}] \quad (1.7)$$

$$[M^aL^bT^c]_C[M^0L^1T^0] = [M^1L^1T^{-2}] \quad (1.8)$$

which gives,

$$a_A = 1, b_A = 0, c_A = 0 \quad (1.9)$$

$$a_B = 1, b_B = 0, c_B = -1 \quad (1.10)$$

$$a_C = 1, b_C = 0, c_C = -2 \quad (1.11)$$

or,

$$A = [M^1L^0T^{-2}], B = [M^1L^0T^{-1}], C = [M^1L^0T^{-2}] \quad (1.12)$$

which are the mass m , the damping coefficient ζ and spring constant k respectively. Using a basic example, the *principle of dimensional homogeneity*, which

allows for mathematical operations on dimensions to maintain consistency, has been illustrated. A brief summary about this principle is put forward here and is explained in more detail in Chapter II.

The concept of homogeneity is of utmost importance in dimensional analysis. The principle essentially ensures that given an equation, the terms involved in the system combine to create the same dimensional form on both sides of the equation. Hence apart from numerical correctness we have to ensure dimensional correctness as well. Further, when an equation is formed by algebraic manipulation of two or more terms, each term must be of the same dimensional form as the output [Szirtes, 1998]. Mathematical constants assume no dimension except for zero, which can theoretically assume any dimension [Hart, 1995]. When a transcendental, exponential or any other function is involved, the function with its arguments cannot assume a residual dimension⁴ [Hart, 1995]. The factors that the function has, may have individual dimensions, but when combined, have to produce a numerical value alone so that the function can be evaluated and has no dimension in its argument. $\tan(3)$ seconds is a valid expression but not $\tan(3 \text{ seconds})$ [Szirtes, 1998]. A similar argument extends to exponential functions as well. If t represents time in seconds, then e^t is a valid time scale only if the entire function is assumed to have dimensions of seconds. Expanding e^t in powers of t gives,

$$e^t = 1 + t + \frac{t^2}{2!} + \dots \quad (1.13)$$

Substituting the simple time scale (seconds) in the above equation generates terms involving higher order powers of seconds which is neither dimensionally correct nor has any physical relevance. Hence in a given system, if t represents time in seconds, another system can exist where e^t seconds is the time scale but not $e^t \text{ seconds}$. Dimensional homogeneity thus is a guiding tool to capture effects of all relevant influencing parameters such that the net result produced by the combination has physical attributes that are both measurable

⁴The argument must be dimension free.

and quantifiable.

Consider another example (see Figure 1.3) where establishing the dimensions of thermal conductivity k of a material is of interest. Heat content

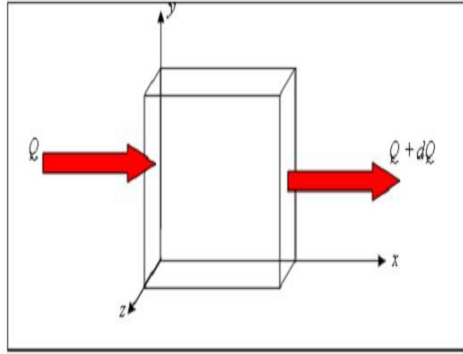


Figure 1.3: Heat conduction through a block

in conduction Q , is given by Fourier's law to be -

$$Q \propto \frac{A\Delta\theta t}{d} = \frac{kA\Delta\theta t}{d} \quad (1.14)$$

where A is area, t is time, d is characteristic length and $\Delta\theta$ is the change in temperature across the length. In dimensional form,

$$[ML^2T^{-2}] = \frac{k[M^0L^2T^0] \times [M^0L^0T^0\theta^1] \times [M^0L^0T^1]}{[M^0L^1T^0]} \quad (1.15)$$

or,

$$[ML^2T^{-2}] = k[M^0L^1T^1\theta^1] \quad (1.16)$$

and hence,

$$k = [MLT^{-3}\theta^{-1}] \quad (1.17)$$

Thus, basic engineering identities and dimensional homogeneity can be combined to obtain the dimensions of system specific constants. Further, this is a good way to verify answers when solving problems as any mismatch in dimensions points to lack of a variable, overuse of a variable or wrong choice

of variables altogether. Even the most complex of problems is constrained by this property and hence dimensionality has to be maintained for correctness in solution. The next section walks through the use of models and prototypes that employ this technique of dimensional analysis in engineering regimes.

1.2 Models and Prototypes

Models and prototypes play significant roles in engineering studies. These tools are often employed to convey certain information about a proposed design or a hypothetical device such as *fit* and *form*. Models in particular are extensively used for understanding analytical behavior of a system. In this context it is necessary to fathom the subtle differences between these two entities and how these are incorporated into similitude analysis. A *model* is a virtual, mathematical or a scaled version of a system. Sketches, engineering drawings, 3D CAD images, clay models, scaled architectural designs, analytical equations and numerical approximations are most common forms of *models*. A *prototype*, on the contrary, is a physical manifestation of the intended design with a definite engineering purpose. It is, more often than not, used to prove the concept of the design *i.e.*, verify functionality of the design. A prototype, like the model, can exist in the virtual world but should necessarily illustrate proposed functionality of the device. Simulations to a certain extent are “prototypes” of the actual solution. Prototypes, thus, are simulated representations of a system, a mimic of the behavior intended to prove the feasibility of the design. Models can thus be interpreted as primitive versions of a prototype and prototypes as refined adaptations of models. However, it is prudent to note that both models and prototypes are employed in the experimental phase of product evolution as is evident, respectively, from wind-tunnel testing (airfoil *models*) and scaling experiments (*prototypes*). In similitude, both these instruments are comprehensively utilized [Langhaar,1951 and Cho, 1999] using *scales*, which are introduced in the next section.

1.3 Scales in Similitude

A scale, from a similitude perspective, is a factor or a number that translates value of a parameter of interest from model domain to the actual system. It is the ratio of actual value to the predicted value and is a dimensionless quantity that relates a parameter evaluated in two different scenarios with no apparent distortion. Put simply,

$$\lambda = \frac{P_{product}}{P_{model}} \quad (1.18)$$

where λ is the scale and P is the parameter of interest evaluated in different conditions. This definition can be extended to intricate geometries with multiple inputs and non-linear material characteristics. A complex 3D body can be visualized as a set or space of well-defined points with functional values attached to them. These functional values (stress, temperature, strain etc) are characteristic of material that the body is made of and define behavior of the structure for various input loads. In most engineering problems, analysis is pursued by making several assumptions to simplify the problem. The idea behind doing so is to ‘idealize’ the system so that a basic understanding is obtained about its working properties. But a rational and realistic analysis would include effects of non-linearity that are inherent in most engineering systems. Such non-linearities, usually in material properties have to be captured for a pragmatic evaluation of the system, and is only plausible if they can be quantified numerically as functional forms.

Consider a mass M moving with a total velocity V . The amount of energy spent is simply $\frac{1}{2}MV^2$ and if another mass $\frac{M}{2}$ has to spend the same amount of energy, then it has to move with a total velocity of $\sqrt{2}V$ where the radical is the *scale* we are interested in. But we have neither accounted for friction loss due to wind resistance nor losses due to kinetic friction from surface interaction, and assumed mass to be independent of time (even though the reduction is negligible). In short, we have analyzed the system in ideal

conditions which limits applicability of similarity analysis to focussed domains. This research thus motivates the need and process of using empirical similarity processes in an effort to extend the applicability of similitude models from linear regimes to non-linear domains, thus allowing for developing scales as matrices instead of numbers. The engineering relevance of similitude scales and models is motivated in the next section.

1.4 Applications of Similitude

Modeling and experimentation are two vital components in design process that seek to identify key parameters influencing a system and affecting its behavior. Many engineering systems are designed for low cost, high reliability, high quality, easy maintenance, simple manufacturability, high durability, toughness and, environment and aesthetics. Each of these parameters has inherent factors that affect its performance. More often than not, capturing such behavior is possible through experimentation alone due to relative modeling complexity. Further, experimentation is often closer to reality than modeling. However, testing the actual system itself is difficult when designs are still hypothetical or if the object is too complex to test (see Figure 1.4). Similitude is used as a predictive instrument in such situations. The process allows for identifying key variables, developing combination of the variables that affect the output parameter and defining scales to map experimental results from model space to the product domain. Hence, similitude plays a vital role in engineering design as a predictive and experimental tool for product validation. Design iteration and synthesis can thus be performed based on results of the technique thus contributing to the product life cycle. The next section explains how test prototypes and specimen can be directly coupled with similitude thus providing an empirical framework for similarity analysis.

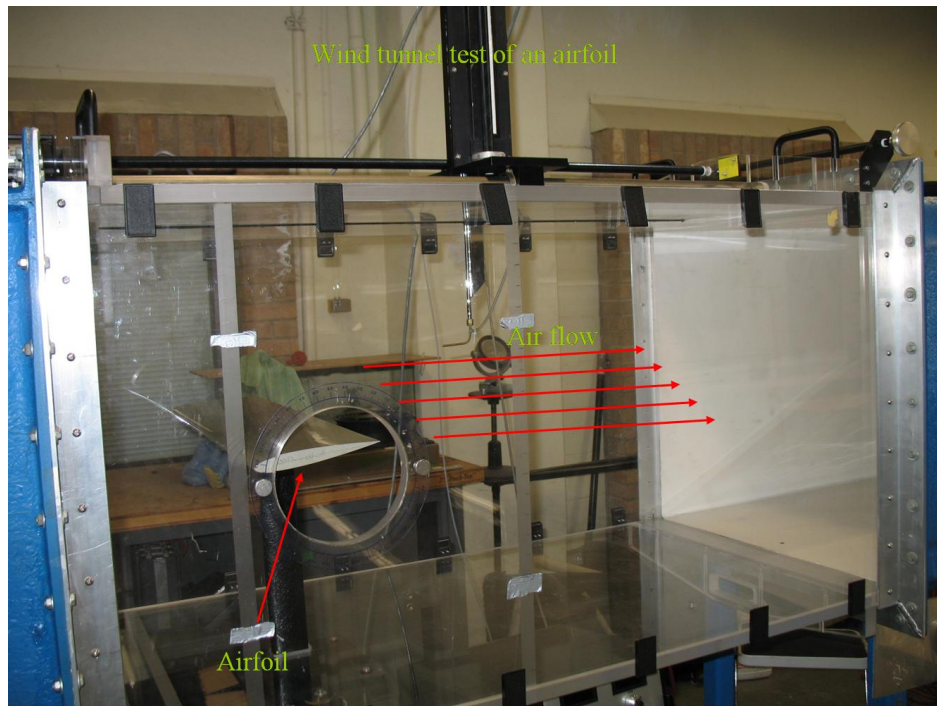


Figure 1.4: A wind tunnel test for dynamic similitude

1.5 Similitude with Experimental Prototypes - The Empirical Similitude Method

Physical prototypes and models fabricated either through rapid prototyping or conventional techniques can represent a complex product sharing similar attributes of geometry and material. When regular analytical approach to parameter (say deflection) evaluation in a certain product requires complicated estimations, these prototypes and models can be experimented with to obtain relevant test data that can be coupled using mathematical procedures to generate the required parameter value in the actual system, thus providing an alternate and accurate mapping strategy. The Empirical Similitude Method (ESM) [Cho, 1999], based on this premise, thus combines the advantages of using simplified geometries (test specimen) and reliability of experimental data of

these geometries to predict the performance of a complex product (see Figure 1.5).

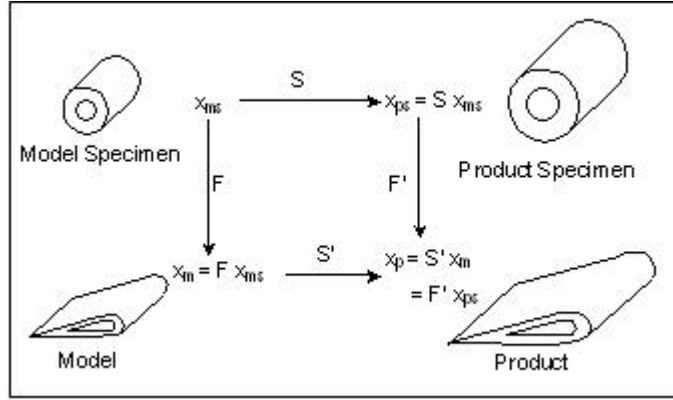


Figure 1.5: The ESM process - Adapted from [Cho, 1999]

Using the experimental data of the three representative geometries called the *model*, the *model specimen* and the *product specimen*, the values of a parameter are predicted for the *product*. Rapid prototyping has lent additional impetus to this method as the *model* and the *model specimen*, on some occasions, can be made directly from RP processes thus negating any manufacturing constraints.

In order to develop the analytical structure to combine such experimental data, [Cho, 1999], [Dutson, 2002] and [Wood, 2002] did pioneering work providing mathematical relations and procedures to obtain insights into prediction and estimation of engineering parameters in products. [Dutson, 2002] also created an initial framework for integrating specimen with different shapes into ESM analysis. However, these developments are quite primitive and do not employ modern computational algorithms which offer many discernible benefits including flexible tolerance levels and iteration characteristics. Further, error minimization through interval and polynomial order refinement coupled with mathematical features such as continuity and adaptivity has not been pursued. Shape factors and their significance in ESM has not been thoroughly investigated. Choice of method and domain (linear *vs.* non-linear) has

also not been properly defined. These avenues for continued research have thus been identified (see Figure 1.6) and form the basis for this effort. The goal of this research is to hence identify procedures for test specimen selection and develop mathematical methods to transform experimental results of such specimen with rigorous accuracy. The process employed for successful completion of these tasks is surmised next.

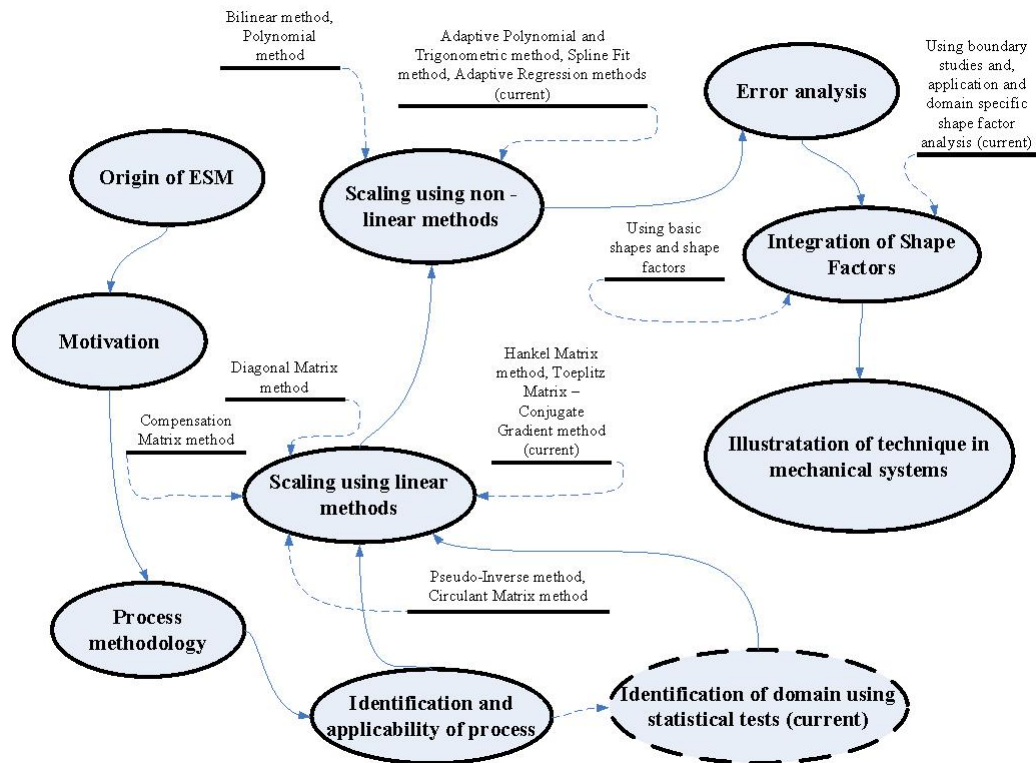


Figure 1.6: The ESM process - Genesis and current status

1.6 Objectives and Hypothesis of Research

The hypothesis for continued research in ESM can be stated as “*Special matrices and adaptive algorithms can be used and developed to accurately evaluate non-linear and distorted systems through the use of experimental spec-*

imens”. The key objectives in proving the hypothesis include:

- Use matrix structures and develop adaptive algorithms to functionally map material and geometric properties.
- Define the proposed methods, principles, working procedures, errors and limitations.
- Show initial validation with engineering examples.
- Compare efficiency and robustness of developed methods with previous ESM techniques.
- Show enhancement of the process using appropriate examples.
- Use a practical example for realistic validation of the process.

1.7 Dissertation Layout

Several sources of information have been consulted in understanding the process of similitude and relevant mathematical background. Theory of similarity and its origins, resulting in development of Buckingham π theorem, and initial applications in practical problems have been identified. This information is compiled concisely in Chapter II and elucidated using a couple of examples. Chapter III continues the use of Traditional Similitude Method (TSM) based on Buckingham π theorem and builds on the technique by extending the process into reduction of non-monomial bases. Graphs and their applications in dimensional analysis is discussed and a novel algorithm and graphical approach are introduced in understanding system dynamics of a toy water-rocket. The premise behind the development of Empirical Similitude Method (ESM) and the advantages over TSM are highlighted in Chapter IV by identifying the limitations of TSM. Further, conditions when ESM is applicable, principles governing its operation and systems that satisfy ESM properties are elaborated.

Chapter V explains linear ESM methods delving into prior and recent processes, presenting advantages of innovations generated with the use of the latest methods. Succinct analytical description is complemented with numerical examples to prove feasibility of these methods and highlight enhancement achieved. Extending into non-linear domains, Chapter VI presents a comprehensive discussion about past methods, their drawbacks and puts forward inventive approaches developed complete with mathematical explanation, limitations, working intervals and applicability in practical systems. Examples are provided to show validity and improvements attained using these developments. Augmentation realized in the linear and non-linear regimes is captured using rigorous mathematical definitions in Chapter VII where meticulous error characterizations and algorithms are presented.

Shape factors are introduced in Chapter VIII illustrating pertinence and integration into ESM and their role in specimen selection. General engineering usage is shown along with a set of examples to provide initial framework for coupling ESM and shape factors. Experimental verification is accomplished in Chapter IX where a relevant experiential process is used in the evaluation of developed techniques. Prediction capabilities brought on by new schemes are offered for analyzing an industrial product. The report culminates in Chapter X where the entire process is summarized, important conclusions are finalized and opportunities for future extensions are identified.

Chapter 2

Background

“I find that a great part of the information I have was acquired by looking up something and finding something else on the way.” - Franklin P. Adams

The previous chapter formally introduced the research topic and presented a foreword on similarity techniques apart from establishing research objectives and motivation for working in empirical domains. In this chapter the essence of similitude and development of similarity procedures are described focusing on analytical relations and their industrial applications.

2.1 Dimensional and Similarity Analysis

Similitude as a formal procedure was introduced by [Rayleigh, 1915] discussing the process of establishing *scales* in an engineering setting. Buckingham [Bridgman, 1931] extended the technique to systems that encompassed several variables affecting the performance of a system. The hypothesis behind dimensional analysis is based on the argument that dimensions remain impervious to changes in numerical magnitude. Energy retains units of *Joules* (assuming that SI units are followed) and dimensions of $[ML^2T^{-2}]$ irrespective of the working domain and magnitude attained. Depending on the kind of problem, energy evaluation can assume a mathematical combination of differ-

ent variables and constants. However, dimensions remain constant and invariant. This characteristic captured the effect of *similarity* analysis, a technique which suggested that a ‘complex’¹ system referred to as *product* (difficult to be evaluated) can be represented by a scaled yet *similar* version called *model* (see Figure 2.1).

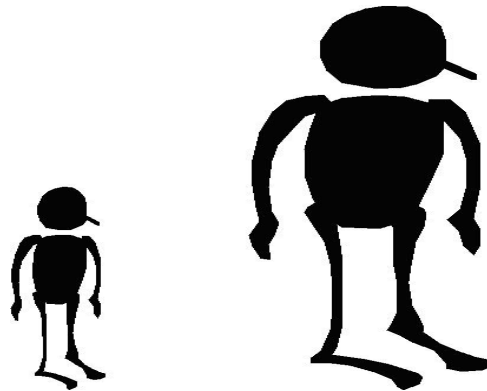


Figure 2.1: Similar figures

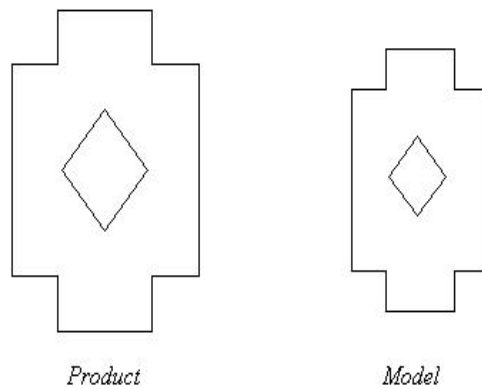


Figure 2.2: Similar geometries

Similarity is not just confined to geometric shapes (see Figure 2.2). Similarity variables and similar matrices are widely used mathematical transformations. The magnetic hysteresis loop and mechanical stress-strain cycle

¹Size, cost, experimental difficulty, hypothetical device still in the design phase.

bear close resemblance implying engineering similarity. Hence, study of one of the systems provides information about the other domain as well. Thus, for similarity to be feasible, being *homologous* [Langhaar, 1951] is essential - a feature that suggests that a variable or a system in one regime corresponds with the same variable or system in another domain with a certain scale involved. It implies that existence, motion and consequence in space and time between two different structures (in their entirety) are exactly identical. Models and products thus need to be homologous in similarity analysis so that a valid prediction can be carried out. In similitude studies, five basic similarity conditions need to be satisfied for an accurate estimate [Skoglund, 1967 and Dutson, 2002] -

- **Geometric Similarity**

Geometric similarity ensures that product and model are structurally similar in shape, size and configuration. All characteristic dimensions and distances are identical relative to a chosen reference frame *i.e.*, *Position Similarity* (see Figure 2.3).

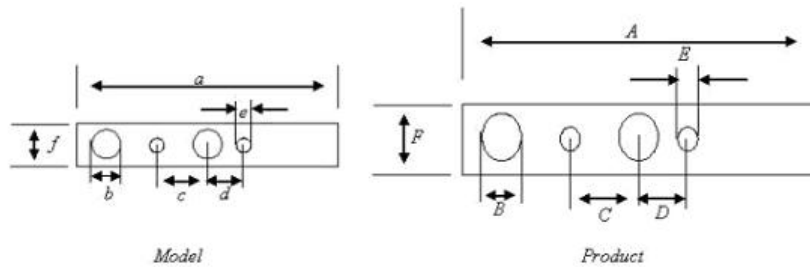


Figure 2.3: Geometric similarity between two beams

$$\frac{A}{a} = \frac{B}{b} = \frac{C}{c} = \frac{D}{d} = \frac{E}{e} = \frac{F}{f} \quad (2.1)$$

- **Kinematic Similarity**

Kinematic similarity ensures that time scale involved in the evaluation of displacement, velocity and acceleration are synonymous in both systems

being evaluated *i.e.*, *Motion Similarity*. If t is time scale in model space and t^* is analogous time scale in product space, then kinematic similarity forces $t \equiv t^*$. For a torsional pendulum,

$$t \propto \sqrt{\frac{I}{k}} \equiv t^* \propto \sqrt{\frac{I^*}{k^*}} \quad (2.2)$$

- **Dynamic Similarity**

Dynamic similarity coerces the constraint that mass distribution, and in combination with kinematic similarity that forces and torques in both systems are similar in magnitude and direction *i.e.*, *Input Force Similarity*.

$$\vec{F} \equiv \vec{F}^* \quad (2.3)$$

- **Thermodynamic Continuum Similarity**

This constraint is the most elaborate and comprehensive of all relations and compels that continuity is never compromised and validity of conservation of mass, momentum and energy holds in fluid, thermal and other related systems *i.e.*, *Continuum Similarity*.

$$q_{cons} \equiv q_{cons}^* \quad (2.4)$$

- **Physical Similarity**

This is the constraint that enforces modeling similarity between two systems, and that true physics of the problem is evaluated similarly in both domains using identical mathematical procedures, numerical approximations and simplifying assumptions *i.e.*, *Modeling Similarity*.

$$system_{PDE} \equiv system_{PDE}^* \quad (2.5)$$

Experimentation and analysis done on the model is now equivalent to

the actual system, and results can hence be mapped between the two as long as the above similarity constraints are maintained. Some leeway can still be expected from *distorted* models [Murphy, 1950 and Taylor, 1974], but necessary correction factors need to be employed². In undistorted systems, mapping between the two geometries is accomplished using π groups that match dimensions of several influencing variables and maintain consistency in the desired output parameter(s) [Langhaar, 1951]. The mathematics of the technique is detailed below.

2.2 Buckingham π Theorem-Traditional Similarity Method (TSM)

Consider a system, *product*, that is influenced by n independent variables $\{x_i\}_{i=1}^n$. Then,

$$f^p(x_1, x_2, \dots, x_n) = 0 \quad (2.6)$$

If the same set of variables, $\{x_i\}_{i=1}^n$, affect another system called the *model* that represents the *product*, then,

$$f^m(x_1, x_2, \dots, x_n) = 0 \quad (2.7)$$

According to Buckingham π theorem [Bridgman, 1931], states x_i 's can be modeled in terms of dimensionless π parameters as -

$$\phi^p(\pi_1, \pi_2, \dots, \pi_{n-k}) = 0 \quad (2.8)$$

$$\phi^m(\pi_1, \pi_2, \dots, \pi_{n-k}) = 0 \quad (2.9)$$

where k is the number of physical dimensions used in modeling the system. The theorem can be thus stated as -

“A dimensionally homogeneous equation can be reduced to a relationship

²These distortions are explained in more detail in Chapter IV.

using a complete set of dimensionless products.” [Langhaar, 1951]

Hence, for two corresponding systems, Buckingham π theorem can be generalized for a particular parameter P [Dutson, 2002] as -

$$\phi^p(P) = \phi^m(P) \quad (2.10)$$

if

$$\pi_i^p = \pi_i^m \quad \forall i \in [1, N] \quad (2.11)$$

Equation (2.10) is called *prediction equation* while Equation (2.11) signifies *similarity constraints* for the system. The combination is generally referred to as *model laws* for the system. The number of dimensionless parameters is now N such that $N = n - k$, hence far smaller in number ($N < n$) and easier to manipulate. Mathematically, k is equivalent to the rank³ of the dimensional matrix formed using the system parameters.

An alternate formulation of the theorem involves classifying and coupling material (M) and geometry (G) variables in steady-state analysis such that for a parameter P ,

$$P_p = \phi(G_p, M_p) \quad (2.12)$$

$$P_m = \psi(G_m, M_m) \quad (2.13)$$

Combining the factors we have,

$$\frac{P_p}{P_m} = \Pi \left(\frac{G_p}{G_m}, \frac{M_p}{M_m} \right) \quad (2.14)$$

$$\frac{P_p}{P_m} = \Pi(\pi_1, \pi_2) \quad (2.15)$$

$$P_p = P_m \Pi(\pi_1, \pi_2) \quad (2.16)$$

The matrix approach however is the ideal method⁴ in dimensional anal-

³Number of independent rows or columns in a matrix.

⁴Most commonly used methods are detailed later in this chapter.

ysis as the number of variables and their dependence on other variables creates a grid-like dependence best captured by matrices. [Corrsin, 1951] provides an alternate but elegant geometrical proof of the Buckingham π theorem to illustrate the idea graphically. Having provided the basis for similarity analysis, the method is elucidated using an example detailed below where results from dimensional analysis and conventional techniques are compared. Thus, the motivation in studying this example is to contrast the effectiveness of Buckingham π theorem against a known solution.

2.3 Buckling of Columns

A column is defined as “*A slender structural member with a substantial axial load component*” [Krenk, 2001]. Buckling of columns occurs in the direction perpendicular to the line of load application. The applied load is usually compressive in nature and for high enough magnitude, the column bends normal to the direction of applied load. Mathematically, buckling is captured using the bending theory of beams as applied to columns. A simple illustration of a *fixed-fixed* beam is shown below (see Figure 2.4).

If P is the applied load on a thin column of length l , and if the horizontal sway at mid-section is y , then basic moment analysis gives,

$$M_y = -Py \tag{2.17}$$

where M_y is the bending moment at section y - y . From elementary bending theory, I being the moment of inertia, E the Young’s modulus, R the radius of curvature and σ the stress, we have,

$$\frac{M_y}{I} = \frac{\sigma}{y} = \frac{E}{R} \tag{2.18}$$

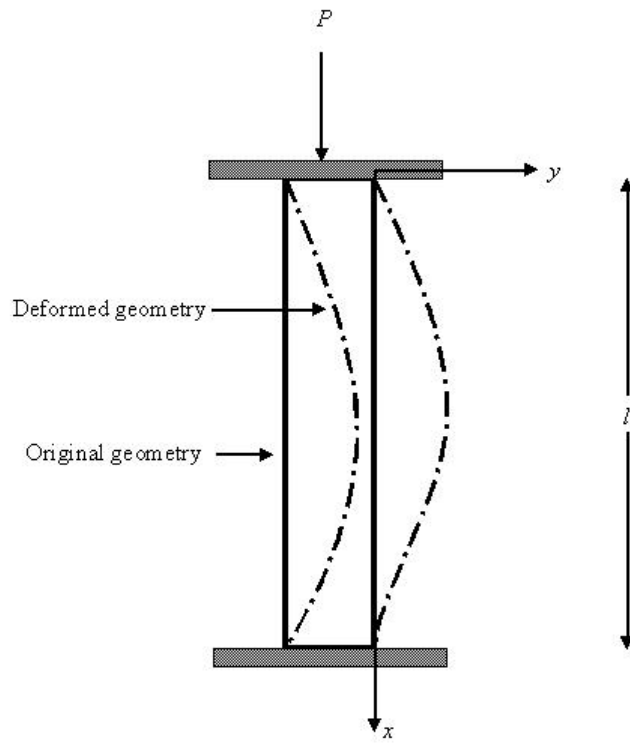


Figure 2.4: Buckling of a *fixed-fixed* column

Combining the two equations, using the relation that $R = \frac{1}{\frac{d^2y}{dx^2}}$, we have,

$$M_y = \frac{EI}{R} = EI \frac{d^2y}{dx^2} \quad (2.19)$$

which is the elementary Euler definition for column buckling [Gere et al., 1961].

Solving the above equation in combination with Equation (2.17), we have,

$$EI \frac{d^2y}{dx^2} + Py = 0 \quad (2.20)$$

or,

$$y(x) = C_1 \sin \sqrt{\frac{P}{EI}}x + C_2 \cos \sqrt{\frac{P}{EI}}x \quad (2.21)$$

where x is distance measured along the vertical axis. Constants C_1 and C_2 are evaluated based on the boundary conditions, $y = 0$ at $x = 0, l$. Notice that the term $\left(\sqrt{\frac{P}{EI}}\right)$ is the eigenvalue of the system and the term $\sin\left(\sqrt{\frac{P}{EI}}\right)$ represents the corresponding eigenfunction. Critical load P_c is now obtained by letting $y = 0$ at $x = l$, which gives,

$$\sqrt{\frac{P}{EI}}l = n\pi \Rightarrow P = \frac{n^2\pi^2 EI}{l^2} \quad (2.22)$$

Generalizing the expression, n being the mode of buckling and l_c being the critical length,

$$P_c = \frac{n^2\pi^2 EI}{l_c^2} \quad (2.23)$$

The critical length depends on type of boundary conditions (fixed, free, hinged, pinned etc). Further, critical load varies from mode to mode and the first mode being fundamental, is used for design purposes. While this approach is analytical for an ‘ideal’ column, we can arrive at the same result using a dimensional approach where parameters are combined based on Buckingham π theorem and the principle of dimensional homogeneity, thus allowing to compare the two techniques. If P_c is parameter of interest, setting up the *dimensional matrix*⁵ (see Table 2.1), let $P_c \equiv f(E, \rho, D, l_c)$, ρ being density and D being the diameter.

Table 2.1: Dimensional matrix for column buckling

<i>Fundamental Dimension</i>	P_c	l_c	ρ	D	E
M	1	0	1	0	1
L	1	1	-3	1	-1
T	-2	0	0	0	-2

A row transformation is now performed by choosing *repeating* variables ($\{P_c, l_c\}$ in this case) to generate the *echelon matrix* (see Table 2.2) where indices of other variables are changed owing to the development of an identity

⁵The development of the dimensional matrix is explained in more detail in Table 2.3.

matrix for the repeating variables.

Table 2.2: Echelon matrix for column buckling

	P_c	l_c	ρ	D	E
π_1	1	0	x_1	x_2	x_3
π_2	0	1	x_4	x_5	x_6

Let

$$A = \begin{pmatrix} 1 & 0 & 1 \\ -3 & 1 & -1 \\ 0 & 0 & -2 \end{pmatrix}$$

\Rightarrow

$$A^{-1} = \begin{pmatrix} 1 & 0 & \frac{1}{2} \\ 3 & 1 & 1 \\ 0 & 0 & -\frac{1}{2} \end{pmatrix}$$

Let

$$B = \begin{pmatrix} 1 & 0 \\ 1 & 1 \\ -2 & 0 \end{pmatrix}$$

\Rightarrow

$$(A^{-1}B)^T = \begin{pmatrix} 0 & 2 & 1 \\ 0 & 1 & 0 \end{pmatrix}$$

From the Fourier's law of dimensional homogeneity [Szirtes, 1998],

$$-(A^{-1}B)^T = \begin{pmatrix} x_1 & x_2 & x_3 \\ x_4 & x_5 & x_6 \end{pmatrix} = \begin{pmatrix} 0 & -2 & -1 \\ 0 & -1 & 0 \end{pmatrix}$$

which gives,

$$\pi_1 = \frac{P_c}{D^2 E} \tag{2.24}$$

$$\pi_2 = \frac{l_c}{D} \tag{2.25}$$

π_1 and π_2 thus represent non-dimensional relations (non-dimensional force and non-dimensional length) combining variables in the system that affect its performance. Thus, an extremely long column can be replaced by a smaller column as long as the π groups in the two systems are similar. Assuming $\pi_1 = K \pi_2^m$ (This is a monomial basis⁶ - a simple relationship between π groups), we have,

$$\frac{P_c}{D^2 E} = K \left(\frac{l_c}{D} \right)^m \quad (2.26)$$

Since $P_c \propto D^4$ (the area moment of inertia), letting $m = -2$, we have,

$$P_c = K D^2 E \left(\frac{l_c}{D} \right)^{-2} = \frac{K E D^4}{l_c^2} \quad (2.27)$$

It is fairly obvious now that $K = 16n^2\pi^4$ so that $P_c = \frac{n^2\pi^2 EI}{l_c^2}$. The technique is thus limited in this regard as constants still need to be evaluated as numerical estimates of experimental data. But for prediction purposes, note that π groups can be used to scale two distinct geometries, *product* and *model* such that,

$$\pi_{1,p} = \pi_{1,m} \leftrightarrow \pi_{2,p} = \pi_{2,m} \quad (2.28)$$

$$\Rightarrow \frac{P_{c,p}}{D_p^2 E_p} = \frac{P_{c,m}}{D_m^2 E_m} \leftrightarrow \frac{l_{c,p}}{D_p} = \frac{l_{c,m}}{D_m} \quad (2.29)$$

The analytical approach and the Buckingham π method thus differ in their mode of execution with the former relying on a calculus based approach while the latter is based on simpler numerical matrix manipulation. The example presented above employed several principles and laws and incorporated the most common form of applying the π theorem. These aspects of the dimensional analysis process are explained in more detail in the next section for a comprehensive and rigorous application procedure.

⁶A monomial basis assumes that a π group is *not* a polynomial form of any other π group and every π group can be represented as a simple product of all other π groups.

2.4 Principles and Rules of Buckingham π theorem

Dimensional analysis and Buckingham π theorem like most methods are governed by a set of laws and principles that regulate applicability and execution of their scaling processes. This section provides a concise collection of the most pertinent rules and constraints together with their physical relevance for completeness. Note that many other laws [Szirtes, 1998], axioms and rules [Murphy, 1950 and Langhaar, 1951] and theorems [Kline, 1965] exist but only the most important and relevant regulations are described below.

- **Choice of variables**

Most engineering systems are governed by a set of inputs such as type and magnitude of the forcing function, boundary conditions that constrain behavior at the boundaries, initial conditions that specify the primary state of the system and state variables that are inherent to the system and the analysis in question. A transient output state y can thus be generalized to be -

$$y(t) = f(x(t), u(t)) + BC + IC \quad (2.30)$$

where $x(t)$ and $u(t)$ are respectively the state variables and inputs. Normalizing initial and boundary conditions,

$$y(t) = f(x(t), u(t)) \quad (2.31)$$

When multiple inputs influence a system and multiple output states are modeled, the above relation assumes a matrix formulation given by,

$$Y(t) = f(X(t), U(t)) \quad (2.32)$$

and for a time invariant system,

$$Y = f(X, U) \quad (2.33)$$

It is important to note that combination of X 's and U 's should necessarily couple to produce Y numerically, mathematically and dimensionally. Any discrepancy in choice of variables implies improper modeling of the system, deviation from true representation of the physics and violation of the governing dynamics. For a given system with a set of states $\{X_i\}_{i=1}^n$ and inputs $\{U_j\}_{j=1}^k$, the following relations needs to hold true for physical sense.

$$X_i \oplus X_j \cup X_i \oplus U_j \cup U_i \oplus U_j \equiv Y \quad (2.34)$$

The above relation simply suggests that inputs operated (\oplus) with states, states coupled with other states and inputs combined with other inputs in any of the six basic mathematical forms shown below, need to produce an output quantity that is representative of the physics of the system and is the desired parameter of interest. For three variables a , b and c , primary coupling modes are given to be -

$$c = a + b \quad (2.35)$$

$$c = a - b \quad (2.36)$$

$$c = a \times b \quad (2.37)$$

$$c = a \div b \quad (2.38)$$

$$c = a^b \quad (2.39)$$

$$c = f(a, b) \quad (2.40)$$

Dimensional analysis in the conventional form primarily focuses on relations (2.37) through (2.39) to combine π groups. The first two relations provide conservation to a technical system while the last relation is the most pertinent in engineering analysis as most products assume complex

relationships transcending intricate interactions. Involving conservation relations (Equations 2.35 and 2.36) in dimensional analysis requires modifications in the process which is shown in the next chapter. Modeling convoluted relations (Equation 2.40) needs experimental evolution that forms the basis for Empirical Similitude Method (ESM) described in chapter IV. However, it is important to note that for simple dimensional analysis, choice of variables assumes significant importance. In evaluating force in a pure magnetic field, magnetic intensity (B), length (l) and velocity (v) are necessary and often times sufficient conditions to estimate magnitude of the force⁷. It is imperative to identify these three parameters as the only influencing parameters. Any other selection leads to physical absurdity.

- **Choice of dimensions**

Choice of dimensions like choice of variables affects the solution of dimensional grouping. It is prudent to understand that dimensions are *not* unique. Energy, a scalar positive definite quantity shares dimensions with torque, which is a direction dependent vectorial parameter. Likewise, pressure and stress share the same dimensions but when analyzing fluid systems, pressure assumes a characteristic that is intuitive while stress is a quantity that is primarily relevant to solids. When modeling systems, choice of dimensions needs to be correspond with choice of variables, as any mismatch leads to erroneous conclusions despite dimensional equivalence.

$$E = \frac{1}{2}MV^2 \leftarrow \textit{dimensionally correct, physically true} \quad (2.41)$$

$$\tau = \frac{1}{2}MV^2 \leftarrow \textit{dimensionally correct, physically not true} \quad (2.42)$$

It is also wise to bear in mind that some parameters assume different dimensions, the choice of which depends strictly on the problem at hand

⁷Lorentz's force in scalar form is given by $F = Blv$.

and the dimension system chosen. Young's modulus can assume dimensions $[FL^{-2}]$, F being force or $[ML^{-1}T^{-2}]$ depending on the situation and transformation from one to the other is required sometimes to maintain invariance in the system, a property discussed later.

- **Dimensional homogeneity**

Dimensional homogeneity reigns supreme in dimensional analysis. It is the principle and law that takes cognizance of dimensional character of a system acknowledging the need to maintain attributes in analysis that are comparable in all forms. An equation has relevance in engineering and mathematics only if it is numerically stable and dimensionally true. All physical processes stem from the basic premise that nature forces non-singular behavior which governs numerical magnitude of the process parameters. However, it is dimensional homogeneity that enforces likeness and identical representation of terms in the equation. In layman terms, homogeneity implies same dimensions in all terms, combined and independent. Put simply,

$$7 \text{ pieces of fruit} = 3 \text{ apples} + 4 \text{ carrots} \quad (2.43)$$

↑ *numerically correct, dimensionally wrong*

$$7 \text{ pieces of fruit} = 3 \text{ apples} + 4 \text{ oranges} \quad (2.44)$$

↑ *numerically correct, dimensionally right*

In a given equation $\mathbf{x} = a\mathbf{y} + b\mathbf{z} + c\mathbf{w} + d\mathbf{v} + e\mathbf{u}$, a , b , c , d and e being constants, dimensional homogeneity ensures that \mathbf{x} has same dimensions as \mathbf{y} , \mathbf{z} , \mathbf{w} , \mathbf{v} and \mathbf{u} . Even in complex relationships, the residual dimension needs to match dimensions of the output even though the arguments of the relationship may assume different dimensions. Hence, homogeneity is a regulator of dimensional accuracy in a mathematical relationship. Analytically, if $y_1 = f(x_1, x_2, \dots, x_n)$ represents a physical process and

$y_2 = f(tx_1, tx_2, \dots, tx_n)$ represents a scaled process, t being a scalar quantity, dimensional homogeneity coerces $y_2 = f(tx_1, tx_2, \dots, tx_n) = t^n f(x_1, x_2, \dots, x_n) = t^n y_1$ [Skoglund, 1967]. In use with dimensional analysis and π group combination, dimensional homogeneity assumes a different notation. If $\pi_1 = \prod_{j=2}^n a_j \pi_j^{b_j}$ represents a system of dimensionless quantities, then $j \in \aleph$, *homogeneity of products* gives [Langhaar, 1951],

$$[M^x L^y T^z]_{\pi_1} = \prod_{j=2}^n [M^{k_j} L^{l_j} T^{m_j}]_{\pi_j} \quad (2.45)$$

$$x = \sum_{j=2}^n k_j \quad (2.46)$$

$$y = \sum_{j=2}^n l_j \quad (2.47)$$

$$z = \sum_{j=2}^n m_j \quad (2.48)$$

Similarly, if $\pi_1 = \sum_{j=2}^n a_j \pi_j^{b_j}$ represents a system of dimensionless quantities, then for $j \in \aleph$, *homogeneity of sums* gives [Langhaar, 1951],

$$[M^x L^y T^z]_{\pi_1} = \{[M^{k_j} L^{l_j} T^{m_j}]_{\pi_j}\} \forall j \in [2, n] \quad (2.49)$$

$$x = k_j \forall j \in [2, n] \quad (2.50)$$

$$y = l_j \forall j \in [2, n] \quad (2.51)$$

$$z = m_j \forall j \in [2, n] \quad (2.52)$$

The essence of homogeneity with specific relation to Buckingham π theorem is captured in the next rule.

- **System invariance**

The elemental ideology of Buckingham π theorem is to reduce the dimen-

sional matrix to the echelon matrix through a series of row⁸ operations. However, Fourier [Dutson, 2002] suggested a matrix approach where a single inversion replaced all row operations and hence simplified the generation of π groups. A typical dimensional-echelon matrix looks like the table shown below (see Table 2.3). In the evaluation of π groups, initial columns are reserved for fundamental dimensions and outputs by convention. The latter columns are populated using influencing variables. Fourier's law requires the matrix A to be square. This condition compels the necessity to choose the number of *independent* variables in forming A matrix to be exactly the same in number as the fundamental dimensions needed to represent the system. If the matrix A is of size $n \times n$, then the matrix B is of size $n \times k$ where k is rank of A . The number of π groups developed is $n - k$. Hence, mathematically, difference between number of variables and rank of the A matrix (number of independent variables) should be number of π groups needed to model the system. The matrix I is an identity matrix of size $k \times k$.

Table 2.3: A typical dimensional-echelon matrix

The diagram shows a matrix with 6 columns and 5 rows. The columns are labeled: Fundamental Dimensions, Output₁, Output₂, Variable₁, Variable₂, and Variable₃. A bracket above the entire matrix is labeled 'Matrix B'. A bracket to the right of the matrix is labeled 'Matrix A'. A bracket below the first column is labeled 'Fundamental Dimensions'. A bracket below the first three columns is labeled ' π groups'. A bracket below the next two columns (Output₁ and Output₂) is labeled 'Matrix I'. A bracket below the last three columns (Variable₁, Variable₂, and Variable₃) is labeled 'Matrix X'.

	Fundamental Dimensions	Output ₁	Output ₂	Variable ₁	Variable ₂	Variable ₃

⁸Only row operations are allowed as they involve all pertinent variables in the dimensional matrix. A column operation can exclude some variables.

The matrix X of size $k \times n$ holds information about actual constants of the scaling process. Hence,

$$A_{n \times n} X_{n \times k}^T = -B_{n \times k} I_{k \times k} \quad (2.53)$$

$$X_{n \times k}^T = -A_{n \times n}^{-1} B_{n \times k} \quad (2.54)$$

$$X_{k \times n} = -(A^{-1} B)_{k \times n}^T \quad (2.55)$$

$$X = -(A^{-1} B)^T \quad (2.56)$$

For system invariance, matrix A needs to be square and non-singular so that X can be uniquely evaluated. To ensure non-singularity of matrix A , the dimensions and/or the choice of variables need to be changed constrained to the condition that a square matrix is still generated that models the system. Further, fundamental dimension set can also be altered to reduce the number while retaining system information. This modification also eliminates singularity conditions in some instances.

- **Non-dimensional form of the π groups**

The next rule is to ensure the dimensionless form of all generated π groups. Further manipulation of π groups in terms of coupling and combining is only possible if developed π groups are parameters which are free of dimension. The analytical combination will be one of the six forms listed earlier.

- **Completeness of the π groups**

Before any combination of π groups can be established, caution needs to be exercised in ensuring that the set of π groups generated is complete - all variables affecting the system, irrespective of their numerical magnitude and dimensions, are captured in *at least* one of the π groups and the resultant π group is dimensionless and *unique* for the chosen variable and dimension set.

- **Existence of monomial basis**

The next condition of dimensional analysis caters to the mathematics of the process. Once π groups are generated, the combination of the π groups can be established *iff* a monomial basis exists. [Szirtes, 1998] shows how some non-monomial bases can be developed but the process is lot more intricate involving analytical reasoning and experimentation. A modified analysis approach is also presented in the next chapter involving a dynamic system with simple reduction of a non-monomial basis. However, the existence of a monomial⁹ is assumed and persisted with in this explanation. A monomial is a simple polynomial of degree and order 1. Hence if $\{\pi_j\}_{j=1}^n$ are the π groups generated, then a monomial basis implies,

$$\pi_i = \prod_{j \neq i, j=1}^n a_j \pi_j^{b_j} \quad (2.57)$$

The principle of *homogeneity of products* allows for the evaluation of indices $\{b_j\}_{j=1}^n$. However, the constant $A = \prod_{j=1}^n a_j$ can only be established through experimentation.

- **Interchangeability of π groups**

Interchangeability of the π groups is a consequence of the previous rule. For a monomial basis between three π groups, π_1 , π_2 and π_3 ,

$$\pi_1 = a_1 \pi_2^{b_1} \pi_3^{b_2} \Rightarrow \pi_2 = a_2 \pi_1^{b_3} \pi_3^{b_4} \quad (2.58)$$

$$\Rightarrow \pi_3 = a_3 \pi_2^{b_5} \pi_1^{b_6} \quad (2.59)$$

- **Uniqueness of constants and indices**

Note that the developed π groups are unique only for chosen variable and dimension set and vary when either or both are altered. However, if the variable and dimension set are finalized, then developed indices have to be unique as the π groups themselves are unique. This implies that

⁹Is an outcome of approximation theory [Szirtes, 1998].

algebraic equations,

$$[M^x L^y T^z]_{\pi_1} = \prod_{j=2}^n [M^{k_j} L^{l_j} T^{m_j}]_{\pi_j} \quad (2.60)$$

$$x = \sum_{j=2}^n k_j \quad (2.61)$$

$$y = \sum_{j=2}^n l_j \quad (2.62)$$

$$z = \sum_{j=2}^n m_j \quad (2.63)$$

represent a homogeneous and consistent set thus ensuring uniqueness of indices $\{x, y, z\}$.

- **Uniqueness of relationship**

The final condition relates to the constant involved in the monomial basis. This is the constant $A = \prod_{j=1}^n a_j$ that can only be established through experimentation by varying one or more of the π groups while holding the rest constant. Evaluation of the constant needs to incorporate experimental error and quality of numerical solutions and curve fits, and it can at best be a close approximation to the true value. However, this value is also unique, thus ensuring uniqueness of supposed solution of three hypothetical π groups,

$$\pi_1 = A\pi_2^x \pi_3^y \quad (2.64)$$

The mathematical identities presented in the rules above are general guidelines to maintain analytical integrity of the Buckingham π theorem method. However, it is important to demonstrate its application in engineering analysis where numerical results provide more meaningful insights. Thus, summariz-

ing the above principles and rules, the following process is presented that illustrates a systematic procedure of applying the Buckingham π theorem to develop scaling factors.

Process 1: Procedure for applying Buckingham π theorem

Step 1: Identify if symmetry exists - If it exists find the plane and/or axis of symmetry

Step 2: Identify inputs, outputs and key parameters

Step 3: Identify constraints

Step 4: Identify assumptions

Step 5: Setup the dimensional matrix

Step 6: Identify A and B matrices

Step 7: Is matrix A invertible - else alter selection of key parameters and/or modify dimensional forms

Step 8: Develop the echelon matrix

Step 9: Develop π group relations

Step 10: Derive functional relationship based on a choice of basis form

The described rules and regulations along with the application procedure are put to practice in the next section where a common product is analyzed for deflection at free end caused by a force input. Hence, the main objective in presenting this example is to illustrate the functionality of the Buckingham π theorem method as applied to engineering systems using the procedure detailed above.

2.5 Backpack Buckle

Some of the design problems commonly encountered can be effectively solved using the dimensional analysis approach. While the functional form can be established - with some effort and skill - between state variables, inputs and outputs, values of coefficients and exponents would still have to be derived from experimentation. A methodical approach is illustrated below using a simple example to exemplify the rules discussed before.



Figure 2.5: A simple backpack clip

A backpack buckle is a clip-lock mechanism where the lock shaft is under bending for the locking piece to move underneath the corresponding holding part (see Figure 2.5). This movement requires that the shaft be made of flexible material capable of producing the required bend without breaking under high force input or repeated usage. In this design analysis, we are interested in estimating deflection produced for a particular input force, analyzing the clip as a cantilever beam. Taking advantage of symmetry, $\frac{1}{2}$ section is modeled as a representative geometry with an end load of magnitude P producing the required bend (see Figure 2.6).

Applying the procedure of Buckingham π theorem systematically to analyze this system, we have,

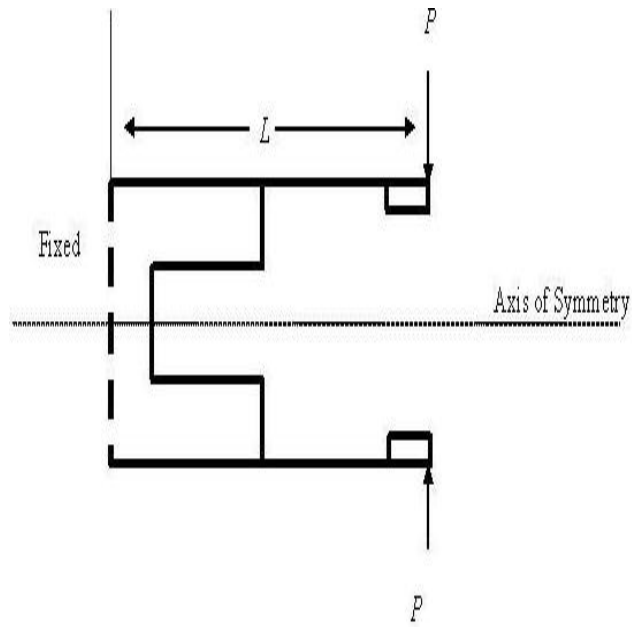


Figure 2.6: Clip geometry

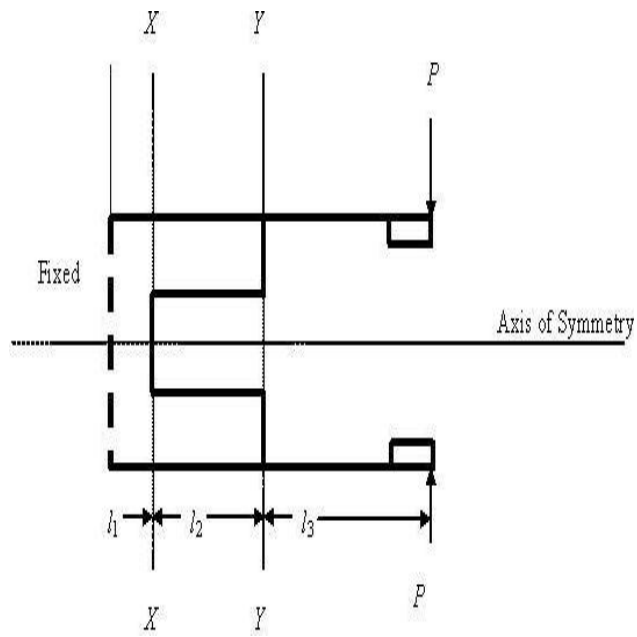


Figure 2.7: Configuration of the clip

**Process 2: Applying Buckingham π theorem
to the Backpack Buckle system**

Step 1: Identify if symmetry exists - If it exists find the plane and/or axis of symmetry

In this case the buckle geometry is symmetric about x - axis.

Step 2: Identify inputs, outputs and key parameters

Input - Load (P)

Parameters - Young's Modulus (E), Area Moment of Inertia (I),

Length (L)

Output - Deflection (δ)

Step 3: Identify constraints

Since the geometry varies across different length scales (see Figure 2.7), define I^* as equivalent effective area moment of inertia.

Step 4: Identify assumptions

E is assumed to be constant (material isotropic); beam does not rotate in the plane of paper.

Step 5: Setup the dimensional matrix

Table 2.4: Dimensional matrix for clip deflection

	P	δ	E	I^*	L
M	1	0	1	0	0
ℓ	1	1	-1	4	1
T	-2	0	-2	0	0

Step 6: Identify A and B matrices

$$A = \begin{pmatrix} 1 & 0 & 0 \\ -1 & 4 & 1 \\ -2 & 0 & 0 \end{pmatrix}, B = \begin{pmatrix} 1 & 0 \\ 1 & 1 \\ -2 & 0 \end{pmatrix}$$

Step 7: Is matrix A invertible - else alter selection of key parameters and/or modify dimensional forms

Matrix A is singular requiring a change either in dimensional forms or modification in choice of key parameters or both. Choosing density ρ in place of I^* , the dimensional matrix changes to the form shown in Table 2.5. The matrices are now altered to -

Table 2.5: Refined dimensional matrix for clip deflection

	P	δ	E	ρ	L
M	1	0	1	1	0
ℓ	1	1	-1	-3	1
T	-2	0	-2	0	0

$$A = \begin{pmatrix} 1 & 1 & 0 \\ -1 & -3 & 1 \\ -2 & 0 & 0 \end{pmatrix}, B = \begin{pmatrix} 1 & 0 \\ 1 & 1 \\ -2 & 0 \end{pmatrix}$$

such that,

$$A^{-1} = \begin{pmatrix} 0 & 0 & -\frac{1}{2} \\ 1 & 0 & \frac{1}{2} \\ 3 & 1 & 1 \end{pmatrix}$$

Inversion of the matrix A is required under the principle of dimensional homogeneity to eliminate system invariance. Further, for a linear system, a square matrix guarantees existence and uniqueness of solution vector \vec{x} as matrix A in the linear equation $Ax = B$ is invertible.

Step 8: Develop the echelon matrix

Table 2.6: Echelon matrix for clip deflection

	P	δ	E	ρ	L
π_1	1	0	x_1	x_2	x_3
π_2	0	1	x_4	x_5	x_6

Step 9: Develop π group relations

Using the homogeneity principle,

$$x = -(A^{-1}B)^T = \begin{pmatrix} -1 & 0 & -2 \\ 0 & 0 & -1 \end{pmatrix}$$

Hence,

$$\pi_1 = \frac{P}{EL^2} \quad (2.65)$$

$$\pi_2 = \frac{\delta}{L} \quad (2.66)$$

Thus, if an equivalent model (m) is constructed to determine the deflection of the buckle (p) then,

$$\frac{P_p}{E_p L_p^2} = \frac{P_m}{E_m L_m^2} \quad (2.67)$$

$$\Leftrightarrow \frac{\delta_p}{L_p} = \frac{\delta_m}{L_m} \quad (2.68)$$

Step 10: Derive functional relationship based on a choice of basis form

Assuming a monomial basis such that $\pi_1 = k\pi_2^m$, for $m = 1$,

$$\frac{P}{EL^2} = k \left(\frac{\delta}{L} \right)^m \Rightarrow \delta = k \left(\frac{P}{EL} \right) = k \left(\frac{PL^3}{EI^*} \right) \quad (2.69)$$

which is the governing equation for deflection in a cantilever beam [Gere et al., 1985]. Classic solid mechanics suggests that k assumes a value of $\frac{1}{3}$. This value can also be established (approximately) numerically, by changing the value of P and observing corresponding values of δ (while holding all other variables constant) and fitting a curve between them. Note also that the choice of $m = 1$ is not arbitrary. We know intuitively that larger P implies greater δ . In this sense $m \neq 0$ and $m > 0$. Further to have a contribution from effect of length of beam, $1 - \frac{2}{m} \neq 0 \Rightarrow m \neq 2$ in the equation $\delta = k \left(\frac{P}{E}\right)^{\frac{1}{m}} (L)^{1-\frac{2}{m}}$.

Another intuitive observation is that for a given load and Young's modulus, it is easier to bend a longer beam than a shorter beam due to the relative stiffness and flexure difference between the two which implies that deflection and length hold an inverse relationship. Hence $1 - \frac{2}{m} < 0 \Rightarrow m < 2$

Hence, mathematically, $m \in (0, 2)$, *i.e.*, $|m| < 2$ where $m = 1$ is a valid integer data point. Notice that lumped approximation has been highlighted by defining effective area moment of inertia I^* . Further, the process of setting up the problem is shown such that 'correct' dimensional form and 'right' parameters are chosen to avoid system invariance. A final problem simplification is also shown where a square matrix is generated. The entire process is encapsulated in a flow chart shown below (see Figure 2.8).

The procedure commences with proper identification and definition of the problem. Subsequently, all influencing variables and required outputs need to be characterized along with possible symmetry conditions. Next, constraints and assumptions need to be incorporated to simplify the analysis. Following this initial study, the dimensional matrix is setup and A and B matrices are identified for verification of possible singularity conditions. Depending on the characteristics of matrix A , refinement of dimensional forms is sought or alteration of variables is pursued until the matrix is non-singular. Thereafter, the echelon matrix is developed resulting in construction of the π groups. Depending on the existence and relevance of a monomial basis, a final functional relationship is developed to generate the model laws.

While this example has illustrated the technique of Buckingham π the-

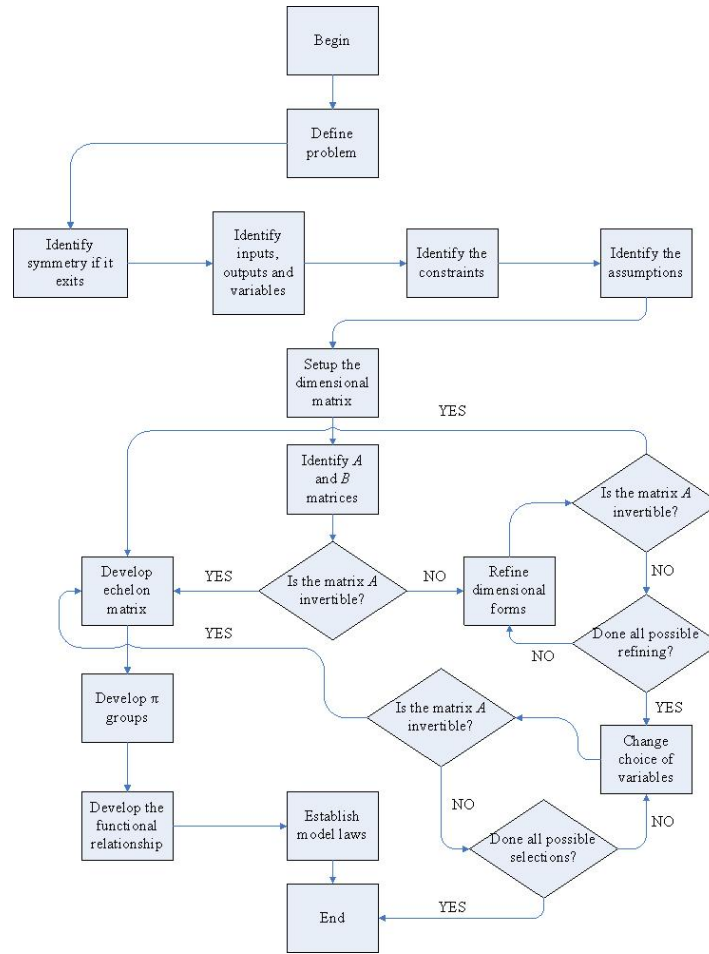


Figure 2.8: Flow chart for applying Buckingham π theorem

orem in all its elegance, other methods do exist that offer similar benefit in developing scales in similarity analysis. The most important of such methods are explicated below.

2.6 Other Methods of TSM

Buckingham π theorem is the most widely employed procedure for dimensional analysis, using a matrix approach to mathematically define scales

and constants of similarity. However, generation of square and non-singular matrices is absolutely necessary in the dimensional matrix for the technique to be feasible as was illustrated in the previous section. In this section four other methods are introduced that incorporate same functionality as the echelon matrix method but are not constrained by the restrictions that affect the Buckingham π theorem. In all these methods, dimensionless groups, or B -numbers [Happ, 1967,] are generated *individually* by simple numerical manipulation of dimensions unlike the Buckingham π theorem method where a matrix approach develops π groups *collectively*. While there are several other methods [Deb et al., 1986] and variants of each method [Barr, 1982], the following four *principal* methods are offered as an introductory exposition to non-matrix dimensional reasoning. Consider, a system parameter P affected by variables q_1 and q_2 .

- **Rayleigh's Method**

In this method, dimensions of the system parameter P are matched to dimensions of influencing variables q_1 and q_2 assuming dimensions of the system parameter to be proportional to each individual variable. “[]” indicating dimensions,

$$[P] \propto [q_1]; [P] \propto [q_2] \tag{2.70}$$

$$\Rightarrow [P] \propto [q_1][q_2] \tag{2.71}$$

$$\Rightarrow [P] \equiv K[q_1][q_2] \tag{2.72}$$

$$\Rightarrow [MLT]_P \equiv K[MLT]_{q_1}^\alpha [MLT]_{q_2}^\beta \tag{2.73}$$

$$\Rightarrow [M]_P = [M]_{q_1}^\alpha + [M]_{q_2}^\beta \tag{2.74}$$

$$\Rightarrow [L]_P = [L]_{q_1}^\alpha + [L]_{q_2}^\beta \tag{2.75}$$

$$\Rightarrow [T]_P = [T]_{q_1}^\alpha + [T]_{q_2}^\beta \tag{2.76}$$

where K is a constant, which can have no dimensions. Solving any two

of the three equations gives unique values for α and β .

- **Buckingham's Method**

This method is a minor variation of Rayleigh's method where dimensions of the system parameter P combined with dimensions of influencing variables q_1 and q_2 , are matched to *null* dimensions of a constant. This method is not to be confused with Buckingham π theorem.

$$[P][q_1][q_2] = [K] \quad (2.77)$$

$$\Rightarrow [M]_{P+q_1^\alpha+q_2^\beta} = 0 \quad (2.78)$$

$$\Rightarrow [L]_{P+q_1^\alpha+q_2^\beta} = 0 \quad (2.79)$$

$$\Rightarrow [T]_{P+q_1^\alpha+q_2^\beta} = 0 \quad (2.80)$$

Like before, solving any two of the three equations gives unique values for α and β .

- **Taylor's Method**

Taylor's method is a systematic reduction of the dimensional matrix to a form given by $\phi(B_1, B_2, \dots, B_n) = 0$ where B_i 's are the B -numbers of the system.

$$\phi[f(P, q_1), g(P, q_2)] = 0 \quad (2.81)$$

- **Proportionalities Method**

The Proportionalities method is similar to Taylor's method in that a systematic reduction is employed to develop $\phi(B_1, B_2, \dots, B_n) = 0$ but the reduction process employed is slightly different. Variables are all listed first in the form given by $\phi(P, q_1, \dots, q_n) = 0$, their dimensions noted, and multiple reductions done sequentially to reduce $\phi(P, q_1, \dots, q_n) = 0$ to have dimensions of just *one* of the fundamental dimensions. A final step is then undertaken to reduce $\phi(P, q_1, \dots, q_n) = 0$ to be dimension

free by integrating the fundamental dimension.

$$\phi[f(P, q_1), g(P, q_2)]_{FD} = 0 \quad (2.82)$$

$$\phi[f(P, q_1), g(P, q_2)] = 0 \quad (2.83)$$

where FD is a fundamental dimension.

Each of these processes is illustrated below using a basic example. The objective behind presenting this example is to demonstrate the generation of functional relationships of influencing variables in engineering systems using dimensional analysis techniques different from the Buckingham π theorem method thereby highlighting possible advantages and limitations of each process.

2.7 A Simple Pendulum

In this section, time period of oscillation of a simple pendulum (see Figure 2.9) is evaluated using the four methods described above. The general modeling equation is $t = \phi(l, g)$, the objective being development of the functional form of ϕ .

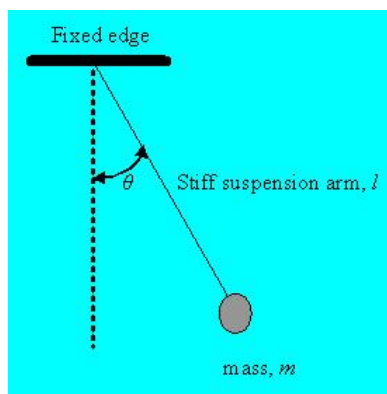


Figure 2.9: A simple pendulum

- **Rayleigh's Method**

$$[t] \propto [l]; [t] \propto [g] \quad (2.84)$$

$$\Rightarrow [t] \propto [l][g] \Rightarrow [t] = K[l][g] \quad (2.85)$$

$$\Rightarrow [MLT]_t \equiv K[MLT]_l^\alpha [MLT]_g^\beta \quad (2.86)$$

$$\Rightarrow [L]_t = [L]_{l^{\alpha+g^\beta}} \quad (2.87)$$

$$\Rightarrow [T]_t = [T]_{l^{\alpha+g^\beta}} \quad (2.88)$$

$$\Rightarrow 0 = \alpha + \beta; 1 = -2\beta \quad (2.89)$$

$$\Rightarrow \alpha = \frac{1}{2}; \beta = -\frac{1}{2} \quad (2.90)$$

$$\Rightarrow t = K\sqrt{\frac{l}{g}} \quad (2.91)$$

- **Buckingham's Method**

$$[t][l][g] = [K] \quad (2.92)$$

$$\Rightarrow [L]_{t+l^{\alpha+g^\beta}} = 0 \quad (2.93)$$

$$\Rightarrow [T]_{t+l^{\alpha+g^\beta}} = 0 \quad (2.94)$$

$$0 + \alpha + \beta = 0 \quad (2.95)$$

$$1 + 0 - 2\beta = 0 \quad (2.96)$$

$$\Rightarrow \alpha = \frac{1}{2}; \beta = -\frac{1}{2} \quad (2.97)$$

$$\Rightarrow t = K\sqrt{\frac{l}{g}} \quad (2.98)$$

- **Taylor's Method**

Eliminating the length dimension from the dimensional matrix (see Table 2.7), the reduced matrix (see Table 2.8) is developed with just the dimension of time. A further reduction by eliminating the time dimension results in a B -number from the final matrix (see Table 2.9) which

is the desired dimensionless group. Hence, $\phi\left(\frac{gt^2}{l}\right) = 0$.

Table 2.7: Dimensional matrix for Taylor's method

<i>Fundamental Dimension</i>	<i>t</i>	<i>l</i>	<i>g</i>
<i>L</i>	0	1	1
<i>T</i>	1	0	-2

Table 2.8: Reduced matrix for Taylor's method

<i>Fundamental Dimension</i>	<i>t</i>	$\frac{g}{l}$
<i>T</i>	1	-2

Table 2.9: Final matrix for Taylor's method

$$\boxed{\frac{gt^2}{l}}$$

• **Proportionalities Method**

$$\phi(t, l, g) = 0 \tag{2.99}$$

$$\phi\left(t, \sqrt{\frac{l}{g}}\right) = 0 \leftarrow \text{dimensions of time alone} \tag{2.100}$$

$$\phi\left(\frac{t}{\sqrt{\frac{l}{g}}}\right) = 0 \tag{2.101}$$

$$\phi\left(\sqrt{\frac{g}{l}}t\right) = 0 \tag{2.102}$$

$$\phi\left(\frac{gt^2}{l}\right) = 0 \tag{2.103}$$

Equations (2.99) through (2.103) represent systematic reductions in the evaluation as functions are converted to mathematical forms with time dimensions alone and then to a number before finally resulting in a simplified dimensionless form. Notice also that all methods presented do not rely on matrix

inversion and do not develop constants, which in some sense is a limitation of these processes. The latter two methods develop B -numbers in a functional formulation. It is through experimentation alone that values of constants and functional form of ϕ can be established. In case of Taylor's method and Proportionalities method, $\phi\left(\frac{gt^2}{l}\right) = 0$ would evaluate to $\frac{gt^2}{l} = K$, reducing finally to $t = K\sqrt{\frac{l}{g}}$. The value of K , from theory, would be equal to 2π , a value that can be established in similitude, approximately, using mathematical manipulation of experimental data. It is however important to note that Buckingham π theorem method would not have worked in this scenario as the matrix developed with variables l and g is not square and hence not invertible. Concluding this profound discussion on TSM, it is imperative to realize three important limitations of the process -

1. The dimensionless π groups can be combined only if a monomial basis exists or if a basic non-monomial basis - basis involving polynomial, trigonometric or transcendental functions - can be constructed without excessive difficulty. Complex formulations are not apparently intuitive.
2. Values of constants cannot be directly estimated and experimentation needs to be done irrespective of the choice of basis. Further, non-singularity of the dimensional matrix needs to be ensured.
3. Establishing values of indices of the π groups is also intricate sometimes and presupposes some engineering background.

2.8 Summary

This chapter summarized Traditional Similitude Method (TSM) by elaborating scaling processes and supplementing with examples for clarity. All relevant principles and laws in the use of traditional similarity methods have been discussed and explained. The development of Buckingham π theorem and its applications has been provided. Alternate methods and formulations

have been identified and illustrated. Furthering the use of similitude, the next chapter applies dimensional analysis to dynamic systems through the use of newer techniques.

Chapter 3

Advances in Traditional Similitude Method

“Science... never solves a problem without creating ten more.” - George
Bernard Shaw

Dimensional Analysis (DA) is a tool used to relate models and specimens to the actual product or system based on the hypothesis that the two regimes follow same physical laws and are hence dimensionally equivalent. Analyzing static and time invariant systems has been the conventional use of the process but the technique is definitely not constricted to such systems. Dynamic systems can also be evaluated using DA and this chapter extends the technique to analyzing time varying systems in an effort to develop state equations that allow for design studies through parametrization. This augmentation into transient modeling using DA is detailed with an example of a toy water-rocket assembly [Otto et al., 2001]. A modified methodology is also discussed to condense non-monomial basis systems (often encountered in engineering modeling) using simple physical laws and a novel reduction process. This chapter thus realizes the potential of DA as a holistic approach to prediction spanning static and dynamic systems.

As documented in the last chapter, several challenges lie in the proper execution of Buckingham π theorem including maintaining matrix non-singularity, simple monomial basis selection and dimensional homogeneity. However, minor modification in applying the process can be extremely useful in the analysis of dynamic systems. This innovation is shown inductively using an example of a simple dynamic system followed by incorporation of graphs, another advancement achieved for topological visualization of DA. The need for using such modified methods is motivated in the next section.

3.1 Similarity Methods in Design

Scaling and similarity offer ease and flexibility in analysis that is commonly attributed to conventional closed-form methods. DA can be used in different forms in design techniques. As a predictive tool the process serves the purpose of design validation but its inherent ability lies in the incorporation of parametric and configurational design principles. These modeling methods are often discussed as forms of embodiment design where a proven and/or chosen functional form is given shape and structure with material properties assigned to different sub-systems and assemblies.

Designers often need to prove technical feasibility of a particular concept or a re-design which involves thorough analytical understanding and implementation of complex mathematical formulations that are associated with physical functioning of the device. While traditional techniques have encompassed analysis for most commonly used designs, modern day requirements necessitate use of devices that are made of multiple materials and/or various shapes to meet certain customer requirements. Conjuring up an analysis procedure in such systems for a parameter of interest is inevitably a complicated task requiring use of numerical and computational methods. However, DA offers an alternate procedure where even such complex systems can be modeled using simple yet representative models whose experimental data can be mapped to the actual system. It is in this regard that DA plays an important

role in the physical manifestation of a design. Repetition and iteration can be integrated into the technique for a more robust design. DA thus embraces several design strategies including robustness and analyzability by using parametric and embodiment principles. This is better illustrated in analysis of a rocket assembly where several design parameters including shape and size of the rocket and nozzle are modeled for optimizing performance.

3.2 Water-Rocket: Analysis of a Dynamic System

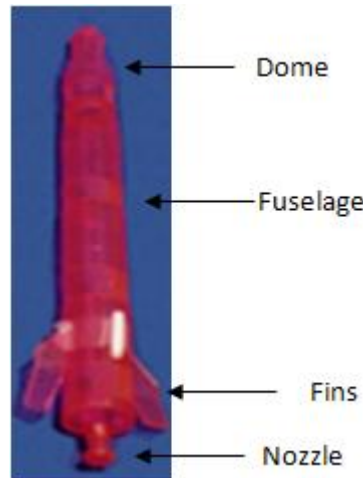


Figure 3.1: A basic water-rocket assembly

Consider a bottle rocket (see Figure 3.1) charged with pressurized air-water mixture. The objective is to develop state equations of the system using DA by identifying all pertinent variables and combining them to capture flight motion till the assembly runs out of charge. From basic mass and momentum conservation principles, we know that the rocket rises due to change in momentum causing a thrust to be developed that propels the rocket upwards. This momentum change is primarily due to mass flow rate occurring due to pressure difference between internal charge and external atmosphere. Assume

that all measurements are made with respect to the inertial reference frame fixed at ground level. Even when the system is open like in this example, the developed methodology can be appropriately modified so that feasibility in analysis can be demonstrated. Like before a structured process is initiated for a systematic approach.

Process 3: Applying Buckingham π theorem to the Water-Rocket system

Step 1: Identify if symmetry exists - If it exists find the plane and/or axis of symmetry

In this case the entire rocket is treated as a system and hence symmetry does not hold.

Step 2: Identify inputs, outputs and key parameters

Parameters - liquid density (ρ_l), nozzle area (A_r), gravity (g), total instantaneous mass of the rocket (m), nozzle jet velocity (v_n), air density (ρ_a), rocket area (A_r), coefficient of drag (C_d), velocity of rocket (v_r), coefficient of nozzle (C_N), mass of water (m_l), pressure difference (ΔP), coefficient of expansion ($C_{isentropic}$), volume of rocket (V_r), gas constant (K) Output - System State equations (Net upward thrust)

It is important to understand physics of the problem so that all relevant variables are identified. Any incorrect choice leads to several discrepancies as discussed in the homogeneity principle. In this system, it is prudent to realize that air undergoes isentropic expansion during water ejection phase caused by pressure differential between internal air and outside atmosphere. Further, nozzle shape plays an important role in determining ejection velocity.

Step 3: Identify constraints

Initial volume of the charge and charge distribution ratio (air-liquid) is known and pressure is suitably adjusted.

Step 4: Identify assumptions

Nozzle is completely turned open and resistance to flow is assumed to be negligible. Flow pattern is discounted as turbulence effects are not considered. Any incorporation of flow characteristics and viscosity effects complicates the evaluation process.

Step 5: Setup the dimensional matrix

Table 3.1: Output and system variables for the water-rocket

	F	ρ_l	A_n	g
L	1	-3	2	1
M	1	1	0	0
T	-2	0	0	-2

Table 3.2: System variables for the water-rocket

	m	v_n	ρ_a	A_r
L	0	1	-3	2
M	1	0	1	0
T	0	-1	0	0

Table 3.3: System variables and constants for the water-rocket

	C_d	v_r	C_N	m_l
L	0	1	0	0
M	0	0	0	1
T	0	-1	0	0

Step 6: Identify total independent (repeating) variables (m) and total variables (n)

Table 3.4: System variables and constants for the water-rocket

	ΔP	$C_{isentropic}$	V_r	K
L	-1	0	3	0
M	1	0	0	0
T	-2	0	0	0

In this case $\{A_r, v_n, \rho_a\}$ is a viable repeating variable set. Hence $n - m = 13 - \pi$ groups - one each accounting for the variations in thrust, liquid density, nozzle area, gravity, mass of the rocket, coefficient of drag, velocity of the rocket, coefficient of nozzle, mass of liquid, pressure difference, coefficient of expansion, volume of the rocket and the gas constant will be generated. It is extremely important that mutual independence in repeating variable set be established. Any dependence causes an improper or an impossible evaluation [Szirtes, 1998].

Step 7: Develop π group relations

Define π groups as -

$$\pi_1 \equiv \pi_1(F, A_r, v_n, \rho_a) \quad (3.1)$$

$$\pi_2 \equiv \pi_2(\rho_l, A_r, v_n, \rho_a) \quad (3.2)$$

$$\pi_3 \equiv \pi_3(A_n, A_r, v_n, \rho_a) \quad (3.3)$$

$$\pi_4 \equiv \pi_4(g, A_r, v_n, \rho_a) \quad (3.4)$$

$$\pi_5 \equiv \pi_5(m, A_r, v_n, \rho_a) \quad (3.5)$$

$$\pi_6 \equiv \pi_6(C_d, A_r, v_n, \rho_a) \quad (3.6)$$

$$\pi_7 \equiv \pi_7(v_r, A_r, v_n, \rho_a) \quad (3.7)$$

$$\pi_8 \equiv \pi_8(C_N, A_r, v_n, \rho_a) \quad (3.8)$$

$$\pi_9 \equiv \pi_9(m_l, A_r, v_n, \rho_a) \quad (3.9)$$

$$\pi_{10} \equiv \pi_{10}(\Delta P, A_r, v_n, \rho_a) \quad (3.10)$$

$$\pi_{11} \equiv \pi_{11}(C_{isentropic}, A_r, v_n, \rho_a) \quad (3.11)$$

$$\pi_{12} \equiv \pi_{12}(V_r, A_r, v_n, \rho_a) \quad (3.12)$$

$$\pi_{13} \equiv \pi_{13}(K, A_r, v_n, \rho_a) \quad (3.13)$$

Table 3.5: Combined matrix for the water-rocket

	F	ρ_l	A_n	g	m	C_d	v_r	C_N	m_l	ΔP	$C_{isentropic}$	V_r	K	A_r	v_n	ρ_a
L	1	-3	2	1	0	0	1	0	0	-1	0	3	0	2	1	-3
M	1	1	0	0	1	0	0	0	1	1	0	0	0	0	0	1
T	-2	0	0	-2	0	0	-1	0	0	-2	0	0	0	0	-1	0
π_1	1	0	0	0	0	0	0	0	0	0	0	0	0	x_1	x_2	x_3
π_2	0	1	0	0	0	0	0	0	0	0	0	0	0	x_4	x_5	x_6
π_3	0	0	1	0	0	0	0	0	0	0	0	0	0	x_7	x_8	x_9
π_4	0	0	0	1	0	0	0	0	0	0	0	0	0	x_{10}	x_{11}	x_{12}
π_5	0	0	0	0	1	0	0	0	0	0	0	0	0	x_{13}	x_{14}	x_{15}
π_6	0	0	0	0	0	1	0	0	0	0	0	0	0	x_{16}	x_{17}	x_{18}
π_7	0	0	0	0	0	0	1	0	0	0	0	0	0	x_{19}	x_{20}	x_{21}
π_8	0	0	0	0	0	0	0	1	0	0	0	0	0	x_{22}	x_{23}	x_{24}
π_9	0	0	0	0	0	0	0	0	1	0	0	0	0	x_{25}	x_{26}	x_{27}
π_{10}	0	0	0	0	0	0	0	0	0	1	0	0	0	x_{28}	x_{29}	x_{30}
π_{11}	0	0	0	0	0	0	0	0	0	0	1	0	0	x_{31}	x_{32}	x_{33}
π_{12}	0	0	0	0	0	0	0	0	0	0	0	1	0	x_{34}	x_{35}	x_{36}
π_{13}	0	0	0	0	0	0	0	0	0	0	0	0	1	x_{37}	x_{38}	x_{39}

Step 8: Derive functional relationship for each π group based on dimensions alone

Notice that the matrix formed by independent variables is square and non-singular and thus invertible. Further, it guarantees a unique solution on inversion [Grewal, 1998]. Let A be the matrix formed by independent variables and B be the matrix formed by rest of the variables. Then,

$$A = \begin{pmatrix} 2 & 1 & -3 \\ 0 & 0 & 1 \\ 0 & -1 & 0 \end{pmatrix}$$

$$B = \begin{pmatrix} 1 & -3 & 2 & 1 & 0 & 0 & 1 & 0 & 0 & -1 & 0 \\ 1 & 1 & 0 & 0 & 1 & 0 & 0 & 0 & 1 & 1 & 0 \\ -2 & 0 & 0 & -2 & 0 & 0 & -1 & 0 & 0 & -2 & 0 \end{pmatrix}$$

From Fourier's law of dimensional homogeneity [Dutson, 2002], the matrix X is given by $X = -(A^{-1}B)^T$ or,

$$X = \begin{pmatrix} -1 & -2 & -1 \\ 0 & 0 & -1 \\ -1 & 0 & 0 \\ \frac{1}{2} & -2 & 0 \\ -\frac{3}{2} & 0 & -1 \\ 0 & 0 & 0 \\ 0 & -1 & 0 \\ 0 & 0 & 0 \\ -\frac{3}{2} & 0 & -1 \\ 0 & -2 & -1 \\ 0 & 0 & 0 \\ -\frac{3}{2} & 0 & 0 \\ 0 & 0 & 0 \end{pmatrix}$$

Hence,

$$\pi_1 = \frac{F}{A_r v_n^2 \rho_a}; \pi_2 = \frac{\rho_l}{\rho_a}; \pi_3 = \frac{A_n}{A_r}; \quad (3.14)$$

$$\pi_4 = \frac{g A_r^{\frac{1}{2}}}{v_n^2}; \pi_5 = \frac{m}{A_r^{\frac{3}{2}} \rho_a}; \pi_6 = C_d; \quad (3.15)$$

$$\pi_7 = \frac{v_r}{v_n}; \pi_8 = C_N; \pi_9 = \frac{m_l}{A_r^{\frac{3}{2}} \rho_a}; \quad (3.16)$$

$$\pi_{10} = \frac{\Delta P}{\rho_a v_n^2}; \pi_{11} = C_{isentropic}; \pi_{12} = \frac{V_r}{A_r^{\frac{3}{2}}}; \quad (3.17)$$

$$\pi_{13} = K \quad (3.18)$$

Notice that all π groups have no units or dimensions, a condition required for further manipulation.

Step 9: Derive functional relationship between the π groups based on a basis assumption

Since thrust is desired output, the motivation now is to derive relationship between thrust achieved and rest of the variables. Let $\pi_1 = \Psi (\prod \pi_j)_{j=2}^{13}$ such that $\pi_1 = k\pi_2^a\pi_3^b \dots \pi_{13}^l$, assuming a monomial basis. Then,

$$F = k(\rho_l^a)(\rho_a^{1-(a+d+h+i)})(A_n^b)(A_r^{1-b+\frac{c}{2}-\frac{3d}{2}-\frac{3h}{2}-\frac{3k}{2}})(g^c)(v_n^{2-2c-f-2i})(m^d)(m_l^h)(v_r^f)(C_N^g)(C_d^e)(C_{is.}^j)(\Delta P^i)(V_r^k)(K^l) \quad (3.19)$$

Based on observation and simple judgment, the following conditions can be deduced about the constants.

$$a \neq 0 \quad (3.20)$$

$$a + d + h + i \neq 1 \quad (3.21)$$

$$b - \frac{c}{2} + \frac{3d}{2} + \frac{3h}{2} + \frac{3k}{2} \neq 1 \quad (3.22)$$

$$c \neq 0 \quad (3.23)$$

$$2c + f + 2i \neq 2 \quad (3.24)$$

$$d, f, h, i, k \neq 0 \quad (3.25)$$

$$e, g, j, l = 1 \quad (3.26)$$

The system of equations above, constitute an incomplete collection and thus equation (3.19) is almost impossible to evaluate without use of some basic logic from system dynamics as is presented in the following section.

3.3 Modified Analysis

To simplify evaluation, the modified procedure is introduced and evaluated in a systematic process. All steps described henceforth are part of the

new approach.

Step 10: Is problem decomposition possible?

The original problem can be decomposed into several sub-problems with the notable condition that each sub-problem capture a physical parameter or event. In this case force causing motion upward is equal to difference between fluid thrust developed and net resistance (gravity and drag).

Step 11: Repeat steps 1 through 9 for each factor

Collecting fluid thrust (F_f) terms, we have,

Table 3.6: Combined matrix for fluid thrust

	F_f	ρ_l	A_n	v_n
L	1	-3	2	1
M	1	1	0	0
T	-2	0	0	-1
π_1	1	x_1	x_2	x_3

Homogeneity delivers $X = (-1 - 1 - 2)$ or $\pi_1 = \frac{F_f}{\rho_l A_n v_n^2}$. Since only one π group exists, evaluation is possible only if the group itself is equal to a constant and since all the dimensions are consistent, $\pi_1 = \frac{F_f}{\rho_l A_n v_n^2}$ must evaluate to a number. Hence $F_f = k_1 \rho_l A_n v_n^2$. Dividing through with rocket mass, fluid thrust per unit mass is obtained to be $F_f^* = \frac{F_f}{m} = k_1 \left(\frac{\rho_l A_n v_n^2}{m} \right)$. Evaluating net resistance¹ (R) (see Table 3.7) and using homogeneity, we have,

$$X = \begin{pmatrix} -1 & -1 & -2 \\ -1 & -\frac{3}{2} & 0 \\ 0 & 0 & 0 \\ 0 & \frac{1}{2} & -2 \end{pmatrix}$$

¹Technically we can split and individually evaluate resistances but further decomposition leads to loss of matrix invertibility in gravity resistance.

Table 3.7: Combined matrix for resistance

	R	m	C_d	g	ρ_a	A_r	v_r
L	1	0	0	1	-3	2	1
M	1	1	0	0	1	0	0
T	-2	0	0	-2	0	0	-1
π_1	1	0	0	0	x_1	x_2	x_3
π_2	0	1	0	0	x_4	x_5	x_6
π_3	0	0	1	0	x_7	x_8	x_9
π_4	0	0	0	1	x_{10}	x_{11}	x_{12}

such that,

$$\pi_1 = \frac{R}{\rho_a A_r v_r^2}; \pi_2 = \frac{m}{\rho_a A_r^{\frac{3}{2}}}; \pi_3 = C_d; \pi_4 = \frac{g\sqrt{A_r}}{v_r^2} \quad (3.27)$$

A monomial basis produces an erroneous result as all relevant π groups are multiplied but from basic conservation principles, resistances need to be added. Thus, a novelty is introduced in the form of the new algorithm that could not be executed in the initial analysis (up until step 9) due to higher number of π groups. The current grouping is limited to 4, which is ideal for the following analysis.

Step 12: If decomposition produces a monomial consistent with conservation, stop, else invoke modified algorithm²

Assume several different simple variations of the monomial. It is quite evident that $\pi_1 = \psi(\pi_2, \pi_3, \pi_4)$, π_1 being the output π group. Three possible variations in the monomial form considered here are -

$$\pi_1 = k_2 \pi_2^a \pi_3^b + k_3 \pi_4^c \quad (3.28)$$

$$\pi_1 = k_2 \pi_2^a \pi_4^b + k_3 \pi_3^c \quad (3.29)$$

$$\pi_1 = k_2 \pi_3^a \pi_4^b + k_3 \pi_2^c \quad (3.30)$$

²A rule of thumb is that analysis is ideal for no more than 4 π groups. Existence of more than 4 π groups necessitates further decomposition.

Notice that in all three cases, only the output π group is being related. In general,

$$(\pi_j)_{output} = M\pi_i^a \pi_k^b + N\pi_l^c \quad (3.31)$$

where

$$i \neq j \neq k \neq l \quad (3.32)$$

$$M \neq N \quad (3.33)$$

$$a \neq b \neq c \quad (3.34)$$

$$i, j, k, l \in [1, 4] \quad (3.35)$$

We can continue decomposing to a point where all factors are in pure summation implying complete linearity between factors. Such a solution is superposition of each individual contribution. However, a suitable match can be obtained in a previous iteration. Hence reality check needs to be performed before the next step is invoked. In each of the cases listed above, we have,

$$R = k_2(\rho_a^{1-a})(A_r^{1-\frac{3a}{2}})(v_r^2)(m^a)(C_d^b) + k_3(\rho_a)(A_r^{1+\frac{c}{2}})(g^c)(v_r^{2-2c}) \quad (3.36)$$

$$R = k_2(\rho_a^{1-a})(A_r^{1-\frac{3a}{2}+\frac{b}{2}})(v_r^{2-2b})(m^a)(g^b) + k_3(\rho_a)(A_r)(C_d^c)(v_r^2) \quad (3.37)$$

$$R = k_2(\rho_a)(A_r^{1+\frac{b}{2}})(v_r^{2-2b})(C_d^a)(g^b) + k_3(\rho_a^{1-c})(A_r^{1-\frac{3c}{2}})(m^c)(v_r^2) \quad (3.38)$$

Resorting to classical dynamics again, letting gravity, mass and coefficient of drag have exponents equal to unity for physical certainty³, the equations are simplified to -

$$R = k_2(\rho_a^{1-a})(A_r^{1-\frac{3a}{2}})(v_r^2)(m)(C_d) + k_3(\rho_a)(A_r^{1+\frac{c}{2}})(g^c)(v_r^{2-2c}) \quad (3.39)$$

$$R = k_2(\rho_a^{1-a})(A_r^{1-\frac{3a}{2}+\frac{b}{2}})(v_r^{2-2b})(m)(g) + k_3(\rho_a)(A_r)(C_d)(v_r^2) \quad (3.40)$$

$$R = k_2(\rho_a)(A_r^{1+\frac{b}{2}})(v_r^{2-2b})(C_d)(g) + k_3(\rho_a^{1-c})(A_r^{1-\frac{3c}{2}})(m)(v_r^2) \quad (3.41)$$

³Another guideline is to set indices of mass, gravity and any coefficient to 1 always. This does not work before decomposition as several different inertia modes might exist.

Using unity indices for mass, gravity and coefficient of drag in the three equations accordingly, we have,

$$R = k_2 C_d m v_r^2 (A_r^{-\frac{1}{2}}) + k_3 g \rho_a (A_r^{\frac{3}{2}}) \quad (3.42)$$

$$R = k_2 m g + k_3 C_d \rho_a v_r^2 A_r \quad (3.43)$$

$$R = k_2 \rho_a g C_d (A_r^{\frac{3}{2}}) + k_3 m v_r^2 (A_r^{\frac{1}{2}}) \quad (3.44)$$

To help assist with the final choice we invoke the final step of the method⁴. Caution needs to be followed when dealing with indices of inertia elements. Existence of multiple inertia elements causes a system interaction that can only be solved after numerous decompositions and iterations. The above equation set cannot be properly developed sometimes by simple substitution. In such cases other alternatives need to be pursued. The two suggested here are to equate indices to the same value (first selectively and then cumulatively) and follow evaluation based on technical reasoning (like presented in the buckle example) thereafter [Szirtes, 1998]. In situations when such reasoning does not yield any palpable result, it usually indicates existence of fractional exponents which can be tried, at best, to be modeled using a polynomial equivalent between π groups. Every coefficient in the series represents a degree of freedom (DOF) that captures scalar contribution of the particular π group in the system solution. This method though needs comprehensive experimentation and does not guarantee a solution. The quality of the solution depends on goodness of fit which might not always be acceptable.

Step 13: If two or more equations are developed without any indices, use dimensional homogeneity principle coupled with physical significance to decide for the correct choice. One and only one choice would be dimensionally accurate and have terms that are of physical relevance.

Resistance being a force, all terms on the parameter side have to evaluate to force dimensions with physical significance *i.e.*, they need to capture

⁴Note that setting these parameters to 1 is a reasonable start for iteration.

a physical event. All equations are consistent in dimensions but terms in first and last equation have no attached physical meaning. The second equation though has terms signifying weight and drag force respectively. Hence, second equation is the correct choice. Thus,

$$R = k_2mg + k_3C_dA_r\rho_a v_r^2 \quad (3.45)$$

Dividing through with rocket mass, resistance per unit mass is evaluated to be -

$$R^* = \frac{R}{m} = k_2g + k_3\frac{C_dA_r\rho_a v_r^2}{m} \quad (3.46)$$

The net thrust of the system for unit mass or acceleration is given by,

$$T^* = F_f^* - R^* \quad (3.47)$$

$$\frac{dv_r}{dt} = k_1\left(\frac{\rho_l A_n v_n^2}{m}\right) - k_2g - k_3\left(\frac{C_d A_r \rho_a v_r^2}{m}\right) \quad (3.48)$$

Developing rest of the state equations using a similar approach of identifying right set of affecting variables and then applying DA we obtain the variable listing depicted in Table 3.8.

Table 3.8: Combined matrix for Bernoulli's equation

	v_n	ρ_l	C_N	ΔP
L	1	-3	0	-1
M	0	1	0	1
T	-1	0	0	-2
π_1	1	x_1	x_2	x_3

Since a singular matrix is generated for all variations in choice of columns, we need to apply modified DA and use homogeneity subsequently. Following the dimensions, we have to combine variables such that dimensionless groups are created. Using the nozzle coefficient as a scaling parameter, we have,

$$\left[\frac{v_n^2}{\Delta P} \right] = \frac{[L^2 T^{-2}]}{[M L^{-1} T^{-2}]} = [M^{-1} L^3] [M^0 L^0 T^0]^b = \left[\frac{k_4^a}{\rho_l} \right] [C_N]^b \quad (3.49)$$

$$v_n^2 = \frac{(k_4^a)(C_N^b)\Delta P}{\rho_l} \quad (3.50)$$

Note that a unique correlation would exist between variables as dictated by laws of physics and for a problem with 4 coefficients or less, the task of correlating dimensions becomes trivial once the right combination is established⁵. Defining $\Delta P = P_a - P_{atm}$ and like before, setting $a = b = 1$, we have,

$$v_n^2 = \frac{k_4 C_N (P_a - P_{atm})}{\rho_l} \quad (3.51)$$

Continuing with development of rest of the state equations, modifying dimensions of pressure as specific density of volume of air per unit mass, we have,

Table 3.9: Combined matrix for isentropic expansion

	P_a	K	$C_{isentropic}$	m_l	ρ_l	V_r
L	3	0	0	0	-3	3
M	0	0	0	1	1	0
T	0	0	0	0	0	0
π_1	1	0	0	x_1	x_2	x_3
π_2	0	1	0	x_4	x_5	x_6
π_1	0	0	1	x_7	x_8	x_9

A singular condition again coerces use of variation of DA. Using gas constant K as magnifying parameter,

⁵When coefficients are encountered, a general rule of thumb is to manipulate them such that they always figure in numerator of a fraction.

$$\left[V_r - \frac{m_l}{\rho_l} \right] = [M^0 L^3 T^0] = \pi_1 \quad (3.52)$$

$$\left[\frac{1}{P_a} \right] [C_{isentropic}]^b = [M^0 L^{-3} T^0] = \pi_2 \quad (3.53)$$

Using a simple monomial basis such that $\pi_2 = k_5(\pi_1)^c$ where $c = K$ we have,

$$P_a \left(V_r - \frac{m_l}{\rho_l} \right)^K = k_5 (C_{isentropic})^b \quad (3.54)$$

Following the convention of letting $b = 1$, we have,

$$P_a \left(V_r - \frac{m_l}{\rho_l} \right)^K = k_5 C_{isentropic} \quad (3.55)$$

This might be tricky for initial users but recognition of the fact that air undergoes isentropic expansion allows designers to model the system correctly in DA. Establishing the final state equation,

Table 3.10: Combined matrix for continuity

	\dot{m}	ρ_l	A_n	v_n
L	0	-3	2	1
M	1	1	0	0
T	-1	0	0	-1
π_1	1	x_1	x_2	x_3

Again from the principle of homogeneity, $X = (-1 \ -1 \ -1)$ or $\pi_1 = \frac{\dot{m}}{\rho_l A_n v_n}$ or $\frac{dm}{dt} = k_6 \rho_l A_n v_n$. Notice that in their general form, the above equations capture the momentum equation, Bernoulli's equation, isentropic process and continuity equation respectively. All that remains to be done is to establish values of constants k 's which is done combining numerical and experimental analysis.

3.4 Numerical and Experimental Analysis

Evaluation of constants in the state equations is performed through a combination of physical reasoning, numerical simulation and experimental verification. State equations have six different constants whose value need to be ascertained. The experimental procedure provides values for height achieved alone, which is the only available benchmark. An initial guess for all six constants commences process of estimation. Bear in mind that choice of initial guess greatly affects convergence and hence an educated guess needs to be employed. Further, optimality is dependent on inputs as well and hence, the optimal combination varies as values of inputs differ. The system is simulated for known inputs to establish net numerical height achieved *i.e.*, the maximum height reached by the rocket that includes the two individual events of flight during water drain and subsequent flight. For an initial volume of 50% water pressurized to 4 *atm* gage, simulations are run up until the system reaches its net height which is evaluated to be 17.52 *m* as compared to an experimental value of 17.92 *m* causing an error of 0.40 *m*. This error, specific to an initial volume of 50% water and pressure of 4 *atm* gage, is minimized using the solver technique to obtain sub-optimal values for constants. Excel solver is used to minimize error from numerical evaluation using conjugate search and central derivatives (see Figure 3.2). Shown below is an optimization procedure summarizing the process.

Step 1: Consider system of equations. Set all constants to an initial guess.

Go to step 2.

Step 2: Estimate height with assumed values of constants for one test condition (say %vol of water = 0.5). Go to step 3.

Step 3: Compare simulated numerical height with experimental value for the test condition. Estimate error and go to step 4.

Step 4: Setup an optimization scheme to minimize error for the particular test condition by altering values of constants. Go to step 5.

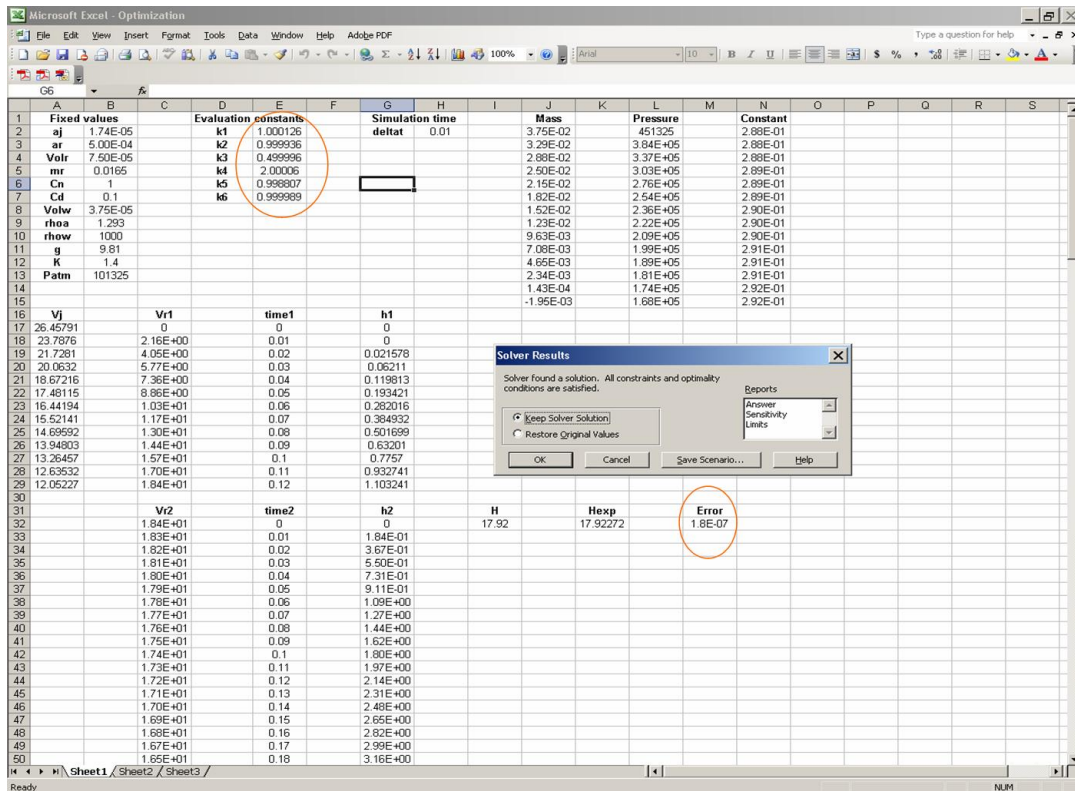


Figure 3.2: Optimal values using Excel solver

Step 5: Obtain a sub-optimal set of values for the specific test condition. Go to Step 6.

Step 6: Using the sub-optimal values, compare for different input conditions to generate individual errors for each of the test condition. Go to Step 7.

Step 7: Alter the sub-optimal values of the constants such that each individual error **and** the net root mean square of the individual errors are minimized to obtain global optimal values.

Hence, the optimization problem can be mathematically defined as -

$$\begin{aligned}
& \text{find } \{k_i\}_{i=1}^6 \ni \varepsilon_i \text{ and } \sqrt{\frac{\sum_{i=1}^6 \varepsilon_i^2}{6}} \text{ are minimized } \forall i \in [1, 6] \\
& \text{where } \varepsilon_i = |\text{num}_i - \text{exp}_i| \forall i \in [1, 6]
\end{aligned}$$

In essence, the procedure iterates till an optimal combination of constants is obtained where each individual error and the net RMS error across all six readings are minimized. Once the optimal set of constants is established (see Table 3.12), the values are incorporated into the state equations and simulated for varying levels of %water in the system. Since constants are specific to a particular condition, errors are still generated but remain convergent when inputs change. The algorithm is put to test with the set of initial values for all parameters and constants as shown below [Otto et al., 2001]. All units are given in SI system (see Table 3.11).

Table 3.11: Input parameters and values for the algorithm

Input	Parameter	Initial value
Area of jet	A_j	0.174×10^{-4}
C/S area of rocket	A_r	5.0×10^{-4}
Volume of rocket	V_r	75.0×10^{-6}
Mass of rocket	m_r	0.0165
Nozzle coefficient	C_N	1.0
Drag Coefficient	C_d	0.1
Pressure of air	P_a	451325
Volume of water	V_w	37.5×10^{-6}
Density of air	ρ_a	1.293
Density of water	ρ_w	1000
Acceleration due to gravity	g	9.81
Expansion coefficient	K	1.40
Atmospheric pressure	P_{atm}	101325

Table 3.12: Estimated values of constants using the algorithm

Parameter	Estimated value
k_1	1.00
k_2	0.99
k_3	0.49
k_4	2.00
k_5	0.99
k_6	0.99

Hence the state equations are -

$$\frac{dv_r}{dt} = \left(\frac{\rho_l A_n v_n^2}{m} \right) - 0.99g - 0.49 \left(\frac{C_d \rho_a A_r v_r^2}{m} \right) \quad (3.56)$$

$$v_n^2 = \frac{2C_N(P_a - P_{atm})}{\rho_l} \quad (3.57)$$

$$P_a \left(V_r - \frac{m_l}{\rho_l} \right)^K = 0.99C_{isentropic} \quad (3.58)$$

$$\frac{dm}{dt} = -0.99\rho_l A_n v_n \quad (3.59)$$

Comparing developed state equations to traditional state equations given below [Otto et al., 2001], we have,

$$\frac{dv_r}{dt} = \left(\frac{\rho_l A_n v_n^2}{m} \right) - g - \left(\frac{C_d \rho_a A_r v_r^2}{2m} \right) \quad (3.60)$$

$$v_n^2 = \frac{2C_N(P_a - P_{atm})}{\rho_l} \quad (3.61)$$

$$P_a \left(V_r - \frac{m_l}{\rho_l} \right)^K = C_{isentropic} \quad (3.62)$$

$$\frac{dm}{dt} = -\rho_l A_n v_n \quad (3.63)$$

such that the DA solution is close to theoretical development captured by the second set of equations which are developed using conventional control volume

and control surface analysis. The only variation occurs in the constants which can be attributed to numerical evaluation. Differences in actual values are too small to be even considered for any subsequent analysis. As part of further validation, experimental authentication is provided by comparing maximum height achieved. Three different solutions are plotted comparing accuracy and precision of the traditional model and the DA solution with experimental values (see Table 3.16). In the experimental analysis, volume of water is varied from 10% to 60% (see Table 3.13) as a fraction of rocket volume and in each case the system is simulated. In order to accommodate experimental features (see Figure 3.3), the state equation that models flight after all water is drained, is also incorporated. This is captured traditionally and by DA respectively as

$$\frac{dv_r}{dt} = -g - \left(\frac{C_d \rho_a A_r v_r^2}{2m} \right) \quad (3.64)$$

$$\frac{dv_r}{dt} = -0.99g - 0.49 \left(\frac{C_d \rho_a A_r v_r^2}{m} \right) \quad (3.65)$$

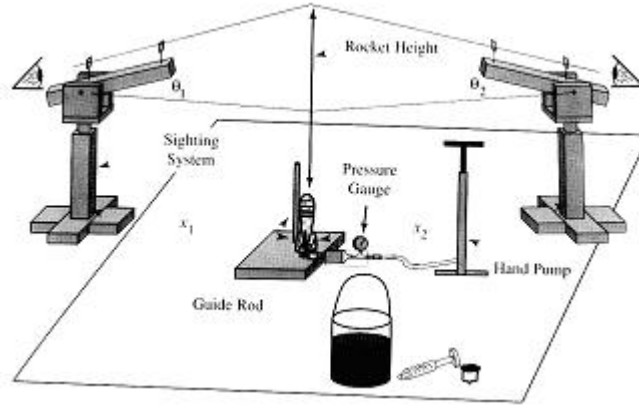


Figure 3.3: Experimental setup for water rocket - Adapted from [Otto et al., 2001]

This allows for evaluating maximum height reached by the rocket that includes the two individual events of flight during water drain and flight thereafter. The results are shown below (see Tables 3.14-3.17 and Figures 3.4-3.5).

Table 3.13: Input conditions to experimental setup of the water-rocket

<i>%Volume of Water</i>	<i>Air Pressure ($\frac{N}{m^2}$)</i>
0.6	4.51×10^5
0.5	4.51×10^5
0.4	4.51×10^5
0.3	4.51×10^5
0.2	4.51×10^5
0.1	4.51×10^5

Table 3.14: Results from traditional simulation

<i>Height₁(m)</i>	<i>Height₂(m)</i>	<i>Net Height(m)</i>
1.869320	11.980500	13.849820
1.252020	17.034100	18.286120
0.840102	18.215900	19.056002
0.514656	16.001500	16.516156
0.258050	10.944300	11.202350
0.076049	6.304970	6.381019

Table 3.15: Results from DA simulation

<i>Height₁(m)</i>	<i>Height₂(m)</i>	<i>Net Height(m)</i>
1.656450	12.316380	13.972830
1.103240	16.823760	17.927900
0.641710	18.945100	19.586810
0.297770	16.304260	16.602030
0.114010	10.957570	11.071580
0.075690	6.284110	6.359800

The constants developed in the equation remain impervious to magnitude changes in parameters (geometric or otherwise) indicating the uniqueness of the model and the underlying physical phenomena. Hence, this is a procedure where a design model is derived from a limited set of data points and experiments. Repetition and reevaluation of constants is not necessary as they are invariant to changes in magnitudes in parameters and are thus dependent

Table 3.16: Experimental values from the water-rocket setup

Net Height (m)
14.14528
17.92272
19.34916
15.86360
12.27667
7.03618

Table 3.17: Error margins comparing traditional and DA solutions

% Error (Traditional Approach)	% Error (DA Approach)
2.09	1.22
2.03	0.02
1.52	1.23
4.11	4.65
8.75	9.82
9.31	9.61

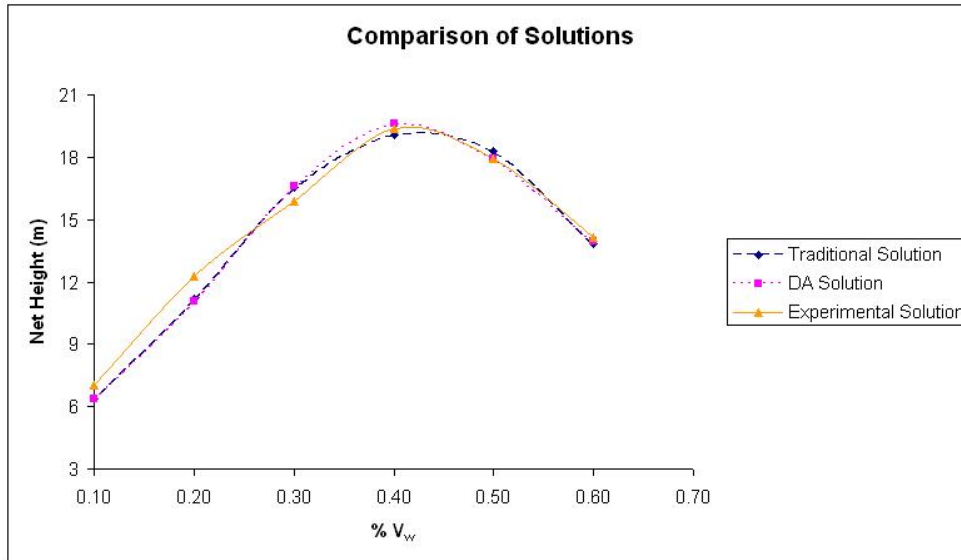


Figure 3.4: Comparison of different solutions

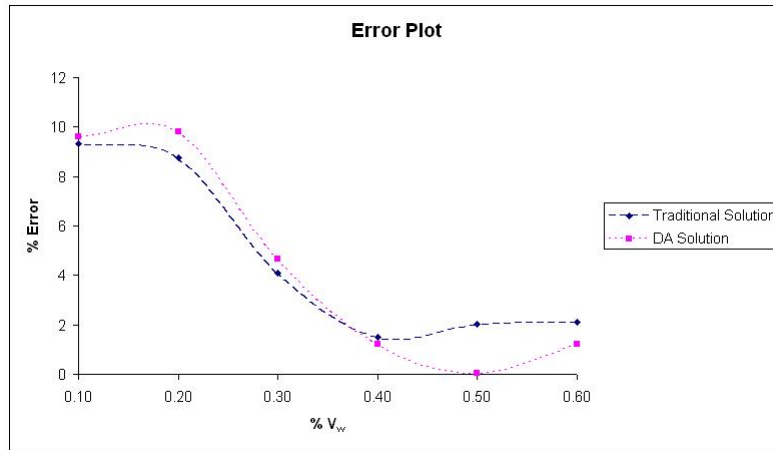


Figure 3.5: Error trends from different solutions

on the system and its physics alone rather than the numerical magnitude that each parameter attains. To validate this argument, pressure is changed and in each case the experimental and numerical solutions are compared where the numerical solutions incorporate the derived constants. The two solutions are shown below for varying levels of pressure and %water level fixed at 0.4 (see Figure 3.6). Notice that the differences between the values are marginal implying robustness in the developed design model.

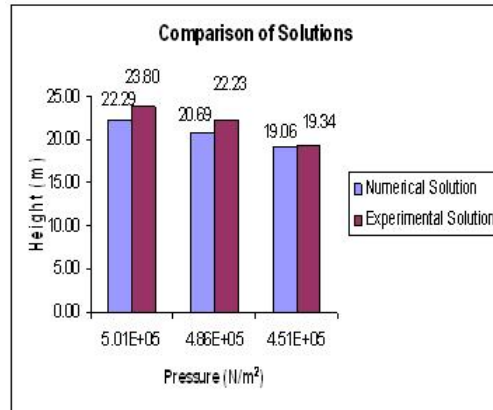


Figure 3.6: Comparison of numerical and experimental solutions for varying pressure levels

The entire development is summarized using a flow chart approach for ease and elucidation (see Figures 3.7 and 3.8). The conventional TSM technique follows the procedure detailed earlier. However, problem decomposition, a novelty in this flow chart, arises to simplify the original formulation to develop domain specific monomial basis instead of a global monomial basis that does not exist or is complex and not insightful. This condition would thus initiate use of the modified approach. In the modified approach, each domain is treated as a separate sub-problem and is solved independent of the other domains. The functional relationships of each domain are thus generated with their specific variables and parameters. The values of constants in each domain are approximated using numerical optimization coupled with experimental results.

This example thus deviates from TSM but is still a powerful tool to develop functional relations between variables affecting a physical system. Versatility in incorporating several different energy domains has been illustrated. Further, the method has allowed for dimensional manipulation of diverse parameters digressing from conventional differential element analysis in system dynamics. However, the modified analysis has retained mathematically mundane calculations without genuine visual insight. Continuing the effort to build simpler and more intuitive engineering tools, a graphical and topological combination is presented next. This exposition acts as a learning instrument where complex engineering equations are derived and interpreted through visual perception similar to a block diagram.

3.5 System Dynamics

Modeling system dynamics requires thorough knowledge of fundamental processes at work and associated physical laws. Many complex systems are analyzed using simplification procedures where components and sub-systems are isolated and modeled. The governing dynamics of each component is influenced by physics of the problem and extent to which the particular com-

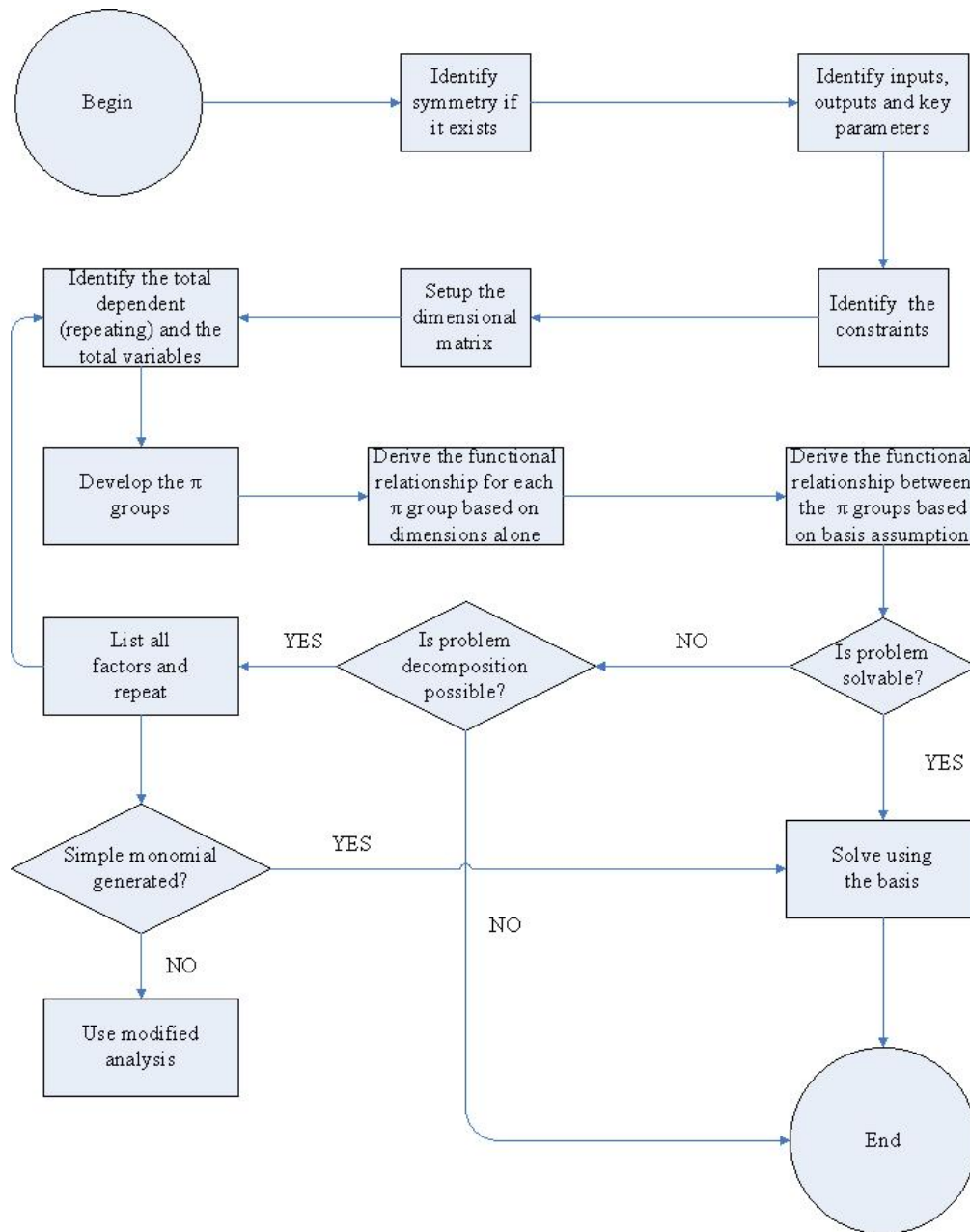


Figure 3.7: Conventional TSM analysis

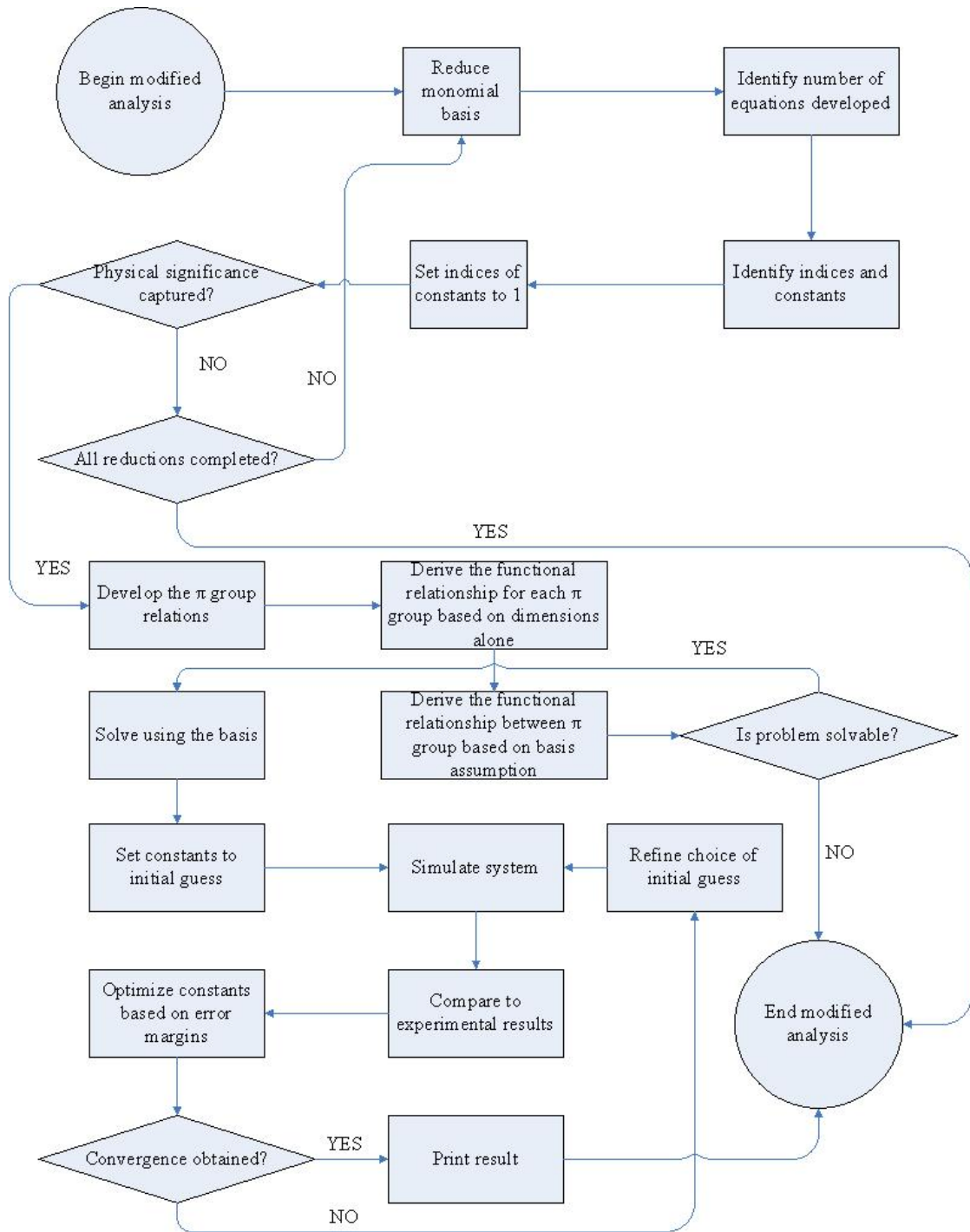


Figure 3.8: Modified TSM analysis

ponent affects response of the system. For systems with multiple components and interactions, a systematic approach needs to be employed to individually model each sub-system that forms the basis for system level response. Bond graphs [Karnopp et al., 2006] are one such graphical visualization tools for interpreting system dynamics and provide means for evaluating state equations through a combination of conservation statements and fundamental laws. However, modeling thermal interactions in bond graph process presupposes intimate knowledge of the topic and is not as intuitively apparent as other techniques. Dimensional analysis used in the conventional form [Bridgman, 1931] also requires skill in matrix manipulation and is constrained by the possibility of having to solve or simplify systems with non-monomial basis [Szirtes, 1998]. A graphical approach with limited mathematical effort mitigates need to evaluate complex analytical relations while providing a visual aid for better understanding of data flow in the system. Such a process is elaborated in this section supported by evaluation of the dynamic system introduced earlier.

3.6 Nodes and Graphs

Graphs have been widely used in engineering applications with signal flow graphs [Deo, 1974] and state transition diagrams [Johnson et al., 1972] being most commonly employed visual tools in modeling electrical and control systems. Happ [1971] introduced the concept of illustrating dimensional analysis through the use of directed graphs. Using methods of path inversion and transmittances, Happ [1971] established several engineering identities. However, the basic limitation of these graphs is their inability to model transient or dynamic systems and thus most engineering phenomenon modeled are linear or quasi-linear steady state problems. Further, all systems shown by Happ [1971] have simple fundamental laws that are coupled only through variable multiplication and no parameter is added or subtracted which is an inherent requirement for conservation statements. However, the process pioneered use of graphs in dimensional analysis.

Shown below are a couple of illustrations depicting Happ’s approach, focusing on energy transfer in the mechanical (see Figure 3.9) and electrical domains (see Figure 3.10). The weights on each edge indicate value with which the respective node is scaled. The dimensional form of energy $[ML^2T^{-2}]$ is graphically modeled as the dimensional product of mass $[M]$ and square of velocity $[V^2]$ in Figure 3.9 and equivalence of energy is shown in Figure 3.10, where two different domains are combined using the scalar equality operator “=” indicating dimensional equivalence.

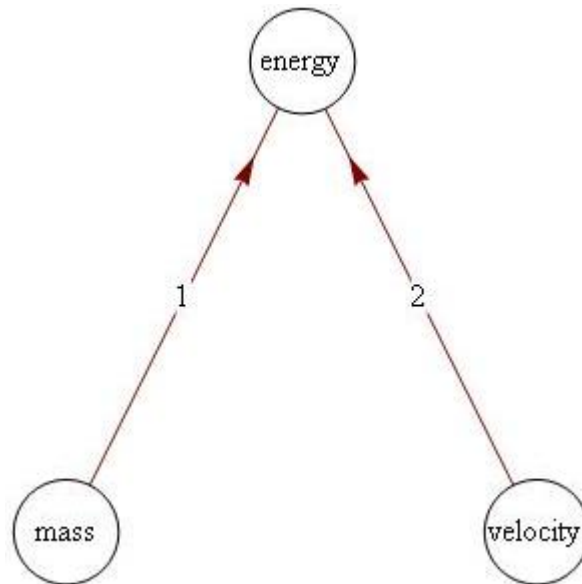


Figure 3.9: A simple flow graph

This technique is modified to make it more conducive to mechanical engineering design applications, specifically to dynamic systems modeling, by introducing the $\Pi - \Sigma$ approach.

3.7 Development of the Graph

A graph is an ordered collection of nodes and edges and is defined as $G = \{N, e\}$, where N is number of nodes and e is the number of edges. In engi-

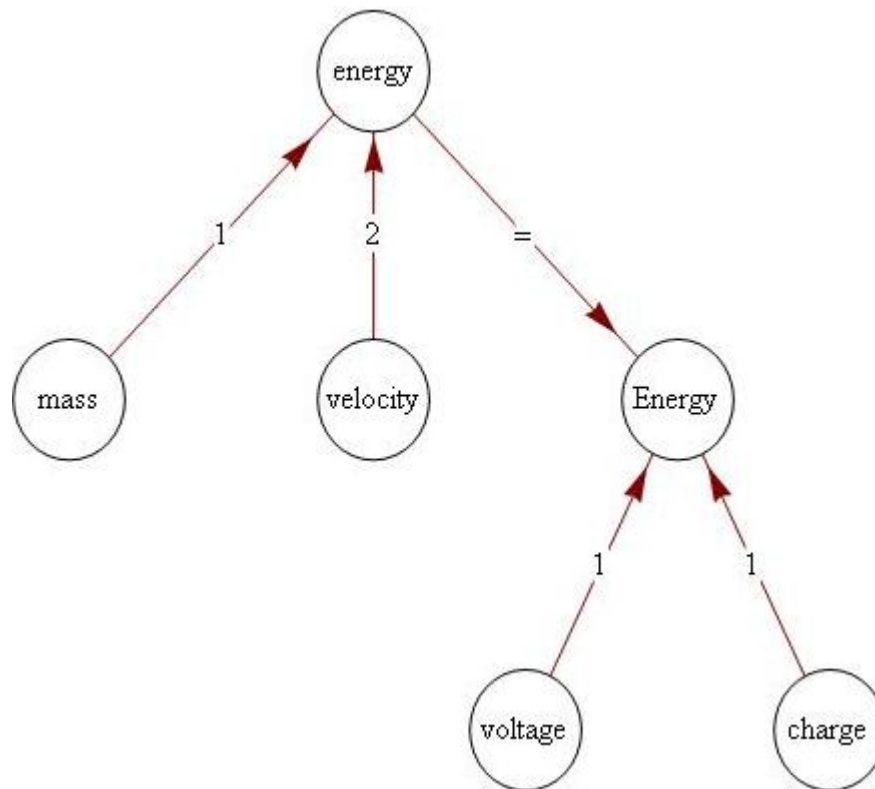


Figure 3.10: Multiple domain flow graph

neering systems, nodes represent variables affecting a system and edges capture how these variables interact with each other. This interaction is quantified by edge weight which is finite for a well-defined relationship (see Figure 3.11) and indefinite for an unknown or non-existent relationship (see Figure 3.12). The graph in Figure 3.11 implies that density is dimensionally equivalent to the ratio of mass and volume, *i.e.*, the product of mass raised to the power of “1” and volume raised to the power of “-1”. Hence, the graph is complete and needs no further information to define it. On the contrary Figure 3.12 emphasizes the idea that no plausible relationship can be established between mass and area without further information relating the two. Hence this graph is incomplete and a broken link is shown with no definitive edge weight.

The motivation now is to establish a graph structure that has only finite

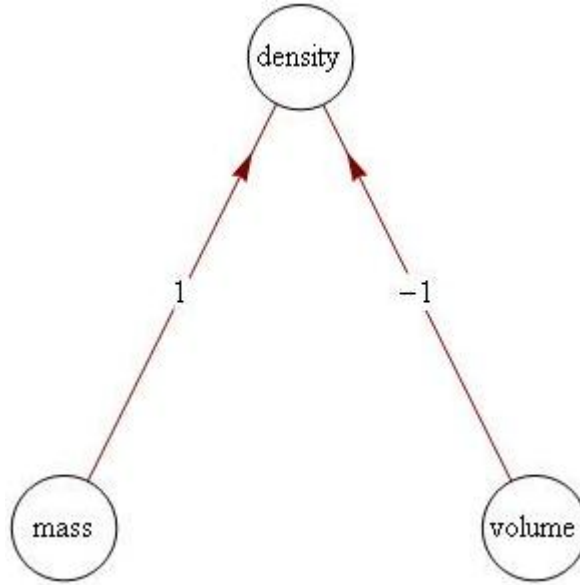


Figure 3.11: Graph for a known relationship - finite edge weight

edge weights to capture true physics of a dynamic system. Any graph with an infinite edge is discarded as it represents a physical law that is improbable or unknown⁶. Modifying the relation for the system graph we have,

$$G_{sys} = \{N_{sys}, e_f\} \quad (3.66)$$

where N_{sys} are nodes in the system and e_f are edges with finite edge weights. A node indicating a variable must have dimensions and hence has an associated dimension vector or D -vector. The D -vector is a row vector with elements equal to indices of the fundamental vector $[M, L, T, \theta, q]$ (mass - length - time - temperature - charge) corresponding to the basic dimensional analysis variables. A node representing a force value would have a D -vector equal to $[1, 1, -2, 0, 0]$.

With this basic graph structure in mind, the following nodes are introduced that are developed to simplify the analysis for dynamic system evalua-

⁶Rules and constraints for graph construction are elaborated later in this section.

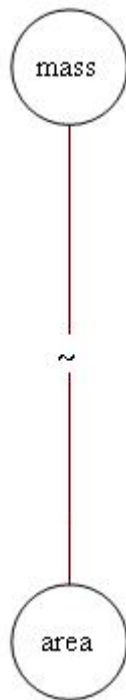


Figure 3.12: Graph for an unknown relationship - infinite edge weight

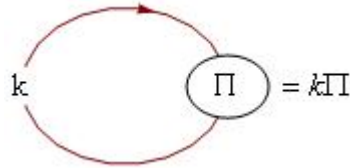
tion -

1. *Independent node* - A node representing an independent variable.
2. *Dependent node* - A node representing a variable that is dependent on at least one other variable, *i.e.*, node.
3. *Derived node* - These nodes are Π and Σ nodes representing product and the sum of two independent or dependent nodes. These are dependent nodes by default.
4. *Differential node* - A node that contains a derivative *w.r.t* a variable.
5. *Constant node* - A node with constant numerical value.
6. *0 node* - A node with zero numerical value.

7. *F node* - A node indicating a known functional form.

These nodes constitute the basic graph nomenclature needed to represent design models for dynamic systems. A set of rules is now needed to develop an approach for deriving graph models. The rules and constraints for the generation of such graphs include -

1. A Π or a Σ node can have only two inputs.
2. An independent or dependent node cannot directly interact with another independent or dependent node. All interactions have to be through a Π or a Σ node to satisfy dimensional analysis properties.
3. Every Π and Σ node must represent a valid physical law or principle.
4. A graph can have any number of Π and Σ nodes, *i.e.*, there is no limitation on the number of Π and Σ nodes.
5. Any two nodes can be used to produce a Π node as long as the resulting Π node is dimensionally correct, physically measurable and has a D -vector with at least one element larger in power magnitude than the input nodes.
6. A Σ node can be used to combine two nodes of same dimensional form due to principle of dimensional homogeneity [Murphy, 1950] and hence cannot have inputs with inconsistent dimensional forms.
7. An edge weight of “+” or “-” indicates positive or negative of the concerned nodes.
8. A constant node can be used only as a scaling parameter when combined with a Π node. A constant node can never be used with a Σ node.
9. A loop indicates that the concerned node is scaled by the constant of the loop only once as shown below.



10. A θ node indicates culmination or sink of the graph. Input to a θ node can have any dimensional form.
11. A graph can have edges with finite edge weight alone.
12. All logarithmic, exponential and transcendental relations can only be combined after reducing to the correct dimensional form - a number. Output of a F node has to be a number [Hart, 1995].
13. A sub-graph of a system graph must also represent a physical phenomenon.
14. Number of sub-graphs must be the same as number of terms in the conservation statement.
15. A node can be combined with itself through a Π or Σ node in conjunction with the looping condition as long as resulting output is dimensionally correct and physically measurable.
16. A system will have one and only one graph to represent its dynamics ensuring uniqueness of physics and fundamental laws *i.e.*, despite the existence of multiple design models, graphs modeling particular physics laws are unique.

Using the definitions and rules developed, the water-rocket dynamic system is evaluated that incorporates functionality and versatility of $\Pi - \Sigma$ approach. The system evaluated like before, as an illustration of the process, is a simple water-rocket assembly using water as charge for propulsion [Otto et al., 2001]. Recall that the travel of the rocket is governed by momentum

conservation principle where thrust developed upward is a consequence of exit of water jet downward. A systematic procedure is employed to evaluate the system and develop state equations. This problem serves as a pilot project in establishing feasibility of $\Pi - \Sigma$ approach as it combines principles from thermodynamics, fluid mechanics and translational dynamics.

Process 4: Applying $\Pi - \Sigma$ approach to the Water-Rocket system

Step 1: Identify different domains in the system

Thermodynamics - Isentropic expansion of air causes pressure differential within the rocket and outside atmosphere.

Fluid Mechanics - Exit of jet from the rocket is governed by continuity equation, momentum equation and Bernoulli's principle.

Translational Dynamics - Motion of the rocket upward is determined by Newton's laws incorporating drag and gravitational or inertial effects.

This is probably the most critical step in the analysis to ensure proper dimensional evaluation of the system. Some technical knowledge and skill is expected of users to identify and understand the principles governing the behavior of the system. The process of recognizing and distinguishing different forces at play in such systems is implicit to the evaluation procedure.

Step 2: Setup conservation statement for each domain

The conservation statement for translational dynamics is presented, which can be generalized for the entire system. But using a simpler approach where each domain is analyzed for its system parameters offers greater flexibility and ease in computation. The translational dynamics is governed by,

$$Force_{net} = Thrust\ Developed - Drag - Inertia \quad (3.67)$$

Like in the previous step, without any loss of generality, an assumption is made that relations like above can be developed without major concerns.

Further, when working with complex systems involving multiple conservation statements and multiple terms in each statement, it is imperative that each term be evaluated individually for greater accuracy in estimation and simplicity in analysis. When numerous variables affect a system, it is judicious to simplify the system for modeling ease.

Step 3: Evaluate each term by identifying influencing variables

Identification of these variables is sometimes not trivial but careful analysis and understanding of the physics of the problem allows proper evaluation of the system. In this system, since the thrust is caused by the change in momentum, the two moving objects causing such change need to be identified first. While the rocket (object 1) motion is the output momentum, the input momentum is the result of rapidly exiting fluid (object 2). The fluid (water) exits because the air within the rocket pushes down on the liquid column forcing discharge. Hence, the thrust developed is governed by liquid density (ρ_l), nozzle area (A_n) and nozzle jet velocity (v_n) as these determine flow resistance, flow speed and flow properties respectively.

In order to combine these variables, simple combinations of material and geometry attributes are resorted to. Consider the variables ρ_l and A_n . While the former is a *material* specific flow parameter of the liquid used, the latter is a *geometry* specific variable of the rocket nozzle. Hence, it is fairly obvious that they cannot be directly related. Thus, another variable is needed that couples these two variables *i.e.*, v_n , which combines with each of them independently thereby associating them indirectly. Therefore one of the five identities (see Equations 2.35 - 2.39) must hold true and have physical significance. Note that addition and subtraction would be dimensionally incorrect due to disparity in dimensions between the parameters. Thus, the set of possible operators reduces to multiplication, division and power. The next challenge is to understand if any parameter needs to be scaled to a power *i.e.*,

$$\{A_n, \rho_l\} \odot v_n^k$$

where \odot is \times for $k = n$ and \div for $k = -n, n \in \aleph$

This issue is resolved using the rules and constraints developed for construction of the graph. Let $k = 1$, a condition that generates $A_n v_n$ and $\rho_l v_n$. For $k = -1$, we have $\frac{A_n}{v_n}$ and $\frac{\rho_l}{v_n}$. The latter two are unknown physical quantities as is the second relation of the first set. However, the first relation of the first set, $A_n v_n$, bears dimensional and measurable features of a known quantity, that of volume flow rate. Thus for $k = 1$, a valid physical parameter consistent with the rules has been identified and isolated and hence no more iterations of k are needed. Proceeding with the construction of the entire graph using similar logic, we have (see Figure 3.13),

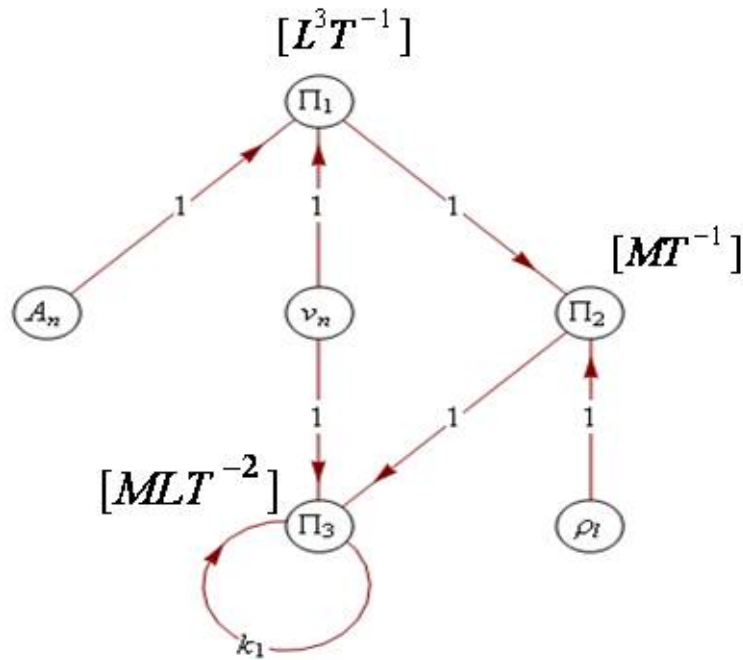


Figure 3.13: Flow graph for thrust

The graph thus represents thrust given by $k_1 \rho_l v_n^2 A_n$ with dimensions of force. Notice that all edge weights are numerically finite, every influencing variable has been incorporated and each Π group has a D -vector greater than or equal to preceding nodes. Every Π group represents a dimensionally sound measurable quantity with Π_1 accounting for volume flow rate, Π_2 indicating mass flow rate and Π_3 signifying force. Notice also that no other combination of variables produces a measurable quantity thus validating the uniqueness property of the graph. Note also that the final node Π_3 is scaled by a constant since dimensional analysis does not yield any constants in an equation. Moving on to evaluating drag experienced by the rocket and inertial effects encountered in its flight path, the influencing parameters are coefficient of drag (C_d), velocity of the rocket (v_r), air density (ρ_a) and rocket area (A_r). The only two factors affecting inertial effects are total instantaneous mass of the rocket (m) and acceleration due to gravity (g). Setting up the graphs, we obtain the relations provided in Figures 3.14 and 3.15.

Step 4: Combine graphs if all terms are evaluated in the conservation statement

Since all terms in the conservation statement are accounted for, we can now put the sub-graphs together to generate a parameter graph for translational dynamics. Notice that all end Π groups in each sub-graph *i.e.*, Π_3 , Π_8 and Π_9 have dimensions of force and thus principle of homogeneity is satisfied. Combining these forms in the relation $\frac{\Pi_i \Pi_j}{\Pi_k}$ still generates an output form that is dimensionally equivalent to force but violates the conservation statement and is hence not valid. Therefore the only plausible relation that is both dimensionally accurate and valid from a conservation standpoint has to have a relation given by,

$$Force_{net} = \Pi_3 - \Pi_8 - \Pi_9 \quad (3.68)$$

Σ nodes are now invoked using “+ -” convention to combine Π nodes for the parameter graph of translational dynamics as shown below (see Figure 3.16). The parameter graph indicates net force upward which is a combination

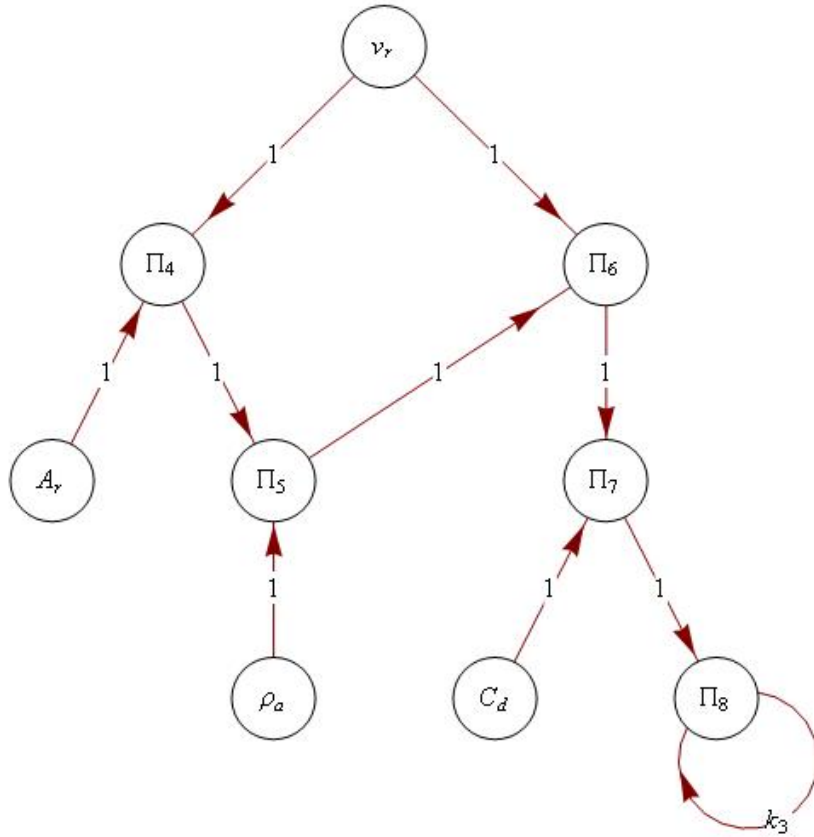


Figure 3.14: Flow graph for drag

of mass and acceleration upward and hence the following graph is generated. Thus Π_{10} in the graph below indicates force upward given by $m \frac{dv_r}{dt}$ which is the thrust Π_3 minus total resistance Σ_1 (drag + gravity).

Notice that the node v_r is associated with the differential node Dt with a unit scale on the bond indicating a first order derivative. Therefore, the scale signifies the order of differentiation of the variable node with respect to the differential node. The flow graph hence represents the analytical relation given by,

$$m \frac{dv_r}{dt} = \rho_l v_n^2 A_n - mg - \frac{1}{2} C_d \rho_a v_r^2 A_r \quad (3.69)$$

The flow graph for translational dynamics is complete, dimensionally

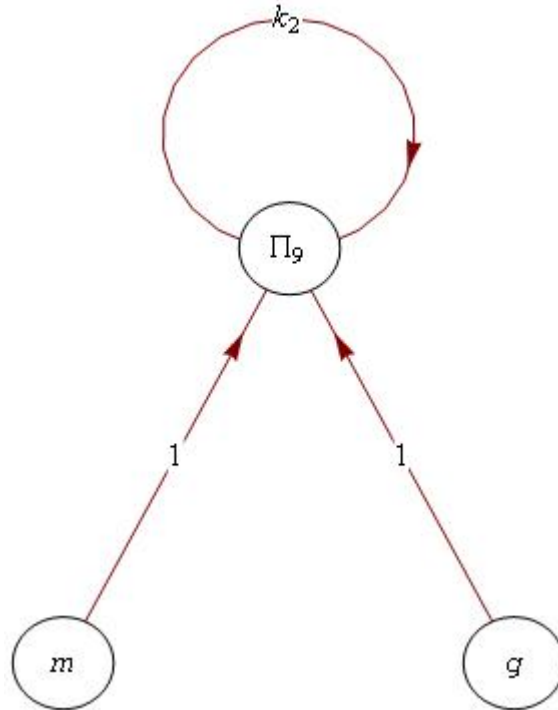


Figure 3.15: Flow graph for inertial effects

homogeneous and has finite edge weights. The above equation thus represents a basic first-order, non-linear model for the translational dynamics of the system. Further, notice that all variables are constants except for v_n , a parameter introduced for completeness. Thus, v_n needs to have a state equation of its own to define its behavior. We thus seek state equations to completely model the system and every time a new variable is introduced that is neither a constant nor a known parameter, the equation set is refined to update a new state equation iterating till all the domains listed in Step 1 are captured. Equation (3.69) is now derived using conventional control volume-control surface (see Figure 3.17) analysis to contrast the graphical approach and the closed-form technique. Conserving momentum, we have,

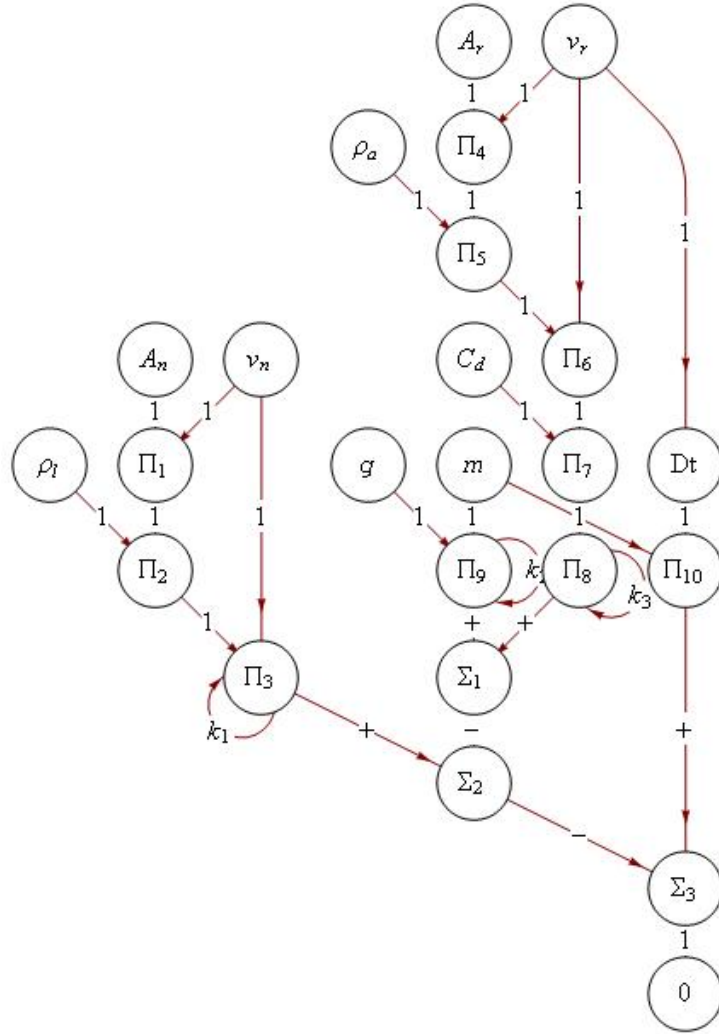


Figure 3.16: Flow graph for translational dynamics

$$\sum \vec{F}_{ext} = \frac{d\vec{P}}{dt} = \sum_{CS} \vec{v} \rho \vec{v} \cdot \vec{A} + \frac{d}{dt} \int_{CV} \vec{v} \rho \cdot d\vec{V} \quad (3.70)$$

\vec{v} being velocity vector, \vec{A} being area vector and \vec{V} being volume vector. Since forces acting on the system are aligned along z - axis (vertical direction)

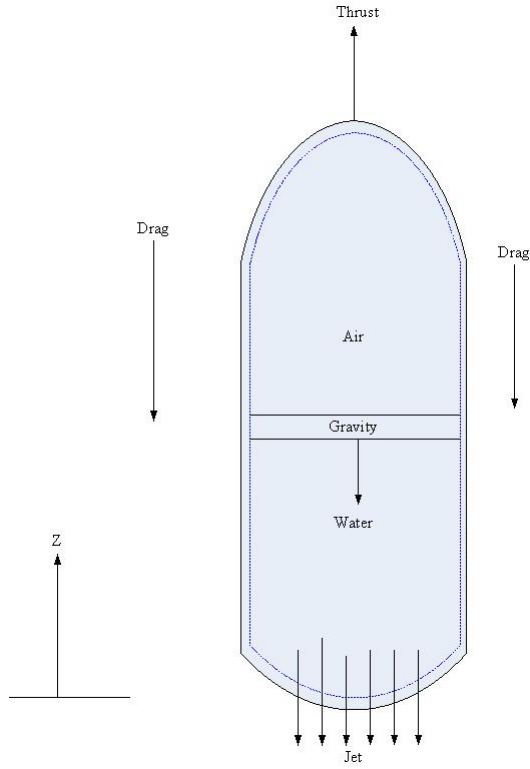


Figure 3.17: Control volume for the water-rocket

alone,

$$\sum F_z = \sum_{CS} \vec{v}_n \rho_l \vec{v}_2 \cdot \vec{A}_n + \frac{d}{dt} \int_{CV} \vec{v}_n \rho_l \cdot d\vec{V} \quad (3.71)$$

where \vec{v}_n is jet velocity vector *w.r.t* vertical reference frame and \vec{v}_2 is velocity vector *w.r.t* control volume. This implies that -

$$\vec{v}_n = \vec{v}_2 + \vec{v}_r \quad (3.72)$$

where \vec{v}_r is rocket velocity vector. Combining the two previous equations, we have,

$$\sum F_z = (v_r - v_n) \rho_l v_n A_n + \frac{d}{dt} \int_{CV} v_2 \rho_l dV + \frac{d}{dt} \int_{CV} v_r \rho_l dV \quad (3.73)$$

Since velocity vector *w.r.t* control volume, \vec{v}_2 , does not change with time internal to control volume,

$$\frac{d}{dt} \int_{CV} v_2 \rho_l dV = 0 \quad (3.74)$$

Further since $\int_{CV} \rho_l dV = m$, we have,

$$\sum F_z = (v_r - v_n) \rho_l v_n A_n + \frac{d}{dt} (m v_r) \quad (3.75)$$

or,

$$\sum F_z = (v_r - v_n) \rho_l v_n A_n + m \frac{dv_r}{dt} + v_r \frac{dm}{dt} \quad (3.76)$$

From continuity relation,

$$\frac{dm}{dt} = -\rho_l A_n v_n \quad (3.77)$$

Substituting in the previous equation,

$$\sum F_z = (v_r - v_n) \rho_l v_n A_n + m \frac{dv_r}{dt} - \rho_l A_n v_n v_r \quad (3.78)$$

Simplifying,

$$\sum F_z = m \frac{dv_r}{dt} - \rho_l A_n v_n^2 \quad (3.79)$$

Recognizing the fact that the only two external forces acting on the system are weight and drag resistance, we have,

$$\sum F_z = m \frac{dv_r}{dt} - \rho_l A_n v_n^2 = -mg - \frac{1}{2} \rho_a C_d A_r v_r^2 \quad (3.80)$$

Reorganizing the equation,

$$m \frac{dv_r}{dt} = \rho_l A_n v_n^2 - mg - \frac{1}{2} \rho_a C_d A_r v_r^2 \quad (3.81)$$

Equations (3.69) and (3.81) are identical except the derivation process is lot more intricate in the conventional approach. The graphical approach on the other hand offers a visual perspective where transition from one term to

the other is simple and unequivocal. Thus, an entire mathematical development can be replaced by a single dimensional graph. On the downside, the conventional method does account for constants in the equation unlike the dimensional approach.

Step 5: Generate graphs for each domain

Using similar procedures for Bernoulli's (see Figure 3.18), isentropic expansion (see Figure 3.19) and continuity (see Figure 3.20) equation, parameter graphs are generated using variables liquid density (ρ_l), nozzle area (A_r), total instantaneous mass of the rocket (m), nozzle jet velocity (v_n), coefficient of nozzle (C_N), mass of water (m_l), pressure difference (ΔP), coefficient of expansion ($C_{isentropic}$), volume of rocket (V_r) and gas constant (K).

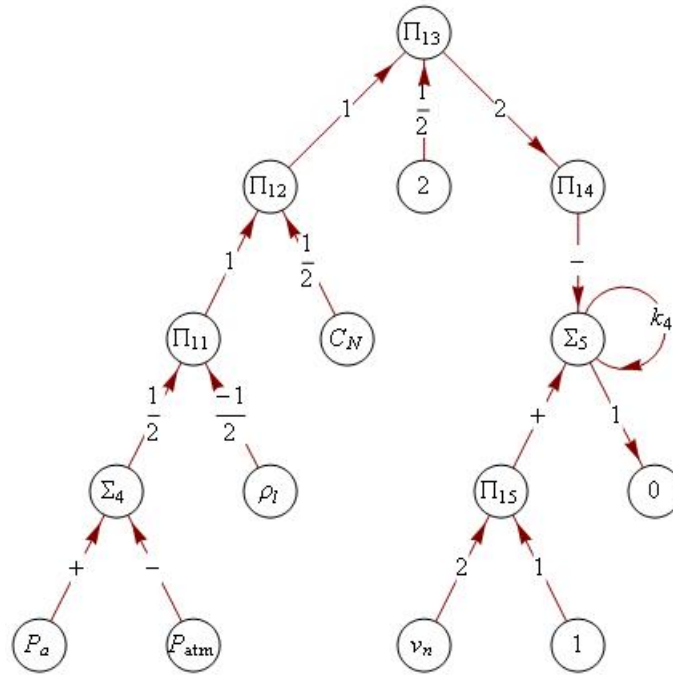


Figure 3.18: Flow graph for Bernoulli's equation

This graph thus gives the relation, $v_n^2 = \frac{k_4 C_N (P_a - P_{atm})}{\rho_l}$ where an unknown parameter P_a is introduced. The rest of the equation has terms that

have been used before or are known constants. To model the variation in pressure, we invoke the next state equation captured by isentropic expansion (see Figure 3.19) given by $P_a \left[V_r - \frac{m_l}{\rho_l} \right]^K = k_5 C_{isentropic}$ thus introducing an additional unknown parameter m_l , which is modeled using the continuity equation (see Figure 3.20) as $\frac{dm}{dt} = -k_6 \rho_l A_n v_n$ where m is total instantaneous mass of the rocket. At this point, we have neither introduced a new variable nor have any unknown parameters in the latest state equation suggesting that all domains have been captured. Thus, the number of state equations spans the list of domains. Hence, the state equations given by the dimensional graphs are -

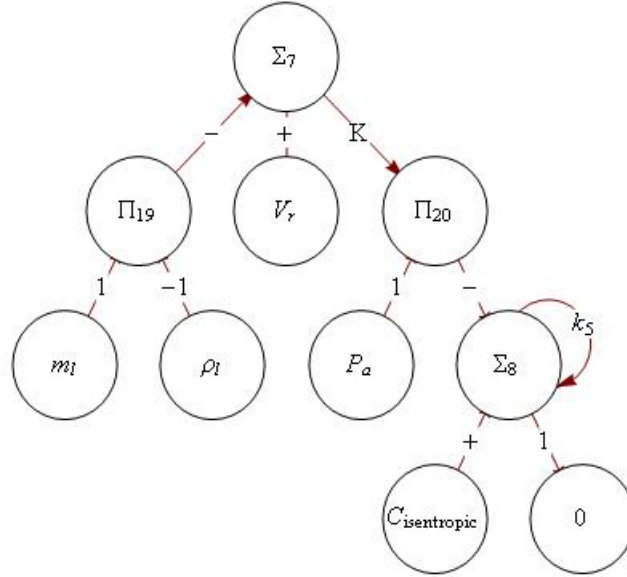


Figure 3.19: Flow graph for isentropic expansion

$$\frac{dv_r}{dt} = k_1 \left(\frac{\rho_l A_n v_n^2}{m} \right) - k_2 g - k_3 \left(\frac{C_d \rho_a A_r v_r^2}{m} \right) \quad (3.82)$$

$$v_n^2 = \frac{k_4 C_N (P_a - P_{atm})}{\rho_l} \quad (3.83)$$

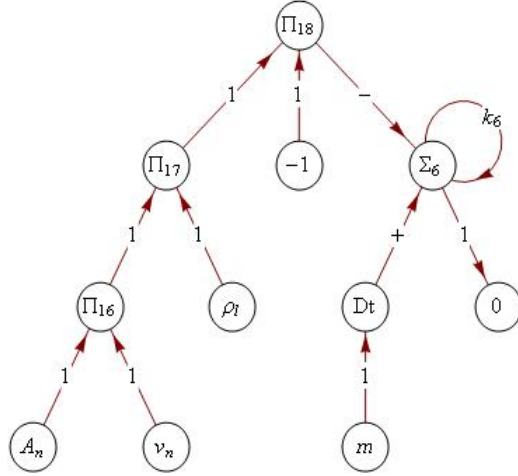


Figure 3.20: Flow graph for continuity

$$P_a \left(V_r - \frac{m_l}{\rho_l} \right)^K = k_5 C_{isentropic} \quad (3.84)$$

$$\frac{dm}{dt} = -k_6 \rho_l A_n v_n \quad (3.85)$$

where the constants are established using the numerical-experimental combination procedure detailed earlier.

A system graph can now be established which is a global scheme where all influencing parameters are accounted for and their interactions with each other are quantified. Such a pictorial representation allows a designer to traverse the graph for nodes which can be tweaked, like geometric constants, and the effect such a manipulation causes in the graph in terms of functional dependence. Since each Π node represents a variable that can be controlled, the global graph presents an opportunity of identifying and isolating key controllable variables so that system response can be adjusted accordingly. Note that a system modeled using n -differential equations would still result in a single system graph with several interactions and such a representation allows for referencing and combining all influencing variables in a single plot unlike traditional approach. Having established the working procedure of graphical

dimensional analysis method and illustrated an example of a dynamic system, the technique is summarized using a flow chart below (see Figure 3.21). The procedure begins with proper identification of different domains influencing the system, for which concerned conservation statements need to be developed. Every term of the conservation statement in each domain is isolated next and a particular graph is generated to model its behavior. All terms are thus accounted for and domain specific conservation statements are graphically modeled to develop parameter graphs that can then be coupled to form a global system graph.

Graphs thus provide visual understanding of engineering principles by simple pictorial representations of complex analytical relations. Combined with dimensional analysis, they offer an alternate evaluation procedure for system dynamics and thus provide diagrammatic insight into working processes of engineering phenomena. As a learning tool, graphs and dimensional analysis illustrate applications of engineering parameters in scientific study of physical systems. The system graph can be coupled with simulator programs to visually model and simulate response of a given mechanical system.

3.8 Summary

This chapter presented two novel approaches in dimensional analysis and their applications in the design evaluation of a dynamic system. Complete with mathematical and visual formulations, the procedures presented a meticulous blueprint for extension into complex systems. The technique of DA though remains largely dependent on experimental data for evaluation of constants and indices. Non-monomial bases problems, when encountered, produce tough similarity challenges which are resolved *only* through experimentation. Realizing this constraint and the need to overcome such challenges motivated the development of Empirical Similitude Method (ESM) which is introduced in the next chapter.

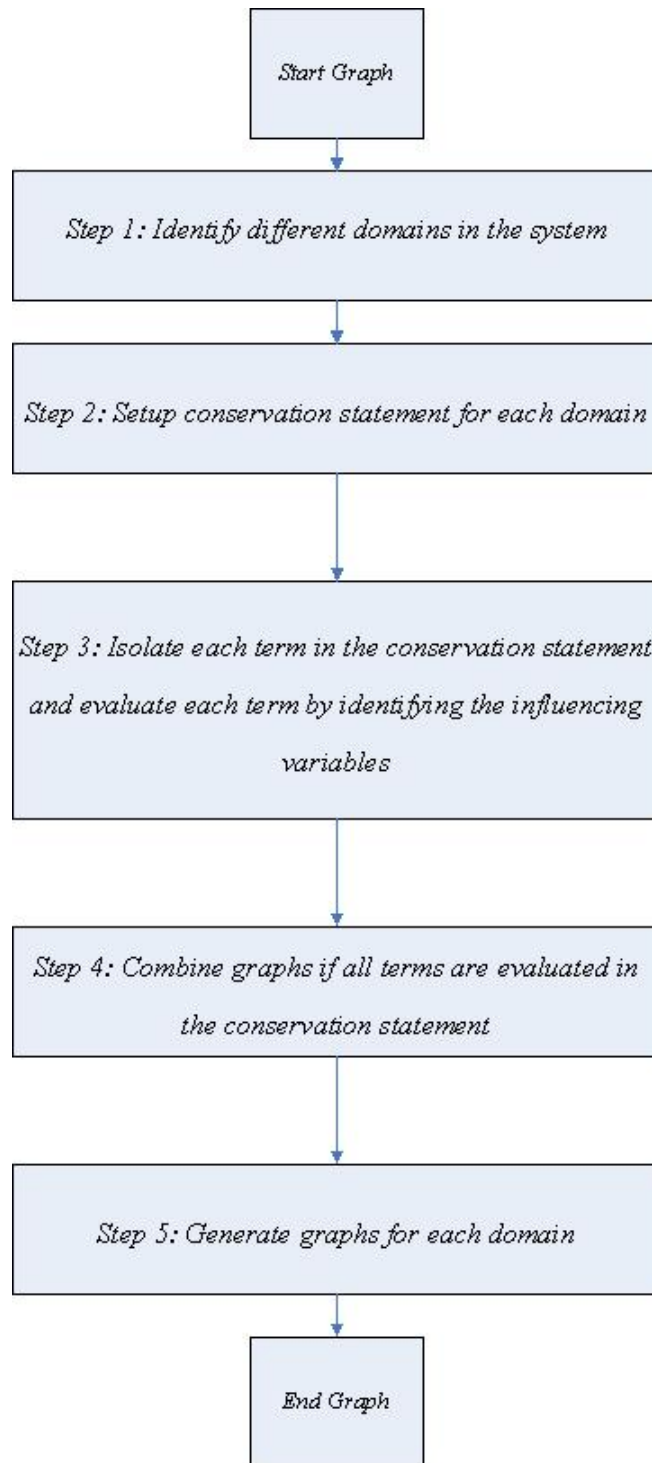


Figure 3.21: Flow chart for graphical dimensional analysis

Chapter 4

Development of Empirical Similitude Method (ESM)

“There is a single light of science, and to brighten it anywhere is to brighten it everywhere.” - Isaac Asimov

The inevitability of experimentation in TSM when non-monomial bases are encountered or in establishing constants for monomial bases is a foregone conclusion. The requirement however compounds when non-linear relationships need to be established involving multiple non-monomial bases necessitating extensive testing. To mitigate the effect of non-linear behavior, the ESM method has been developed and this chapter describes the process motivating *direct* integration of experimental analysis into similitude studies for an empirical approach to similarity methods thereby eliminating need for combining π groups.

4.1 Limitations of TSM

Traditional Similitude Method has provided an initial outlook towards applying dimensional analysis in studying engineering phenomena. However, naturally occurring processes tend to assume complex relationships which are

difficult to capture using techniques and methods described earlier. One such example is illustrated below. Assume that pressure-height relationship needs to be established, commonly referred to as the barometric formula. From classic thermodynamics, the result for a molar mass m and temperature θ^* is given by $P = P_o \exp\left(-\frac{mgh}{R\theta^*}\right)$ [Reiss, 1997] where P_o is base pressure, g is gravity and R is the universal gas constant. Using conventional dimensional analysis,

Table 4.1: Combined matrix for barometric formula

	P	P_o	m	g	h	R	θ^*
M	1	1	1	0	0	1	0
L	-1	-1	0	1	1	2	0
T	-2	-2	0	-2	0	-2	0
θ	0	0	0	0	0	-1	1
π_1	1	0	0	x_1	x_2	x_3	x_4
π_2	0	1	0	x_5	x_6	x_7	x_8
π_3	0	0	1	x_9	x_{10}	x_{11}	x_{12}

$$X = -(A^{-1}B)^T = \begin{pmatrix} 0 & 3 & -1 & -1 \\ 0 & 3 & -1 & -1 \\ 1 & 1 & -1 & -1 \end{pmatrix}$$

or,

$$\pi_1 = \frac{Ph^3}{R\theta^*} \quad (4.1)$$

$$\pi_2 = \frac{P_o h^3}{R\theta^*} \quad (4.2)$$

$$\pi_3 = \frac{mgh}{R\theta^*} \quad (4.3)$$

Assumption of monomial basis gives $\pi_1 = k\pi_2^a\pi_3^b$ or,

$$\frac{Ph^3}{R\theta^*} = k \left(\frac{P_o h^3}{R\theta^*}\right)^a \left(\frac{mgh}{R\theta^*}\right)^b \quad (4.4)$$

Equating indices of like terms gives $a = 1$ and $b = 0$, reducing the relationship to -

$$P = kP_o \quad (4.5)$$

which is illogical. The true basis that needs to be used is $\pi_1 = k\pi_2 e^{-\pi_3}$ which is not a monomial. But development of this basis is not directly intuitive and cannot be done arbitrarily without any engineering relevance. *A priori* knowledge of the physical process is warranted in such situations which is not always available. Technical reasoning is also not conducive in this example as bounds for indices a and b cannot be established for any reasonable argument. The same interpretation holds true for transcendental functions, fractional indices and polynomial combinations which encompass major portion of engineering processes. Non-existence of monomial basis is thus a major shortcoming of TSM. Likewise several other restrictions constrain applicability of TSM, the most important of which are presented below [Cho, 1999, Dutson, 2002] -

- **Product/Model has distortions**

Distortions, in simple terms, are deviations from normalcy and regularity. In similitude studies, these signify conditions when one or more of the similarity constraints and/or prediction equations do not hold in the product and model space. Such distortions occur frequently in similarity methods like in experimental modeling of river flow to predict actual river flow [Taylor, 1974] where depth perspective is lost between the two domains. However such models are economically viable and therefore necessary for similitude. Using distorted models coerces use of distortion (prediction) factors [Murphy, 1950 and Skoglund, 1967] to compensate for the deviation from the actual system. Like before, if

$$\pi_1^p = f(\pi_2, \pi_3, \dots, \pi_n) \quad (4.6)$$

represents a product and

$$\pi_1^m = g(\pi_2, \pi_3, \dots, \pi_n) \quad (4.7)$$

denotes an equivalent model, then for a completely similar system,

$$\pi_1^p = \pi_1^m \Leftrightarrow \pi_i^p = \pi_i^m \quad \forall i \geq 2 \quad (4.8)$$

But for a dissimilar system,

$$\pi_1^p = \delta \pi_1^m \quad (4.9)$$

where δ is the distortion factor and at least one ratio of the π groups scales accordingly *i.e.*,

$$\delta = \frac{\pi_j^p}{\pi_j^m} \quad (4.10)$$

where $j \neq 1$. Needless to say, $\delta = 1$ indicates a system with no distortion. When each π group is affected by individual distortions, then the similarity constraints change to -

$$\delta_j = \frac{\pi_j^p}{\pi_j^m}, j \geq 2 \quad (4.11)$$

and the prediction equation transforms to -

$$\pi_1^p = \Delta \pi_1^m \quad (4.12)$$

where

$$\Delta = \prod_{i=1}^n \delta_j \quad (4.13)$$

To simplify the effect of distortions, a compensated approach [Murphy, 1950] is employed sometimes such that,

$$\Delta = \prod_{j=1}^n \delta_j = 1 \Rightarrow \delta_j = \frac{1}{\delta_k} \quad (4.14)$$

where $j, k \in [1, n]$ and $j \neq k$. However, this approach is time consuming

and complex as constructing distortion factors which are of reciprocal value to the existing distortion factors might not always be feasible. Further, the values of δ can only be obtained from experimentation. For practical purposes, if ϵ was the allowable error (numerically small), then $|\delta - 1| = \epsilon$ would imply a completely similar system, $|\delta - 1| > \epsilon$ would indicate a semi-similar system and $|\delta - 1| < \epsilon$ would signify a quasi-similar system, all of which have engineering relevance and applications [Skoglund, 1967].

It is important to note that most distortions can be identified and quantified. The most common forms of distortion are shown below (see Figure 4.1). Bear in mind that this list is not comprehensive but is the best compilation thus far. The major distortions can be categorized into primary (see Figure 4.2), secondary and tertiary (see Figure 4.3) distortions. The primary distortions are due to geometry, material forms, time scales involved, input and initial and boundary conditions which signify the deviation in structure, shape and state. The secondary distortions are due to the modeling and numerical schemes employed that capture the variation due to physical phenomena, identification of right system parameters and solution strategy used. The tertiary distortions arise from experimental vagaries caused by discrepancies due to instrumentation, resolution and parallax. These distortions can be further classified as shown below.

- **Product has material non-linear responses**

One of the important advancements in modern products is the use of lightweight structures that yield comparable strength as metal compounds. These structures typify plastic, ceramic, composite and polymer usage to produce highly durable and environmentally safe products while not compromising on the health and safety standards. While this has been an important achievement, scaling from a similitude perspective is affected as typical polymer based compounds exhibit non-linear mechan-

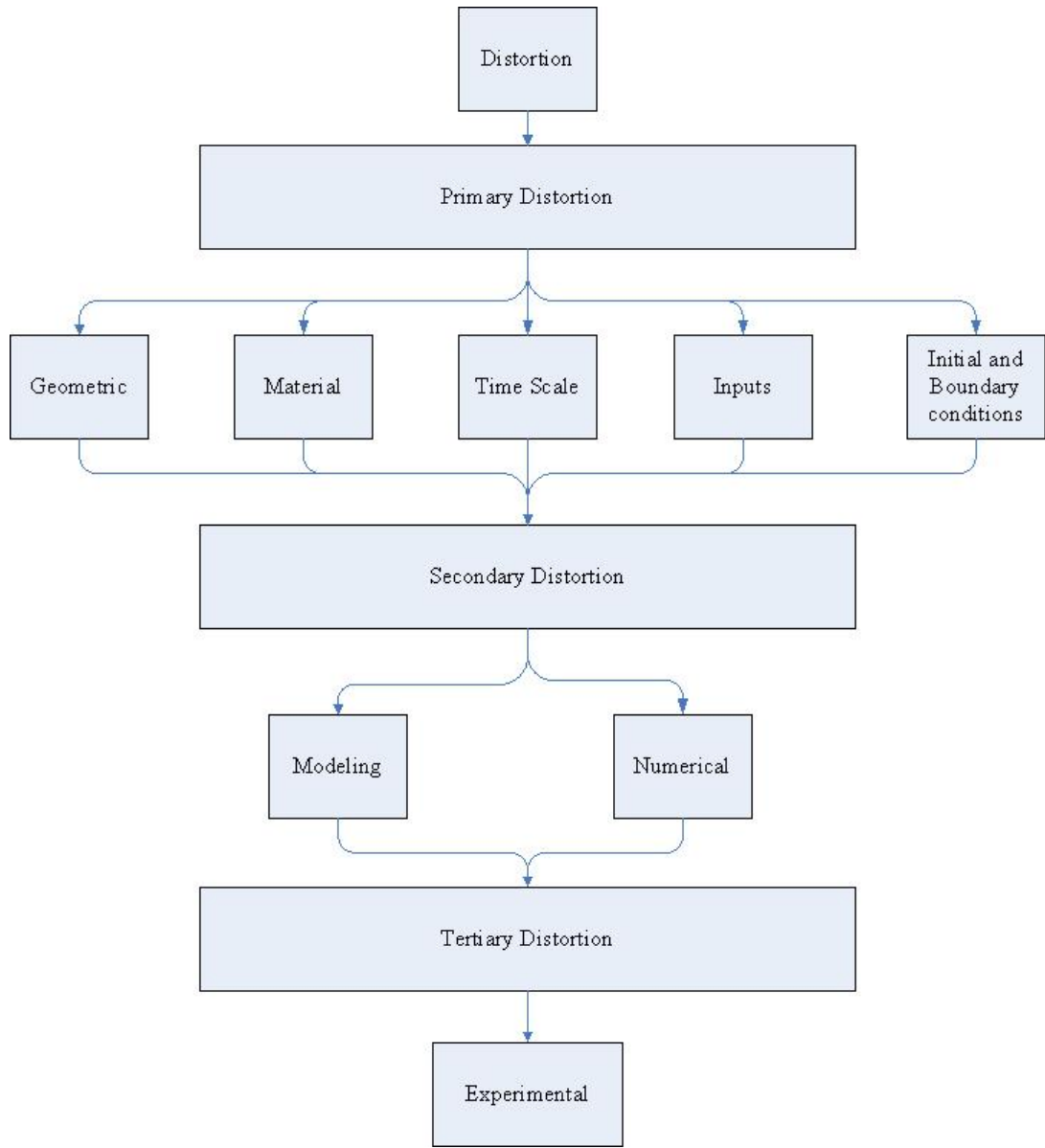


Figure 4.1: Distortions in engineering systems

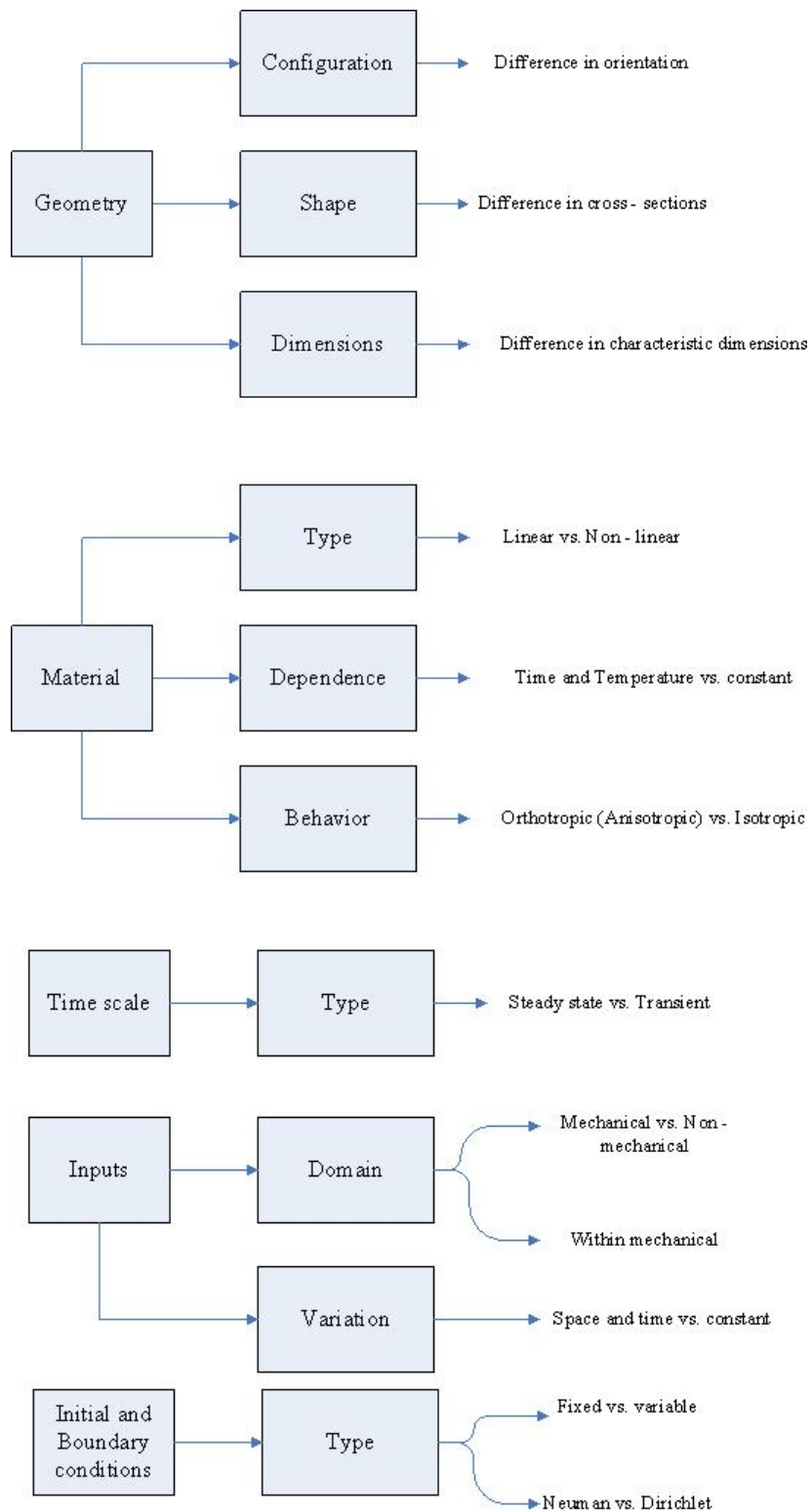


Figure 4.2: Detailed primary distortions

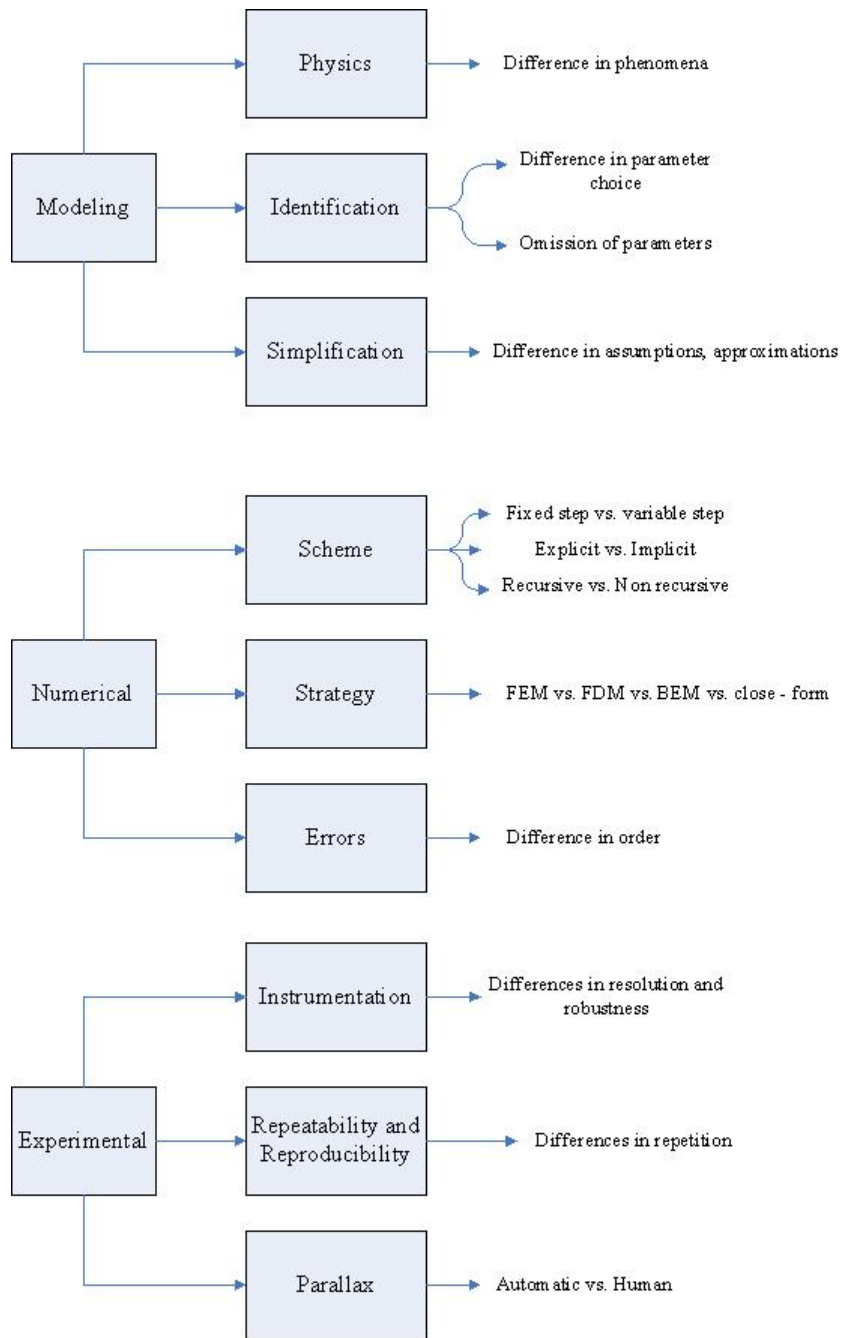


Figure 4.3: Detailed secondary and tertiary distortions

ical behavior. Developing a model to capture such non-linear behavior in a product would necessitate the use of the exact same material that the product is made of, which might not always be economical either in production or experimentation. Also in the scaled model space, elastic and plastic regions cannot be ensured to remain exactly the same as in the product (see Figure 4.4).

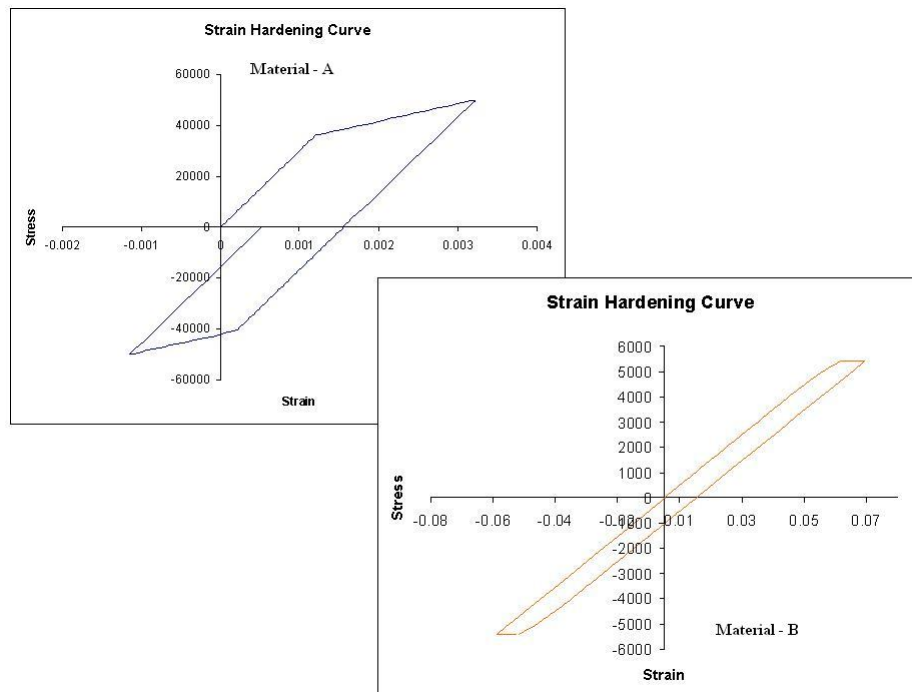


Figure 4.4: Dissimilarity in material response

- **Product has multiple materials**

A typical product these days incorporates benefits of multiple material usage to devise a design that is optimal in terms of weight and cost while providing the required functionality. Such products are hard to scale into a model form as every material needs to be appropriately scaled forcing the model to be made of the same set of multiple materials as well which again is redundant from a manufacturing and cost stand point. On

the contrary, using a single material form in the model to capture the characteristics of all the materials in the product would be an engineering nightmare as such an approximation is extremely difficult and unreliable due to temperature and time dependencies (see Figure 4.5).

Plastic fan



Fibreglass board

Metal casing

Figure 4.5: Product with multiple materials - The CPU of a computer

- **Product has variable inputs and, initial and boundary conditions**

If the product P is influenced by a set of inputs $\{q_i\}_{i=1}^n$ with initial and boundary conditions IC_1 and BC_1 , then

$$P = f(q_1, q_2, \dots, q_n) + IC_1 + BC_1 \quad (4.15)$$

If the inputs are functions of time, then,

$$P(t) = f(t, q_1, q_2, \dots, q_n) + IC_1 + BC_1 \quad (4.16)$$

where $q_i \equiv q_i(t)$. To develop a model synonymous with the product would necessitate,

$$M(t) = g(\lambda t, \lambda q_1, \lambda q_2, \dots, \lambda q_n) + \lambda IC_1 + \lambda BC_1 \quad (4.17)$$

where $\lambda \neq 0$. Since $q_i(t)$ is not necessarily identical to $q_j(t)$, the scaling factor λ would itself be a function of time and $\lambda(t)M(t) = P(t)$ would not be necessarily true. Hence, a variation due to time dependency is created causing a time scale deviation or $\left(\frac{q_i}{q_j}\right)_P \neq \left(\frac{q_i}{q_j}\right)_M$ and TSM does not hold.

- **Product has space and time varying properties**

Consistent with the previous condition, if the product P has system (material) properties that change with time and space (viscoelastic, anisotropic and orthotropic) material, then product to model scaling assumes highly intricate relationships and a simple scale is not feasible. If

$$P = f(G, m(x, y, z, t)) \quad (4.18)$$

and

$$M = g(G, m(x, y, z, t)) \quad (4.19)$$

then for TSM to hold, $\left(\frac{G_P}{G_M}\right)$ must be equal to $\left(\frac{m_P}{m_M}\right)$, which would not always hold true as the material dependencies in both geometries need not be identical as time and space constraints offer variable responses in the same material.

- **Product to model scaling is not uniform or constant**

Building on the two previous conditions, if analysis does yield a scale that is time invariant and constant, then there is no guarantee that the scale would be uniform in the entire working domain of both geometries, *i.e.*,

$$\frac{q_1^P}{q_1^M} = \frac{q_2^P}{q_2^M} \neq \frac{q_3^P}{q_3^M} \quad (4.20)$$

- **Product behavior has no or complex governing equation**

Many products exhibit extremely complex behavior where responses can be evaluated only numerically using computational power built on massive algorithms and numerous assumptions and approximations. This implies that a closed-form solution does not exist or is extremely intricate and time consuming to estimate. In such cases, using a model for the physical process in question would not be advisable as a complex phenomenon is being observed whose influencing parameters are either unknown or not captured completely.

- **Product has no realizable simple model**

Assuming that the product does exhibit a known physical characteristic, it is sometimes not possible to build a simple model consistent in scale in all parameters, due to sheer size or cost limitations. TSM in such situations becomes a luxury rather than a feasible tool. A building can have a scaled model but analysis on the scaled model would not necessarily translate to the building as the scaling effects need to be consistent in all affecting parameters.

- **Parameters have no realizable experiment**

If the product does have a realizable model but is being analyzed for a process whose parameters or constants cannot be verified using a conceivable experiment, then using TSM does not offer any advantage as no conclusive results can be derived due to lack of experimental evidence.

- **Experimentation has unrealistic time scale**

If an experiment can be conjured to verify the scaling results between the model and the product, then it is extremely important to ensure that the time scales involved are realistic *i.e.*, if the scale in geometry (G) and material characteristics (m) do turn out to be consistent but generate a scale that is numerically not finite, then experimentation needs to be done using extremely fast or slow time scales (T) which is not technically viable. If $P_P = f(G, m, T)$ and $P_M = g(G, m, T)$ and a common scale

of 10^6 is produced in geometry and material, then scaling uniformity in TSM requires that $\frac{T_P}{T_M} = 10^6$ which might not be physically achievable due to experimental constraints like resolution and instrumentation capabilities.

The existence of such variations and deviations in industrial systems and products, and the associated difficulty in modeling and simulating such systems for functional validation has uncovered options for exploring uncharted research territories, specially in similarity methods. Broadening the reach of experimental similitude models, the ESM method developed to address the above concerns is motivated in the next section clarifying the driving principle and associated geometries.

4.2 Motivation for ESM

Several problems in engineering realm pose modeling and simulation difficulty due to severe non-linear behavior and debilitating singular or stiff conditions that act as additional impediments. In many such instances advanced numerical schemes are employed to either relax or simplify the PDE that defines the physical process to obtain reasonable output from the simulation. The assertion behind such a simplification is the existence of a PDE, which is not always guaranteed. Further, most technical problems encountered in industrial systems have complex interactions of sub-systems and components unlike conventional problems in the academic world. Analyzing the behavior of a system with a network of components requires multifaceted approximations to reasonably simplify the modeling effort. More often than not, a dominant phenomenon is isolated that captures a major segment of the system response without compromising the integrity of the governing dynamics of the associated physical process. Such a simplification cannot be achieved with considerable ease and requires numerous approximations and assumptions. This feature is more profound in product design, especially in the evolution phase of the product when the geometry is still hypothetical.

When a design needs to be qualified parametrically [Otto et al., 2001], the system has to be evaluated mathematically using a procedure that is both accurate and robust. Such a procedure must also encompass uncertainty indicators and error definitions for the designer to take advantage of, to maintain rigorous quality and reliability standards. Keeping in mind that most modern designs are intricate in geometry and are manufactured from multi-material composites or involve multiple material effects, any traditional effort like bond graphs [Karnopp et al., 2006] or Finite Element Methods (FEM) [Becker et al., 1981] necessitate increased graphical and computational effort. The Empirical Similitude Method (ESM) [Cho, 1999] thus provides an alternate evaluation practice that directly combines the physical experimental data with the scaling parameters superseding the need to model the physics of the system *i.e.*, the PDE of the system.

Much of the development of ESM has been motivated by the premise of forging a relationship between experiential information and physical systems that have inherent non-linear variables and factors affecting their response. Considering the fact that the applicability of TSM process is determined by the ability to determine the constants and the exponents of the scaling factors [Szirtes, 1998], the technique is limited by the degree of non-linearity and independence of the affecting geometric and material variables. While some headway can still be expected using more advanced methods like those described earlier, the associated experimental and computational effort also compounds relatively. In an effort to ease this effort, the ESM process [Cho, 1999] was developed that simplified the conversion by disassociating geometry and material properties and provided a means for independent and individual scaling. ESM thus provides relief by,

- Simplifying the analysis effort by incorporating scaling methods using experimental data thus nullifying the need to generate a PDE of the system dynamics.
- Accurately mapping realistic test information rather than simulating

conditions which are unreliable without experimental evidence.

- Eliminating the need to formulate complex analytical relationships for any parameter of interest.
- Providing direct numerical values and trends for the parameter of interest with minimal computational simplification.
- Developing methods and techniques that use robust numerical schemes to produce infallible prediction results.

Thus we skip the conventional top-down modeling effort (PDE - Numerical Solution - Experimental Verification) and venture directly into the experimental phase for the required parameter of interest. Shown below is an illustration of the working domains of each process (see Figure 4.6).

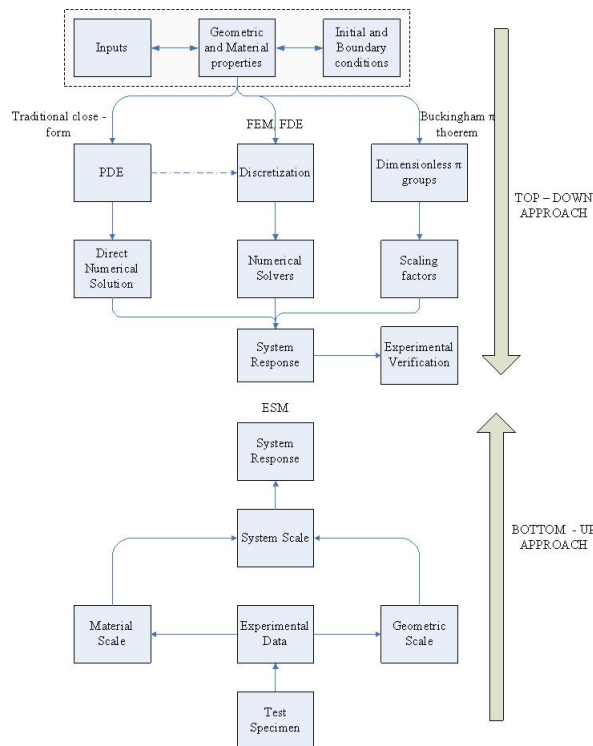


Figure 4.6: Different approaches of system modeling

Note that in all approaches we are interested in estimating hypothetical product behavior. Further, notice that ESM employs intermediate specimen to estimate individual and independent geometric and material scales. The reason for such an assumption stems from the idea that these two scales can be combined to form a comprehensive system scale [Cho, 1999 and Dutson, 2002]. The need for two different scales arises from the fact that has been adhered to in the earlier part of this chapter - that of intricate geometries and multi-material effects. In essence, we thus seek a geometry called the product specimen (*ps*) that is a simplification of the product (*p*) geometry while retaining the same material form, and another geometry called the model specimen (*ms*) that is of the same geometry as the product specimen but of another material form. Like in the original Buckingham π theorem, the model (*m*) is retained to be a scaled version of the product but is now of the material form that the model specimen is comprised of. In total, we hence have three test specimens instead of just one as in the Buckingham π theorem.

To further the benefit of ESM, typically, the model and the model specimen are fabricated using rapid prototyping (RP) processes and are thus impervious to intricate geometric features. Development of rapid prototyping (RP) techniques have allowed for the fabrication of the most intricate designs. Any complexity desired in the product's geometry can still be incorporated in the model due to rapid prototyping to thus generate a true representation and simplification of the product. Using the leverage that Selective Laser Sintering (SLS) and other RP processes have provided, geometric constraints not being an impediment, similitude models can be developed for certain material forms like polymers and soft metals. These models can then be extended to incorporate behavior of common engineering materials and systems. The primary motivation therefore, is to couple the advantage of precise fabrication with testing, to enhance similarity studies. Similar work using rapid prototyping specimen has been done earlier with considerable success in the industrial arena [Dornfeld, 1995 and Farrar et al., 1994]. Shown below is an illustration of the ESM process (see Figure 4.7) using all inherent geometries followed by

the mathematical description of the process and initial system evaluation.

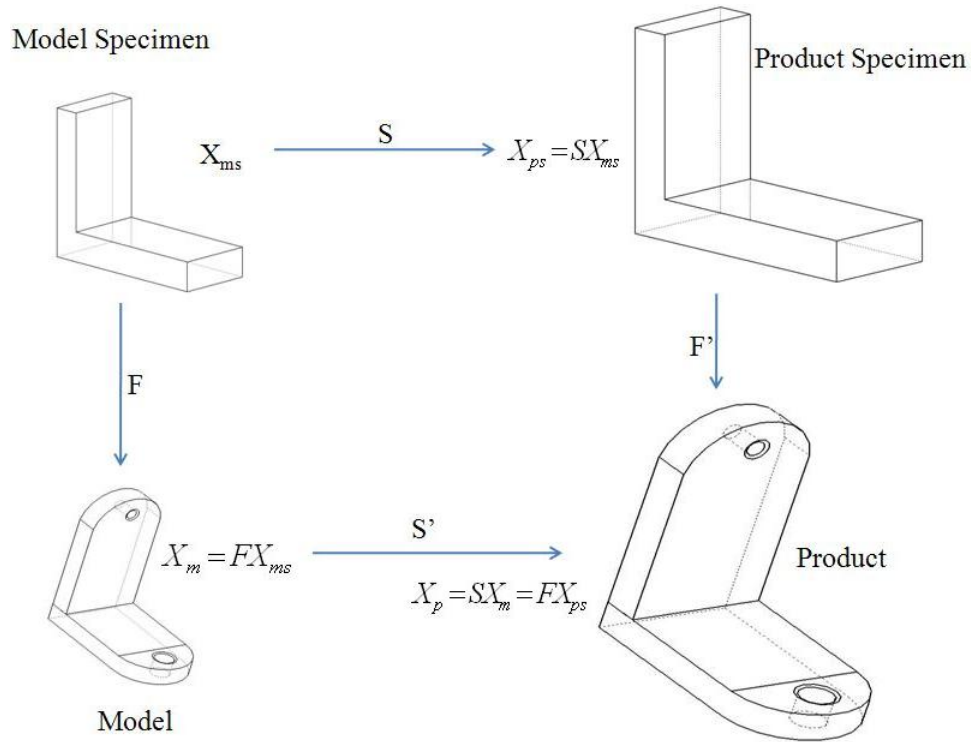


Figure 4.7: ESM process

4.3 Method and Systems in ESM

The main hypothesis of ESM is to assume that the prediction equation for any parameter of interest P can be written as -

$$P = f_1(F) * f_2(S) \tag{4.21}$$

for null boundary and initial conditions, and steady-state analysis. Put in a mathematical form, the method assumes that the geometric (*form* F) and the material properties (*scale* S) are not interrelated. [Wood, 2002] gave another

expression by modifying the relation to -

$$P = f_1(F) * f_2(S) + R(F, S) \quad (4.22)$$

where $R(F, S)$ represents the error in the system which needs to be minimized with an appropriate choice of f_1 and f_2 . The idea behind this method is to use the original mapping theorem (Buckingham π theorem) as a two stage process rather than one, where the two stages account for the individual and independent scaling of geometry and material. Such a simplification allows for the product state vector to be interpreted as -

$$x_p = f(x_m, x_{ms}, x_{ps}) \quad (4.23)$$

where the state vectors of the model specimen, the model, the product specimen and the product are respectively given by x_{ms} , x_m , x_{ps} and x_p . The parameters F and S are matrices that capture the geometry (*form*) and the material (*scale*) changes in the system. The product of these two matrices is the net system transformation. This allows for the evaluation of the product response at every point i in its domain based on the values in the other three geometries measured at the same corresponding point. Such an evaluation thus circumvents the necessity to obtain a governing equation to describe the engineering process and focuses on the estimation of the parameter through experimental (more realistic) and numerical transformations. Hence, the *scale* equation takes the form given by,

$$x_{ps} = Sx_{ms} \quad (4.24)$$

and the *form* equation is written as -

$$x_m = Fx_{ms} \quad (4.25)$$

The product is assumed to have a variation *w.r.t* the model that is sim-

ilar to the above equation and hence the prediction equation is now developed to be -

$$x_p = Fx_{ps} = Sx_m = (S \times F)x_{ms} \quad (4.26)$$

and from symmetry,

$$x_p = (F \times S)x_{ms} \quad (4.27)$$

The ability to make an accurate prediction for the product state vector is dependent now on the precise evaluation of the square matrices S and F . The model and the model specimen combine to indicate the geometric change (the material is constant between the two) referred to as the form matrix (F) of ESM. The model specimen and the product specimen couple to capture the material transition (the geometry is constant between the two) referred to as the scale matrix (S) of ESM. The assumption of independence and symmetry of operation allows us to define $S \times F$ as the system matrix that has both geometric and material information imbibed in it. But the two important queries that need unequivocal response are - what systems follow ESM procedure and, what features and properties do they share that allows them to have said correspondence with ESM. The answer, an important outcome of this research, is provided below.

“Any physical system, mechanical or otherwise, that violates TSM in one or more of the ten criteria mentioned earlier and cannot be suitably scaled using either monomial or non-monomial bases (with experimentation) even after including distortion factors, is a potential candidate for ESM”.

As a consequence, an important and noteworthy insight is that ESM is thus applicable at the product level and at the component level with varying degrees of detail and difficulty. Consider some of the earliest examples modeled using ESM [Cho, 1999 and Dutson, 2002], a heat sink, an archery bow and head phones. These products exhibit non-linear transient response owing to material properties that are characteristically non-linear, have structural and functional distortions (conduction and convection convoluting in the heat

sink example), are relatively complex and have no realistic governing equation for their respective parameter of interest. The analysis performed thereafter categorically proves that ESM outperforms TSM in terms of accuracy [Cho, 1999].

However, the examples discussed above do not offer a robust reasoning for their correspondence with ESM. Building on their working processes and physical relations, the following principles of ESM are offered as more rigorous guidelines. These principles are another important consequence of this research as they constitute the first ever documentation of such rules.

4.4 Principles of ESM

1. Principle of complete and unique correspondence

The fundamental principle of ESM requires that “*Two different structures and material forms sharing similar inputs and output parameters of interest that are measurable, with the expectation of a finite numerical value from a possibly feasible experiment, will scale uniquely and completely at every well-defined point in the domain relaying information consistent with geometry and material that the structures are comprised of (See Figure 4.8).*”

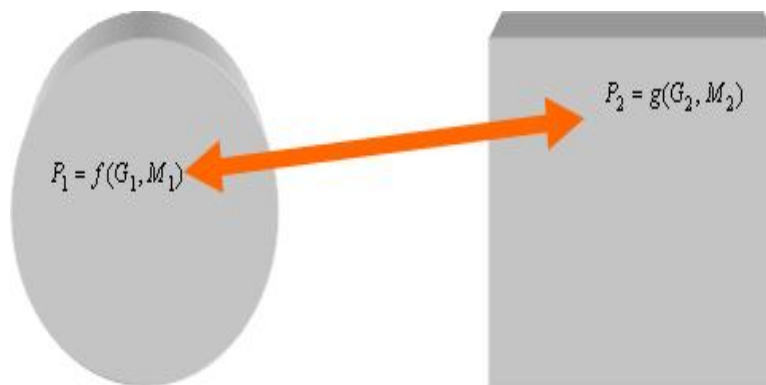


Figure 4.8: Unique mapping between two distinct geometries

2. Principle of simplified representation

Every complex mechanical product with distortions, can be represented by a simpler yet representative structure that models the system by either changing or retaining geometric attributes that signify similar yet simplified shapes (See Figure 4.9).

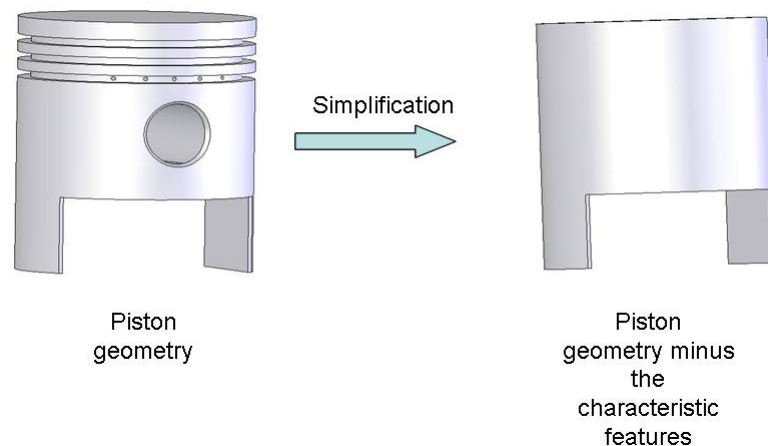


Figure 4.9: Simplified representation of a piston

3. Principle of manufacturability

Every geometry referred to as a specimen, which is supposed to characterize a complex object, can only be termed representative iff it is impervious to manufacturing constraints. It is thus finite in size, has known quantifiable material characteristics and can be physically manifested.

4. Principle of experimentation

Empirical similarity induces the existence and validity of a conceivable experiment that generates the required test data for the parameter of interest. Alternately, ESM applies to those parameters that can be estimated by direct experimentation or further manipulation of experimental data. Strain can be measured while strain energy is a manipulated quantity.

5. Principle of measurability

As a consequence of the principle of experimentation, the principle of measurability ensures that if an experiment can be devised that is repeatable and reproducible for a parameter of interest, then there exists enough control and instrumentation to gauge the response or the numerical reading of the parameter of interest within accepted error bounds. No geometric impediment exists in physically recording the required reading.

6. Principle of mathematical transformation

A set of finite numerical values with or without any apparent trend or pattern in ESM can be transformed to a different domain for computational ease without losing any relevant engineering information in the transfer.

These principles thus form the core ingredients of the ESM process. Every system or product that follow these principles will allow for ESM evaluation as was alluded to in the examples introduced earlier. Many more examples are offered and studied in subsequent chapters that relate to the ESM process based on their agreement with the principles mentioned above. Presence of distortions in physical systems and the working principles of ESM thus stimulated the advent of the technique and is the underlying reason why ESM enjoys considerable accuracy over TSM when such systems are analyzed. Building on this development, the following section seeks to quantify these distortions for a numerical estimate of similarity in solution.

4.5 Quantifying Similarity and Distortion in ESM

Recall that the prediction equation in ESM is $x_p = (S \times F)x_{ms}$ and that the matrix $(S \times F)$ is square since the matrices S and F are square. These matrices are representative of the change or the transformation that has occurred

in the system in terms of geometric alteration and material adaptation. They carry numerical information indicative of such a transformation and using established properties of matrices allows us to define estimates that qualify and quantify the transformation. Let $\| \bullet \|$ indicate *norm*¹ of a matrix A , Frobenius in particular given by [Dunford et al., 1958],

$$\| A \|^2 = \sum_{i=1}^n \sum_{j=1}^n A_{ij}^2 \quad (4.28)$$

and let $T \equiv (S \times F)$. The Frobenius norm is chosen to account for possible negative values in the matrix T . [Wood, 2002] gave an elegant expression where the matrix T is split into a diagonal matrix D (called the similarity matrix) and a perturbation matrix δD (called the distortion matrix) such that,

$$T = D + \delta D \quad (4.29)$$

$$D = \{T_{ii}\}_{i=1}^n \quad (4.30)$$

$$\delta D = T - D \quad (4.31)$$

The objective now is to establish D and δD such that similarity is maximized and distortion is minimized whose measures are respectively given by,

$$\textit{similarity index} = \sum_{i=1}^n D_{ii}^2 \quad (4.32)$$

$$\textit{distortion} = \frac{\sum_{i=1}^n \sum_{j=1}^n \delta D_{ij}^2}{\sum_{i=1}^n D_{ii}^2} \quad (4.33)$$

$$\textit{similarity} = 1 - \textit{distortion} \quad (4.34)$$

Notice that greater the value of the norm in the similarity matrix D implies greater correspondence in the system and lesser distortion. The only limitation of the process though, is in setting up the matrix D whose diagonal

¹Norm in \Re^2 signifies length or distance [Finkbiener II, 1978].

elements have to be all numerically equal, which is not certain. Hence, the choice of the matrix D has been arbitrary as in the example illustrated below [Wood, 2002]. To account for this limitation, a slightly modified expression is suggested that retains the original strength while injecting robustness into the estimation -

$$T = D + \delta D \quad (4.35)$$

$$D = \{mean(\{T_{ii}\}_{i=1}^n)\}_{i=1}^n \quad (4.36)$$

$$\delta D = T - D \quad (4.37)$$

For a hypothetical matrix [Wood, 2002] given by,

$$T = \begin{pmatrix} 3.5 & -0.033 & -0.067 & -0.1 & -0.133 \\ 0 & 3.517 & 0.033 & 0.05 & 0.067 \\ 0 & 0.033 & 3.567 & 0.1 & 0.133 \\ 0 & 0.017 & 0.033 & 3.55 & 0.067 \\ 0 & -0.033 & -0.067 & -0.1 & 3.367 \end{pmatrix}$$

and an arbitrary choice of 3.5 for the diagonal element generates,

$$D = \begin{pmatrix} 3.5 & 0 & 0 & 0 & 0 \\ 0 & 3.5 & 0 & 0 & 0 \\ 0 & 0 & 3.5 & 0 & 0 \\ 0 & 0 & 0 & 3.5 & 0 \\ 0 & 0 & 0 & 0 & 3.5 \end{pmatrix}$$

and

$$\delta D = \begin{pmatrix} 0 & -0.033 & -0.067 & -0.1 & -0.133 \\ 0 & 0.017 & 0.033 & 0.05 & 0.067 \\ 0 & 0.033 & 0.067 & 0.1 & 0.133 \\ 0 & 0.017 & 0.033 & 0.05 & 0.067 \\ 0 & -0.033 & -0.067 & -0.1 & -0.133 \end{pmatrix}$$

while the modified robust definition gives,

$$D_{modified} = \begin{pmatrix} 3.5002 & 0 & 0 & 0 & 0 \\ 0 & 3.5002 & 0 & 0 & 0 \\ 0 & 0 & 3.5002 & 0 & 0 \\ 0 & 0 & 0 & 3.5002 & 0 \\ 0 & 0 & 0 & 0 & 3.5002 \end{pmatrix}$$

and

$$\delta D_{modified} = \begin{pmatrix} -0.0002 & -0.033 & -0.067 & -0.1 & -0.133 \\ 0 & 0.0168 & 0.033 & 0.05 & 0.067 \\ 0 & 0.033 & 0.0668 & 0.1 & 0.133 \\ 0 & 0.017 & 0.033 & 0.0498 & 0.067 \\ 0 & -0.033 & -0.067 & -0.1 & -0.1332 \end{pmatrix}$$

The corresponding values for similarity and distortion measures are given in Table 4.2. Notice that marginal improvement is achieved but lot more robust definition is created that eliminates arbitrariness in estimation. It is important to note that in the development of these measures, the distortion matrix had elements that are numerically smaller than the similarity matrix thus providing greater similarity index and consequently lesser distortion. However, in the development of these matrices, if the magnitude of the off diagonal elements surpass the mean of diagonal elements then the two matrices are switched. This ensures that similarity and distortion measures are always less than one irrespective of the magnitude of the off diagonal elements. Hence, in special situations when off diagonal elements gain numerical precedence over the mean of diagonal elements, the similarity matrix assumes the role of the distortion matrix and vice versa. Such situations arise when interactions between elements are considerable as will be apparent in examples provided later. These measures of similarity and distortion are also used later in the report in conjunction with methods of scaling in linear range.

Table 4.2: Similarity and distortion measures

Analysis	Similarity	Distortion
<i>Prior</i>	99.809739%	0.190261%
<i>Modified</i>	99.809761%	0.190239%

4.6 Summary

Expanding on TSM, this chapter has introduced the ESM process complete with limitations of TSM leading to the development of ESM, the hypothesis of ESM and the method of usage in some preliminary systems together with improvements acquired thereby answering the *what*, *why* and *when* of the process. More importantly, illustrating each restriction, the constraints of TSM have been discussed in great detail. The first known principles of ESM have been developed to vindicate the empirical approach. A final analytical treatment of similarity and distortion measures has also been presented. The next chapter uses this development, providing the *how* of the process.

Chapter 5

Linear Methods

“A sense of curiosity is nature’s original school of education.” - Smiley
Blanton

The essence of similitude in traditional and empirical settings has been established thus far. This chapter augments the technique by providing a mathematical structure for the process and its applications in the linear range. Several methods have been adopted for scaling in linear ESM [Dutson, 2002 and Cho, 1999 and Wood, 2002] and have provided valuable insights into the underlying engineering phenomena. To invoke these methods, *a priori* knowledge of the probable linear response of a certain product or design is required. This vital piece of information can be extracted from the test data of the specimens and the model. The trends and the distribution of the experimental results are pretty good indicators of the expected response of the product as all inherent affecting factors (geometry, material and boundary conditions) are accounted for. Robust statistical procedures also exist that lend analytical credibility to the linearity assumption. Thus, the main motivation in this chapter is to define linear range of operation, employ and compare linear ESM methods to analyze mechanical systems and document enhancement attained using modern numerical solvers.

5.1 Test for Linearity-Statistical Procedures

Analyzing a parameter in a hypothetical product assumed to behave in the linear range requires mathematical evidence corroborating such trend. Remember that only the test data from the specimens and the model is available and establishment of linearity in these data points suggests linearity in the hypothetical product too. Consider for lucidity,

$$X_{ms} = \begin{pmatrix} 1.0 \\ 2.0 \\ 3.0 \\ 4.0 \\ 5.0 \end{pmatrix}, \quad X_{ps} = \begin{pmatrix} 2.0 \\ 4.0 \\ 6.0 \\ 8.0 \\ 10.0 \end{pmatrix}, \quad X_m = \begin{pmatrix} 3.0 \\ 6.0 \\ 9.0 \\ 12.0 \\ 15.0 \end{pmatrix}$$

which gives,

$$X_{ps} = 2X_{ms} \tag{5.1}$$

$$X_m = 3X_{ms} \tag{5.2}$$

and linearity is confirmed thereby validating $X_p = 2X_m = 3X_{ps} = 6X_{ms}$. This process is not robust though as data points are seldom integers and developing the preceding equations is not usually trivial. Establishing linearity in complex problems necessitates more rigorous mathematical processes that encompass all possible variations in the real number system.

Consider the same matrices for illustration. Two statistical tests are introduced that test pairs of data points for possible linear relation and the degree of such relationship. In essence, the correspondence of two independent variables is being tested to understand if any plausible linear relationship can be derived with a certain degree of confidence. It is therefore imperative that

the data collected be independent for a bivariate¹ correlational statistic to be developed. The two tests described below are chosen as measurements are nominal² and independent.

- **Pearson's product-moment correlation coefficient**

The most common correlation index is the Pearson's coefficient [Spiegel, 1992] given by,

$$r = \frac{(\sum XY) - \left(\frac{\sum X \sum Y}{N}\right)}{\sqrt{(\sum(X^2) - \frac{(\sum X)^2}{N})(\sum(Y^2) - \frac{(\sum Y)^2}{N})}} \quad (5.3)$$

where X and Y are the two independent variables and N is the number of measurements. Note that the Pearson's test assumes linearity between the two variables and a correlation value of 1 or -1 indicates perfect positive or negative linearity and 0 represents no linear relation between the two variables. Values are very rarely 1, -1 or 0 but closer the value of the coefficient to the value of 1 greater the accuracy of the linearity assumption. Hence r^2 indicates the degree of variation in the estimation which can be interpreted as the measure of variability caused in the variable Y due to the variation in X . Note also that a value much lesser than 1 *only* signifies non-existence of a linear relationship but does not discount the possible existence of a non-linear relationship. This test is simple and for a limited number of observations like in ESM, it is quite practical for establishing and using the linear methods. For the matrices defined above,

$$\sum X_{ms} = 15; \sum X_{ps} = 30; \sum X_m = 45 \quad (5.4)$$

$$\sum X_{ms}X_{ps} = 110; \sum X_{ms}X_m = 165 \quad (5.5)$$

$$\sum X_{ms}^2 = 55; \sum X_{ps}^2 = 220; \sum X_m^2 = 495 \quad (5.6)$$

¹Two independent variables.

²Measurements can be nominal, ordinal, interval or ratio [Stevens, 1946].

$$r(X_{ms}, X_{ps}) = 1 \quad (5.7)$$

$$r(X_{ms}, X_m) = 1 \quad (5.8)$$

indicating a perfectly linear relationship.

- **Spearman's rank correlation coefficient**

The Spearman's test unlike the Pearson's test does not assume a linear relationship between the variables X and Y . This test is based on an ordinal scale where measurement values are ranked in order of magnitude and assumes equidistant intervals between the rankings [Edwards, 1976]. Hence, if multiple values have same magnitude, then Pearson's test becomes more lucrative as this test gives a monotone association. The Spearman's rank correlation coefficient is given by,

$$\rho = 1 - 6 \sum \frac{d^2}{N(N^2 - 1)} \quad (5.9)$$

where d is the statistical rank for all N measurements. A value closer to 1 indicates an accurate linear relationship while a value close to 0 indicates lack of any such linear relationship. Bear in mind that the validity is only being tested for linearity and does not in any way account for possible non-linear associations. For the matrices defined above, the rank table is generated (see Table 5.1) between the model specimen and the product specimen. A similar table is defined using the model specimen and the model (see Table 5.2).

Table 5.1: Spearman's test for X_{ms} and X_{ps}

X_{ms}	X_{ps}	$rank(X_{ms})$	$rank(X_{ps})$	d	d^2
1.0	2.0	1	1	0	0
2.0	4.0	2	2	0	0
3.0	6.0	3	3	0	0
4.0	8.0	4	4	0	0
5.0	10.0	5	5	0	0

which gives,

$$\rho(X_{ms}, X_{ps}) = 1 - 6 \times 0 = 1 \quad (5.10)$$

Similarly,

Table 5.2: Spearman's test for X_{ms} and X_m

X_{ms}	X_m	$rank(X_{ms})$	$rank(X_m)$	d	d^2
1.0	3.0	1	1	0	0
2.0	6.0	2	2	0	0
3.0	9.0	3	3	0	0
4.0	12.0	4	4	0	0
5.0	15.0	5	5	0	0

which also leads to -

$$\rho(X_{ms}, X_m) = 1 - 6 \times 0 = 1 \quad (5.11)$$

thereby indicating perfectly linear relationships. For ESM, these two techniques are sound indicators for the usage of linear methods as linear or near linear values in the coefficients are employed to gauge the applicability of linear methods described in the next section.

5.2 Linear ESM Methods

The ESM equation $x_p = (S \times F)x_{ms}$ represents a classic problem in linear algebra similar to $Ax = B$ with minor modifications. In the conventional form, the matrices A and B are respectively square and column and hence well defined. In the ESM equation, the known matrices x_{ms} , x_{ps} and x_m are column vectors that need to be coupled in the forms mentioned above. It is however known that the scale and form matrices S and F have to be square for mathematical correctness.

$$[x_{ps}]_{n \times 1} = [S]_{n \times n} [x_{ms}]_{n \times 1} \quad (5.12)$$

$$[x_m]_{n \times 1} = [F]_{n \times n} [x_{ms}]_{n \times 1} \quad (5.13)$$

$$[x_p]_{n \times 1} = ([S]_{n \times n} \times [F]_{n \times n}) [x_{ms}]_{n \times 1} \quad (5.14)$$

Several methods have been embraced in establishing elements of the matrices S and F which are then used subsequently in the prediction equation $x_p = (S \times F)x_{ms}$. The first two equations (5.12 and 5.13) thus represent similarity constraints in ESM and together with the prediction equation (5.14) constitute model laws in ESM distinct yet similar to those mentioned in TSM. Each of these linear methods is described below complete with analytical development.

5.2.1 Diagonal Matrix Method

The diagonal matrix (DM) method [Dutson, 2002] is the fastest and easiest process of coupling state vectors to generate the elements of S and F . i denoting a point in the domain of the geometry, the scaling parameters are assumed to be simple ratios given by,

$$S_{ii} = \frac{[x_{ps}]_{ii}}{[x_{ms}]_{ii}} \quad (5.15)$$

$$F_{ii} = \frac{[x_m]_{ii}}{[x_{ms}]_{ii}} \quad (5.16)$$

$$x_p = \left(\frac{[x_{ps}x_m]_{ii}}{[x_{ms}^2]_{ii}} \right) [x_{ms}]_{ii} \quad (5.17)$$

Hence, the elements of the transformation matrices are all numerically finite along the diagonal with the off diagonal elements set to 0. The diagonal matrix approach is particularly useful when there is only one measurement value in the model and the specimens. Thus,

$$x_{ps} = \begin{pmatrix} a & 0 & 0 & \dots \\ 0 & b & 0 & \dots \\ 0 & 0 & c & \dots \\ \vdots & \vdots & \vdots & \ddots \end{pmatrix} x_{ms}, \quad x_m = \begin{pmatrix} d & 0 & 0 & \dots \\ 0 & e & 0 & \dots \\ 0 & 0 & f & \dots \\ \vdots & \vdots & \vdots & \ddots \end{pmatrix} x_{ms}$$

This method cannot be used if one or more of the entries in the model specimen vector are 0, which leads to numerical complexity. However, for finite values, it is an invaluable technique to establish the prediction equation. For a perfectly scaled undistorted system, the diagonal elements would be equal and finite resulting in zero distortion and generation of the similarity matrix alone. However, existence of distortions would create unequal diagonal elements resulting in both similarity and distortion matrices. Further, since $\left(\frac{[x_{ps}x_m]_{ii}}{[x_{ms}^2]_{ii}} \right) = \left(\frac{[x_mx_{ps}]_{ii}}{[x_{ms}^2]_{ii}} \right)$, the condition for symmetry is satisfied. For hypothetical experimental values given by,

$$x_{ms} = \begin{pmatrix} 1.0 \\ 2.0 \\ 3.0 \\ 4.0 \\ 5.0 \end{pmatrix}, \quad x_{ps} = \begin{pmatrix} 2.0 \\ 4.0 \\ 6.0 \\ 8.0 \\ 10.0 \end{pmatrix}, \quad x_m = \begin{pmatrix} 3.0 \\ 6.0 \\ 9.0 \\ 12.0 \\ 15.0 \end{pmatrix}$$

$$S = \begin{pmatrix} 2.0 & 0.0 & 0.0 & 0.0 & 0.0 \\ 0.0 & 2.0 & 0.0 & 0.0 & 0.0 \\ 0.0 & 0.0 & 2.0 & 0.0 & 0.0 \\ 0.0 & 0.0 & 0.0 & 2.0 & 0.0 \\ 0.0 & 0.0 & 0.0 & 0.0 & 2.0 \end{pmatrix}, \quad F = \begin{pmatrix} 3.0 & 0.0 & 0.0 & 0.0 & 0.0 \\ 0.0 & 3.0 & 0.0 & 0.0 & 0.0 \\ 0.0 & 0.0 & 3.0 & 0.0 & 0.0 \\ 0.0 & 0.0 & 0.0 & 3.0 & 0.0 \\ 0.0 & 0.0 & 0.0 & 0.0 & 3.0 \end{pmatrix}$$

and

$$x_p = \begin{pmatrix} 6.0 & 0.0 & 0.0 & 0.0 & 0.0 \\ 0.0 & 6.0 & 0.0 & 0.0 & 0.0 \\ 0.0 & 0.0 & 6.0 & 0.0 & 0.0 \\ 0.0 & 0.0 & 0.0 & 6.0 & 0.0 \\ 0.0 & 0.0 & 0.0 & 0.0 & 6.0 \end{pmatrix} x_{ms}$$

5.2.2 Pseudo-Inverse Method

The pseudo-inverse (PI) method [Cho, 1999] was the first method developed to model system interactions while also accounting for possible 0 values in the specimen set or the model. The scale (and independently form) equation in the ESM system given by $x_{ps} = Sx_{ms}$ is modified by using appropriate operators to convert the element vectors to invertible forms. Post-multiplying the equation using x_{ms}^T where the super-script T denotes the conjugate transpose of the matrix, we have,

$$x_{ps}x_{ms}^T = S(x_{ms}x_{ms}^T) \quad (5.18)$$

Linear algebra suggests that a matrix multiplied by its transpose generates a square matrix [Bernstein, 2005] for linearly independent columns and hence the term $(x_{ms}x_{ms}^T)$ is square and invertible. Simplifying the equation,

$$S = (x_{ps}x_{ms}^T) (x_{ms}x_{ms}^T)^{-1} \quad (5.19)$$

$$S = (x_{ps}) (x_{ms}^+) \quad (5.20)$$

where x_{ms}^+ is the pseudo-inverse of x_{ms} [Penrose, 1955] given by $x_{ms}^T (x_{ms}x_{ms}^T)^{-1}$. Similarly,

$$F = (x_m x_{ms}^T) (x_{ms} x_{ms}^T)^{-1} \quad (5.21)$$

$$F = (x_m) (x_{ms}^+) \quad (5.22)$$

and hence,

$$x_p = (x_{ps} x_{ms}^+) x_m \quad (5.23)$$

$$x_p = (x_m x_{ms}^+) x_{ps} \quad (5.24)$$

The pseudo-inverse method thus provides a least square solution to the linear ESM equation by minimizing the error specified by the Euclidean norm given by $\|Ax - b\|^2$ where A , x and b are used in the conventional form [Robinson, 1981]. For the example matrices used earlier,

$$S = \begin{pmatrix} \frac{2}{55} & \frac{4}{55} & \frac{6}{55} & \frac{8}{55} & \frac{2}{11} \\ \frac{4}{55} & \frac{8}{55} & \frac{12}{55} & \frac{16}{55} & \frac{4}{11} \\ \frac{6}{55} & \frac{12}{55} & \frac{18}{55} & \frac{24}{55} & \frac{6}{11} \\ \frac{8}{55} & \frac{16}{55} & \frac{24}{55} & \frac{32}{55} & \frac{8}{11} \\ \frac{2}{11} & \frac{4}{11} & \frac{6}{11} & \frac{8}{11} & \frac{10}{11} \end{pmatrix}, \quad F = \begin{pmatrix} \frac{3}{55} & \frac{6}{55} & \frac{9}{55} & \frac{12}{55} & \frac{2}{11} \\ \frac{6}{55} & \frac{12}{55} & \frac{18}{55} & \frac{24}{55} & \frac{4}{11} \\ \frac{9}{55} & \frac{18}{55} & \frac{27}{55} & \frac{36}{55} & \frac{6}{11} \\ \frac{12}{55} & \frac{24}{55} & \frac{36}{55} & \frac{48}{55} & \frac{8}{11} \\ \frac{2}{11} & \frac{6}{11} & \frac{9}{11} & \frac{12}{11} & \frac{15}{11} \end{pmatrix}$$

and for $S \times F$,

$$x_p = \begin{pmatrix} \frac{6}{55} & \frac{12}{55} & \frac{18}{55} & \frac{24}{55} & \frac{6}{11} \\ \frac{12}{55} & \frac{24}{55} & \frac{36}{55} & \frac{48}{55} & \frac{12}{11} \\ \frac{18}{55} & \frac{36}{55} & \frac{54}{55} & \frac{72}{55} & \frac{18}{11} \\ \frac{24}{55} & \frac{48}{55} & \frac{72}{55} & \frac{96}{55} & \frac{24}{11} \\ \frac{6}{11} & \frac{12}{11} & \frac{18}{11} & \frac{24}{11} & \frac{30}{11} \end{pmatrix} x_{ms}$$

or,

$$x_p = \begin{pmatrix} \frac{6}{5} & 0 & 0 & 0 & 0 \\ 0 & \frac{6}{5} & 0 & 0 & 0 \\ 0 & 0 & \frac{6}{5} & 0 & 0 \\ 0 & 0 & 0 & \frac{6}{5} & 0 \\ 0 & 0 & 0 & 0 & \frac{6}{5} \end{pmatrix} x_{ms} + \begin{pmatrix} \frac{-60}{55} & \frac{12}{55} & \frac{18}{55} & \frac{24}{55} & \frac{6}{11} \\ \frac{12}{55} & \frac{-42}{55} & \frac{36}{55} & \frac{48}{55} & \frac{12}{11} \\ \frac{18}{55} & \frac{36}{55} & \frac{-12}{55} & \frac{72}{55} & \frac{18}{11} \\ \frac{24}{55} & \frac{48}{55} & \frac{72}{55} & \frac{30}{55} & \frac{24}{11} \\ \frac{6}{11} & \frac{12}{11} & \frac{18}{11} & \frac{24}{11} & \frac{84}{55} \end{pmatrix} x_{ms}$$

Notice that there is lot more system interaction captured in the pseudo-inverse approach than in the diagonal matrix method and the distortion matrix

is thus completely populated with significant values. This method is however, constrained by the fact that a true inverse is not generated as the original equation (5.18) is improperly formed. Symmetry of ESM is also lost as $S \times F \neq F \times S$ in this process as matrix multiplication in equations (5.23) and (5.24) is non-commutative. The disadvantage of such a limitation is the quandary in selecting the correct prediction equation which is detrimental to the final estimation.

5.2.3 Circulant Matrix Method

The circulant matrix (CM) approach [Cho, 1999] is a method developed to address the limitations of the previous two techniques. In the process of evaluating the scale and form matrices, this method generates square matrices (that guarantee unique solution upon “true” inversion), using the circulant operator that transforms row (and column) vectors into their respective square forms by populating other elements based on the values of the elements in the vector. The original ESM scale equation is modified to a more useful form by invoking the circulant operator³ such that,

$$circ(x_{ps}) = S circ(x_{ms}) \quad (5.25)$$

$$S = circ(x_{ps})circ(x_{ms})^{-1} \quad (5.26)$$

Similarly,

$$circ(x_m) = F circ(x_{ms}) \quad (5.27)$$

$$F = circ(x_m)circ(x_{ms})^{-1} \quad (5.28)$$

and

$$circ(x_p) = (S \times F)circ(x_{ms}) \quad (5.29)$$

Notice that the final evaluation generates a $n \times n$ matrix while the product state vector in reality is of dimension $n \times 1$. Thus, only the first

³The circulant operator is also commutative [Davis, 1979].

column of the final matrix is selected for prediction purposes. Like before, using the example matrices,

$$\text{circ}(x_{ms}) = \begin{pmatrix} 1 & 5 & 4 & 3 & 2 \\ 2 & 1 & 5 & 4 & 3 \\ 3 & 2 & 1 & 5 & 4 \\ 4 & 3 & 2 & 1 & 5 \\ 5 & 4 & 3 & 2 & 1 \end{pmatrix}$$

Hence, for any matrix given by [Davis, 1979],

$$A = \begin{pmatrix} a_1 \\ a_2 \\ a_3 \\ a_4 \\ a_5 \end{pmatrix}, \quad \text{circ}(A) = \begin{pmatrix} a_1 & a_5 & a_4 & a_3 & a_2 \\ a_2 & a_1 & a_5 & a_4 & a_3 \\ a_3 & a_2 & a_1 & a_5 & a_4 \\ a_4 & a_3 & a_2 & a_1 & a_5 \\ a_5 & a_4 & a_3 & a_2 & a_1 \end{pmatrix}$$

Thus,

$$S = \begin{pmatrix} 2.0 & 0.0 & 0.0 & 0.0 & 0.0 \\ 0.0 & 2.0 & 0.0 & 0.0 & 0.0 \\ 0.0 & 0.0 & 2.0 & 0.0 & 0.0 \\ 0.0 & 0.0 & 0.0 & 2.0 & 0.0 \\ 0.0 & 0.0 & 0.0 & 0.0 & 2.0 \end{pmatrix}, \quad F = \begin{pmatrix} 3.0 & 0.0 & 0.0 & 0.0 & 0.0 \\ 0.0 & 3.0 & 0.0 & 0.0 & 0.0 \\ 0.0 & 0.0 & 3.0 & 0.0 & 0.0 \\ 0.0 & 0.0 & 0.0 & 3.0 & 0.0 \\ 0.0 & 0.0 & 0.0 & 0.0 & 3.0 \end{pmatrix}$$

and

$$\text{circ}(x_p) = \begin{pmatrix} 6.0 & 0.0 & 0.0 & 0.0 & 0.0 \\ 0.0 & 6.0 & 0.0 & 0.0 & 0.0 \\ 0.0 & 0.0 & 6.0 & 0.0 & 0.0 \\ 0.0 & 0.0 & 0.0 & 6.0 & 0.0 \\ 0.0 & 0.0 & 0.0 & 0.0 & 6.0 \end{pmatrix} \text{circ}(x_{ms})$$

Notice similarity with the DM approach but more robustness is brought on by true inversion of square matrices. Further, a smoothing effect is caused by the use of the entire column vector and thus the capture of true interaction of all elements. This method though is hindered by the possibility of having to invert stiff or large matrices but the assumption of symmetry in ESM is satisfied due to the commutative nature of circulant operators. The circulant matrix is however completely populated due to its formal definition but certain elements can be eliminated (set to 0) due to redundancy. Setting some elements to 0 without losing generality would expedite the solution. Such an innovation is brought on in the Hankel matrix method described later.

5.2.4 Compensation Matrix Method

Building on the premise of regression methods, the compensation matrix (CpM) approach [Wood, 2002] lends a linear curve fit process to the ESM equations such that error (Euclidean norm) in such approximation is minimized using a least square solution. Using mathematical formulations similar to the PI method [Robinson, 1981], this technique seeks to identify and fit the “best” linear curve for the scale and form equation such that,

$$x_{ps} = a^* + b^* x_{ms} \quad (5.30)$$

$$x_m = a_1^* + b_1^* x_{ms} \quad (5.31)$$

where a^* , b^* , a_1^* and b_1^* are the constants of the best fit linear curve given by,

$$\begin{pmatrix} a^* \\ b^* \end{pmatrix} = [1 \ x_{ms}]^+ x_{ps}, \quad \begin{pmatrix} a_1^* \\ b_1^* \end{pmatrix} = [1 \ x_{ms}]^+ x_m$$

where the ‘+’ operator indicates the pseudo-inverse and hence,

$$x_p = a^* + b^* x_m = a^* + b^* (a_1^* + b_1^* x_{ms}) \quad (5.32)$$

$$x_p = a_1^* + b_1^* x_{ps} = a_1^* + b_1^*(a^* + b^* x_{ms}) \quad (5.33)$$

Using the matrices defined earlier,

$$\begin{pmatrix} a^* \\ b^* \end{pmatrix} = \begin{pmatrix} 0 \\ 2 \end{pmatrix}, \quad \begin{pmatrix} a_1^* \\ b_1^* \end{pmatrix} = \begin{pmatrix} 0 \\ 3 \end{pmatrix}$$

and therefore $x_p = 2x_m$ or $x_p = 3x_{ps}$. Thus,

$$x_p = \begin{pmatrix} 6.0 & 0.0 & 0.0 & 0.0 & 0.0 \\ 0.0 & 6.0 & 0.0 & 0.0 & 0.0 \\ 0.0 & 0.0 & 6.0 & 0.0 & 0.0 \\ 0.0 & 0.0 & 0.0 & 6.0 & 0.0 \\ 0.0 & 0.0 & 0.0 & 0.0 & 6.0 \end{pmatrix} x_{ms}$$

Symmetry of ESM is satisfied only if $a^* + b^* a_1^* = a_1^* + b_1^* a^*$ which is true in this example and hence $x_p = 6x_{ms}$ is a valid (and unique) prediction equation similar to the DM and CM techniques. Like the PI method, this process also negates some of its mathematical prowess due to lack of clarity in the choice of final prediction equation.

5.2.5 Hankel Matrix Method

Seeking further refinement of the square matrix inversion process, the Hankel matrix approach is detailed below which retains all the benefits of the circulant operator and improves on it by setting redundant elements to 0, thereby accelerating the solution further. The Hankel matrix [Peller, 2003] is a linear operator that also allows conversion of a row (or column) vector to its corresponding square form with the following notation. For a row vector $A = (a \ b \ c \ d \ e)$, the corresponding Hankel form is,

$$H(A) = \begin{pmatrix} a & b & c & d & e \\ b & c & d & e & 0 \\ c & d & e & 0 & 0 \\ d & e & 0 & 0 & 0 \\ e & 0 & 0 & 0 & 0 \end{pmatrix}$$

The Hankel operator thus generates a sparse matrix because the entries in the first column are not completely reproduced and is also a special case of Toeplitz matrices⁴ as it is a mirror image of $U(Toep)$ where U is the upper triangular form of a matrix. The incorporation of Hankel forms reduces complexity further due to the sparseness of the matrix. Notice again, the diagonal (anti) dominance maintained for a square but sparse definition. The scale equation of ESM given by $x_{ps} = Sx_{ms}$ is now modified to $H(x_{ps}) = S H(x_{ms})$ where $H()$ is the Hankel operator. Hence,

$$H(x_{ps}) = S H(x_{ms}) \quad (5.34)$$

$$S = H(x_{ps})H(x_{ms})^{-1} \quad (5.35)$$

Similarly,

$$H(x_m) = F H(x_{ms}) \quad (5.36)$$

$$F = H(x_m)H(x_{ms})^{-1} \quad (5.37)$$

and

$$H(x_p) = (S \times F)H(x_{ms}) \quad (5.38)$$

Adopting the examples matrices again,

$$H(x_{ms}) = \begin{pmatrix} 1 & 2 & 3 & 4 & 5 \\ 2 & 3 & 4 & 5 & 0 \\ 3 & 4 & 5 & 0 & 0 \\ 4 & 5 & 0 & 0 & 0 \\ 5 & 0 & 0 & 0 & 0 \end{pmatrix}$$

⁴Described later in this chapter.

Thus,

$$S = \begin{pmatrix} 2.0 & 0.0 & 0.0 & 0.0 & 0.0 \\ 0.0 & 2.0 & 0.0 & 0.0 & 0.0 \\ 0.0 & 0.0 & 2.0 & 0.0 & 0.0 \\ 0.0 & 0.0 & 0.0 & 2.0 & 0.0 \\ 0.0 & 0.0 & 0.0 & 0.0 & 2.0 \end{pmatrix}, \quad F = \begin{pmatrix} 3.0 & 0.0 & 0.0 & 0.0 & 0.0 \\ 0.0 & 3.0 & 0.0 & 0.0 & 0.0 \\ 0.0 & 0.0 & 3.0 & 0.0 & 0.0 \\ 0.0 & 0.0 & 0.0 & 3.0 & 0.0 \\ 0.0 & 0.0 & 0.0 & 0.0 & 3.0 \end{pmatrix}$$

and

$$H(x_p) = \begin{pmatrix} 6.0 & 0.0 & 0.0 & 0.0 & 0.0 \\ 0.0 & 6.0 & 0.0 & 0.0 & 0.0 \\ 0.0 & 0.0 & 6.0 & 0.0 & 0.0 \\ 0.0 & 0.0 & 0.0 & 6.0 & 0.0 \\ 0.0 & 0.0 & 0.0 & 0.0 & 6.0 \end{pmatrix} H(x_{ms})$$

Notice likeness to DM, CM and CpM approaches while maintaining symmetry of ESM despite the use of a sparse matrix (HM). The characteristics of the Hankel operator are similar to the circulant operator in that inverting large or stiff matrices remains a numerical challenge and only the first column holds values of interest. Before a formal comparison is initiated for the procedures described above, a brief explanation is given regarding the diagonal dominance⁵⁶ of each method, which can be explained mathematically using the similarity and distortion indices developed earlier. The similarity matrix hypothesized the maximization of diagonal norm so that there is minimal distortion. This feature is captured and translated to the matrices in the scale and form equation thus generating diagonally dominant matrices, an effect that becomes more apparent in an example provided later in this chapter.

⁵This is not the conventional diagonal dominance where $a_{ii} > \sum_{j \neq i} a_{ij} \forall i$.

⁶It is just an indicator of how presence of values along the diagonal is absolutely necessary in the similarity matrix, especially in conditions of zero distortion, for any plausible scaling.

5.2.6 Comparison of Methods

The methods explained above are gauged for efficiency based on the parameters chosen below (see Table 5.3). The assumption of symmetry plays a pivotal role in ESM and is important for analysis though not vital. Robustness of each method is qualified based on the ability of the method to incorporate and evaluate possible 0 values in the model and/or specimen matrices. Interactions are also studied as not all methods duly accommodate such features. The evaluation pattern is next probed which targets the capability of the method to allow for variable settings in the estimation implying freedom to choose the magnitude of the error margin, the number of steps required to reach the error margin, the tolerance value, the starting step size and the maximum step size. As all the methods used above are direct techniques, they do not allow flexibility in estimation or choice of acceptable error. They provide exact solution in a finite number of steps which is not always viable in mechanical systems analysis where iterative methods provide more meaningful and feasible solutions. Iteration also enjoys the feature of self-correction implying progression toward the right value while maintaining the trend in the solution.

Table 5.3: Comparison of linear methods

Method	Symmetry	Robustness	Interactions	Evaluation	Flexibility
DM	Yes	No	No	Fixed	No
PI	No	Yes	Partial	Fixed	No
CM	Yes	Yes	Yes	Fixed	No
CpM	No	Yes	Yes	Fixed	No
HM	Yes	Yes	Yes	Fixed	No

Notice that the linear methods discussed thus far incorporated features from prior techniques and built on them to improve the estimation process and imbibed a greater variety of problems, thus overcoming the limitations of null values, developing square definitions and providing for error minimization schemes. Notice that symmetry is not attached as much importance because

a prediction equation can still be generated that may not be unique as was illustrated in the PI and CpM approach. However, all these methods are constrained by the limitation of rigidity - they are fixed techniques and cannot provide the freedom of choosing the estimation strategy. They can be time consuming and often times encounter impossible situations when inverting large or stiff systems. Therefore, need exists in developing and using solution processes which are robust, diagonally dominant, capture interactions and are numerically stable iterative schemes that are immune to large or stiff systems. Such a method using iteration is introduced below.

5.2.7 Toeplitz Matrix-Conjugate Gradient Method

The importance of creating and maintaining square matrices has been elaborated earlier as has been the necessity to model interactions. The emphasis being given to square matrix generation is due to one its inherent mathematical properties - existence of *condition number*. The condition number determines stability of a system and its sensitivity to numerical operations and minor fluctuations in input values. In ESM, it is imperative to characterize the condition number of the system matrix $S \times F$ so that its stability⁷ can be ensured. Further, accuracy desired compels thorough and exhaustive experimentation of specimens and model yielding column vectors of considerable length. Generating and inverting square matrices of such size requires significant computational effort and hence cost. Alternate iterative methods are thus sought with indifference towards size of the matrices, which can be best captured using the order of complexity involved in inverting matrices. *Stationary* iterative methods⁸ require lot more operations and only converge

⁷A condition number of 1 typically indicates a stable system *i.e.*, well-conditioned. A general rule is that finite condition numbers are acceptable as against extremely high (orders of 10) magnitudes *i.e.*, ill-conditioned.

⁸Iterative methods, where a fixed point or a pivot point is used to decompose the original matrix - Gauss Elimination, Gauss-Siedel method, Jacobi method, Richardson iteration, SOR approximation [Ng, 2004].

for an *educated* initial guess if the spectral radius⁹ is less than 1 [Golub et al., 1996]. Hence, the spectral radius determines feasibility of stationary methods. Gaussian elimination, for instance, is a process with $O(n^3)$ operational complexity [Ng, 2004]. However, Krylov space methods exist that are not stationary [Ng, 2004] and are significantly better - the conjugate gradient (CG) method in particular [Shewchuk, 1994] which is a $O(n \ln n)$ process. A further advantage of these methods is the ability to speed up estimation using pre-conditioners to “condition” the matrices before evaluation, a feature that is absent in stationary methods. A third benefit of numerical methods is the ability to choose an acceptable residual¹⁰ in the solution. Depending on the stiffness¹¹ of the system, a nominal residual can be chosen so that the solution converges without any major deviation from the actual solution. The numerical scheme of the conjugate gradient method is detailed in Appendix A. The CG method is now used in solving the linear ESM scale and form equation after invoking the Toeplitz operator and subsequent simplification.

The Toeplitz matrix [Grenander et al., 1958] is an operator that allows conversion of a row (or column) vector to its corresponding square form with the notation $A_{i,j} = a_{i-1,j-1}$ where A is the square form of the vector of values given by a_i . For a row vector $A = (a \ b \ c \ d \ e)$, the corresponding Toeplitz form is,

$$Toep(A) = \begin{pmatrix} a & b & c & d & e \\ b & a & b & c & d \\ c & b & a & b & c \\ d & c & b & a & b \\ e & d & c & b & a \end{pmatrix}$$

The circulant matrix is a special case of Toeplitz matrices and $U(circ) = U(Toep)$ where U is the upper triangular form of a matrix. Thus, the circulant operator can be replaced with the Toeplitz operator and the developed ma-

⁹The largest eigenvalue of the matrix [Bernstein, 2005].

¹⁰Residual is the difference between the actual and the predicted values in a certain norm.

¹¹Given by the condition number of a matrix $A = \|A\| \|A^{-1}\|$.

trices can be inverted like before to develop scale and form matrices. However, incorporation of Toeplitz forms reduces complexity from $O(n^2)$ to $O(2n-1)$ as most of the values are repeated. This enhancement is achieved while maintaining diagonal dominance and square definitions, which thus are added benefits. Combined with the advantages of CG methods that are impervious to stiffness issues, a successful solution combination is established. The scale equation of ESM given by $x_{ps} = Sx_{ms}$ is now modified to $Toep(x_{ps}) = S Toep(x_{ms})$ where $Toep()$ is the Toeplitz operator. T indicating the conjugate transpose,

$$Toep(x_{ps})^T = [S Toep(x_{ms})]^T = Toep(x_{ms})^T S^T \quad (5.39)$$

Similarly,

$$Toep(x_m)^T = [F Toep(x_{ms})]^T = Toep(x_{ms})^T F^T \quad (5.40)$$

These equations are reminiscent of the standard linear $Ax = b$ form with $A = Toep(x_{ms})^T$ and $b = Toep(x_{ps})^T$ or $b = Toep(x_m)^T$ which can be solved quite easily using standard mathematical software including *Matlab*TM and *Mathematica*TM. Solving the system of equations using the CG method generates the required scale and form matrices. Hence,

$$S_{CG}^T = [Toep(x_{ps})^T, Toep(x_{ms})^T]_{CG} \quad (5.41)$$

$$F_{CG}^T = [Toep(x_m)^T, Toep(x_{ms})^T]_{CG} \quad (5.42)$$

and

$$Toep(x_p) = (F_{CG}^T \times S_{CG}^T)^T Toep(x_{ms}) \quad (5.43)$$

$$Toep(x_p) = (S_{CG} \times F_{CG}) Toep(x_{ms}) \quad (5.44)$$

Using the matrices described earlier,

$$Toep(x_{ms}) = \begin{pmatrix} 1 & 2 & 3 & 4 & 5 \\ 2 & 1 & 2 & 3 & 4 \\ 3 & 2 & 1 & 2 & 3 \\ 4 & 3 & 2 & 1 & 2 \\ 5 & 4 & 3 & 2 & 1 \end{pmatrix}$$

Thus,

$$S = \begin{pmatrix} 2.0 & 0.0 & 0.0 & 0.0 & 0.0 \\ 0.0 & 2.0 & 0.0 & 0.0 & 0.0 \\ 0.0 & 0.0 & 2.0 & 0.0 & 0.0 \\ 0.0 & 0.0 & 0.0 & 2.0 & 0.0 \\ 0.0 & 0.0 & 0.0 & 0.0 & 2.0 \end{pmatrix}, \quad F = \begin{pmatrix} 3.0 & 0.0 & 0.0 & 0.0 & 0.0 \\ 0.0 & 3.0 & 0.0 & 0.0 & 0.0 \\ 0.0 & 0.0 & 3.0 & 0.0 & 0.0 \\ 0.0 & 0.0 & 0.0 & 3.0 & 0.0 \\ 0.0 & 0.0 & 0.0 & 0.0 & 3.0 \end{pmatrix}$$

and

$$Toep(x_p) = \begin{pmatrix} 6.0 & 0.0 & 0.0 & 0.0 & 0.0 \\ 0.0 & 6.0 & 0.0 & 0.0 & 0.0 \\ 0.0 & 0.0 & 6.0 & 0.0 & 0.0 \\ 0.0 & 0.0 & 0.0 & 6.0 & 0.0 \\ 0.0 & 0.0 & 0.0 & 0.0 & 6.0 \end{pmatrix} Toep(x_{ms})$$

This solution is identical to DM, CM, CpM and HM methods and hence shows the feasibility of using the Toeplitz operators in conjunction with CG methods (TCG). Notice also that symmetry is obtained. Remember that like the circulant matrix, only the first column holds elements of interest. Note also that all methods converge to the DM method when there is only one measurement value to be scaled.

Application of all developed methods in mechanical systems analysis is tested as the mathematical behavior should be more coherent for random values as is illustrated in the example below - a simple deflection problem

construed to make a comparison between all the available methods for contrast and validity in terms of error margins. This example thus signifies a deviation from the mathematical comparison (see Tables 5.4 and 5.5) done thus far and investigates physical substantiation.

Table 5.4: Improvements over earlier linear methods - I

Method	Symmetry	Robustness	Interactions	Evaluation	Flexibility
TCG	Yes	Yes	Yes	Iterative	Yes

Table 5.5: Improvements over earlier linear methods - II

Method	Complexity	Pre-conditioning	Large Systems	Stiff Systems
TCG	Reduced	Yes	Does not matter	Does not matter

5.3 USB Clip-Deflection Analysis

The developed linear strategies are tested for numerical accuracy by evaluating the methods using a product. The device studied is a simple USB clip (see Figure 5.1) whose deflection is estimated for a force applied at its free ends (for unlatching from the lock position). Since the product is symmetric (see Figure 5.2 - all dimensions in mm) about the x - plane, a $\frac{1}{2}$ section (see Figure 5.3) is modeled and analyzed. The specimen used is also shown (see Figure 5.4). Thus, the primary objectives in analyzing this product are -

- Establish the feasibility of TCG and HM techniques in terms of error margins and compare them with other procedures, for a perfectly linear system.
- Demonstrate diagonal dominance discussed earlier in this chapter.
- Establish distortion and similarity measures using maximization of the diagonal norm, and condition number for each method.

- Identify system interactions and highlight corresponding changes in distortion and similarity estimation.



Figure 5.1: USB Clip

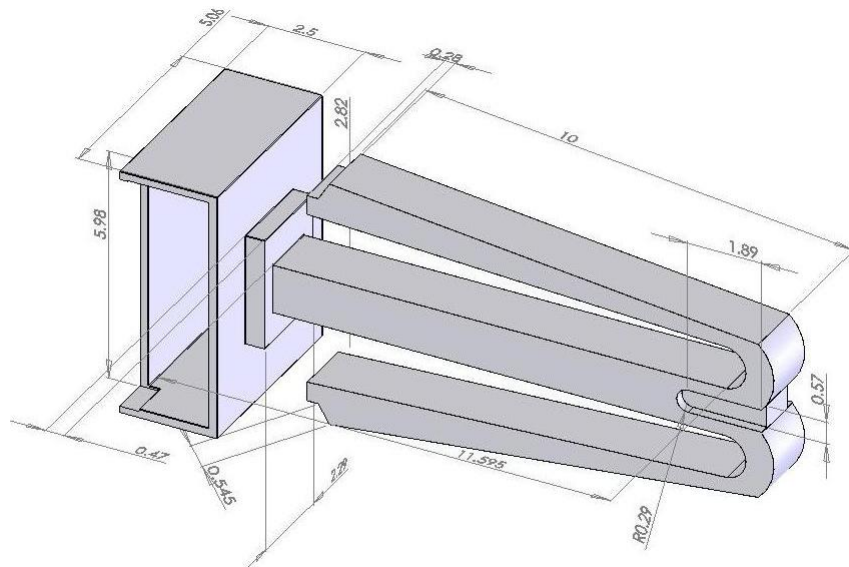


Figure 5.2: USB Clip - Solid model

In order to address each of the objectives listed above, the ESM procedure is employed using all linear solution strategies. The selected product is made from a plastic based compound and the specimen chosen is assumed

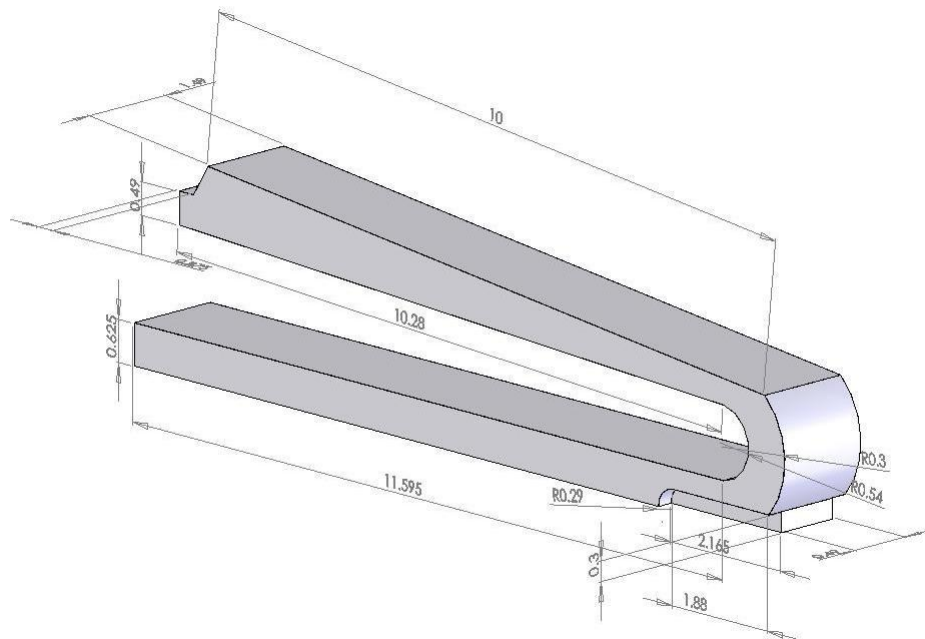


Figure 5.3: USB Clip - Half section

to be made of Nylon. Hence, the four corners of the ESM quadrant traveling counter-clockwise are respectively represented by the following table (see Table 5.6). Notice that all inherent variables affecting the system such as Poisson's ratio, Young's modulus, yield limit, ultimate strength etc. are imbibed in the retrieved deflection numerical data.

Table 5.6: ESM representation of the clip

Geometry	Material
Product	Plastic
Product Specimen	Plastic
Model Specimen	Nylon
Model	Nylon

The three representative geometries are thus analyzed using *ABAQUSTM* software for different values of force (0.5 - 2.5 *N*) applied to the free end and the associated deflection (see Table 5.7) is plotted (see Figure 5.5). Notice

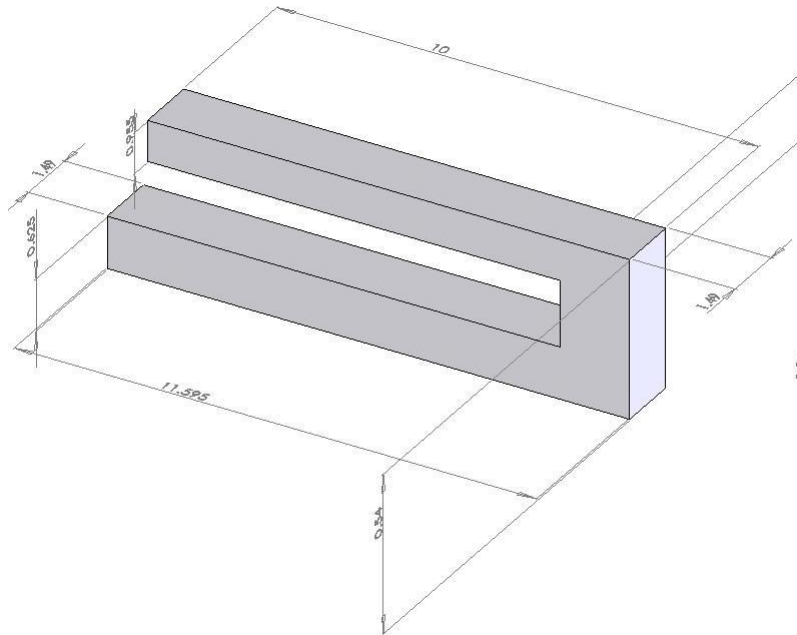


Figure 5.4: USB Clip - Specimen

that all three geometries show a linear trend but with different slopes as one would expect due to changing shapes, sizes and material properties. A safe conclusion could now be arrived at suggesting that the product would behave linearly as well and using linear methods to solve for the required parameter of interest is a valid approach. This conclusion is concretized by the Pearson's statistical test as well, shown below. Hence, linear working range of the clip deflection can be hypothesized without testing the actual product itself.

Table 5.7: Test data from representative geometries of the clip

Load (N)	δ_{ms} (in)	δ_{ps} (in)	δ_m (in)	δ_p (in)
0.5	0.0244947	0.0319442	0.0356637	0.0452190
1	0.0293936	0.0383330	0.0427964	0.0542628
1.5	0.0342925	0.0447218	0.0499291	0.0633066
2.0	0.0391915	0.0511100	0.0570619	0.0723504
2.5	0.0440904	0.0574995	0.0641940	0.0813942

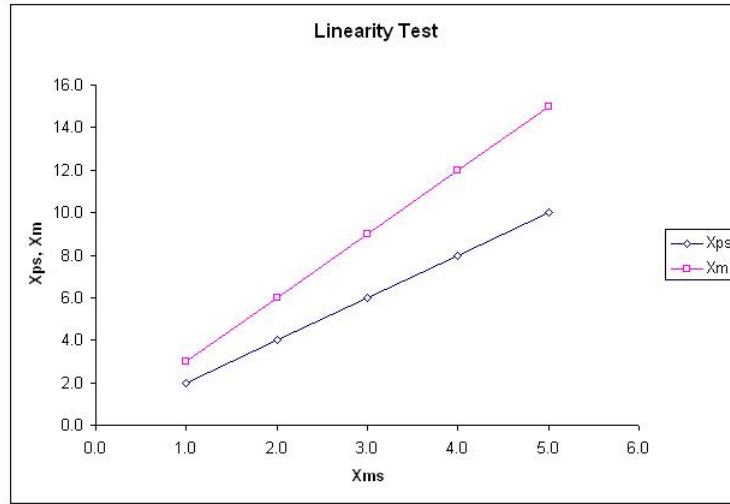


Figure 5.5: Linearity of test data from representative geometries of the clip

$$r(X_{ms}, X_{ps}) = 1 \quad (5.45)$$

$$r(X_{ms}, X_m) = 1 \quad (5.46)$$

The developed methods are now invoked with the idea of establishing their respective system transformations, which are shown below.

$$(S \times F)_{DM} = \begin{pmatrix} 1.89878 & 0.0 & 0.0 & 0.0 & 0.0 \\ 0.0 & 1.89878 & 0.0 & 0.0 & 0.0 \\ 0.0 & 0.0 & 1.89878 & 0.0 & 0.0 \\ 0.0 & 0.0 & 0.0 & 1.89875 & 0.0 \\ 0.0 & 0.0 & 0.0 & 0.0 & 1.89876 \end{pmatrix}$$

$$(S \times F)_{PI} = \begin{pmatrix} 0.186155 & 0.223385 & 0.260616 & 0.297847 & 0.335078 \\ 0.223385 & 0.268062 & 0.312739 & 0.357416 & 0.402093 \\ 0.260616 & 0.312739 & 0.364862 & 0.416985 & 0.469108 \\ 0.297843 & 0.357411 & 0.41698 & 0.476549 & 0.536117 \\ 0.335078 & 0.402093 & 0.469108 & 0.536125 & 0.60314 \end{pmatrix}$$

$$(S \times F)_{CM} = \begin{pmatrix} 1.89875 & -3.55 \times 10^{-6} & -3.55 \times 10^{-6} & 4.22 \times 10^{-5} & -1.32 \times 10^{-11} \\ -1.32 \times 10^{-11} & 1.89875 & -3.55 \times 10^{-6} & -3.55 \times 10^{-6} & 4.22 \times 10^{-5} \\ 4.22 \times 10^{-5} & -1.32 \times 10^{-11} & 1.89875 & -3.55 \times 10^{-6} & -3.55 \times 10^{-6} \\ -3.55 \times 10^{-6} & 4.22 \times 10^{-5} & -1.32 \times 10^{-11} & 1.89875 & -3.55 \times 10^{-6} \\ -3.55 \times 10^{-6} & -3.55 \times 10^{-6} & 4.22 \times 10^{-5} & -1.32 \times 10^{-11} & 1.89875 \end{pmatrix}$$

$$(S \times F)_{CPM} = \begin{pmatrix} 1.3041 + a & b & c & d & e \\ f & 1.3041 + g & h & i & j \\ k & l & 1.3041 + m & n & o \\ p & q & r & 1.3041 + s & t \\ u & v & w & x & 1.3041 + y \end{pmatrix}$$

where the constants are given by,

$$10^{-5} \begin{pmatrix} -0.0024 & -0.0029 & -0.0034 & -0.0039 & -0.0044 \\ 0.0292 & 0.0351 & 0.0409 & 0.0468 & 0.0526 \\ 0.0609 & 0.0731 & 0.0853 & 0.0974 & 0.1096 \\ -0.1998 & -0.2397 & -0.2797 & -0.3196 & -0.3596 \\ 0.1121 & 0.1345 & 0.1569 & 0.1793 & 0.2017 \end{pmatrix}$$

$$(S \times F)_{HM} = \begin{pmatrix} 1.8988 & 0.0 & 0.0 & 0.0 & 0.0 \\ 0.0 & 1.8988 & 0.0 & 0.0 & 0.0 \\ 0.0 & 0.0 & 1.8988 & 0.0 & 0.0 \\ 0.0 & 0.0 & 0.0 & 1.8988 & 0.0 \\ 0.0 & 0.0 & 0.0 & 0.0 & 1.8988 \end{pmatrix}$$

$$(S \times F)_{TCG} = \begin{pmatrix} 1.89878 & 1.66 \times 10^{-9} & -1.14 \times 10^{-4} & 1.38 \times 10^{-4} & -3.36 \times 10^{-5} \\ -1.12 \times 10^{-5} & 1.89879 & -1.23 \times 10^{-9} & -1.14 \times 10^{-5} & 1.03 \times 10^{-4} \\ -3.02 \times 10^{-6} & 1.93 \times 10^{-11} & 1.89879 & 1.93 \times 10^{-11} & -3.02 \times 10^{-6} \\ 1.03 \times 10^{-4} & -1.14 \times 10^{-4} & -1.23 \times 10^{-9} & 1.89879 & -1.12 \times 10^{-5} \\ -3.36 \times 10^{-5} & 1.38 \times 10^{-4} & -1.14 \times 10^{-4} & 1.66 \times 10^{-9} & 1.89878 \end{pmatrix}$$

Notice that all methods develop completely populated matrices where presence of values along the diagonal is ensured. Collecting distortion and similarity measures using the definitions introduced in chapter IV, and values of condition number, we have (see Table 5.8),

Table 5.8: Distortion, similarity measure and condition number for all linear methods

Method	Distortion	Similarity	Condition Number
DM	0	1	1
PI	0.25	0.75	1.7219×10^{33}
CM	0	1	1
CpM	0	1	1
HM	0	1	1
TCG	0	1	1.00027

Similarity and distortion matrices are switched in the PI method as off diagonal elements are larger in magnitude than mean of diagonal elements. Interpreting these measures, the values signify degree of correspondence in scaling and are only *general* indicators of how accurate the final solution would be.

A similarity of 1 does not necessarily mean that the solution would be perfect. It just means that the terms and factors contributing towards similarity have been well captured. Distortion, similarly does not completely indicate the accuracy of the final prediction. It should be interpreted as the change that the system has *seen* in terms of geometry, material and other variables *w.r.t* the similarity of the transformation. These values are dependent on numerical entries in scale and form matrices and are specific to the method chosen. Note also that all methods except the PI method are stable implying that this technique is highly sensitive to minor changes in the input values. Notice also reduction in similarity and increase in distortion with rise in condition number. In this example though, where the key motivation is to prove feasibility of TCG and HM approaches, and limited values are used in prediction, the final solution should not be significantly different as the variation in estimation would be negligible due to the values themselves being numerically small. This is illustrated below (see Tables 5.9 and 5.10) where the response values of the actual product are also obtained using *ABAQUSTM* simulations.

Table 5.9: Predicted values for clip deflection

Load	Actual Deflection	DM	PI	CM	CpM	HM	TCG
0.5	0.0452	0.0465	0.0465	0.0465	0.0465	0.0465	0.0465
1.0	0.0542	0.0558	0.0558	0.0558	0.0558	0.0558	0.0558
1.5	0.0633	0.0651	0.0651	0.0651	0.0651	0.0651	0.0651
2.0	0.0723	0.0744	0.0744	0.0744	0.0744	0.0744	0.0744
2.5	0.0813	0.0837	0.0837	0.0837	0.0837	0.0837	0.0837

Notice that the predicted plot (see Figure 5.6) is close to the actual plot and all methods generate values that are almost equal to each other. Also note that error values¹² (see Figure 5.7) are almost identical with insignificant change occurring in the fourth decimal. Linear trend of product response predicted by statistical tests is also confirmed. This example thus proves

¹²Estimation of errors and concerned mathematical definitions are explained thoroughly in Chapter VII.

Table 5.10: Error values for clip deflection

Load	DM	PI	CM	CpM	HM	TCG
0.5	2.85%	2.85%	2.85%	2.85%	2.85%	2.85%
1.0	2.85%	2.85%	2.85%	2.85%	2.85%	2.85%
1.5	2.85%	2.85%	2.85%	2.85%	2.85%	2.85%
2.0	2.85%	2.85%	2.85%	2.85%	2.85%	2.85%
2.5	2.85%	2.85%	2.85%	2.85%	2.85%	2.85%
RMS Error	2.85%	2.85%	2.85%	2.85%	2.85%	2.85%

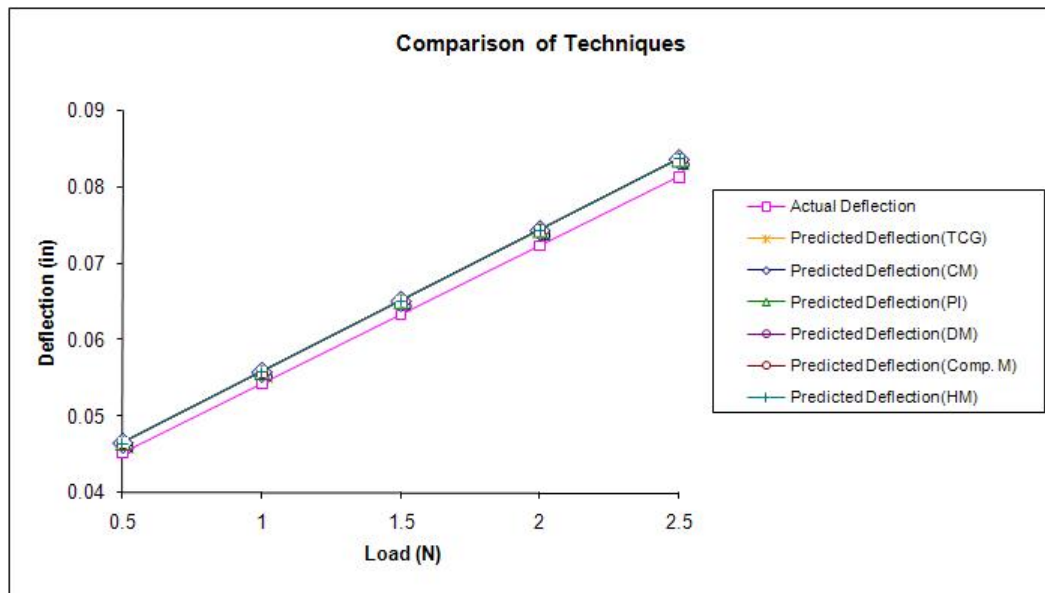


Figure 5.6: Prediction plot for clip deflection

numerical validity of TCG and HM approach and authenticates viability of these processes in comparison with other established methods. Bear in mind that no pre-conditioning matrix was used in this example and simulation has been performed using an in-built default residue automatically chosen by the software. The objectives listed for this example are achieved as both processes are shown to be as effective as the earlier methods. Further, distortion and similarity measures have been illustrated along with their estimation when off diagonal elements gain numerical precedence as was the condition that finite

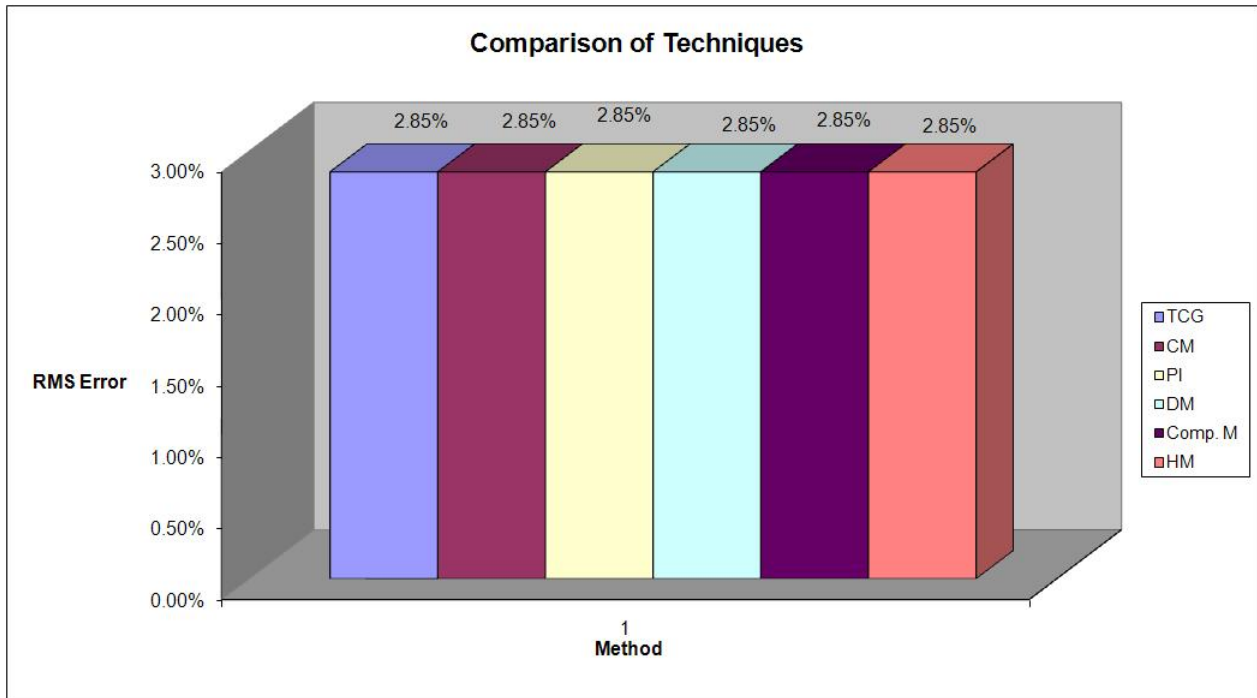


Figure 5.7: Error plot for clip deflection

non-zero elements must exist along the diagonal. Building on this conclusion, the next example illustrates benefit and enhancement achieved using the TCG method.

5.4 Transformer-Magnetic Flux Analysis

Seeking diversity in applications of ESM, this example pursues prediction of flux values of an anisotropic material used in transformers in a particular phase by evaluating a simpler isotropic material modeled in a different phase (distortion in test conditions). Before embarking on establishing the description of the problem and associated scaling parameters, a brief explanation is provided regarding transformers and their applications. Transformers are electrical devices that condition voltage by either stepping up or stepping

down the numerical magnitude of input voltage thus transmitting the required amounts of electrical power over large distances [Daniels, 1985]. Transformers work on principles of electromagnetism and electromagnetic induction where changing electricity in the primary coil induces voltage across the secondary coil due to the magnetic flux generated in the transformer core (see Figure 5.8), the magnitude of which is governed by Faraday's laws [Winders, 2002]. Transformers are typically made from laminated steel cores whose permeability is much larger than free space. However usage of such material results in considerable anisotropic behavior whose flux values are the parameters of interest. [Gyselinck et al., 2001] studied the behavior of overlap joints in transformer cores in two different phases to develop a 2-D finite element model of the responses of different parameters. Incorporating the results of that exercise into ESM, this example correlates the flux values of anisotropic steel in phase B (magnetic flux lines are symmetric [Gyselinck et al., 2001]) using a piecewise isotropic model of steel in phase A (magnetic flux lines are rotational [Gyselinck et al., 2001]) for varying values of current (see Figure 5.9). ESM representation of the problem is given below (see Table 5.11). The main objectives in this experiment are -

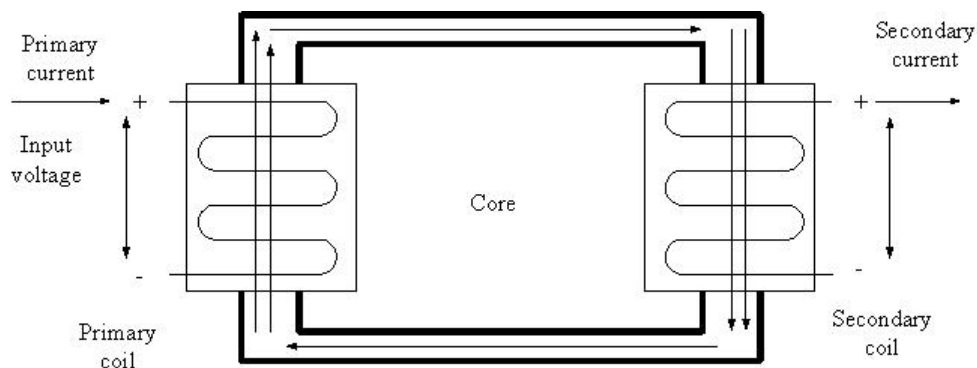


Figure 5.8: Transformer layout and operation

- Demonstrate prediction improvement achieved using the iterative method.

- Illustrate applicability of ESM when test conditions alter along with material properties.
- Show versatility of linear ESM processes when systems are distorted and are not perfectly linear.

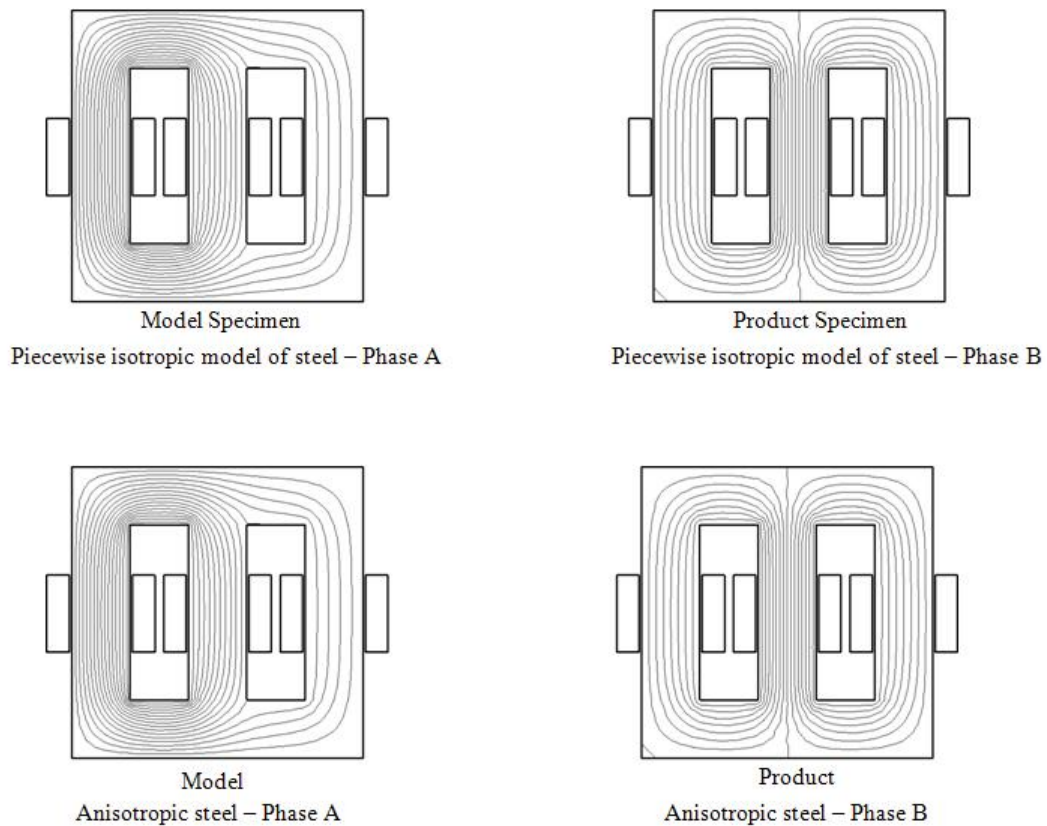


Figure 5.9: ESM quartet for the transformer system [Adapted from Gyselinck et al., 2001]

[Gyselinck et al., 2001] provide summarized data about these structures and relevant data for this analysis has been approximated from *Two-dimensional finite element modelling of overlap joints in transformer cores* [Gyselinck et al., 2001] (see Table 5.12).

Table 5.11: ESM representation of the transformer system

Geometry	Material	Test Conditions
Product	Anisotropic steel	Phase B
Product Specimen	Piecewise isotropic model of steel	Phase B
Model Specimen	Piecewise isotropic model of steel	Phase A
Model	Anisotropic steel	Phase A

Table 5.12: Test data from representative geometries of the transformer system

Current (A)	ψ_{ms} (Wb)	ψ_{ps} (Wb)	ψ_m (Wb)	ψ_p (Wb)
0.045	0.06000	0.04000	0.08000	0.07000
0.085	0.16500	0.15000	0.25000	0.20000
0.125	0.39000	0.36000	0.61000	0.58000
0.175	0.62500	0.58500	0.85500	0.82500
0.225	0.77500	0.74000	0.96000	0.94500
0.260	0.88000	0.82000	1.00000	0.99500
0.290	0.94000	0.89500	1.25000	1.15000
0.335	0.96500	0.92000	1.30000	1.20000
0.375	0.97500	0.95500	1.35000	1.25000
0.420	0.99500	0.97500	1.40000	1.30000
0.460	1.05000	0.98000	1.45000	1.35000
0.500	1.15000	0.98500	1.50000	1.40000

Pearson's test shown below, provides near linear values between the model specimen and the product specimen, and the model specimen and the model thus authenticating use of linear methods.

$$r(X_{ms}, X_{ps}) = 0.9948 \quad (5.47)$$

$$r(X_{ms}, X_m) = 0.9888 \quad (5.48)$$

Notice that test values are numerically small and hence estimation using matrices needs caution against potential noise induction during matrix inversion and multiplication. To simplify analysis and allow choice of user

desired residue, the Jacobi pre-conditioner¹³ is used in the TCG method along with the smallest possible residue (machine precision). All linear methods are invoked to determine predicted values of flux (see Table 5.13). Intermediate analysis and associated relations are summarized in Appendix B. The TCG approach being iterative allow flexibility in choosing number of iterations and acceptable residual thus permitting refinement in solution unlike other fixed linear ESM processes. Shown below are results of analysis.

Table 5.13: Predicted values for transformer flux measurement

Current	DM	PI	CM	CpM	HM	TCG
0.045	0.05330	0.05330	0.06110	0.05390	0.06020	0.07025
0.085	0.22730	0.19980	0.23710	0.22880	0.23460	0.19896
0.125	0.56310	0.47960	0.55770	0.56510	0.55410	0.57281
0.175	0.80030	0.77930	0.78660	0.80090	0.78520	0.81610
0.225	0.91660	0.98570	0.90720	0.91830	0.90910	0.94187
0.260	0.93180	1.09230	0.93930	0.93110	0.94450	0.96598
0.290	1.19020	1.19220	1.19020	1.19080	1.19300	1.16177
0.335	1.23940	1.22550	1.24480	1.23980	1.24560	1.21128
0.375	1.32230	1.27210	1.32420	1.32080	1.32330	1.29270
0.420	1.37190	1.29880	1.36620	1.36940	1.36490	1.35920
0.460	1.35330	1.30540	1.34550	1.35420	1.34720	1.43960
0.500	1.28480	1.31210	1.28870	1.28270	1.28480	1.34901

Observe near linear trend in final predicted values (see Figure 5.10) and notice that the TCG procedure outperforms other methods (see Table 5.14 and Figure 5.11) since refined iteration causes smaller residuals leading to greater accuracy while the HM process ranks second. This improvement is statistically significant as the difference is about two standard deviations away from the mean of the RMS errors. Further, all objectives for this experiment have been realized with the demonstration of ESM for near linear and distorted systems when test conditions change along with material properties.

¹³The matrix P with just the diagonal elements of matrix A to condition the equation $Ax = b$ to $P^{-1}Ax = P^{-1}b$.

Table 5.14: Error values for transformer flux measurement

Current	DM	PI	CM	CpM	HM	TCG
0.045	23.86%	23.86%	12.71%	23.00%	14.00%	0.36%
0.085	13.65%	0.10%	18.55%	14.40%	17.30%	0.52%
0.125	2.91%	17.31%	3.84%	2.57%	4.47%	1.24%
0.175	2.99%	5.54%	4.66%	2.92%	4.82%	1.08%
0.225	3.00%	4.31%	4.00%	2.83%	3.80%	0.33%
0.260	6.35%	9.78%	5.60%	6.42%	5.08%	2.92%
0.290	3.50%	3.67%	3.50%	3.55%	3.74%	1.02%
0.335	3.28%	2.13%	3.73%	3.32%	3.80%	0.94%
0.375	5.78%	1.77%	5.94%	5.66%	5.86%	3.42%
0.420	5.53%	0.09%	5.09%	5.34%	4.99%	4.55%
0.460	0.24%	3.30%	0.33%	0.31%	0.21%	6.64%
0.500	8.23%	6.28%	7.95%	8.38%	8.23%	3.64%
RMS Error	9.02%	9.51%	7.85%	8.92%	7.82%	2.93%

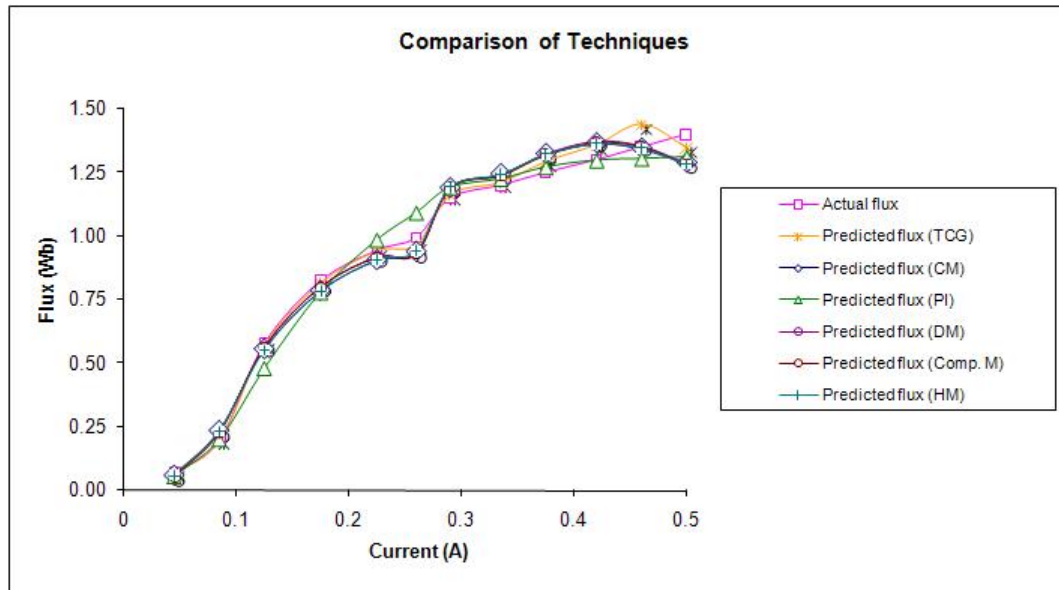


Figure 5.10: Prediction plot for transformer flux measurement

5.5 Summary

Using modern linear systems analysis concentrating on numerical techniques, this chapter introduced linear methods developed earlier and has shown

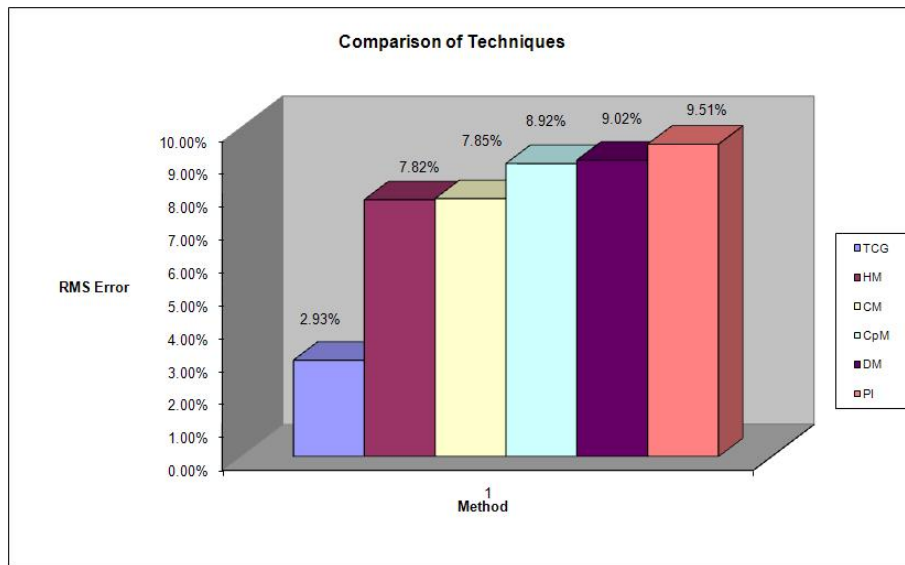


Figure 5.11: Error plot for transformer flux measurement

enrichment through the use of special matrices and modern computational algorithms based on robust statistical definitions. Application of these methods in product evaluation has been illustrated in such designs as the USB clip and transformers. Bolstering need for such algorithms, the next chapter analyzes systems exhibiting non-linear response.

Chapter 6

Non-Linear Methods

“It is not the fruits of scientific research that elevate man and enrich his nature. But the urge to understand, the intellectual work, creative or receptive.” - Albert Einstein

Systems demonstrating non-linear behavior typically indicate changes in magnitude with variable slope. Such systems do not correlate in the linear range with statistical measures typifying swerve from expected values of linearity. Analyzing situations arising from such deviations need mathematical definitions involving higher order approximations as linear scale does not suffice. Buttressing development of non-linear processes, this chapter reflects upon past methods and introduces advances achieved using novel techniques. Potency of mathematical rigor used in the configuration of linear relations is perpetuated to higher order polynomials.

6.1 Test for Non-Linearity-Statistical Procedures

Like before, it is highly recommended to establish non-linearity ahead of any analysis. Such estimation assures proper usage of available techniques

without compromising desired accuracy. Consider for illustration, hypothetical vectors given by,

$$X_{ms} = \begin{pmatrix} 0.141120 \\ 0.279415 \\ 0.656987 \\ 0.756802 \\ 0.958924 \end{pmatrix}, \quad X_{ps} = \begin{pmatrix} 0.420167 \\ 0.990607 \\ 0.650288 \\ 0.287903 \\ 0.961397 \end{pmatrix}, \quad X_m = \begin{pmatrix} 0.846220 \\ 0.905578 \\ 0.132352 \\ 0.762558 \\ 0.756376 \end{pmatrix}$$

Simple observation does not yield any palpable measure of linearity or the lack of it but resorting to statistical measures generates mathematical credit to the argument of non-linearity. Pearson's and Spearman's coefficients provide enough insight into behavior of values to understand possible variations and plausible mathematical description thereafter. For test matrices defined above, Pearson's coefficients evaluate to -

$$r(X_{ms}, X_{ps}) = 0.1257 \tag{6.1}$$

$$r(X_{ms}, X_m) = -0.3279 \tag{6.2}$$

implying lack of linearity and suggesting probable higher order variation. Negative value in the second coefficient implies decrease in the value of variable X_m with increase in X_{ms} . Spearman's test described below provides similar results (see Tables 6.1 and 6.2).

Table 6.1: Spearman's test for X_{ms} and X_{ps}

X_{ms}	X_{ps}	$rank(X_{ms})$	$rank(X_{ps})$	d	d^2
0.141120	0.420167	1	2	-1	1
0.279415	0.990607	2	5	-3	9
0.656987	0.650288	3	3	0	0
0.756802	0.287903	4	1	3	9
0.958924	0.961397	5	4	1	1

which gives,

$$\rho(X_{ms}, X_{ps}) = 1 - 6 \times \left(\frac{1 + 9 + 0 + 9 + 1}{5 \times (25 - 1)} \right) = 1 - \frac{6 \times 20}{5 \times 24} \quad (6.3)$$

$$\rho(X_{ms}, X_{ps}) = 1 - 1 = 0 \quad (6.4)$$

Similarly,

Table 6.2: Spearman's test for X_{ms} and X_m

X_{ms}	X_m	$rank(X_{ms})$	$rank(X_m)$	d	d^2
0.141120	0.846220	1	4	-3	9
0.279415	0.905578	2	5	-3	9
0.656987	0.132352	3	1	2	4
0.756802	0.762558	4	3	1	1
0.958924	0.756376	5	2	3	9

which leads to -

$$\rho(X_{ms}, X_m) = 1 - 6 \times \left(\frac{9 + 9 + 4 + 1 + 9}{5 \times (25 - 1)} \right) = 1 - \frac{6 \times 32}{5 \times 24} \quad (6.5)$$

$$\rho(X_{ms}, X_m) = 1 - 1.6 = -0.6 \quad (6.6)$$

thereby indicating existence of non-linear relationships. Building on this knowledge of non-linear measures, the following section introduces early methods and fortifies pioneering developments in non-linear ESM.

6.2 Non-Linear ESM Methods

In the estimation of parameters in non-linear systems, ESM deviates from point based linear model and assumes continuous functional variations. The ESM problem is modified to accommodate non-linear features such that,

$$x_{ps} = f(x_{ms}) \quad (6.7)$$

$$x_m = g(x_{ms}) \quad (6.8)$$

$$x_p = f(x_m) \quad (6.9)$$

$$x_p = g(x_{ps}) \quad (6.10)$$

$$x_p = (f * g)(x_{ms}) \quad (6.11)$$

where f and g are functional forms relating concerned geometries. Notice that functions are convoluted when relating product and model specimen as simple multiplication does not convey information regarding material and geometry changes. Convolution provides necessary integration and interaction of material properties *as* geometry modifies. Using the convolution formulation defined above, non-linear methods provide required scaling using properties specific to their analytical abilities. The most promising of such techniques are described below.

6.2.1 Polynomial Methods

Polynomial methods represent logical progression to model non-linear systems stepping up order of evaluation from a monomial to functions of order 2 and above. These functions involve $C^{\infty 1}$ characteristics whose approximation engulfs data in the family of curves characterized by smooth continuous definitions and spans entire length of available experimental data. Response values of systems displaying non-linear behavior can be captured using such methods thus providing physical insight. Some of the early methods used are described below followed by more advanced innovations.

6.2.1.1 Bilinear Method

The first method introduced for analyzing non-linear systems is bilinear ESM [Cho, 1999], a combination of two linear forms such that the product state

¹Infinitely differentiable.

vector is represented using the relation,

$$x_p = \frac{ux_m + u_o}{vx_m + v_o} \quad (6.12)$$

where constants of the map $\{u, u_o, v, v_o\}$ are derived using the relation,

$$x_{ps} = \frac{ux_{ms} + u_o}{vx_{ms} + v_o} \quad (6.13)$$

Similarly,

$$x_m = \frac{u'x_{ms} + u'_o}{v'x_{ms} + v'_o} \quad (6.14)$$

The process is a derivative of the Möbius transformation [Grewal, 1998] of a complex number given by,

$$w = \frac{az + b}{cz + d} \quad (6.15)$$

where the condition $\overline{ad - bc} = 0$ characterizes critical points of the transformation. This transformation is symbolized by one - to - one correspondence of all points in z and w plane. Further, the transformation causes cross ratio to hold across all points in the domain, *i.e.*, for any three points in z -plane and w -plane, we have,

$$\frac{(w_1 - w_2)(w_3 - w)}{(w_1 - w)(w_3 - w_2)} = \frac{(z_1 - z_2)(z_3 - z)}{(z_1 - z)(z_3 - z_2)} \quad (6.16)$$

Mathematically, the cross ratio should be invariant² as transformed points are fixed and unique for a given set of initial points. Modifying the cross ratio to adapt to ESM, scale formation is given by,

²Numerically finite and stable.

$$u = z_{ms,2} - z_{ms,1} \quad (6.17)$$

$$u_o = (z_{ms,1} - z_{ms,2})z_{ms,3} \quad (6.18)$$

$$v = z_{ms,2} - z_{ms,3} \quad (6.19)$$

$$v_o = (z_{ms,3} - z_{ms,2})z_{ms,1} \quad (6.20)$$

and form transformation is captured by,

$$u' = z_{ps,2} - z_{ps,1} \quad (6.21)$$

$$u'_o = (z_{ps,1} - z_{ps,2})z_{ps,3} \quad (6.22)$$

$$v' = z_{ps,2} - z_{ps,3} \quad (6.23)$$

$$v'_o = (z_{ps,3} - z_{ps,2})z_{ps,1} \quad (6.24)$$

where $z_{\odot,i}$ represents response value in a particular domain and point. System transformation is now given by,

$$T = (S \times F) = \frac{ux_m + u_o}{vx_m + v_o} \quad (6.25)$$

such that the prediction equation is modified to -

$$x_p = \frac{Tv'_o - u'_o}{u' - Tv'} \quad (6.26)$$

For each triplet of x_m , x_{ms} and x_{ps} , we obtain a single prediction for x_p . Notice that bilinear ESM is inhibited by a potential singularity condition (referred to as invariance of the process) when $z_{ms,1} = z_{ps,1} = z_{m,1}$ and has limited predictions in its domain *i.e.*, it takes 9 initial points (3 points in each geometry in three successive states) to have a single prediction and hence for n states, number of possible predictions is $n - 2$. The final two values need to be generated using reverse estimation or backward evaluation where values are flipped and analysis performed thereafter. The singularity though is removable

by mathematical simplification of the prediction equation. Symmetry of ESM is also lost as -

$$x_p = \frac{ux_m + u_o}{vx_m + v_o} = \frac{u \left(\frac{u' x_{ms} + u'_o}{v' x_{ms} + v'_o} \right) + u_o}{v \left(\frac{u' x_{ms} + u'_o}{v' x_{ms} + v'_o} \right) + v_o} \quad (6.27)$$

$$\neq \frac{u' x_{ps} + u'_o}{v' x_m + v'_o} = \frac{u' \left(\frac{ux_{ms} + u_o}{vx_{ms} + v_o} \right) + u'_o}{v' \left(\frac{ux_{ms} + u_o}{vx_{ms} + v_o} \right) + v'_o} \quad (6.28)$$

Using the test vectors defined earlier in this chapter,

$$\begin{pmatrix} [u \ u_0 \ v \ v_0]_1 \\ [u \ u_0 \ v \ v_0]_2 \\ [u \ u_0 \ v \ v_0]_3 \\ [u \ u_0 \ v \ v_0]_4 \\ [u \ u_0 \ v \ v_0]_5 \end{pmatrix} = \begin{pmatrix} 0.138295 & -0.090858 & -0.377572 & 0.053283 \\ 0.377572 & -0.285747 & -0.099815 & 0.0278898 \\ 0.099815 & -0.095715 & -0.202122 & 0.132792 \\ -0.099815 & 0.0278898 & 0.377572 & -0.285747 \\ -0.202122 & 0.132792 & 0.099815 & -0.095715 \end{pmatrix}$$

$$\begin{pmatrix} [u' \ u'_0 \ v' \ v'_0]_1 \\ [u' \ u'_0 \ v' \ v'_0]_2 \\ [u' \ u'_0 \ v' \ v'_0]_3 \\ [u' \ u'_0 \ v' \ v'_0]_4 \\ [u' \ u'_0 \ v' \ v'_0]_5 \end{pmatrix} = \begin{pmatrix} 0.57044 & -0.37095 & 0.340319 & -0.142991 \\ -0.340319 & 0.0979789 & 0.362385 & -0.358981 \\ -0.362385 & 0.348396 & -0.673494 & 0.437965 \\ 0.362385 & -0.358981 & -0.340319 & 0.0979789 \\ -0.673494 & 0.437965 & -0.362385 & 0.348396 \end{pmatrix}$$

and thus,

$$\begin{pmatrix} T_1 \\ T_2 \\ T_3 \\ T_4 \\ T_5 \end{pmatrix}_{Bilinear} = \begin{pmatrix} -0.0982999 \\ -0.898772 \\ -0.778047 \\ -22.1897 \\ 0.993638 \end{pmatrix}$$

Further, modifying Equation (6.12),

$$x_p = \frac{ux_m + u_o}{vx_m + v_o} = \frac{1}{v_o} \left(\frac{ux_m + u_o}{\frac{vx_m}{v_o} + 1} \right) \quad (6.29)$$

$$x_p = \left(\frac{ux_m + u_o}{v_o} \right) \left(1 + \frac{vx_m}{v_o} \right)^{-1} \quad (6.30)$$

$$x_p \approx \left(\frac{ux_m + u_o}{v_o} \right) \left(1 - \frac{vx_m}{v_o} + \frac{v^2x_m^2}{v_o^2} - \dots \right) \quad (6.31)$$

provided $\frac{vx_m}{v_o} \ll 1$. This condition is severely restrictive and magnitude of the fraction is really dependent on the problem and associated values. Hence, a more generic polynomial mapping is desired where order can vary to higher degrees instead of simple linear relations. This method though is an initial attempt at non-linear ESM and has provided basis for the development of the next technique that incorporates general polynomial mapping of test data.

6.2.1.2 Polynomial Method

The second method is the classic polynomial ESM process [Cho, 1999] where the product state vector is defined by,

$$x_p = \sum_{i=0}^n a_i x_m^i \quad (6.32)$$

where n is order of the polynomial used and constants a_i 's are derived using the relation,

$$x_{ps} = \sum_{i=0}^n a_i x_{ms}^i \quad (6.33)$$

Similarly,

$$x_m = \sum_{i=0}^n b_i x_{ms}^i \quad (6.34)$$

In this case, the state and system transformations are given by,

$$S = x_{ps}x_{ms}^+; F = x_mx_{ms}^+; T = [(x_{ps}x_{ms}^+) \times (x_mx_{ms}^+)] \quad (6.35)$$

where x_{ms}^+ is pseudo-inverse of x_{ms} [Albert, 1972]. The prediction equation is written as -

$$x_p = Tx_{ms} = Sx_m = Fx_{ps} \quad (6.36)$$

where we select only the second column of the resulting matrix for consideration [Cho, 1999]. Notice that polynomial ESM does not suffer from any singularity drawbacks but the biggest impediment to the process is establishing the right order of polynomial, n , to use. Conventionally, the method has been used where the order, starting from 2, has been incremented in steps of 1 and error at end of each step compared to estimate “best” fit. The inherent limitation of this strategy is unavailability of (hypothetical) product data to estimate errors which then inhibits use of correct order of polynomial. Lack of knowledge of order of polynomial can be detrimental when analyzing systems with numerous measurements as order can rise dramatically introducing complexity and unwarranted noise. For the test vectors defined earlier, several different polynomials can be derived such that,

$$x_{ps,2} = 0.780501 - 0.898443x_{ms} + 0.948328x_{ms}^2 \quad (6.37)$$

$$x_{ps,3} = -1.18049 + 15.2991x_{ms} - 31.6671x_{ms}^2 + 18.7914x_{ms}^3 \quad (6.38)$$

$$x_{ps,4} = 0.14299 - 1.31039x_{ms} + 32.744x_{ms}^2 - 73.7835x_{ms}^3 + 43.7887x_{ms}^4 \quad (6.39)$$

Thus,

$$X_{ps} = \begin{pmatrix} 0 & 0 & 0.948328 & -0.898443 & 0.780501 \\ 0 & 18.7914 & -31.6671 & 15.2991 & -1.18049 \\ 43.7887 & -73.7835 & 32.744 & -1.31039 & 0.14299 \end{pmatrix} \begin{pmatrix} x_{ms}^4 \\ x_{ms}^3 \\ x_{ms}^2 \\ x_{ms} \\ 1 \end{pmatrix}$$

such that,

$$S = \begin{pmatrix} 0 & 0 & 0.948328 & -0.898443 & 0.780501 \\ 0 & 18.7914 & -31.6671 & 15.2991 & -1.18049 \\ 43.7887 & -73.7835 & 32.744 & -1.31039 & 0.14299 \end{pmatrix}$$

Similarly,

$$X_m = \begin{pmatrix} 0 & 0 & 2.47492 & -2.95076 & 1.32825 \\ 0 & 4.44731 & -5.24409 & 0.882681 & 0.864144 \\ -113.654 & 244.727 & -172.424 & 43.993 & -2.57097 \end{pmatrix} \begin{pmatrix} x_{ms}^4 \\ x_{ms}^3 \\ x_{ms}^2 \\ x_{ms} \\ 1 \end{pmatrix}$$

such that,

$$F = \begin{pmatrix} 0 & 0 & 2.47492 & -2.95076 & 1.32825 \\ 0 & 4.44731 & -5.24409 & 0.882681 & 0.864144 \\ -113.654 & 244.727 & -172.424 & 43.993 & -2.57097 \end{pmatrix}$$

Hence, a set of nine choices (3 in S combined with 3 in F) are created for the system transformation T^3 . Selection of the best polynomial combination is now non-trivial and might involve use of unnecessary or incorrect higher order polynomials. Remember that a 4th order scale curve and a 4th order form curve couple to produce a 8th order prediction curve. A reasonable estimate can be obtained using lower order curves even when the number of measurements or data points is fairly large. This estimation though, needs to be done based on judgement and computational ease using test data from the three representative geometries judiciously. Further, notice that the technique employs a pseudo-inverse since the matrix formed by coefficients of polynomial might not be square. Also, when such global schemes are used, mix and

³More higher order curves can still be forced using advanced data fit techniques.

match of different methods is impossible thereby losing potential and probable benefits obtained from concoction of techniques.

Based on these constraints, five novel methods have been developed that -

- Do not have any singularity conditions.
- Provide an accurate estimate of what the best order of the fit is or do not need one.
- Provide flexibility of using alternate methods in intermediate intervals.

While first two conditions are apparently intuitive, the third condition is elaborated for lucidity. The two methods presented above do not complement each other in the sense that one method cannot be used in conjunction with the other. In a given working domain, a designer needs to choose one of the methods but can never use both either partially or to complement the other. Thus, both methods lack flexibility to incorporate other methods into their working process. Such a feature can be accomplished if methods are adaptive and local as against global schemes. Adaptivity is done to reap benefits of discretization of working intervals and allows piecewise (interval specific) error check⁴. Since the working interval is discretized into several sub-intervals, we can adapt polynomial order and interval width, and combine individual interval solutions to form the system response by coupling points and slopes at end of each interval, a feature explained in more detail later in this chapter.

Working range discretization and subsequent individual scaling of each interval, allows for comparison of experimental and estimated data so that right order of polynomial can be established without any ambivalence. Methods relying on power of adaptivity provide added advantage of notification of potential error induced when orders of polynomials greater than the required

⁴These errors and their significance, and their implication in adaptive ESM methods are discussed in the next chapter.

order are used. [Cho, 1999] identified how higher order polynomials are not always suitable for scaling in his heat conduction example where errors increased after a certain order of polynomial was used depicting noise generation and propagation. But, obtaining the particular order before noise sets in is a cumbersome task. Order needs to be incremented in steps of 1 till such noise is observed, hinting that the previous order was the last potential polynomial map that can be extracted where noise to signal ratio is small. Higher order curves thus are not completely satisfactory and are computationally inefficient when artificial noise is introduced. Adaptive methods however have the ability to pick the next data point and order only when estimated interval error for a given order is not in the acceptable margin, an iteration that continues till diminishing returns phenomena is observed thereby nullifying noise development. Hence in the limiting condition,

$$\textit{Adaptive Polynomial ESM} \rightarrow \textit{Polynomial ESM as } k \rightarrow 1$$

k being number of intervals. The current focus though is to demonstrate improved estimation achieved while adhering to stringent error margins. The first of such developed adaptive methods is detailed below.

6.2.1.3 Adaptive Polynomial Method

The adaptive polynomial process is a variant of polynomial ESM method where estimation is still based on a curve fit given by,

$$[x_p]_k = \left[\sum_{i=0}^n a_i x_m^i \right]_k \quad (6.40)$$

where n is order of the polynomial and constants a_i 's still derived using the relation,

$$[x_{ps}]_k = \left[\sum_{i=0}^n a_i x_{ms}^i \right]_k \quad (6.41)$$

Similarly,

$$[x_m]_k = \left[\sum_{i=0}^n b_i x_{ms}^i \right]_k \quad (6.42)$$

However, the notable difference is use of interval k and hence individual and independent maps are produced to obtain scale and form transformations. Collecting individual transformations produces required system scale and form transformation which is then used for prediction purposes. The state and system transformations are now modified to -

$$S_k = (x_{ps}x_{ms}^{-1})_k; F_k = (x_m x_{ms}^{-1})_k; T_k = [(x_{ps}x_{ms}^{-1}) \times (x_m x_{ms}^{-1})]_k \quad (6.43)$$

and prediction equation assumes the form,

$$(x_p)_k = T_k (x_{ms})_k = S_k (x_m)_k = F_k (x_{ps})_k \quad (6.44)$$

The polynomial produced uses a combination of approximation and interpolation to establish scale and form transformations, and correct order of polynomial. Consider a system with 3 sets of ordered pairs in product specimen and model specimen, *i.e.*, $\{(x_{ms,1}, x_{ps,1}), (x_{ms,2}, x_{ps,2}), (x_{ms,3}, x_{ps,3})\}$. If $n = 2$ is the starting order of polynomial, then end points $(x_{ms,1}, x_{ps,1})$ and $(x_{ms,3}, x_{ps,3})$, and slope at the end point $(x_{ms,3}, x_{ps,3})$ are chosen for estimating the quadratic function that maps the data. Once the polynomial is obtained, prediction is made at the discarded intermediate point $(x_{ms,2}, x_{ps,2})$ and error comparison is conducted in Euclidean norm⁵. The process is repeated with higher order polynomials and corresponding intermediate points. Hence, several different error values are obtained at intermediate points depending on the order of polynomial used, the smallest of which indicates the best polynomial fit. Therefore, end points and slope at the right end point perform approximation while interpolation is executed at the intermediate point thereby setting up a scheme of iterative approximation and interpolation. Thus, P_k being a

⁵Explained in the next chapter.

polynomial of order k ,

$$\text{approximation} \rightarrow P_2 = f_2 \left[(x_{ms,1}, x_{ps,1}), (x_{ms,3}, x_{ps,3}), |f'_2|_{(x_{ms,3}, x_{ps,3})} \right] \quad (6.45)$$

$$\text{interpolation} \rightarrow x_{ps,2}^{est} = |P_2|_{x_{ms,2}} \quad (6.46)$$

$$\text{error} \rightarrow \epsilon_1 = \|x_{ps,2}^{est} - x_{ps,2}\|_{L^2} \quad (6.47)$$

When multiple interpolations are carried out, the smallest of individual errors indicates the right polynomial. The process is repeated to establish cubic, quartic, quintic and higher order curves based on availability of data points and occurrence of diminishing returns thereby estimating interval specific optimal polynomial order. Further continuity of solution needs to be ensured in position and slope implying that interval end points need to converge with smooth gradients. Slope information at junction points is obtained from the two interacting intervals. The process continues till the final interval where slope information at the left end and all final interval data points are used along with the assumption of zero slope at the right extreme to compile the culminating polynomial subject to existence of data points.

Generalizing for n data points, p representing order of polynomial, m number of intervals, h the interval number and j the corresponding end point, $\forall h \in [1, m], \forall p \in [2, n - 1]$ and $j \leq n$,

$$P_p = f_p \left[(x_{ms,1}, x_{ps,1}), \dots, (x_{ms,j}, x_{ps,j}), |f'_p|_{(x_{ms,j}, x_{ps,j})} \right] \quad (6.48)$$

$$x_{ps,u}^{est} = |P_p|_{x_{ms,u}} \quad \forall u \in [1, j]' \quad (6.49)$$

$$\epsilon_u = \|x_{ps,u}^{est} - x_{ps,u}\|_{L^2} \quad \forall u \in [1, j]' \quad (6.50)$$

$$\epsilon_{min,h} = \min(\epsilon_u) \quad (6.51)$$

$$\left| \left(\frac{dP_p}{dx} \right)^{h^+} \right|_j = \left| \left(\frac{dP_p}{dx} \right)^{h^-} \right|_j \quad (6.52)$$

and

$$Q_p = g_p \left[(x_{ms,1}, x_{m,1}), \dots, (x_{ms,j}, x_{m,j}), |g'_p|(x_{ms,j}, x_{ps,j}) \right] \quad (6.53)$$

$$x_{m,u}^{est} = |Q_p|_{x_{ms,u}} \quad \forall u \in [1, j]' \quad (6.54)$$

$$\varepsilon_u = \|x_{m,u}^{est} - x_{m,u}\|_{L^2} \quad \forall u \in [1, j]' \quad (6.55)$$

$$\varepsilon_{min,h} = \min(\varepsilon_u) \quad (6.56)$$

$$\left| \left(\frac{dQ_p}{dx} \right)^{h^+} \right|_j = \left| \left(\frac{dQ_p}{dx} \right)^{h^-} \right|_j \quad (6.57)$$

where P and Q are scale and form polynomials respectively. The process is highly effective when number of measurements is fairly large but for few measurements (5 or less), a global scheme (cubic or quadratic) would be advantageous as further manipulation is impossible due to lack of data and it is computationally unprofitable to use an adaptive scheme. Also, the method fails for numerically small values since higher order terms become less significant. Hence, this approach fits a polynomial of optimal order irrespective of upper bound on the number of measurements. Notice that matrices formed by the polynomials (coefficient matrix) are always square even if orders change with interval. An optimal order of 2 in interval x and an order of 3 in interval y can still be coupled with an additional 0 element to make the system square thus negating use of pseudo-inverses. In essence, the method scans through every interval, probing at every point and order, to set up error comparison that allows to determine the smallest order polynomial that maps data with a fair degree of accuracy in that particular interval. In the process, interval width is adjusted by incorporating additional data points if they exist. The algorithm to conduct such a search in establishing scale and form polynomials is detailed below and summarized in a flow chart later.

Algorithm 1: The Adaptive Polynomial Method

Step 1: Set $\epsilon_g \rightarrow tol$. Go to step 2.

Initial value of acceptable global error to be equal to some fixed finite tolerance.

Step 2: Set $m \rightarrow 2$, Set $n \rightarrow m$, Set $h \rightarrow 1$. Go to step 3.

Initial search index of polynomial, n , set to degree 2. This implies that a quadratic polynomial is fitted in each interval. Further, we have 3 DOF and hence each interval has 3 nodes - 2 to approximate the polynomial with slope information and 1 to interpolate and verify. This is also the first interval.

Step 3: Set $(z_i) \rightarrow (x_{ms,i}, x_{ps,i})$, the end points of each interval. Go to step 4. If the material is isotropic throughout, then each interval is of uniform length else interval length is determined by end points located exactly where a change in material property occurs.

Step 4: Fit $x_{ps}^{est} \rightarrow \sum_{j=0}^n a_j x_{ms}^j$. Go to step 5.

Curve that fits distribution of values at points between the two geometries in the particular interval.

Step 5: Estimate local error $\epsilon_{l,i} \rightarrow \|x_{ps}^{est} - x_{ps}\|_{L^2}$ at each intermediate point. Go to step 6.

L^2 norm is chosen as it accounts for possible negative values in estimating local errors.

Step 6: Estimate minimum of local errors $\epsilon_{min} \rightarrow \min(\epsilon_{l,i})$. Go to step 7.

Step 7: Include next data point, modify $(z_i) \rightarrow (x_{ms,i+1}, x_{ps,i+1})$. Go to step 8. Inclusion of next data point allows increase of polynomial order.

Step 8: Repeat steps 4 through 7 for order $n \rightarrow 2$ and order $n \rightarrow n + 1$. Go to step 9.

Step 9: Compare 2 different errors. Go to step 10.

ϵ_{min} for order 2 with original end points

ϵ_{min} for order 3 with modified end points

Step 10: Is order 3 better than order 2? If yes, set $n \rightarrow 3$. Repeat steps 4 through 9 until $\epsilon_{min,latest} > \epsilon_{min,previous}$. If no, go to step 11.

Every time order is incremented by 1, number of possible error margins increase.

Step 11: Set $h \rightarrow h + 1$. Go to step 12.

Interval 1 has an optimal order 2 and ends at $(x_{ms,i}, x_{ps,i})$.

Step 12: Set $i \rightarrow i + 1$, redefine bounds of next interval $(z_i) \rightarrow (x_{ms,i}, x_{ps,i})$. Go to step 13.

Step 13: Repeat steps 3 through 12 till all intervals or data points are included. Go to step 14.

Step 14: Obtain the Root Mean Square (RMS) of all local minimum errors to generate net scale error $\epsilon_{scale} \rightarrow \|\epsilon_{min}\|_{RMS}$. Repeat the entire process for form error $\epsilon_{form} \rightarrow \|\epsilon_{min}\|_{RMS}$. Go to step 15.

RMS estimate is used to provide global average of ϵ_{min} .

Step 15: Estimate system error as $E_{sys} \rightarrow \epsilon_{scale} \times \epsilon_{form}$. Go to step 16.

Step 16: Is $E_{sys} \leq \epsilon_g$? If yes, Print n , $x_m^{est} \rightarrow \sum_{j=0}^n b_j x_{ms}^j$ and $x_{ps}^{est} \rightarrow \sum_{j=0}^n a_j x_{ms}^j$ for each interval. End. If no, print convergence not obtained. End.

Consider the following example matrices for illustration. Assume that the scale transformation is of interest.

$$X_{ms} = \begin{pmatrix} 325 \\ 368 \\ 417 \\ 484 \\ 543 \\ 599 \end{pmatrix}, \quad X_{ps} = \begin{pmatrix} 416 \\ 488 \\ 525 \\ 573 \\ 635 \\ 676 \end{pmatrix}$$

The first interval, $h = 1$, when order is 2 is spanned by $\{(325, 416), (417, 525)\}$ and includes three points. Let the curve be defined as -

$$x_{ps}^{h=1} = a_1 x_{ms}^2 + b_1 x_{ms} + c_1 \quad (6.58)$$

where the end points and slope at the right end are used. The second interval, $h = 2$ is spanned by $\{(417, 525), (599, 676)\}$ and includes four points and thus is represented by a cubic curve. Two different options are available to define the cubic polynomial using the four points. Since the end points and the slope at the left end are prescribed, three of the four DOF's are populated leaving just one DOF that is satisfied by either point $(484, 573)$ or $(543, 635)$. Error estimation is performed at the point other than the one chosen for the curve definition. Let the curve be defined as -

$$x_{ps}^{h=2} = a_2 x_{ms}^2 + b_2 x_{ms} + c_2 + d_2 \quad (6.59)$$

Since continuity in position and slope is to be maintained at the interacting point $(417, 525)$,

$$|2a_1 x_{ms} + b_1|_{x_{ms}=417} = |3a_2 x_{ms}^2 + 2b_2 x_{ms} + c_2|_{x_{ms}=417} \quad (6.60)$$

Hence,

$$416 = 325^2 a_1 + 325 b_1 + c_1 \quad (6.61)$$

$$525 = 417^2 a_1 + 417 b_1 + c_1 \quad (6.62)$$

$$2 \times 417 a_1 + b_1 = 3 \times 417^2 a_2 + 2 \times 417 b_2 + c_2 \quad (6.63)$$

$$525 = 417^3 a_2 + 417^2 b_2 + 417 c_2 + d_2 \quad (6.64)$$

$$676 = 599^3 a_2 + 599^2 b_2 + 599 c_2 + d_2 \quad (6.65)$$

$$635 = 543^3 a_2 + 543^2 b_2 + 543 c_2 + d_2 \quad (6.66)$$

or,

$$416 = 325^2 a_1 + 325 b_1 + c_1 \quad (6.67)$$

$$525 = 417^2 a_1 + 417 b_1 + c_1 \quad (6.68)$$

$$2 \times 417 a_1 + b_1 = 3 \times 417^2 a_2 + 2 \times 417 b_2 + c_2 \quad (6.69)$$

$$525 = 417^3 a_2 + 417^2 b_2 + 417 c_2 + d_2 \quad (6.70)$$

$$676 = 599^3 a_2 + 599^2 b_2 + 599 c_2 + d_2 \quad (6.71)$$

$$573 = 484^3 a_2 + 484^2 b_2 + 484 c_2 + d_2 \quad (6.72)$$

Notice that there are 6 equations and 7 unknowns. Thus we need another condition which is the slope information at right extreme of the second interval or the left extreme of the first interval. Progressing in the forward direction typically assures slope information at the right extreme of the second interval (provided it is not the last interval) and thus a marching solution is generated. Hence, in the final interval slope at the right most extreme is warranted which is assumed to be zero. Therefore,

$$3 \times 599^2 a_2 + 2 \times 599 b_2 + c_2 = 0 \quad (6.73)$$

which is the missing equation. Bear in mind that the above discussion is only an illustration of adaptive 2-3 polynomial and depending on the error margins at points (368, 488) and (484, 573)/(543, 635), the algorithm would suitably modify to estimate the optimal combination. For the example above,

$$\begin{pmatrix} a_1 \\ b_1 \\ c_1 \\ a_2 \\ b_2 \\ c_2 \\ d_2 \end{pmatrix}_{using(484,573)} = \begin{pmatrix} -0.0121972 \\ 10.2351 \\ -1622.08 \\ -0.0000482038 \\ 0.0732904 \\ -35.9153 \\ 6252.61 \end{pmatrix} \text{ or } \begin{pmatrix} a_1 \\ b_1 \\ c_1 \\ a_2 \\ b_2 \\ c_2 \\ d_2 \end{pmatrix}_{using(543,635)} = \begin{pmatrix} -0.0191743 \\ 15.4121 \\ -2567.65 \\ -0.0000675822 \\ 0.104587 \\ -52.5491 \\ 9152 \end{pmatrix}$$

Since there are two possible error margins in the second interval, estimating both the values gives,

$$x_{ps,e}(484, 573) = 573 \quad (6.74)$$

$$x_{ps,e}(543, 635) = 635 \quad (6.75)$$

$$\epsilon_{(484,573)} = 0 \quad (6.76)$$

$$\epsilon_{(543,635)} = 0 \quad (6.77)$$

which suggests that either of the two curves is acceptable in the second interval alone. For completeness, estimating at the discarded intermediate point in the first interval,

$$x_{ps,e}(368, 488) = 492.645 \text{ using } (484, 573) \quad (6.78)$$

$$x_{ps,e}(368, 488) = 507.346 \text{ using } (543, 635) \quad (6.79)$$

$$\epsilon_1 = 4.645 \quad (6.80)$$

$$\epsilon_2 = 19.346 \quad (6.81)$$

clearly implying that the two polynomials to be used respectively in each interval are -

$$x_{ps,h=1} = -0.0121972x_{ms}^2 + 10.2351x_{ms} - 1622.08 \quad (6.82)$$

$$x_{ps,h=2} = -0.0000482038x_{ms}^3 + 0.0732904x_{ms}^2 - 35.9153x_{ms} + 6252.61 \quad (6.83)$$

thus generating the scale matrix to be -

$$S = \begin{pmatrix} 0 & -0.0121972 & 10.2351 & -1622.08 \\ -0.0000482038 & 0.0732904 & -35.9153 & 6252.61 \end{pmatrix}$$

Reiterating, this example is just an illustration of adaptive quadratic-cubic polynomial combination and the optimal orders of polynomial in each

interval is the prerogative of the algorithm which is pictorially described below (see Figure 6.1). The procedure commences with the selection of an acceptable global tolerance or error value which is used as a guiding tool for the rest of the algorithm. The initial order of polynomial is set to a value of 2 implying that curve fitting begins with quadratic functions. The end point of each interval is then identified and interval specific quadratic polynomial is fitted where position and slope continuity at each end point is ensured. Local errors are estimated at the discarded intermediate points. Subsequently, the interval span is increased to include the next data point and a cubic polynomial is fitted which allows to have two local errors, the smaller of which is adopted for analysis. This new error and the error from the quadratic polynomial are then compared to gauge any improvement obtained. The process continues till the current local minimum error for a certain order of polynomial is larger than the previous local minimum error for a order of polynomial one less than the current value. Using this pattern, all intervals are spanned and in each interval, a custom polynomial is used to map the data thereby developing a precise scale transformation. The root mean square of each local minimum error is thus the error due to the adaptive optimal scale transformation. Extension into establishing the form matrix follows similar analysis using data from the model. The product of the scale and form errors *i.e.*, the system error is compared to the global tolerance to determine its numerical acceptability. Relaxation of the global tolerance value may be pursued if the conditions are not satisfied and is strictly dependent on the requirements of the physical application. In each degree of relaxation, the algorithm searches for the optimal orders of polynomials to be constructed in every interval.

Thus far, polynomial methods have been elaborated that have varied from bilinear forms to polynomial curves to adaptive methods. This transition has spanned variations in order, from a special linear function to novel developments where optimal orders have been established. Extending this process, the next section introduces a special curve of order 3 that is adaptive by definition and does not skip points as in the adaptive polynomial method.

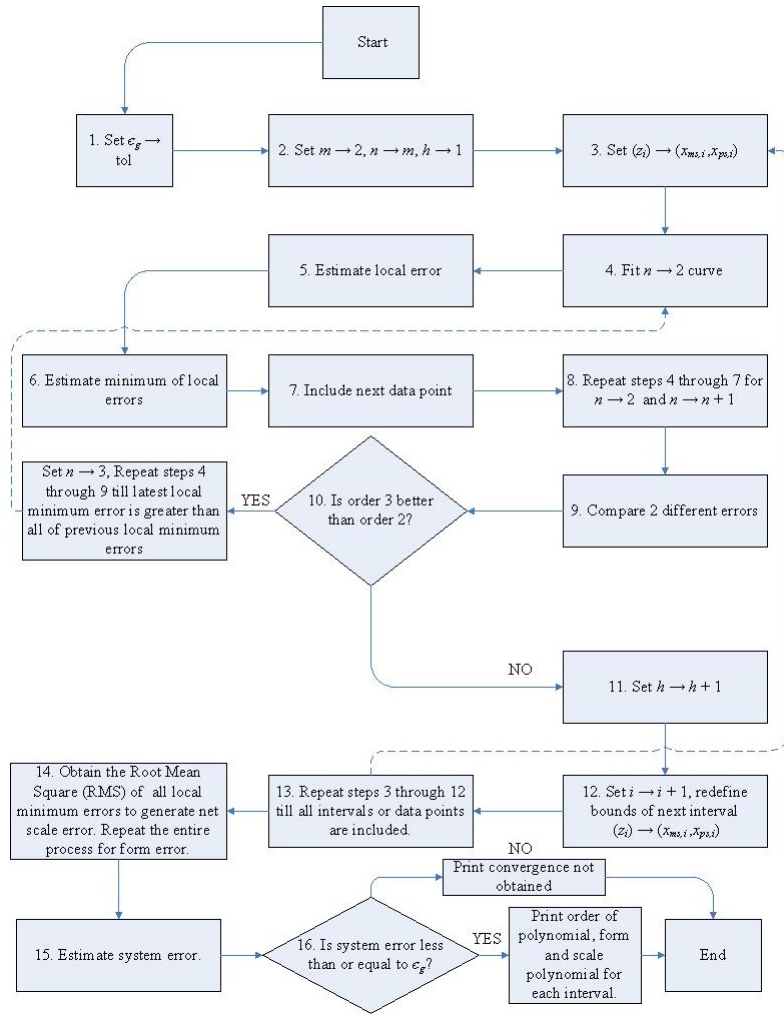


Figure 6.1: Adaptive polynomial method

6.2.1.4 Spline Fit Method

The previous section initiated discussion on adaptive polynomials and associated advantages. Necessity to maintain continuity was also described and such conditions have been enforced at junction points where two different intervals coincide. Illustrated below (see Figure 6.2) is effect of forcing higher order continuity as against simple position correction. Notice the smoothness introduced by using higher order definitions.

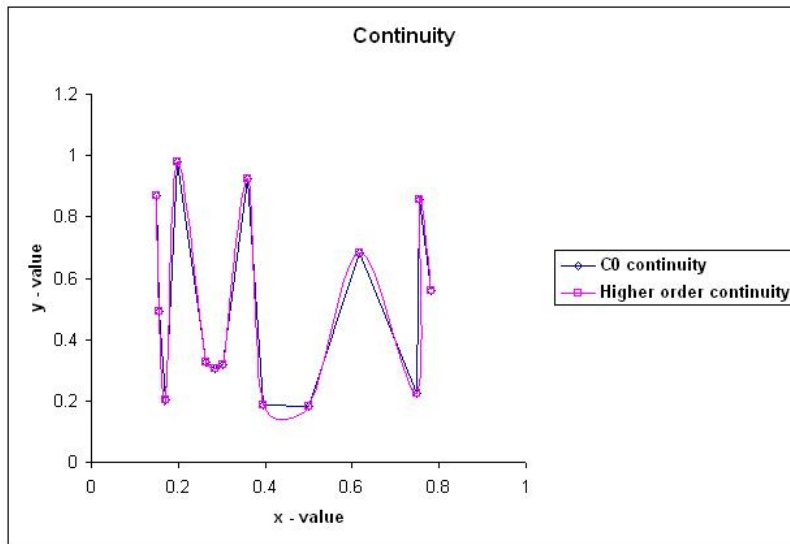


Figure 6.2: Effect of higher order continuity

Piecewise polynomials have been employed in the previous section where junction points were merged by coercing first order slopes to be numerically identical. This compels smoothness of curve but needs additional evaluation of gradient (finite and achievable) at boundaries, might produce oscillatory response and does not always guarantee smoothness [Faux et al., 1979]. To overcome such computational drawbacks, splines are introduced, natural cubic splines in particular that have the following characteristics [Faux et al., 1979]

1. Polynomials of degree ≤ 3 .
2. Interpolate all intermediate points.
3. Have continuous first and second derivatives at internal points.
4. No curvature at starting and ending points.

[Eubank, 1988] defines a spline as a piecewise polynomial joined with other piecewise polynomials at points of intersection with constrained continuity. Natural cubic spline approximation and interpolation, thus, is a structure

where points referred to as *knots* and interval width called *span* of the spline [Eubank, 1988], allows smooth 3rd order uniform and continuous estimation. Hence, all intervals would have the same order of polynomial. Mathematically, a cubic spline ϕ approximating knots $\{(x_i, y_i)\}_{i=0}^n$ is defined as -

$$\phi(x) \leq P_3 \quad (6.84)$$

$$\phi(x_i) = y_i \quad (6.85)$$

$$\phi'(x_i) = \phi''(x_i) \quad \forall 1 \leq i \leq n - 1 \quad (6.86)$$

$$\phi''(x_0) = \phi''(x_n) = 0 \quad (6.87)$$

Adapting the method to ESM, let $\{(x_{ms,1}, x_{ps,1}), (x_{ms,2}, x_{ps,2})\}$ be a set of two knots in estimating scale spline in the span $h_1 = |x_{ms,1} - x_{ms,2}|$. Then,

$$x_{ps} = \frac{a_1(x_{ms,2} - x_{ms})^3 + b_1(x_{ms} - x_{ms,1})^3}{6(x_{ms,2} - x_{ms,1})} + c_1x_{ms} + d_1 \quad (6.88)$$

where

$$a_1 = |x''_{ps}|_{x_{ms,1}} \quad (6.89)$$

$$b_1 = |x''_{ps}|_{x_{ms,2}} \quad (6.90)$$

$$c_1 = x_{ps,1} \quad (6.91)$$

$$d_1 = x_{ps,2} \quad (6.92)$$

Evaluating values of c_1 and d_1 is trivial but constants a_1 and b_1 need information about second derivatives at end points. To estimate these values, we invoke the curve from the next span $h_2 = |x_{ms,2} - x_{ms,3}|$ such that,

$$a_1h_1 + 2b_1(h_1 + h_2) + a_2h_2 = \frac{6(x_{ms,3} - x_{ms,2})}{h_2} - \frac{6(x_{ms,2} - x_{ms,1})}{h_1} \quad (6.93)$$

The above equation has three unknowns a_1 , b_1 and a_2 but each of the internal knot can be used to setup similar equations thus producing a matrix

of size n , leaving the starting and ending second derivatives $|x''_{ps}|_{x_{ms,1}}$ and $|x''_{ps}|_{x_{ms,n+1}}$ of complete span $H = |x_{ms,1} - x_{ms,n+1}|$. Using the final condition of a natural cubic spline, these terms would be 0 and hence n unknowns are evaluated using the matrix of coefficients thereby defining the curve completely. In this case, $a_1 = b_{n+1} = 0$. Hence,

$$x_{ps} = S_{spline}(x_{ms}) \quad (6.94)$$

$$x_m = F_{spline}(x_{ms}) \quad (6.95)$$

$$x_p = S_{spline}(x_m) = F_{spline}(x_{ps}) = (S_{spline} * F_{spline})(x_{ms}) \quad (6.96)$$

For test matrices given by,

$$X_{ms} = \begin{pmatrix} 325 \\ 368 \\ 417 \\ 484 \\ 543 \\ 599 \end{pmatrix}, \quad X_{ps} = \begin{pmatrix} 416 \\ 488 \\ 525 \\ 573 \\ 635 \\ 676 \end{pmatrix}$$

simulating directly from *Matlab*TM generates,

$$S = \begin{pmatrix} 0.0003 & -0.0595 & 3.7400 & 416.0000 \\ 0.0003 & -0.0250 & 0.1031 & 488.0000 \\ -0.0030 & 0.0576 & 3.4513 & 525.0000 \\ 0.0003 & -0.0595 & 3.4261 & 573.0000 \\ 0.0003 & -0.0018 & -0.1897 & 635.0000 \end{pmatrix}$$

with similar estimation possible for the form matrix as well. Splines thus present a wonderful opportunity to develop scale and form polynomials as values at junction points merge seamlessly due to mathematical characteristics of curves that obey natural cubic spline development. The only limiting

condition of splines is that $x_{j+1} > x_j$ or $x_{j+1} < x_j \forall j \in [1, n + 1]$ *i.e.*, distribution of values in x_{ms} has to be monotone increasing or decreasing and non-repetitive. However, most modern mathematical software allow direct evaluation of splines thus injecting ease in numerical computation unlike previous methods that need hard coding. In an effort to continue systematic robust analytical procedures, polynomial based schemes have traversed a path involving bilinear approach covering arbitrary order and adaptive optimal order polynomials before culminating in 3^{rd} order piecewise curves. Continuing such rigorous growth, the next section presents order free regression methods to analyze scale and form changes.

6.2.2 Regression Methods

Regression is a statistical process of establishing the functional form between a response variable y and a set of independent variables $\{x_i\}_{i=1}^n$ [Freedman, 2005]. The equation is usually derived using the least-squares approach in linear domains [Fox, 1997] where error is minimized and constants of the relation are established. Compensation matrix approach [Wood, 2002] described in chapter V is a linear regression model used to analyze sample data. Non-linear regression is a method where observed data is modeled as a curve of higher order since contributions from non-linear terms assume numerical significance [Seber et al., 1989]. In analyzing non-linear ESM problems, two such methods are detailed below.

6.2.2.1 Adaptive Exponential Regression Method

Adaptive exponential regression ESM process is a technique where prediction is based on the relation given by [Bethea et al., 1985],

$$[x_p]_k = [ab^{x^m}]_k \quad (6.97)$$

where constants a and b are derived using,

$$[x_{ps}]_k = [ab^{x_{ms}}]_k \quad (6.98)$$

Similarly,

$$[x_m]_k = [cd^{x_{ms}}]_k \quad (6.99)$$

Hence in a given interval k with sample data $\{(x_{ms,1}, x_{ps,1}), (x_{ms,2}, x_{ps,2})\}$,

$$\ln a = \left(\frac{x_{ms,1}x_{ms,2}}{x_{ms,1} - x_{ms,2}} \right) \ln \left[\frac{\frac{1}{x_{ps,1}}}{\frac{1}{x_{ps,2}}} \right] \quad (6.100)$$

$$\ln b = \left(\frac{1}{x_{ms,1} - x_{ms,2}} \right) \ln \left[\frac{x_{ps,1}}{x_{ps,2}} \right] \quad (6.101)$$

Thus, for every interval k ,

$$\begin{pmatrix} \ln x_{ps,1} \\ \ln x_{ps,2} \end{pmatrix}_k^T = \begin{pmatrix} \ln a & \ln b \end{pmatrix}_k \begin{pmatrix} 1 & 1 \\ x_{ms,1} & x_{ms,2} \end{pmatrix}_k$$

and

$$\begin{pmatrix} \ln x_{m,1} \\ \ln x_{m,2} \end{pmatrix}_k^T = \begin{pmatrix} \ln c & \ln d \end{pmatrix}_k \begin{pmatrix} 1 & 1 \\ x_{ms,1} & x_{ms,2} \end{pmatrix}_k$$

Notice that just two points are required to make a prediction that is specific to the interval of interest and since $x_{ms,1}$ and $x_{ms,2}$ are always unique, condition of singularity is completely avoided. In the limiting condition for a measurement point i , if $x_{ms,i} \rightarrow 0 \Rightarrow a \rightarrow x_{ps,i}$ and b is an arbitrary constant and therefore a free choice (1 DOF). However, even if one of the values of set $\{x_{ps,i}\}_{i=1}^n$ is 0, then scaling cannot be concluded as constant a would necessarily evaluate to 0. The necessity to model at the other extremum at (∞) is discounted as typical mechanical systems and products do not have undefined, indeterminate or infinitely large values for common parameters. Hence, the process is mathematically stable for non-zero finite values and allows comparison of experimental and estimated values of x_{ps} in each interval. This contrast

translates to important scaling information regarding efficiency of the technique. Note that only position continuity can be enforced at junction points as slope continuity becomes impractical. The first derivative at a junction point i for scale regression, $(a_1 b_1^{x_{ms,i}} \ln b_1)$ should be equal to $(a_2 b_2^{x_{ms,i}} \ln b_2)$ implying that $a_1 = a_2$ and $b_1 = b_2$ thereby setting up uniform scaling parameters across all intervals which is contrary to adaptivity. The method does not have enough DOF's to incorporate higher order continuity. Thus, continuity can be established in position alone where the arithmetic mean of left and right direction values is used at the junction (see Figure 6.3).

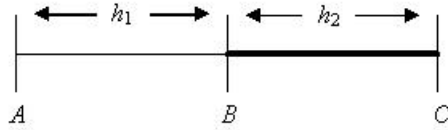


Figure 6.3: Position continuity

If in interval h_1 , predictions made at points A and B are x_A and x_{B^-} , and similarly in interval h_2 , predictions made at points B and C are x_{B^+} and x_C , then in order to maintain position continuity of solution, elemental solutions are modified to -

$$x_A^* = x_A \quad (6.102)$$

$$x_B^* = \frac{x_{B^-} + x_{B^+}}{2} \quad (6.103)$$

$$x_C^* = x_C \quad (6.104)$$

Further, the method is not symmetric as scale and form do not couple independent of direction.

$$[x_p]_k = [ab^{x_m}]_k = [ab^{[cd^{x_{ms}}]}]_k \neq [cd^{x_{ps}}]_k = [cd^{[ab^{x_{ms}}]}]_k \quad (6.105)$$

This method is thus unsuitable when systems depict smooth behavior that is beyond position continuity but is still potent in establishing scaling

values. For test matrices given by,

$$X_{ms} = \begin{pmatrix} 0.141120 \\ 0.279415 \\ 0.656987 \\ 0.756802 \\ 0.958924 \end{pmatrix}, \quad X_{ps} = \begin{pmatrix} 0.420167 \\ 0.990607 \\ 0.650288 \\ 0.287903 \\ 0.961397 \end{pmatrix}, \quad X_m = \begin{pmatrix} 0.846220 \\ 0.905578 \\ 0.132352 \\ 0.762558 \\ 0.756376 \end{pmatrix}$$

we have,

$$\begin{pmatrix} a_1 & b_1 \\ a_2 & b_2 \\ a_3 & b_3 \\ a_4 & b_4 \end{pmatrix}_{Exp.Reg.} = \begin{pmatrix} 0.175119 & 493.593 \\ 1.35262 & 0.327994 \\ 138.748 & 0.000285001 \\ 0.00315158 & 389.758 \end{pmatrix}$$

$$\begin{pmatrix} c_1 & d_1 \\ c_2 & d_2 \\ c_3 & d_3 \\ c_4 & d_4 \end{pmatrix}_{Exp.Reg.} = \begin{pmatrix} 0.789658 & 1.63266 \\ 3.75834 & 0.00613739 \\ 1.30558 \times 10^{-6} & 4.16409 \times 10^7 \\ 0.786157 & 0.960528 \end{pmatrix}$$

Expanding on this development, the next method uses a different regression approach to establish prediction parameters.

6.2.2.2 Adaptive Power Regression Method

Adaptive power regression ESM process obtains prediction values based on the relation given by,

$$[x_p]_k = [ax_m^b]_k \quad (6.106)$$

where k is the interval and constants a and b are derived using the relation,

$$[x_{ps}]_k = [ax_{ms}^b]_k \quad (6.107)$$

Similarly,

$$[x_m]_k = [cx_{ms}^d]_k \quad (6.108)$$

Thus, for every interval k ,

$$\begin{pmatrix} \ln x_{ps,1} \\ \ln x_{ps,2} \end{pmatrix}_k^T = \begin{pmatrix} \ln a & b \end{pmatrix}_k \begin{pmatrix} 1 & 1 \\ \ln x_{ms,1} & \ln x_{ms,2} \end{pmatrix}_k$$

and

$$\begin{pmatrix} \ln x_{m,1} \\ \ln x_{m,2} \end{pmatrix}_k^T = \begin{pmatrix} \ln c & d \end{pmatrix}_k \begin{pmatrix} 1 & 1 \\ \ln x_{ms,1} & \ln x_{ms,2} \end{pmatrix}_k$$

In this case too just two points are needed to make a prediction that is unique to the interval of interest. Hence, for a set of measurement points in model specimen and product specimen given by $\{(x_{ms,1}, x_{ps,1}), (x_{ms,2}, x_{ps,2})\}$, a unique curve fit of the form specified above can be obtained with well determined values for constants a and b . In the limiting condition for a measurement point i , if $x_{ms,i} \rightarrow 0 \Rightarrow x_{ps,i} \rightarrow 0$ and, a and b are now two arbitrary constants and therefore are free choices (2 DOF). If $x_{ps,i} \rightarrow 0$, then for non-zero values of $x_{ms,i}$, $a \rightarrow 0$. Here again mathematical stability is ensured for finite values and necessity to model the other extremum (∞) is refrained from for reasons mentioned earlier. Like before only position continuity can be enforced and symmetry is lost as -

$$[x_p]_k = [ax_m^b]_k = [a(cx_{ms}^d)^b]_k \quad (6.109)$$

$$\neq [cx_{ps}^d]_k = [c(ax_{ms}^b)^d]_k \quad (6.110)$$

Using the test matrices given by,

$$X_{ms} = \begin{pmatrix} 0.141120 \\ 0.279415 \\ 0.656987 \\ 0.756802 \\ 0.958924 \end{pmatrix}, \quad X_{ps} = \begin{pmatrix} 0.420167 \\ 0.990607 \\ 0.650288 \\ 0.287903 \\ 0.961397 \end{pmatrix}, \quad X_m = \begin{pmatrix} 0.846220 \\ 0.905578 \\ 0.132352 \\ 0.762558 \\ 0.756376 \end{pmatrix}$$

we have,

$$\begin{pmatrix} a_1 & b_1 \\ a_2 & b_2 \\ a_3 & b_3 \\ a_4 & b_4 \end{pmatrix}_{PowerReg.} = \begin{pmatrix} 4.91105 & 1.25557 \\ 0.528796 & -0.492303 \\ 0.0578213 & -5.76079 \\ 1.1904 & 5.09384 \end{pmatrix}$$

$$\begin{pmatrix} c_1 & d_1 \\ c_2 & d_2 \\ c_3 & d_3 \\ c_4 & d_4 \end{pmatrix}_{PowerReg.} = \begin{pmatrix} 1.02774 & 0.0992465 \\ 0.0514463 & -2.24934 \\ 24.0248 & 12.3815 \\ 0.755286 & -0.0343879 \end{pmatrix}$$

Summarizing, regression methods offer ease in computation that is time and effort conserving but solution robustness is lost due to lower order continuity. Further, presence of negative or 0 values are detrimental as logarithmic and power functions are not defined for such values. The methods are still highly recommended but with attached conditions. Hence, in analyzing a system where higher order continuity is not of paramount importance, regression methods can prove to be quite efficient since quick estimates can be derived unlike the adaptive polynomial method. Pursuing more rigorous definitions to ensure smoothness and higher order continuity in solution trends, trigonometric transforms are described in the next section where scale and form transformations are analyzed as periodic curves.

6.2.3 Trigonometric Methods

Trigonometric curves offer smoothing of data by fitting piecewise continuous plots. This effect of smoothing is realized by,

$$x_p = a_1 + \sum_{n=1}^r b_n \cos nx_m + \sum_{n=1}^r c_n \sin nx_m \quad (6.111)$$

where constants a_1 , b_n and c_n are derived using,

$$x_{ps} = a_1 + \sum_{n=1}^r b_n \cos nx_{ms} + \sum_{n=1}^r c_n \sin nx_{ms} \quad (6.112)$$

Similarly,

$$x_m = a_1^* + \sum_{n=1}^r b_n^* \cos nx_{ms} + \sum_{n=1}^r c_n^* \sin nx_{ms} \quad (6.113)$$

In each interval, a trigonometric polynomial is constructed starting from order $n = 1$, requiring 2 states of $\{x_{ms,i}, x_{ps,i}\}$ and slope at one of the end points to establish scale trigonometric and, 2 states of $\{x_{ms,i}, x_{m,i}\}$ and slope at one of the end points to establish form trigonometric such that,

$$\begin{pmatrix} x_{ps,1} \\ x_{ps,3} \\ x'_{ps,3} \end{pmatrix}^{est} = \begin{pmatrix} 1 & \cos x_{ms,1} & \sin x_{ms,1} \\ 1 & \cos x_{ms,3} & \sin x_{ms,3} \\ 0 & -\sin x_{ms,3} & \cos x_{ms,3} \end{pmatrix} \begin{pmatrix} a_1 \\ b_1 \\ c_1 \end{pmatrix}$$

and

$$\begin{pmatrix} x_{m,1} \\ x_{m,3} \\ x'_{m,3} \end{pmatrix}^{est} = \begin{pmatrix} 1 & \cos x_{ms,1} & \sin x_{ms,1} \\ 1 & \cos x_{ms,3} & \sin x_{ms,3} \\ 0 & -\sin x_{ms,3} & \cos x_{ms,3} \end{pmatrix} \begin{pmatrix} a_1^* \\ b_1^* \\ c_1^* \end{pmatrix}$$

such that for an intermediate point,

$$\epsilon_2^{n=1} = \|x_{ps,2}^{est} - x_{ps,2}\|_{L^2} \quad (6.114)$$

and

$$\varepsilon_2^{n=1} = \|x_{m,2}^{est} - x_{m,2}\|_{L^2} \quad (6.115)$$

Similar to adaptive polynomial ESM, this process employs using higher order approximations iteratively till current net error is numerically higher in magnitude than previous error. In general, for every interval k ,

$$\begin{pmatrix} x_{ps,1} \\ \vdots \\ x_{ps,n} \\ x'_{ps,n} \end{pmatrix}^{est} = \begin{pmatrix} 1 & \cos & \sin \\ \vdots & \vdots & \vdots \\ 1 & \cos & \sin \\ 0 & -\sin & \cos \end{pmatrix}_{2n+1} \begin{pmatrix} a \\ b \\ c \end{pmatrix}_{2n+1}$$

and

$$\begin{pmatrix} x_{m,1} \\ \vdots \\ x_{m,n} \\ x'_{m,n} \end{pmatrix}^{est} = \begin{pmatrix} 1 & \cos & \sin \\ \vdots & \vdots & \vdots \\ 1 & \cos & \sin \\ 0 & -\sin & \cos \end{pmatrix}_{2n+1} \begin{pmatrix} a^* \\ b^* \\ c^* \end{pmatrix}_{2n+1}$$

such that for any intermediate point t in interval k ,

$$\epsilon_{min} = \min(\|x_{ps,t}^{est} - x_{ps,t}\|_{L^2}) \quad (6.116)$$

and

$$\varepsilon_{min} = \min(\|x_{m,t}^{est} - x_{m,t}\|_{L^2}) \quad (6.117)$$

The technique iterates till ϵ_{min} and ε_{min} are established for an optimal order n (depending on availability of data) such that net system root mean square error,

$$\varepsilon_{sys}^n = (\epsilon_{RMS} \times \varepsilon_{RMS})_n \leq \varepsilon_g \quad (6.118)$$

where ε_g is allowable global tolerance. The algorithm and procedure are identical to adaptive polynomial method with only exception occurring in curve fitting where polynomials are replaced by sinusoidal functions. Higher order continuity is ensured by forcing $-(b_n \sin nx_{ms,i+}) + (c_n \cos nx_{ms,i+}) =$

$-(b_n \sin nx_{ms,i^-}) + (c_n \cos nx_{ms,i^-})$ at junction points i .

Consider a numerical example for elucidation. Assume that estimating the scale transformation is of interest. For adaptive trigonometric polynomials of order 1 and hypothetical test vectors given by,

$$X_{ms} = \begin{pmatrix} 325 \\ 368 \\ 417 \\ 484 \\ 543 \end{pmatrix}, \quad X_{ps} = \begin{pmatrix} 416 \\ 488 \\ 525 \\ 573 \\ 635 \end{pmatrix}$$

we have,

$$416 = \left(\frac{180}{\pi}\right) \left[a_1 + b_1 \cos\left(\frac{325\pi}{180}\right) + c_1 \sin\left(\frac{325\pi}{180}\right) \right] \quad (6.119)$$

$$525 = \left(\frac{180}{\pi}\right) \left[a_1 + b_1 \cos\left(\frac{417\pi}{180}\right) + c_1 \sin\left(\frac{417\pi}{180}\right) \right] \quad (6.120)$$

$$525 = \left(\frac{180}{\pi}\right) \left[a_2 + b_2 \cos\left(\frac{417\pi}{180}\right) + c_2 \sin\left(\frac{417\pi}{180}\right) \right] \quad (6.121)$$

$$635 = \left(\frac{180}{\pi}\right) \left[a_2 + b_2 \cos\left(\frac{543\pi}{180}\right) + c_2 \sin\left(\frac{543\pi}{180}\right) \right] \quad (6.122)$$

Similar to the adaptive polynomial development, slope at the intersecting point (417, 525) is matched for both the intervals and slope at the right extreme of the second interval is assumed to be zero such that,

$$-b_1 \sin\left(\frac{417\pi}{180}\right) + c_1 \cos\left(\frac{417\pi}{180}\right) = -b_2 \sin\left(\frac{417\pi}{180}\right) + c_2 \cos\left(\frac{417\pi}{180}\right) \quad (6.123)$$

$$-b_2 \sin\left(\frac{543\pi}{180}\right) + c_2 \cos\left(\frac{543\pi}{180}\right) = 0 \quad (6.124)$$

thus solving for 6 unknowns using 6 equations. The values of the constants are evaluated to be -

$$\begin{pmatrix} a_1 \\ b_1 \\ c_1 \\ a_2 \\ b_2 \\ c_2 \end{pmatrix} = \begin{pmatrix} 8.26938 \\ -0.333714 \\ 1.28221 \\ 9.8737 \\ -1.20749 \\ -0.0632817 \end{pmatrix}$$

hence creating the polynomials,

$$x_{ps,h=1} = 8.26938 - 0.333714 \cos(x_{ms}) + 1.28221 \sin(x_{ms}) \quad (6.125)$$

$$x_{ps,h=2} = 9.8737 - 1.20749 \cos(x_{ms}) - 0.0632817 \sin(x_{ms}) \quad (6.126)$$

Predicting and estimating errors at the discarded point (368, 488) and (484, 573) using the two polynomials respectively we have,

$$x_{ps,e}(368, 488) = 465.091 \quad (6.127)$$

$$x_{ps,e}(484, 573) = 601.402 \quad (6.128)$$

$$\epsilon_1 = 22.909 \quad (6.129)$$

$$\epsilon_2 = 28.402 \quad (6.130)$$

and

$$S = \begin{pmatrix} 8.26938 & -0.333714 & 1.28221 \\ 9.8737 & -1.20749 & -0.0632817 \end{pmatrix}$$

Bear in mind that these functions are for illustration alone and are first order polynomials in both intervals. The algorithm however searches for the optimal polynomial orders in each interval before diminishing returns is observed. The form transformation is developed using a similar procedure. The

only limitation of the adaptive trigonometric method is a potential complication when extremely small values are encountered which tend to be approximated or extremely large values are observed which cause quadrant specific multi-valued behavior in sinusoidal functions. Remember that in all adaptive methods, individual interval solutions need to be ‘summed’ for a global response curve.

The biggest and single most important innovation in development of these processes is their ability to interact and complement each other - a feature that was sorely missing in the two earliest methods. Consider a situation where the working domain is discretized into five intervals. Flexibility of these methods allows them to be used together implying that adaptive polynomial ESM could be used in first interval while spline fit takes over in the next and adaptive trigonometric ESM thereafter (see Figure 6.4). Remember that such a decision needs to be made based on predicted error values that are expected in each method for every interval and continuity requirements. Based on numerical estimates of error that every method generates in each interval, we can mix and match methods to generate a composite graph of adaptive methods. This phenomenon represents true adaptivity where interval length, polynomial order and scaling method are all combined. Before robustness of adaptive methods is discussed in terms of accuracy in physical system evaluation, it is prudent to contrast all developed methods to fathom their specific advantages and drawbacks. Such a comparison is performed in the next section.

6.2.4 Comparison of Methods

Prior sections discussed non-linear methods with copious mathematical detail and applicability in ESM. To comprehend effect and role of these processes, a comparative study is undertaken (see Tables 6.3, 6.4 and 6.5) that negotiates intricacies of each scheme for chosen criteria. Robustness is measured by potential singularity conditions and applicability over a wide range of values while complexity is determined by time spent in estimating parameters.

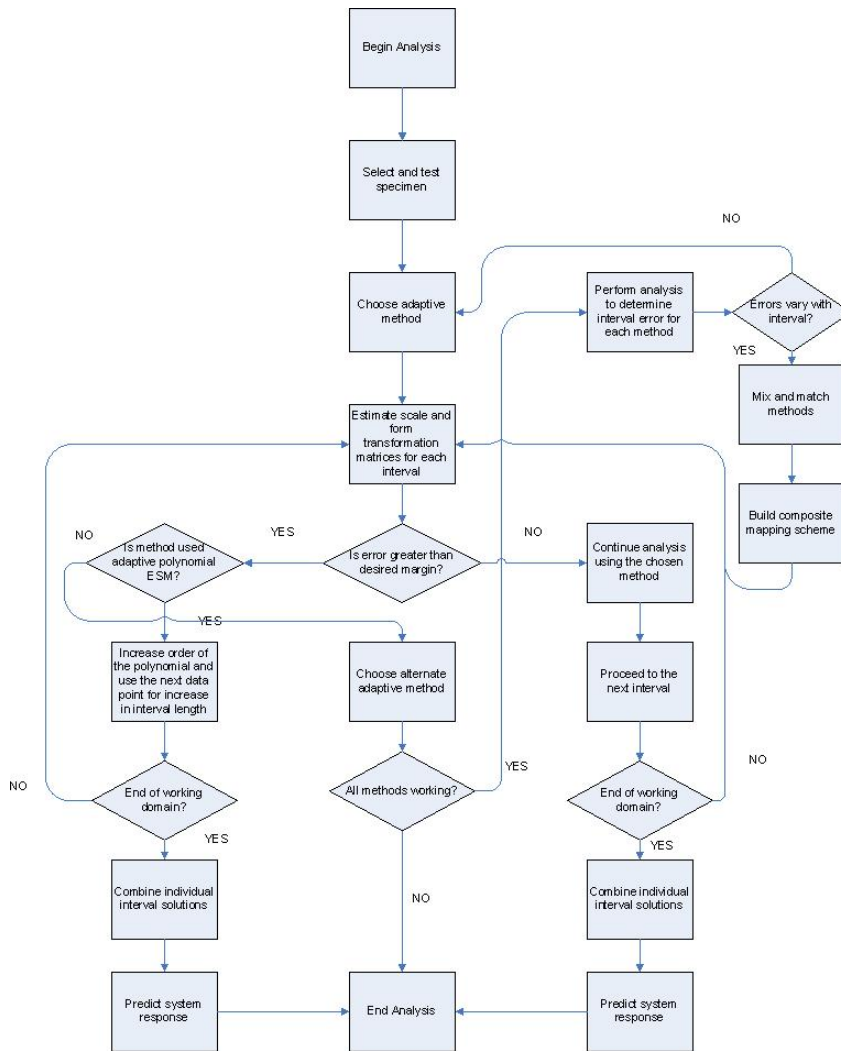


Figure 6.4: Adaptivity of the developed methods

The developed methods are now applied to engineering problems to quantify accuracy achieved and error margins observed. Examples from various domains are sought so that applicability across different conditions can be shown. A simple heat transfer example involving a kitchen utensil is described below.

Table 6.3: Comparison of non-linear methods - I

Method	Symmetry	Robustness
Bilinear	No	Potential removable singularity
Polynomial	Yes	Order unknown
Adaptive Polynomial	Yes	Order optimization needs time, Values must not be $\ll 1$
Spline Fit	Yes	Monotone \uparrow or \downarrow values needed
Adaptive Exp. Reg.	No	Values > 0
Adaptive Power Reg.	No	Values > 0
Adaptive Trig.	Yes	Finite values not approaching approximating conditions

Table 6.4: Comparison of non-linear methods - II

Method	Complexity	Order
Bilinear	Medium	1
Polynomial	Medium	≥ 2
Adaptive Polynomial	High	≥ 2
Spline Fit	High	3
Adaptive Exp. Reg.	Low	None
Adaptive Power Reg.	Low	None
Adaptive Trig.	High	≥ 1

Table 6.5: Comparison of non-linear methods - III

Method	Evaluation	Adaptivity	Continuity
Bilinear	Fixed	No	Position
Polynomial	Fixed	No	Position and slope
Adaptive Polynomial	Iterative	Yes	Position and slope
Spline Fit	Iterative	Yes	Position and slope
Adaptive Exp. Reg.	Fixed	Yes	Position
Adaptive Power Reg.	Fixed	Yes	Position
Adaptive Trig.	Iterative	Yes	Position and slope

6.3 Skillet-Temperature Analysis

The first step in assessing robustness of developed methods is achieved through a numerical experiment, that of temperature distribution of a regu-

lar kitchen skillet based on the prediction of a chosen specimen geometry for a constant heat source applied to the base. The skillet is a copper bottom steel geometry with shape as shown below (see Figure 6.5 - all dimensions are in *mm*). The chosen specimen geometry is a perfect hemisphere (see Figure 6.6) made from nylon. Geometries and materials used in this example are summarized in Table 6.6 as part of its ESM representation. Note that flux applied to the geometries changes from surface loading in product and model to point loading in model specimen and product specimen (distortion level I), and the product specimen is comprised of steel alone and is not a combination of steel and copper (distortion level II). This creates a variation in input conditions and material properties that should affect predicted values but ESM is shown to have minimal effect in such conditions. Further, effect of non-linearity is brought on by convective currents that cool appliances while being used for cooking. This experiment is performed as a validation process to predict behavior of a multi-material geometry using a polymer substance, both exhibiting inherent mild non-linear response. Thus, the main objectives of this experiment are -

- Numerically compare all methods using error margins to illustrate feasibility of the novel adaptive techniques.
- Demonstrate ability of ESM to make accurate prediction for distorted geometries.
- Demonstrate the validity of using a single polymer substance like Nylon to predict a multi-material steel-copper geometry.

The geometries are analyzed using *SolidWorksTM* software for temperature values at discrete points starting from the center of the base. A load of 50 *W* heat is applied to all structures at the geometric center of the base. Temperature values (*°C*) at different points along the surface are simulated and extended for analysis (see Table 6.7).

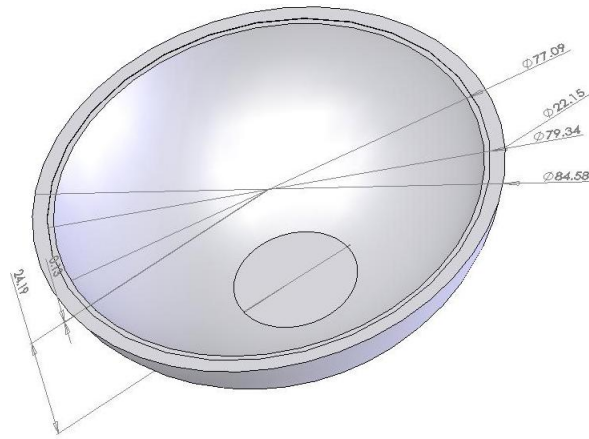


Figure 6.5: Skillet geometry

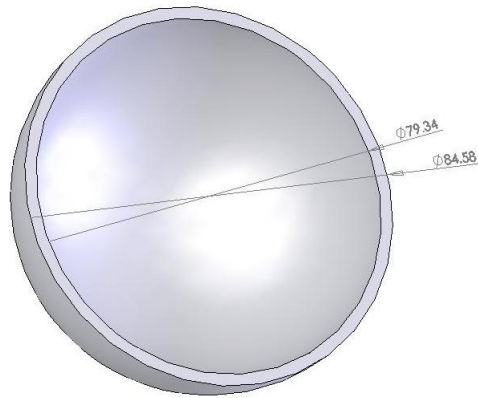


Figure 6.6: Skillet specimen geometry

Table 6.6: ESM representation of the skillet

Geometry	Material
Product	Copper and Steel
Product Specimen	Steel
Model Specimen	Nylon
Model	Nylon

Non-linear trend in distribution of data is analyzed to enforce use of advanced methods. Pearson's coefficients shown below suggest presence of

Table 6.7: Measurement data for skillet experiment

Measurement	T_{ms}	T_{ps}	T_m	T_p
1	89.1900	90.0700	89.2475	91.1413
2	86.4500	83.8400	86.8989	86.0810
3	83.6600	78.5800	82.5019	76.4690
4	79.4500	73.5700	79.3410	72.9822
5	76.4300	69.5500	75.8767	68.5077
6	72.7800	66.2500	72.6897	64.0162
7	69.4500	62.5700	68.2899	60.0667
8	66.6500	60.4400	66.1398	59.0242
9	62.1200	57.6400	61.6081	57.9719
10	58.8400	55.3800	58.1386	54.0897
11	54.5100	54.0400	53.2892	53.8508

mild non-linear effects in the scaling between product specimen and model specimen causing the curve to deviate from constant slope.

$$r(X_{ps}, X_{ms}) = 0.9753 \quad (6.131)$$

$$r(X_m, X_{ms}) = 0.9993 \quad (6.132)$$

This non-linear variation in temperature is expected in the product specimen as metal based structures tend to heat up faster due to higher thermal conductivity while the more benign polymer material that the model is made of shows linear variation due to lower thermal conduction properties. However, the non-linear variation is small since the magnitude of the temperature gradients over the radial length of the skillet is not significant, but motivation enough to warrant use of non-linear methods. Proceeding systematically, scale and form transformation matrices are developed for all polynomial methods, and constants for bilinear and regression methods using relations provided before. System transformation is estimated wherever applicable and used in prediction. Developed metrics are shown below.

$$\begin{pmatrix} [u \ u_0 \ v \ v_0]_1 \\ [u \ u_0 \ v \ v_0]_2 \\ [u \ u_0 \ v \ v_0]_3 \\ [u \ u_0 \ v \ v_0]_4 \\ [u \ u_0 \ v \ v_0]_5 \\ [u \ u_0 \ v \ v_0]_6 \\ [u \ u_0 \ v \ v_0]_7 \\ [u \ u_0 \ v \ v_0]_8 \\ [u \ u_0 \ v \ v_0]_9 \\ [u \ u_0 \ v \ v_0]_{10} \\ [u \ u_0 \ v \ v_0]_{11} \end{pmatrix} = \begin{pmatrix} -2.74 & 229.228 & 2.79 & -248.84 \\ -2.79 & 221.666 & 4.21 & -363.954 \\ -4.21 & 321.77 & 3.02 & -252.653 \\ -3.02 & 219.796 & 3.65 & -289.993 \\ -3.65 & 253.493 & 3.33 & -254.512 \\ -3.33 & 221.944 & 2.8 & -203.784 \\ -2.8 & 173.936 & 4.53 & -314.609 \\ -4.53 & 266.545 & 3.28 & -218.612 \\ -3.28 & 178.793 & 4.33 & -268.98 \\ 3.28 & -218.612 & -4.53 & 266.545 \\ 4.33 & -268.98 & -3.28 & 178.793 \end{pmatrix}$$

$$\begin{pmatrix} [u' \ u'_0 \ v' \ v'_0]_1 \\ [u' \ u'_0 \ v' \ v'_0]_2 \\ [u' \ u'_0 \ v' \ v'_0]_3 \\ [u' \ u'_0 \ v' \ v'_0]_4 \\ [u' \ u'_0 \ v' \ v'_0]_5 \\ [u' \ u'_0 \ v' \ v'_0]_6 \\ [u' \ u'_0 \ v' \ v'_0]_7 \\ [u' \ u'_0 \ v' \ v'_0]_8 \\ [u' \ u'_0 \ v' \ v'_0]_9 \\ [u' \ u'_0 \ v' \ v'_0]_{10} \\ [u' \ u'_0 \ v' \ v'_0]_{11} \end{pmatrix} = \begin{pmatrix} -6.23 & 489.553 & 5.26 & -473.768 \\ -5.26 & 386.978 & 5.01 & -420.038 \\ -5.01 & 348.446 & 4.02 & -315.892 \\ -4.02 & 266.325 & 3.3 & -242.781 \\ -3.3 & 206.481 & 3.68 & -255.944 \\ -3.68 & 222.419 & 2.13 & -141.113 \\ -2.13 & 122.773 & 2.8 & -175.196 \\ -2.8 & 155.064 & 2.26 & -136.594 \\ -2.26 & 122.13 & 1.34 & -77.2376 \\ 2.26 & -136.594 & -2.8 & 155.064 \\ 1.34 & -77.2376 & -2.26 & 122.13 \end{pmatrix}$$

$$\begin{pmatrix} T_1 \\ T_2 \\ T_3 \\ T_4 \\ T_5 \\ T_6 \\ T_7 \\ T_8 \\ T_9 \\ T_{10} \\ T_{11} \end{pmatrix} \underset{\text{Bilinear}}{=} \begin{pmatrix} -95.4324 \\ -10.9968 \\ 7.30893 \\ 49.8032 \\ 12.7314 \\ 79.5452 \\ 3.28732 \\ 19.7604 \\ 10.5037 \\ -8.7864 \\ -9.54926 \end{pmatrix}$$

$$\begin{pmatrix} T_1 \\ T_2 \\ T_3 \\ T_4 \\ T_5 \\ T_6 \\ T_7 \\ T_8 \\ T_9 \\ T_{10} \\ T_{11} \end{pmatrix} \underset{\text{Polynomial}}{=} \begin{pmatrix} 0.524872 & 0.375099 & 0.243358 & 0.0842272 & \dots \\ 0.396115 & 0.301699 & 0.217251 & 0.112154 & \dots \\ 0.194532 & 0.183724 & 0.171021 & 0.148609 & \dots \\ 0.0815258 & 0.114645 & 0.139951 & 0.162054 & \dots \\ -0.0117514 & 0.0540126 & 0.107974 & 0.164564 & \dots \\ -0.0695416 & 0.0120071 & 0.0803859 & 0.155569 & \dots \\ -0.104844 & -0.0240555 & 0.0453129 & 0.125357 & \dots \\ -0.103369 & -0.0324522 & 0.0294315 & 0.103086 & \dots \\ -0.0600215 & -0.030322 & -0.0013302 & 0.0400302 & \dots \\ 0.0100961 & -0.010506 & -0.0224169 & -0.0230709 & \dots \\ 0.161756 & 0.0436231 & -0.0482892 & -0.13278 & \dots \end{pmatrix}$$

$$\begin{pmatrix} -0.000538225 & -0.0702217 & -0.102514 & -0.106568 & -0.0684376 & 0.000770663 & 0.119952 \\ 0.0533093 & 0.000636823 & -0.0298049 & -0.0423953 & -0.0376034 & -0.0118157 & 0.0404526 \\ 0.13013 & 0.105117 & 0.0797384 & 0.0565106 & 0.0152776 & -0.0205033 & -0.0641565 \\ 0.165996 & 0.157476 & 0.137019 & 0.110453 & 0.0493536 & -0.0147748 & -0.103699 \\ 0.186758 & 0.193064 & 0.179228 & 0.15313 & 0.0829235 & 0.00297204 & -0.112875 \\ 0.188757 & 0.205738 & 0.199149 & 0.177301 & 0.110409 & 0.0299611 & -0.0897352 \\ 0.164527 & 0.191521 & 0.196722 & 0.18675 & 0.142865 & 0.0839175 & -0.00807123 \\ 0.141307 & 0.171206 & 0.182926 & 0.181292 & 0.156424 & 0.117337 & 0.0528102 \\ 0.067931 & 0.0996803 & 0.126763 & 0.148146 & 0.18005 & 0.202911 & 0.226162 \\ -0.0107081 & 0.018541 & 0.0588857 & 0.102896 & 0.193613 & 0.282368 & 0.400302 \\ -0.15323 & -0.13317 & -0.0721184 & 0.010784 & 0.205979 & 0.413639 & 0.703806 \end{pmatrix}$$

$$S_{AdaptivePoly.} = \begin{pmatrix} 0.21 & -34.83 & 1498.00 \\ -0.05 & 9.04 & -337.22 \\ 0.09 & -11.56 & 450.14 \\ -0.04 & 5.58 & -145.14 \\ 0.06 & -6.78 & 238.75 \end{pmatrix}, F_{AdaptivePoly.} = \begin{pmatrix} 0.35 & -58.92 & 2576.70 \\ -0.22 & 36.80 & -1427.50 \\ 0.21 & -29.22 & 1095.60 \\ -0.17 & 23.79 & -745.29 \\ 0.14 & -15.66 & 480.11 \end{pmatrix}$$

$$S_{Spline} = \begin{pmatrix} -0.0071 & 0.1345 & -0.1402 & 54.04 \\ -0.0071 & 0.0424 & 0.6261 & 55.38 \\ 0.0032 & -0.0274 & 0.6756 & 57.64 \\ 0.0111 & 0.0166 & 0.627 & 60.44 \\ -0.0219 & 0.11 & 0.9816 & 62.57 \\ 0.0237 & -0.1088 & 0.9856 & 66.25 \\ -0.0287 & 0.1506 & 1.1383 & 69.55 \\ 0.022 & -0.1097 & 1.262 & 73.57 \\ -0.0118 & 0.1681 & 1.5079 & 78.58 \\ -0.0118 & 0.0697 & 2.1712 & 83.84 \end{pmatrix}, F_{Spline} = \begin{pmatrix} 0.0023 & -0.0357 & 1.2314 & 53.2892 \\ 0.0023 & -0.0057 & 1.0518 & 58.1386 \\ -0.008 & 0.017 & 1.0886 & 61.6081 \\ 0.0357 & -0.0924 & 0.747 & 66.1398 \\ -0.0394 & 0.2071 & 1.0683 & 68.2899 \\ 0.0313 & -0.1864 & 1.1373 & 72.6897 \\ -0.0382 & 0.1558 & 1.0254 & 75.8767 \\ 0.0357 & -0.1906 & 0.9202 & 79.341 \\ -0.0469 & 0.2605 & 1.2145 & 82.5019 \\ -0.0469 & -0.1323 & 1.5721 & 86.8989 \end{pmatrix}$$

$$\begin{pmatrix} a_1 & b_1 \\ a_2 & b_2 \\ a_3 & b_3 \\ a_4 & b_4 \\ a_5 & b_5 \\ a_6 & b_6 \\ a_7 & b_7 \\ a_8 & b_8 \\ a_9 & b_9 \\ a_{10} & b_{10} \end{pmatrix}_{Exp.Reg.} = \begin{pmatrix} 8.73576 & 1.0265 \\ 11.26 & 1.0235 \\ 21.2205 & 1.01577 \\ 16.7761 & 1.01878 \\ 25.1324 & 1.01341 \\ 18.9989 & 1.01731 \\ 26.502 & 1.01245 \\ 30.0766 & 1.01053 \\ 27.023 & 1.01227 \\ 39.7008 & 1.00567 \end{pmatrix}, \begin{pmatrix} c_1 & d_1 \\ c_2 & d_2 \\ c_3 & d_3 \\ c_4 & d_4 \\ c_5 & d_5 \\ c_6 & d_6 \\ c_7 & d_7 \\ c_8 & d_8 \\ c_9 & d_9 \\ c_{10} & d_{10} \end{pmatrix}_{Exp.Reg.} = \begin{pmatrix} 37.4625 & 1.00978 \\ 17.3891 & 1.01879 \\ 37.959 & 1.00932 \\ 24.5136 & 1.01489 \\ 30.8948 & 1.01183 \\ 18.5704 & 1.01893 \\ 30.8849 & 1.01149 \\ 23.2773 & 1.01579 \\ 20.5533 & 1.01783 \\ 17.8016 & 1.02032 \end{pmatrix}$$

$$\begin{pmatrix} a_1 & b_1 \\ a_2 & b_2 \\ a_3 & b_3 \\ a_4 & b_4 \\ a_5 & b_5 \\ a_6 & b_6 \\ a_7 & b_7 \\ a_8 & b_8 \\ a_9 & b_9 \\ a_{10} & b_{10} \end{pmatrix}_{PowerReg.} = \begin{pmatrix} 0.00298151 & 2.29714 \\ 0.0125367 & 1.97508 \\ 0.276901 & 1.27592 \\ 0.129288 & 1.45 \\ 0.936459 & 0.993386 \\ 0.354045 & 1.22025 \\ 1.76343 & 0.84163 \\ 3.56658 & 0.673908 \\ 2.74466 & 0.737348 \\ 15.0062 & 0.320444 \end{pmatrix}, \begin{pmatrix} c_1 & d_1 \\ c_2 & d_2 \\ c_3 & d_3 \\ c_4 & d_4 \\ c_5 & d_5 \\ c_6 & d_6 \\ c_7 & d_7 \\ c_8 & d_8 \\ c_9 & d_9 \\ c_{10} & d_{10} \end{pmatrix}_{PowerReg.} = \begin{pmatrix} 1.92185 & 0.85467 \\ 0.0747323 & 1.5828 \\ 2.89641 & 0.756614 \\ 0.513421 & 1.15206 \\ 1.69312 & 0.876893 \\ 0.239384 & 1.33317 \\ 2.52731 & 0.777391 \\ 0.958005 & 1.00839 \\ 0.747339 & 1.06853 \\ 0.559797 & 1.13944 \end{pmatrix}$$

$$S_{Trig.} = \begin{pmatrix} 184.85 & -13.52 & -183.10 \\ 88.87 & -16.40 & -86.21 \\ 55.05 & -16.80 & -51.32 \\ 26.28 & -10.99 & -22.79 \\ 8.08 & -4.14 & -5.81 \end{pmatrix}, F_{Trig.} = \begin{pmatrix} 192.49 & -13.14 & -190.77 \\ 113.61 & -20.34 & -110.60 \\ 84.71 & -25.57 & -79.61 \\ 49.43 & -20.68 & -43.76 \\ 17.42 & -9.57 & -13.42 \end{pmatrix}$$

Notice that in polynomial and adaptive polynomial ESM, 2^{nd} order is used in common as comparison between the two schemes is desired. While selection of second order is unsupported in polynomial ESM (see Figure 6.7), it is completely justified in adaptive polynomial ESM as it produces least error. Further, coefficients of the higher order term in every interval is numerically small implying mild non-linearity. Hence, adaptive polynomial uses 5 intervals (see Figure 6.8) with uniform grid of quadratic curves. Spline fit ESM employs 10 intervals of uniform cubic curves like the regression methods that use 10 intervals but provide C^0 continuity (see Figure 6.9) while trigonometric ESM process establishes 5 intervals modeled as 1^{st} order functions (see Figure 6.10).

Results are shown below (See Table 6.8). Notice that adaptive methods are comparable in terms of error margins with the earlier two methods (see Table 6.9). Notice also trend or distribution of temperature is commensurate with actual distribution for all techniques. This is another feature of adaptive methods that allows them to ‘self-correct’ in order to maintain trend pattern. Even though adaptive methods require more effort, the enterprise pays off in terms of developing robust lower order methods with comparable error values (see Figure 6.11). The only variable that changes in this experiment is time and hence adaptive algorithms treat it as an independent variable. All the objectives laid out in analyzing this system have been realized with ESM demonstrating considerable robustness in scaling non-linear multi-material systems using a single polymer material. This example also confirms numerical validity of adaptive methods which is enhanced in the next example where error margins are significantly improved for a highly non-linear system.

6.4 Airfoil-Coefficient of Drag Analysis

Airfoils are commonly used scaled aerodynamic models that are tested to predict probable aircraft wing behavior under different test conditions. In

Table 6.8: Predicted temperature values for skillet

Bilinear	Polynomial	Adaptive Poly.	Spline Fit	Exp. Reg.	Power Reg.	Trig.
90.2144	89.0785	90.2580	90.2015	90.2056	90.2034	90.7040
84.9240	84.9822	83.7250	84.8276	84.7745	84.7727	88.5790
77.2646	77.9943	77.8280	77.0250	76.8318	76.8204	73.4240
73.3952	73.5240	73.7980	73.4312	73.4328	73.4325	72.1550
69.0907	69.1551	68.6490	68.9623	68.9385	68.9355	65.8580
66.1265	65.6139	64.7660	66.1601	66.1589	66.1590	63.5610
61.6435	61.4961	62.2230	61.5619	61.5076	61.4931	60.1020
60.1415	59.8072	60.8400	60.1240	60.0889	60.0891	58.1810
57.1419	56.9432	57.1460	57.2879	57.3066	57.3044	57.4090
54.8682	55.3865	54.8580	54.9641	55.0345	55.0300	54.8590
53.8017	54.1369	54.1330	54.4245	53.6681	52.7878	54.1330

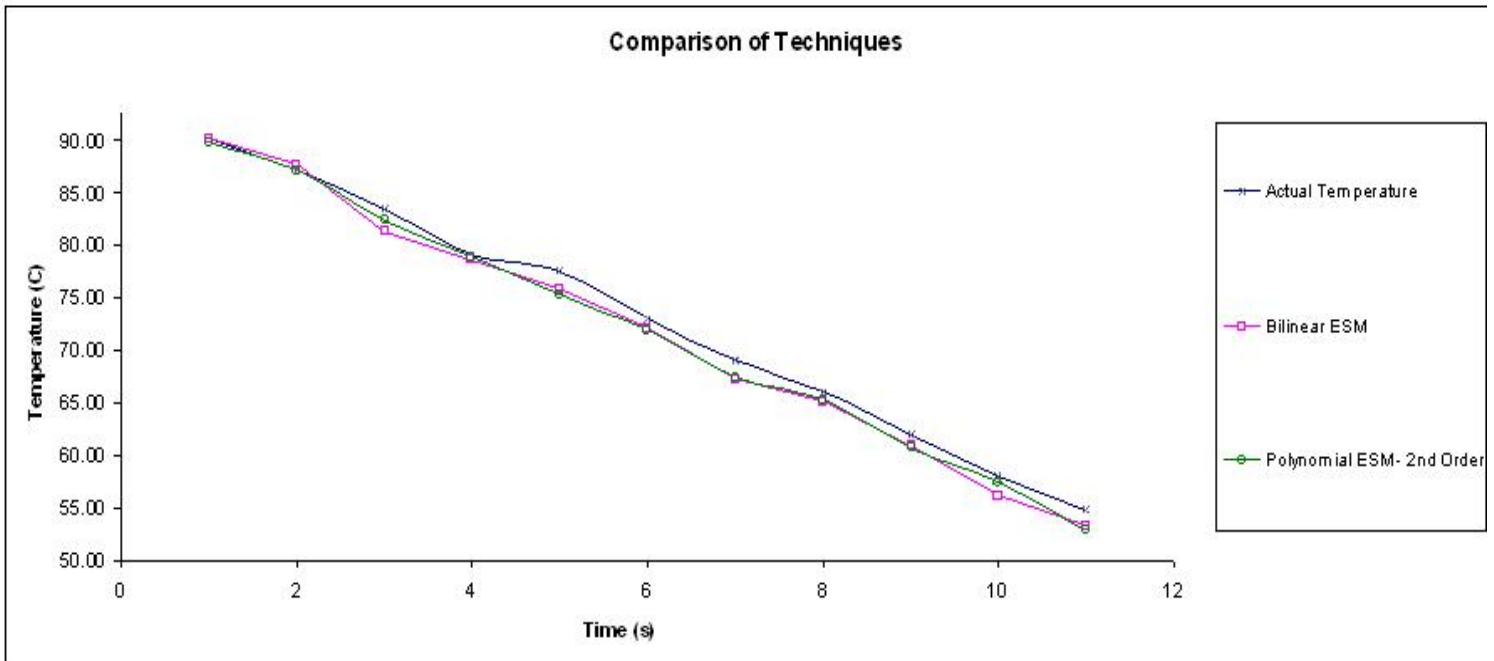


Figure 6.7: Prediction plot for skillet temperature - Bilinear and Polynomial ESM

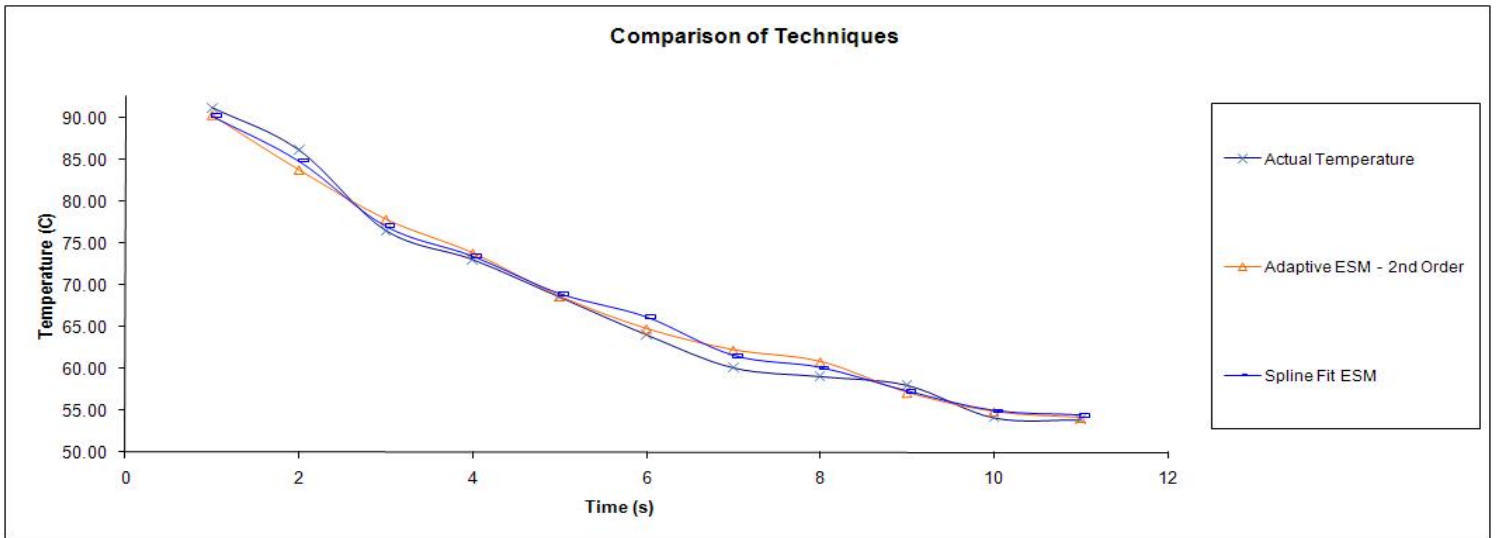


Figure 6.8: Prediction plot for skilket temperature - Adaptive polynomial and Spline fit ESM

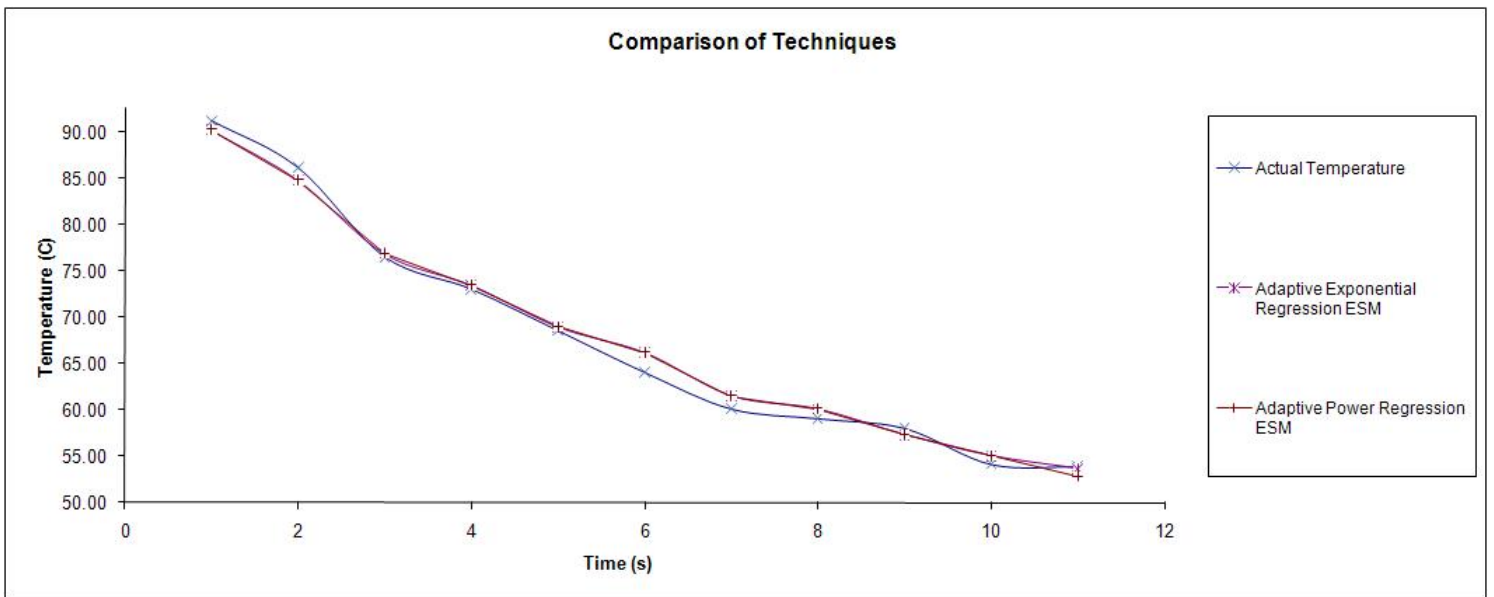


Figure 6.9: Prediction plot for skilket temperature - Regression methods ESM

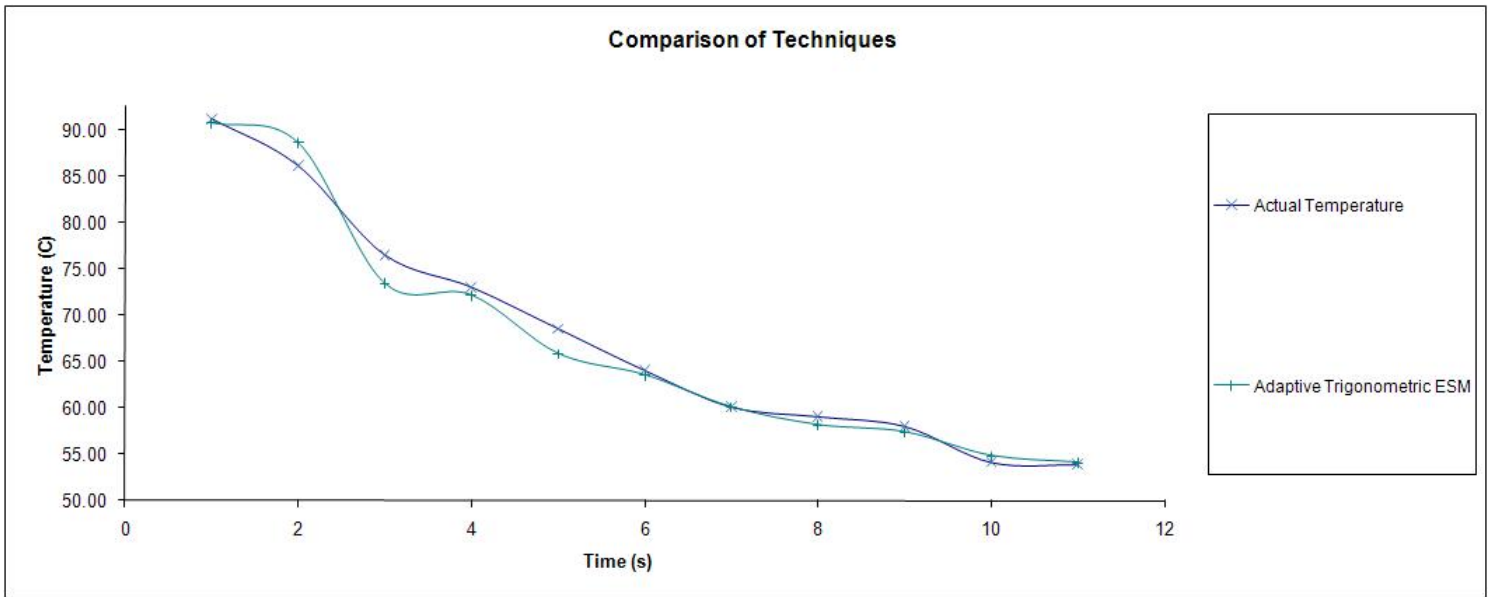


Figure 6.10: Prediction plot for skillet temperature - Trigonometric ESM

Table 6.9: Error values in temperature prediction for skillet

Bilinear	Polynomial	Adaptive Poly.	Spline Fit	Exp. Reg.	Power Reg.	Trig.
1.02%	2.26%	0.97%	1.03%	1.03%	1.03%	0.48%
1.34%	1.28%	2.74%	1.46%	1.52%	1.52%	2.90%
1.04%	1.99%	1.77%	0.73%	0.47%	0.46%	3.98%
0.57%	0.74%	1.12%	0.62%	0.62%	0.62%	1.13%
0.85%	0.95%	0.21%	0.66%	0.63%	0.62%	3.87%
3.30%	2.50%	1.17%	3.35%	3.35%	3.35%	0.71%
2.63%	2.38%	3.59%	2.49%	2.40%	2.37%	0.06%
1.89%	1.33%	3.08%	1.86%	1.80%	1.80%	1.43%
1.43%	1.77%	1.42%	1.18%	1.15%	1.15%	0.97%
1.44%	2.40%	1.42%	1.62%	1.75%	1.74%	1.42%
0.09%	0.53%	0.52%	1.07%	0.34%	1.98%	0.52%
1.66%	1.78%	1.93%	1.67%	1.63%	1.72%	2.06%
↑	↑	↑	↑	↑	↑	↑
RMS Error						

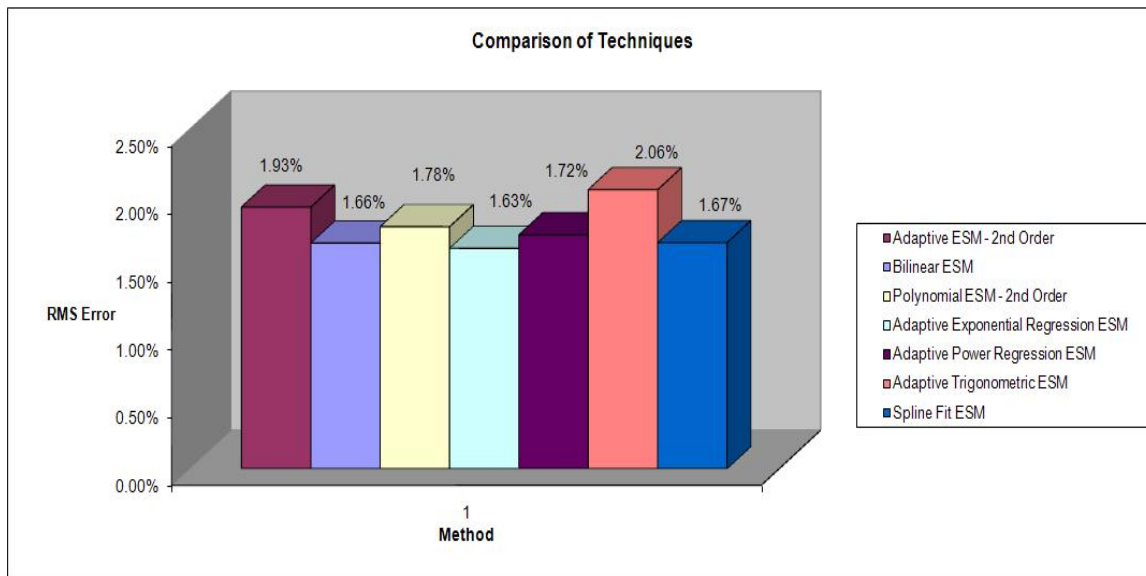


Figure 6.11: Error plot in temperature prediction for skillet

an effort to conclusively present numerical evidence showing profound impact of novel non-linear methods in terms of improvement in prediction accuracy, these airfoils are studied to characterize their drag response for various values of Reynolds number and angles of attack. The two airfoil models used (Gemini and E387) in analysis are shown below (see Figure 6.12) followed by ESM representation of these geometries (see Table 6.10). This experiment first studied by [Wood, 2002] also serves the purpose of illustrating pertinence of ESM when test conditions alter instead of material properties, requiring modification in the development of the scale transformation. Notice that the ratio of Reynolds number between the model specimen and the product specimen is different from that of the model and the product causing distortion in the system. Further, this experiment allows study of prediction limitations of some of the developed methods, which are discussed later. Hence the main objectives in this experiment are -

- Demonstrate prediction improvement achieved using the novel non-linear

methods for a highly non-linear distorted system.

- Illustrate applicability of ESM when test conditions alter instead of material properties.
- Highlight potential limitations of the developed methods.

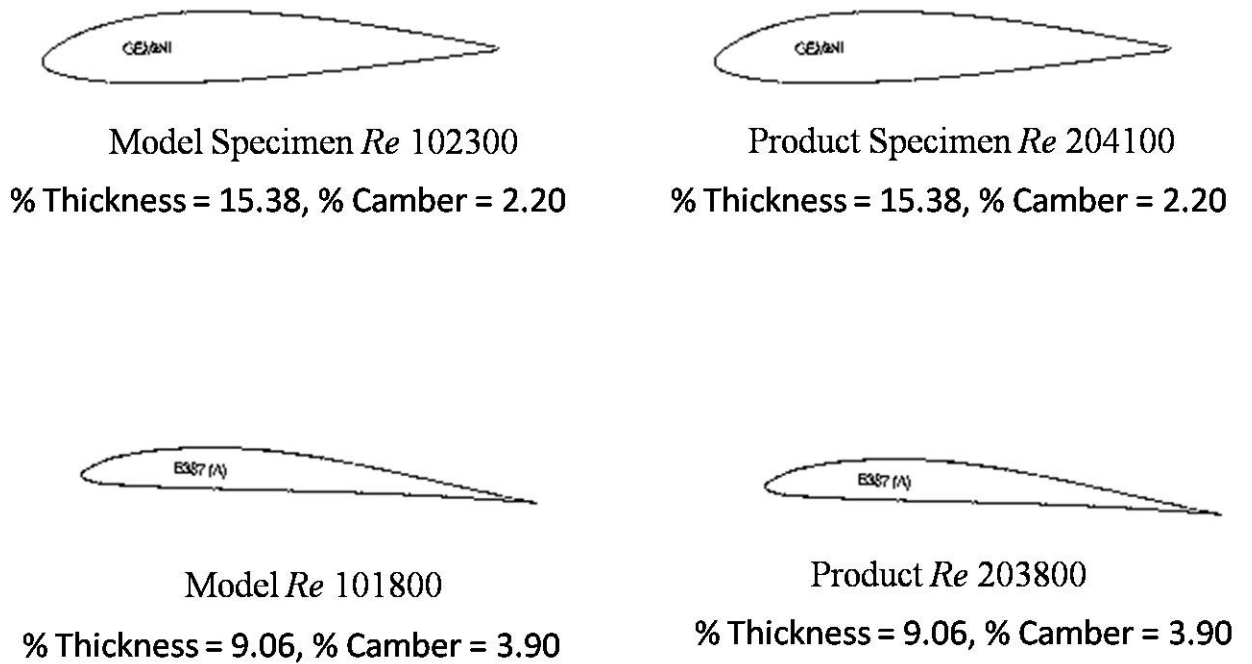


Figure 6.12: ESM quartet for the airfoil system [Adapted from Selig et al., 1995]

Table 6.10: ESM representation of the airfoil system

Geometry	Test Conditions
Product E387	Re 203800
Product Specimen Gemini	Re 204100
Model Specimen Gemini	Re 102300
Model E387	Re 101800

[Selig et al., 1995] provide summarized data about these structures and relevant data for this analysis has been retrieved from *Summary of Low-Speed Airfoil Data* [Selig et al., 1995] (see Table 6.11).

Table 6.11: Test data from representative geometries of the airfoil system

Measurement	Cd_{ms}	Cd_{ps}	Cd_m	Cd_p
1	0.017600	0.012000	0.027500	0.019400
2	0.016000	0.011750	0.019500	0.014400
3	0.016900	0.011900	0.016600	0.011950
4	0.017200	0.012000	0.016650	0.010650
5	0.019500	0.012350	0.017800	0.010500
6	0.020000	0.012350	0.019800	0.011300
7	0.018600	0.012500	0.021500	0.012300
8	0.018900	0.013150	0.022600	0.013300
9	0.020400	0.014250	0.022950	0.014050
10	0.023800	0.015750	0.022980	0.014600
11	0.025500	0.017800	0.022750	0.015100
12	0.027000	0.020000	0.022700	0.015800
13	0.028500	0.021500	0.023700	0.020200

This range of values is of particular interest since the numerical magnitude is less than 1, a feature that allows to test the integrity of some of the developed methods where this condition is shown to be quite critical. Pearson's test shown below, provides non-linear correlation between the model specimen and the product specimen, and the model specimen and the model thus authenticating use of non-linear methods.

$$r(X_{ms}, X_{ps}) = 0.9708 \quad (6.133)$$

$$r(X_{ms}, X_m) = 0.4241 \quad (6.134)$$

Concerned intermediate relations for all methods are presented in Appendix C. The polynomial ESM is modeled using a 3rd order fit while the adaptive polynomial ESM employs a mix of polynomial combinations. The

span of 13 data points is modeled using 3 intervals of quadratic curves and 1 sixth order polynomial. Trigonometric ESM uses 4 intervals with the first three modeled as first order variations and the last captured by a cubic fit, the latter two techniques being consequences of the algorithm. Splines method adopts 12 intervals similar to the regression methods but is a uniform 3rd order mesh. Results from analysis are presented below (se Table 6.12).

Table 6.12: Predicted values for airfoil drag

Bilinear	Polynomial	Adaptive Poly.	Spline Fit	Exp. Reg.	Power Reg.	Trig.
0.012704	0.012120	0.018527	0.020600	0.013670	0.013243	0.018530
0.010955	0.011521	0.012198	0.012400	0.012324	0.012288	0.012198
0.011768	0.011883	0.011820	0.011800	0.011825	0.011825	0.011820
0.012350	0.012120	0.011807	0.011800	0.011868	0.011864	0.011807
0.012350	0.012918	0.012479	0.012000	0.012220	0.012222	0.012479
0.012341	0.012918	0.012343	0.012000	0.012361	0.012360	0.012343
0.014508	0.013247	0.013558	0.017200	0.016298	0.015992	0.013649
0.015326	0.014577	0.014824	0.016700	0.020302	0.019521	0.015326
0.015201	0.016504	0.015043	0.016300	0.015848	0.015756	0.015576
0.014894	0.018545	0.015064	0.016300	0.015111	0.015098	0.015598
0.009107	0.020421	0.014913	0.016500	0.014490	0.014322	0.015432
0.014618	0.021554	0.014882	0.016600	0.015288	0.014950	0.015396
0.013278	0.021976	0.015655	0.015800	0.017059	0.016800	0.016149

Observe that the polynomial ESM holds some resemblance to the final solution in terms of proper trend progression unlike the bilinear ESM (see Figure 6.13). This occurs due to the inherent limitation of the bilinear method (two-linear curves) to capture higher order variations. The splines method and adaptive ESM (see Figure 6.14) show much better variation of solution with adaptive ESM outperforming splines due to the flexibility of the process to allow for order variation (2226) unlike a uniform 3rd order grid that the splines employ. Further intermediate control of continuity ensures that slope information is relayed to and accounted for in the algorithm. Splines are also limited due to the mixed nature of the input data (a combination of decreasing and increasing values). The regression methods also deviate from the expected

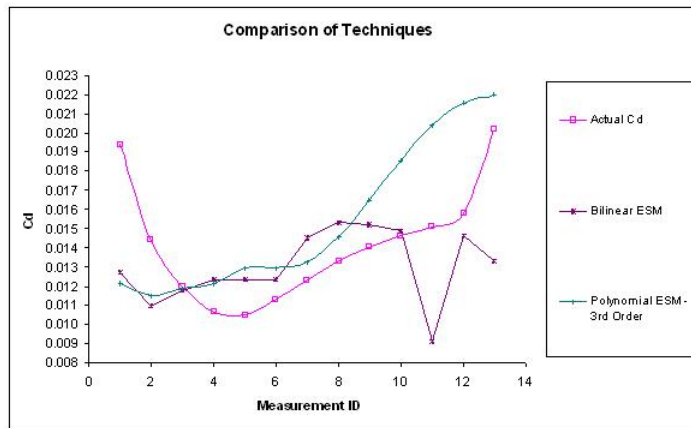


Figure 6.13: Prediction plot for airfoil drag - Bilinear and Polynomial ESM

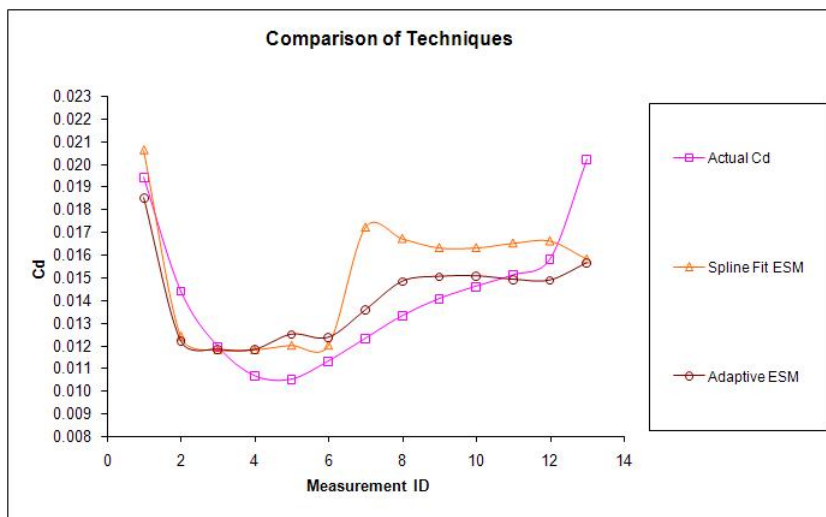


Figure 6.14: Prediction plot for airfoil drag - Adaptive polynomial and Spline fit ESM

evolution of solution (see Figure 6.15) as they do not allow for derivative continuity to be enforced at intermediate points thereby losing data relating to slope direction. The trigonometric ESM process and adaptive ESM generate near identical solutions (see Figure 6.16) which can be explained by the fact that for small values of parameters, trigonometric functions converge to polynomial definitions as dictated by Taylor series approximation in the interval of

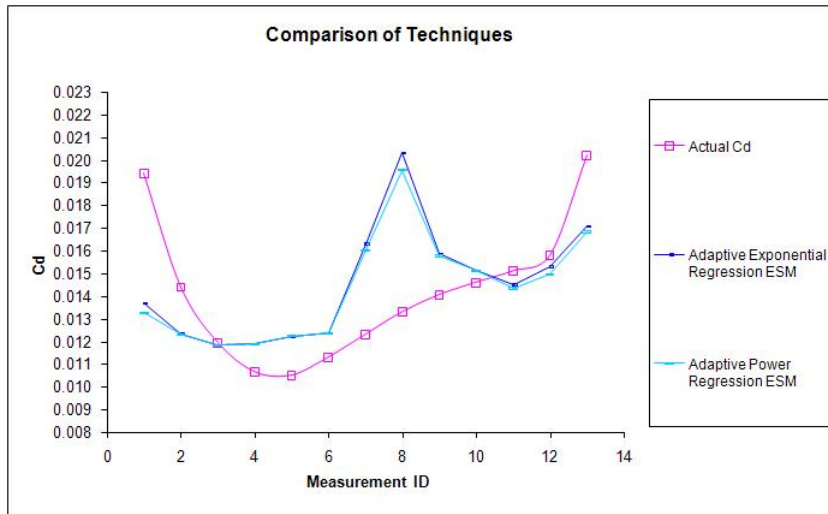


Figure 6.15: Prediction plot for airfoil drag - Regression methods ESM

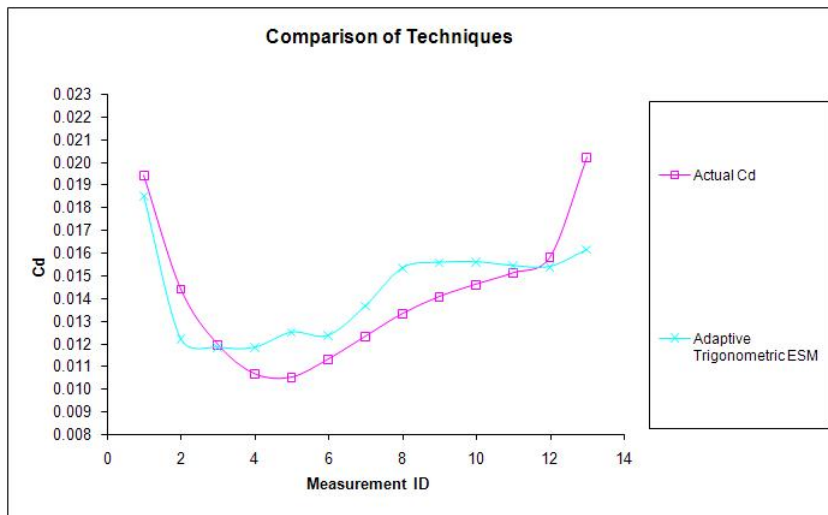


Figure 6.16: Prediction plot for airfoil drag - Trigonometric ESM

convergence. Both these processes remain stable despite the numerical values themselves being small since adaptivity reduces the span from the entire domain to smaller and manageable intervals resulting in generation of scale and form matrices of lower dimension. Inversion of such lower dimension matrices (4×7 in this example) is easier and can avoid potential singularity conditions

(and associated noise) than a matrix developed using all the data points in the domain (for instance, 13×13 in the polynomial method). All the techniques used differ in terms of accuracy achieved as compiled below with the adaptive methods proving to be more efficient (see Table 6.13 and Figure 6.17). Setting polynomial ESM as the benchmark for comparison, improvement of over 45% is achieved in adaptive ESM and trigonometric method thus asserting their overall supremacy in modeling highly non-linear response. The objectives listed for this examples have been achieved with the illustration of improved prediction abilities of the novel methods for highly non-linear distorted systems that are affected by altering test conditions.

Table 6.13: Error values for airfoil drag

Bilinear	Polynomial	Adaptive Poly.	Spline Fit	Exp. Reg.	Power Reg.	Trig.
34.52%	37.53%	4.50%	6.19%	29.54%	31.74%	4.48%
23.93%	19.99%	15.29%	13.89%	14.42%	14.67%	15.29%
1.52%	0.56%	1.09%	1.26%	1.04%	1.05%	1.09%
15.96%	13.80%	10.86%	10.79%	11.43%	11.39%	10.86%
17.62%	23.03%	18.85%	14.29%	16.38%	16.40%	18.84%
9.21%	14.32%	9.23%	6.19%	9.39%	9.38%	9.23%
17.95%	7.70%	10.23%	39.84%	32.50%	30.02%	10.97%
15.23%	9.60%	11.46%	25.56%	52.65%	46.77%	15.23%
8.19%	17.47%	7.07%	16.01%	12.80%	12.14%	10.86%
2.01%	27.02%	3.18%	11.64%	3.50%	3.41%	6.84%
39.69%	35.28%	1.24%	9.27%	4.04%	5.15%	2.20%
7.48%	36.41%	5.81%	5.06%	3.24%	5.38%	2.56%
34.27%	8.79%	22.50%	21.78%	15.55%	16.83%	20.05%
21.21%	22.47%	11.27%	17.12%	21.20%	20.19%	11.58%
↑	↑	↑	↑	↑	↑	↑
RMS Error	RMS Error	RMS Error	RMS Error	RMS Error	RMS Error	RMS Error

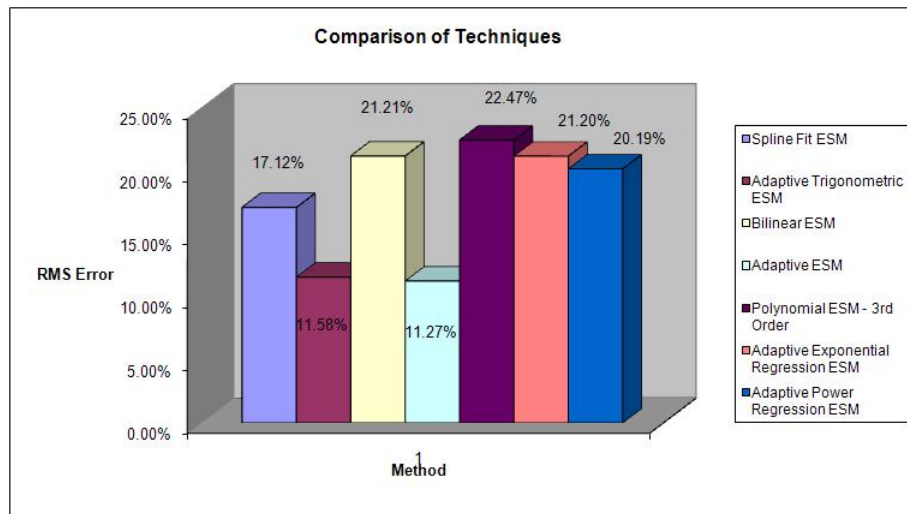


Figure 6.17: Error plot for airfoil drag

6.5 Summary

Non-linear ESM process has been described in this chapter replete with analytical relations and numerical examples. Methodology and procedure have been elaborated to a point where it can be directly incorporated into mechanical design work for numerical and analytical validations of future designs or re-designs. Developed adaptive methods present an interesting choice for mathematical reasoning in parametric design process selection. Several intermediate innovations have been described including establishing optimal polynomial order, developing methods that do not require orders and ability to use methods that interact with each other. All this enhancement has been achieved while maintaining or bettering accuracy margins of earlier methods. Future developments in the field of ESM must incorporate these trends for comprehensive evaluation of non-linear systems. In an effort to conclude cogent development of linear and non-linear methods, the next chapter provides mathematical treatment of error estimation that is intrinsic to both domains.

Chapter 7

Error Estimations

“An error doesn’t become a mistake until you refuse to correct it.” - Orlando
A. Battista

Prior chapters introduced linear and non-linear ESM methods to estimate scaling parameters and establish prediction values. Accuracy and integrity of techniques were presented for some engineering applications in terms of error margins and trends. This chapter briefs analytical understanding of errors, presents means of *a priori* estimation of form, scale and system error, and concludes with definitions for final error in prediction.

7.1 Error Definitions

The simplest definition of error can be interpreted as “*The amount or magnitude by which a parameter deviates numerically from its true value*”. It is thus an estimate and depends solely on how well the parameter is evaluated or approximated. Errors are sometimes referred to as residuals that capture difference between computed and actual values. Accuracy and precision are numerical features that are characterized by error and are inherent in almost all numerical procedures [Kendell, 1988]. Errors are either *random* caused by statistical variations or *systematic* which is bias introduced in a system.

Parallax error is a special kind of error where variability introduced by human observation and involvement is quantified. *Uncertainty* and *resolution* are thus, more commonly employed engineering metrics as measurements and errors themselves are not certain to be repeated or reproduced [Kimothi, 2002]. Most common forms of engineering error definitions include [Becker et al., 1981 and Bourbaki, 1987] -

$$\|e\|_p \triangleq \left(\sum_{i=1}^n |e_i|^p \right)^{\frac{1}{p}} \leftarrow p - norm \quad (7.1)$$

$$\|e\|_2 \triangleq \left(\sum_{i=1}^n |e_i|^2 \right)^{\frac{1}{2}} \leftarrow Euclidean(L^2) - norm \quad (7.2)$$

$$\|e\|_{taxicab} \triangleq \left(\sum_{i=1}^n |e_i| \right) \leftarrow Taxicab - norm \quad (7.3)$$

$$\|e\|_{\infty} \triangleq \max(|e_1|, |e_2|, \dots, |e_n|) \leftarrow \max \text{ or } \infty - norm \quad (7.4)$$

$$\|e\|_{RMS} \triangleq \left(\frac{\sum_{i=1}^n |e_i|^2}{n} \right)^{\frac{1}{2}} \leftarrow RMS - norm \quad (7.5)$$

where $e_i \triangleq |P_{observed,experimental,computed} - P_{actual,true,theoretical}|$, P being the parameter of interest. Characterizing the feasibility of a technique in ESM depends on the potency of its mathematical properties where error margins are assumed to numerically indicate strength of a transformation. The four main errors of interest in ESM include -

- *Scale Error* - Error due to change in material between X_{ms} and X_{ps} .
- *Form Error* - Error due to change in shape between X_{ms} and X_m .
- *System Error* - Product of the independent scale and form errors.
- *Prediction Error* - Error from final comparison of actual and predicted values of X_p and $X_{p,e}$.

In using these definitions in ESM, it is important to realize that error measures are extrinsically applied to all linear methods, and in bilinear, polynomial, regression and spline fit techniques of non-linear methods as they do not have intrinsic error minimization like adaptive polynomial or trigonometric methods. However, error estimates are performed exactly the same way by incorporating similar norms and patterns across all techniques (see Table 7.1).

Table 7.1: Error norms used in ESM

Method	Point	Interval	Scale	Form	System	Prediction
All linear	L^2	N/A	RMS	RMS	Simple product	RMS
Bilinear	L^2	N/A	RMS	RMS	Simple product	RMS
Polynomial	L^2	N/A	RMS	RMS	Simple product	RMS
Adaptive Poly.	L^2	Min	RMS	RMS	Simple product	RMS
Spline Fit	L^2	N/A	RMS	RMS	Simple product	RMS
Adaptive Exp. Reg.	L^2	N/A	RMS	RMS	Simple product	RMS
Adaptive Power Reg.	L^2	N/A	RMS	RMS	Simple product	RMS
Adaptive Trig.	L^2	Min	RMS	RMS	Simple product	RMS

Analytical procedure for numerical estimation of errors in adaptive polynomial and trigonometric ESM is detailed below based on the norms defined above.

7.1.1 Intermediate Error Estimation in Adaptive and Trigonometric ESM

Assume that establishing scale matrix or transformation in ESM process is the problem of interest. If both involved geometries *i.e.*, model specimen and product specimen have $n + 1$ points in their working domain, let $\{P_{ms}\}_{i=0}^n$ and $\{P_{ps}\}_{i=0}^n$ be set of points (measurement values) that are being mapped. For each of the points i in both geometries, an associated finite value for parameter of interest exists. The task now is to establish a functional form that uniquely associates P_i^{ps} with P_i^{ms} . Hence for sets of ordered pairs (P_i^{ms}, P_i^{ps}) , we need to establish a curve that enforces continuous explicit relationship between P_i^{ps}

and P_i^{ms} . Let $f(\bullet)$ be that curve. Then, subscript e denoting estimated value,

$$|P_e^{ps}|_i \approx |f(P^{ms})|_i \quad (7.6)$$

Synonymous with adaptivity, instead of having a single transformation over the entire distance, individual intervals of length h are mapped for closer fits. Hence if k is an interval, then,

$$[|P_e^{ps}|_i]_k \approx [|f(P^{ms})|_i]_k \quad (7.7)$$

Since only discrete nodal point values exist, defining L^2 norm for error estimation in each interval mapping,

$$e_i = e_{y_i} = \|P_{i,e}^{ps} - P_i^{ps}\|_{L^2} = |P_{i,e}^{ps} - P_i^{ps}| \quad \forall i \ni y_i \in k \quad (7.8)$$

$$k \triangleq \{y_i | y_a \leq y_i \leq y_b\} \quad (7.9)$$

where y_a is starting point of interval and y_b is the end point of interval. A similar estimate can be established for form error too.

For all linear and, bilinear and non-linear regression methods, only C^0 continuity can be shown and in spline fit method junction points merge effortlessly while the polynomial method is a global method *i.e.*, uses all the data points to fit a certain higher order curve. Hence, scale and form errors are directly evaluated as -

$$e_{scale} = \left(\sum_{i=1}^n \frac{e_i^2}{n} \right)^{\frac{1}{2}} \quad \forall i \in \{y_i | y_0 \leq y_i \leq y_n\} \quad (7.10)$$

$$E_{form} = \left(\sum_{i=1}^n \frac{E_i^2}{n} \right)^{\frac{1}{2}} \quad \forall i \in \{y'_i | y'_0 \leq y'_i \leq y'_n\} \quad (7.11)$$

The adaptive polynomial and trigonometric methods have an intermediate evaluation to estimate minimum of all interval errors before evaluating

the scale and form errors. This is a process where,

$$e_{min} = \min(e_i) \quad (7.12)$$

$$\forall i \in \{y_i | y_a \leq y_i \leq y_b\} \quad (7.13)$$

$$E_{min} = \min(E_i) \quad (7.14)$$

$$\forall i \in \{y'_i | y'_a \leq y'_i \leq y'_b\} \quad (7.15)$$

such that,

$$e_{scale} = \left(\sum_{i=1}^k \frac{e_{min,i}^2}{k} \right)^{\frac{1}{2}} \quad (7.16)$$

$$E_{form} = \left(\sum_{i=1}^k \frac{E_{min,i}^2}{k} \right)^{\frac{1}{2}} \quad (7.17)$$

Defining average global error to be $e_{scale} \times E_{form}$ generates expected value for net system error in the mapping scheme. Shown below (see Tables 7.2 and 7.3) is an illustration of the process. Notice that the evaluation modifies slightly for adaptive polynomial and trigonometric ESM (see Tables 7.4 and 7.5) but the final prediction error (see Tables 7.6 and 7.7) estimation remains consistent across all methods.

This *a priori* system error estimate directs accuracy of chosen method and its performance. But choice of method is still critical and error is not the only concern that selection is based on. Other constraints exist specific to every method and its analytical properties and working domain. The following section offers insight into making sound decision in method selection.

7.2 Selection of Method in ESM

Linear and non-linear methods are both applicable to physical system evaluation in either range. However, inappropriate use of these methods would

Table 7.2: Error estimation in all linear methods and, bilinear, polynomial, regression and spline fit non-linear methods

X_{ms}	X_{ps}	Point	Evaluation	Point	X_m	X_{ms}
$X_{ms,1}$	$X_{ps,1}$	$\ X_{ps,1} - X_{ps,est,1}\ = e_1$	$\leftarrow\leftarrow L^2\ norm\ \rightarrow\rightarrow$	$\ X_{m,1} - X_{m,est,1}\ = E_1$	$X_{m,1}$	$X_{ms,1}$
$X_{ms,2}$	$X_{ps,2}$	$\ X_{ps,2} - X_{ps,est,2}\ = e_2$	$\leftarrow\leftarrow L^2\ norm\ \rightarrow\rightarrow$	$\ X_{m,2} - X_{m,est,2}\ = E_2$	$X_{m,2}$	$X_{ms,2}$
\vdots	\vdots	\vdots	\vdots	\vdots	\vdots	\vdots
$X_{ms,n}$	$X_{ps,n}$	$\ X_{ps,n} - X_{ps,est,n}\ = e_n$	$\leftarrow\leftarrow L^2\ norm\ \rightarrow\rightarrow$	$\ X_{m,n} - X_{m,est,n}\ = E_n$	$X_{m,n}$	$X_{ms,n}$
		Scale		Form		
		$e_{scale} = \left(\frac{\sum_{i=1}^n e_i^2}{n}\right)^{\frac{1}{2}}$	$\leftarrow\leftarrow\ RMS\ norm\ \rightarrow\rightarrow$	$E_{form} = \left(\frac{\sum_{i=1}^n E_i^2}{n}\right)^{\frac{1}{2}}$		
		\downarrow		\downarrow		
		$\rightarrow\rightarrow$	$\epsilon_{System} = e_{scale} \times E_{form}$	$\leftarrow\leftarrow$		
			\uparrow Simple product			
			System			

Table 7.3: Illustration of error estimation in all linear methods and, bilinear, polynomial, regression and spline fit non-linear methods using the Magnetic Flux example

X_{ms}	X_{ps}	$X_{ps,est}$	Point	Point	$X_{m,est}$	X_m
0.016	0.040	0.040	0.00%	0.00%	0.080	0.080
0.165	0.150	0.150	0.00%	0.00%	0.250	0.250
0.390	0.360	0.360	0.00%	0.00%	0.610	0.610
			Scale	Form		
			0.00%	0.00%		
			ϵ_{System}	0.00%		

introduce undesired anomalies in estimation. A linear method would not scale the system accurately when non-linear terms have greater numerical contribution and non-linear methods are a luxury for linear systems. Within each domain, there are other considerations as well, that need to be addressed - concerns related to mathematical features that have been discussed in plenty detail. Based on collection of all arguments and principles, a concise flowchart

Table 7.4: Error estimation in adaptive polynomial and trigonometric methods

X_{ms}	X_{ps}	Point	Evaluation	Point	X_m	X_{ms}
$X_{ms,1}$	$X_{ps,1}$	$\ X_{ps,k} - X_{ps,est,k}\ = e_k$ $\forall k \in [1, n]'$	$\leftarrow\text{-- } L^2 \text{ norm } \text{--}\rightarrow$	$\ X_{m,u} - X_{m,est,u}\ = E_u$ $\forall u \in [1, m]'$	$X_{m,1}$	$X_{ms,1}$
$X_{ms,2}$	$X_{ps,2}$				$X_{m,2}$	$X_{ms,2}$
\vdots	\vdots				\vdots	\vdots
$X_{ms,n}$	$X_{ps,n}$				$X_{m,m}$	$X_{ms,m}$
\vdots	\vdots				\vdots	\vdots
		Interval		Interval		
		$e_i = \min(e_k)$		$E_i = \min(E_u)$		
\vdots	\vdots	\vdots	\vdots	\vdots	\vdots	\vdots
		Scale		Form		
		$e_{scale} = \left(\frac{\sum_{i=1}^s e_i^2}{n}\right)^{\frac{1}{2}}$	$\leftarrow\text{-- } RMS \text{ norm } \text{--}\rightarrow$	$E_{form} = \left(\frac{\sum_{i=1}^t E_i^2}{n}\right)^{\frac{1}{2}}$		
		\downarrow		\downarrow		
		$\text{--}\rightarrow$	$\epsilon_{System} = e_{scale} \times E_{form}$	$\leftarrow\text{--}$		
			\uparrow Simple Product			
			System			

Table 7.5: Illustration of error estimation in adaptive polynomial and trigonometric methods using the Skillet example

X_{ms}	X_{ps}	$X_{ps,est}$	Point	Interval	Interval	Point	$X_{m,est}$	X_m
89.19	90.07	90.07	0.00%			0.00%	89.24	89.24
86.45	83.84	82.75	1.30%	1.30%	4.20%	4.20%	83.24	86.89
83.66	78.58	78.58	0.00%			0.00%	82.50	82.50
83.66	78.58	78.58	0.00%			0.00%	82.50	82.50
79.45	73.57	73.49	0.10%	0.10%	2.71%	2.71%	81.49	79.34
76.43	69.55	69.55	0.00%			0.00%	75.87	75.87
				Scale	Form			
				$\left(\frac{0.013^2+0.001^2}{2}\right)^{0.5}$	$\left(\frac{0.042^2+0.027^2}{2}\right)^{0.5}$			
				0.92%	3.54%			
			ϵ_{System}	$= 0.92\% \times 3.53\% = 0.03\%$				

Table 7.6: Prediction error estimation in all methods

X_p	$X_{p,est}$	Point	Evaluation
$X_{p,1}$	$X_{p,est,1}$	$\ X_{p,1} - X_{p,est,1}\ = \varepsilon_1$	$\leftarrow L^2 \text{ norm}$
$X_{p,2}$	$X_{p,est,2}$	$\ X_{p,2} - X_{p,est,2}\ = \varepsilon_2$	$\leftarrow L^2 \text{ norm}$
\vdots	\vdots	\vdots	\vdots
$X_{p,n}$	$X_{p,est,n}$	$\ X_{p,n} - X_{p,est,n}\ = \varepsilon_n$	$\leftarrow L^2 \text{ norm}$
		Prediction	
		$\varepsilon_{Prediction} = \left(\frac{\sum_{i=1}^n \varepsilon_i^2}{n}\right)^{\frac{1}{2}}$	$\leftarrow RMS \text{ norm}$

Table 7.7: Illustration of prediction error estimation in all methods using the Magnetic Flux example

X_p	$X_{p,est}$	Point	Evaluation
0.07000	0.07025	0.36%	$\leftarrow L^2 \text{ norm}$
0.20000	0.19896	0.52%	$\leftarrow L^2 \text{ norm}$
0.58000	0.57281	1.24%	$\leftarrow L^2 \text{ norm}$
		Prediction	
		$\varepsilon_{Prediction} = \left(\frac{0.0036^2 + 0.0052^2 + 0.0124^2}{3}\right)^{0.5} = 0.80\%$	$\leftarrow RMS \text{ norm}$

is produced below (see Figure 7.1) that is a road map for process choice. The process begins with collecting the experimental data of the model, the model specimen and the product specimen. Following this initial task, the statistical tests are invoked to identify the degree of linearity depending on which the appropriate domain (linear *vs.* non-linear) is identified. If the system is linear, the numerical values of the test matrices and the condition number of the scale and form matrices would suggest the stiffness in the system. This information would then allow for identification of the appropriate method to evaluate the prediction values. On the contrary, if the system is non-linear, then depending on the type of numerical values of the test vectors a suitable method is chosen to account for positive and negative values, values that do not represent monotonic behavior and extremely small values. All possible numerical values and their variations are thus encompassed and a robust methodology is hence

available to estimate the required prediction values.

7.3 Summary

This chapter formally concludes rigorous mathematical formulation of both linear and non-linear ESM methods by exploring error generation and quantification particular to each method. The exposition has also presented a process to choose a scaling method depending on the working domain and problem specific analytical characteristics. However, all techniques and processes are limited by choice of the specimen and its shape. Properties of these methods becomes relevant only when specimen geometry is chosen and each technique presupposes existence of such geometry. Introducing logical advancement into methodical specimen selection, shape factors are introduced in the next chapter and their integration into ESM is discussed.

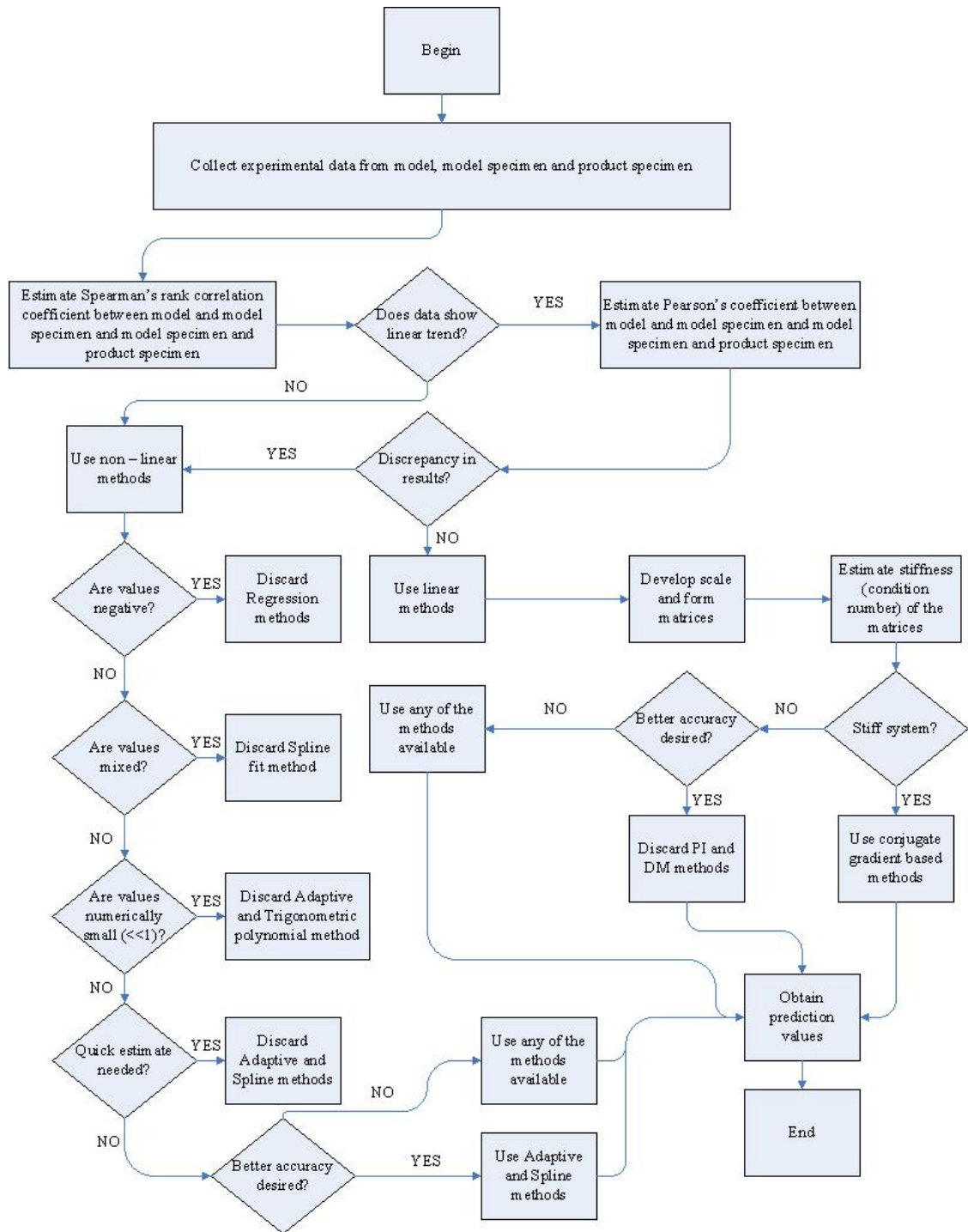


Figure 7.1: Selection of method in ESM

Chapter 8

Shape Factors

“Ideas shape the course of history.”- John Maynard Keynes

Development of ESM thus far encompassed usage procedure permeating applicability and feasibility in analyzing non-linear and distorted systems. The process described how specimen can be used to correlate product behavior using test results and experimental values. Specimen chosen (geometry) in examples provided before have been based on engineering intuition and decisions related to specimen selection included effects of simplicity and need to create simpler representations of products. This chapter formalizes the process of specimen selection incorporating contributions of shape factors to account for changes in cross-sections in product space and specimen geometries.

8.1 Motivation for Shape Factor Study

ESM relies on the ability to create simpler definitions of complex objects which is one of the guiding principles of estimation. Does that mean ESM would not work when simplified representation is not possible? Is ESM heavily dependent on choice of specimen and what if fabrication of a reasonably simplified geometry is not feasible? How then should ESM accommodate changes in geometry and what directs such choices? Does specimen cross-

section affect end solution and how can one maintain consistency in analysis without compromising integrity of the technique? It is questions like these that motivate study of shapes and their effects in ESM. The technique would not be classified as robust if limitations in specimen choice deny the process its due credit and we would like to know if one shape affects another and if it does, how significant that effect is in terms of scaling accuracy.

Assume that a hypothetical product has uniform rectangular cross-section and we desire simplification in specimen geometry that prohibits use of rectangular cross-sections. Among the plethora of shapes available for use, choice needs to be made for specimen geometry with a different cross-section to reflect the product. Logic strongly gravitates to use of square cross-section specimens to maintain consistency in number of boundaries between the two domains. While any other shape offers similar flexibility, only a polygon of 4 boundaries *represents* the original rectangle with square cross-section in particular depicting attributes that closely match the intended design. If the original rectangular cross-section is distorted implying variance in lengths and angles, then any 4-sided polygon would be ideal for specimen geometry. However, since specific choice of a quadrilateral with exact values of lengths and angles is open to interpretation, certain “correction” factor is needed that modifies the end solution to scale according to particular geometric change *w.r.t* the original shape. For example, in mechanical structures, a spline shaft can be represented by a circular shaft and an elliptical shaft - both having same number of boundaries but different cross-sections (see Figure 8.1).

Hence, consistency in number of boundaries is not the only criterion but is a good starting point for further analysis. Incorporation of shape factors capturing such translation would then represent ideal progression to error free ESM analysis. Before integration of shape factors in ESM is elucidated, a brief note is presented below explaining conventional use of shape factors and the like in engineering analysis. This study allows us to deduce certain characteristics of shape factors and understand their significance and practice in engineering.

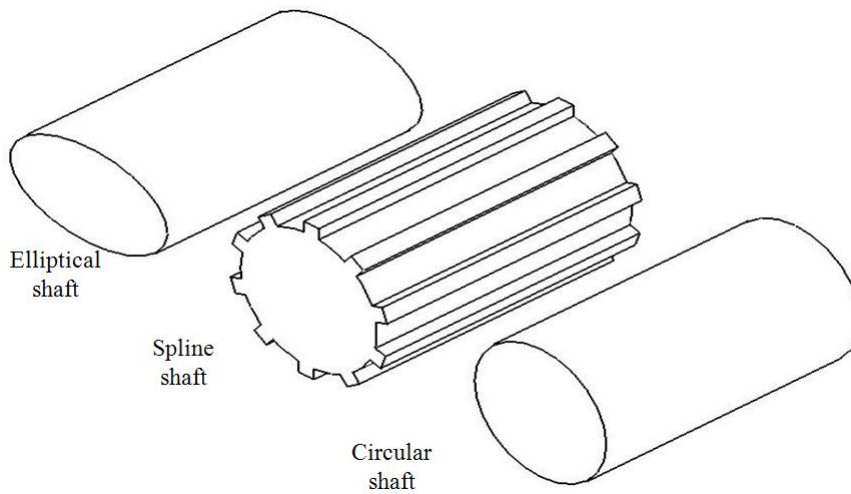


Figure 8.1: Spline shaft representation using circular and elliptical cross-sections

8.2 Applications of Shape Factors in Engineering

This section is designed to obtain insights into shape factors and their utility in engineering through a survey of historical treatment. Several applications and usage in a variety of domains has been studied to compile brief but perceptive observations regarding shape factors. Thus, the key objectives in this literature review are to establish answers to -

- What are shape factors and what do they depend on - *extract information regarding the functional dependence of shape factors.*
- What are they meant for and what do they signify - *extract information regarding their physical interpretation.*
- How are they determined and used in engineering - *observe and deduce trends in typical engineering applications for integration into ESM.*

The required characteristics of shape factors alluding specifically to the above questions is achieved methodically beginning with the study in struc-

tures and solids. A structure is typically used as a beam (horizontal layout, a column (vertical arrangement) or as a truss/strut (angular orientation) [Gere et al., 1985], each employed for a different purpose. The beam configuration is designed to resist axial (compressive and tensile) elongations along with providing constrained bending as they mainly distribute weight. Columns are intended to withstand weight and are hence restrained from buckling or twisting (torsion). Trusses and struts are members that provide additional buttressing to beams and columns thereby imparting more stiffness and minimizing deflection. In determining the optimal shape for each of these structures it is important to realize their application and loading conditions. It is quite trivial to note that a strong material with a solid cross-section would suffice all structural requirements. However, this configuration would involve considerable expenditure and weight due to greater material usage. Desired strength (the hypothetical performance index in this case) might coerce usage of heavy metallic structures thus inducing large weights and high costs, an inconvenience compounded by manufacturing and assembly constraints. Solid sections are hence, not always feasible and the same performance can be derived using alternate materials and shapes.

Materials research has focussed on developing polymers that yield comparable performance, analogous to composites and ceramics using honeycomb structures and corrugated geometries that offer similar mechanical benefits as metals with reduced expense, weight and fabrication restraints. Further, these material forms are environmentally viable and aesthetic. However, the challenge remains if whether solid sections continue to be the only acceptable form for these structures too.

In mechanics of solids, it is common knowledge that I-beams (see Figure 8.2) are highly efficient and provide more stiffness than a regular solid in bending and shear due to area moment of inertia of the shape dictating the performance metric (stress) [Gere et al., 1985]. The Euler bending equation given by,

$$\sigma = \frac{My}{I} \quad (8.1)$$

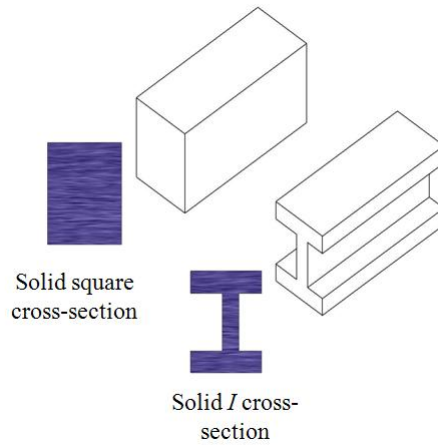


Figure 8.2: Regular square vs. I cross-section

inherits the properties of the shape via the moment of inertia term I , which for any cross-section is determined by its characteristic dimensions. It is thus quite conventional that I-beams are used in railroads and as cross members in cement and steel construction. However, note that an I-beam is not a regular section but is still solid in its shape *i.e.*, it is unlike hollow beams that exist and offer similar structural advantages especially in torsion mode [Gere et al., 1985] where the polar moment of inertia, J , plays a pivotal role as described by,

$$\tau = \frac{Tr}{J} \quad (8.2)$$

again, a shape specific value. However, the analytical relations for estimating polar moment of inertia assume complex variations due to the hollow cross-section requiring more characteristic dimensions to define the shape. Since the effect of shape in design performance has been established, it is imperative to analytically associate a shape and its contribution to parameter evaluation. [Ashby, 1991] provides a useful mechanism of such an association with a relation given by,

$$P = f(F, G, M) \quad (8.3)$$

where P is the parameter of evaluation, F represents the functional requirements, G is the geometry and M the material properties. In the separable form, where the assumption of mutual independence is made [Ashby, 1991], we have,

$$P = f_1(F) \times f_2(G) \times f_3(M) \quad (8.4)$$

Notice the close similarity that the above equation has with the standard ESM equation. Incorporating shape factor ϕ , the equation is modified to -

$$P = f_1(F) \times f_2(G) \times f_3(\phi M) \quad (8.5)$$

Note that the material properties are scaled with the shape factor value thus altering the choice of material form that satisfies the above equation. Generalizing, [Ashby, 1991] defines shape factors as “*Dimensionless numbers that characterize the efficiency of a section shape, regardless of scale, in a given mode of loading*”. For any solid, dimensionless and unit less shape factor is defined for bending and buckling modes to be [Ashby, 1992] -

$$\phi = \frac{4\pi I}{A^2} \quad (8.6)$$

where I is second area moment of inertia and A is the cross-sectional area. If mass m is being minimized through selection of optimal shape and geometry, for a prescribed torsional stiffness k , then [Ashby, 1991],

$$k = \frac{GJ}{L} \quad (8.7)$$

$$\phi = \frac{2\pi J}{A^2} \quad (8.8)$$

$$k = \frac{G\phi A^2}{2\pi L} \quad (8.9)$$

$$m = \left(\sqrt{2\pi k}\right) \left(L^{\frac{3}{2}}\right) \left(\frac{\rho^2}{G\phi}\right)^{\frac{1}{2}} \leftarrow f_1(F) \times f_2(G) \times f_3(\phi M) \quad (8.10)$$

where G is the rigidity modulus, L is length, ρ is density and ϕ is the shape factor. Hence, material choice needs to be done in parallel with shape selection as both collaborate towards the performance objective. Bear in mind that these shape factors are characteristics of mechanical domain alone and will vary for thermal or other systems. For regular geometries with one characteristic dimension (circle, square), shape factor reduces to a fixed constant but for a geometry like an ellipse which has two characteristic dimensions, shape factor is variable and is given by the ratio of the two dimensions.

$$\phi_{cir} = \frac{4\pi I_{cir}}{A_{cir}^2} = 4\pi \left(\frac{\pi r^4}{4}\right) \left(\frac{1}{\pi^2 r^4}\right) = 1 \quad (8.11)$$

$$\phi_{sq} = \frac{4\pi I_{sq}}{A_{sq}^2} = 4\pi \left(\frac{b^4}{12}\right) \left(\frac{1}{b^4}\right) = \frac{\pi}{3} \quad (8.12)$$

$$\phi_{elp} = \frac{4\pi I_{elp}}{A_{elp}^2} = 4\pi \left(\frac{\pi a^3 b}{4}\right) \left(\frac{1}{\pi^2 a^2 b^2}\right) = \frac{a}{b} \quad (8.13)$$

Notice from the two graphs illustrated below that as number of characteristic dimensions increase, shape factor locus transforms from simple line (see Figure 8.3) to more complex curves (see Figure 8.4) when plotted against the two main characteristic dimensions of semi-major and semi-minor axis for an ellipse, a feature made apparent in examples provided later. Bear in mind also that shape factors change with evaluation criterion (elastic to failure), class of problems (axial to torsional and all other modes), type of cross-section (regular to irregular), type of shape (solid to hollow) and orientation of load (aligned to non-aligned) [Ashby 1991].

[Burgess, 2000] and [Burgess et al., 2001] along with [Ashby, 2001] provide additional relations for beams, columns and shafts for various constraints, loading conditions and performance metrics to isolate the best material form to be used for the intended design in conjunction with the shape. Not restricted to solids, [İmrak et al., 2007] provide the shape factor (f) for undercut

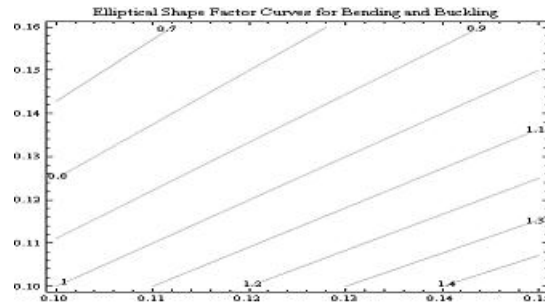


Figure 8.3: Shape factor distribution in an ellipse without thickness - Bending and Buckling modes

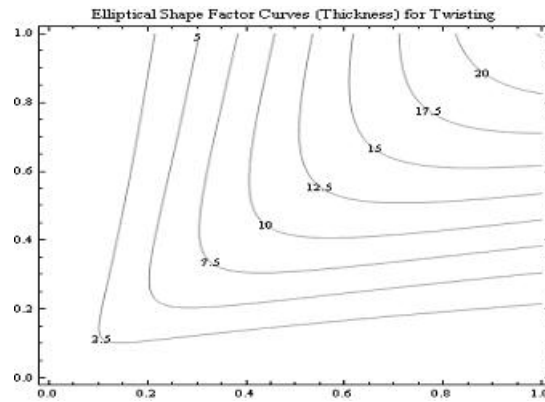


Figure 8.4: Shape factor distribution in an ellipse with thickness - Twisting mode

grooves and ropes using the formula -

$$f = \frac{8 \cos \frac{\beta}{2}}{\delta - \beta + \sin \delta - \sin \beta} \quad (8.14)$$

where δ is the angle of the outer normal of the contact area and β is the angle of undercutting. Similar to the above development, shape factors are also used slightly modified in mechanical design where they appear as stress concentration and safety factors [Juvinal et al., 2006]. Remember that irrespective of the application, shape factors remain unit less and dimension free shape dependent numbers as has been illustrated in the above discussion.

Transitioning, in fluid studies, shape factors assume analogous relationships capturing flow related characteristics. Form factors in potential studies establish number of intersecting flux and potential lines thereby resolving flow pattern, in fluid systems they affect hydraulic conductance of porous media through the use of Mason-Morrow shape factor given by [Patzek et al., 2001],

$$\phi = \frac{R_h}{P} \quad (8.15)$$

where R_h is the hydraulic radius of the pore and P its perimeter. This porosity is of particular interest in drilling and oil retrieval where flow through sub-terrain geology needs to be ensured. Shape factors are also included in dual porosity models to obtain the permeability of fractured media given by [Zimmerman, 2005],

$$\phi = \frac{k\pi^2}{L^2} \quad (8.16)$$

where k is a shape dependent constant and L is the characteristic length of the shape. Hydraulic conductance is also captured by Hvorslev's shape factors, which for a well hole extended at impervious boundary is given by [Butler et al., 2006],

$$\phi = \frac{2\pi R}{\sinh \left[\tanh^{-1} \left(\frac{R}{L} \right) \right] \ln \left[\coth \left\{ 0.5 \tanh^{-1} \left(\frac{R}{L} \right) \right\} \right]} \quad (8.17)$$

where R is radius and L is the length of the well. In watershed hydrology, the relation [Guo, 2008] -

$$\phi = \frac{B}{L} \quad (8.18)$$

where B is the watershed width and L is the watershed length represents the overland flow collected in the watershed. The relation [Valiantzas, 1997] -

$$\phi = \frac{\int_0^x Z ds}{Z_0 x} \quad (8.19)$$

signifies the amount of water infiltration into the subsurface, Z and Z_0 respectively being the actual and cumulative infiltration over the distance x . Aerosol

agglomerates use a correction factor represented by the dynamic shape factor where drag forces are related for a moving particle. This dynamic shape factor is given by [Colbeck et al., 1996],

$$\phi = \frac{d_{me}}{d_{ve}} \quad (8.20)$$

where d_{me} and d_{ve} are respectively the mobility-equivalent and volume-equivalent diameter. Again, notice the strong dependence of shape factors on dimensions alone in all of the examples above where they have pronounced physical significance. Digressing towards usage of shape factors in particle analysis, the apparent mean shape factor given by [Ulusoy, 2008],

$$\phi = \frac{50\% \text{ by mass passing size}}{\text{geometric mean sieve size}} \quad (8.21)$$

reflects the particle size distribution required for understanding flotation and wetting characteristics of a particle. Sedimentation properties are typified by particle size captured by volume and surface shape factors as [Heywood, 1947]

$$\phi_{surface} = \frac{k_e}{m\sqrt{n}} \quad (8.22)$$

$$\phi_{volume} = 1.57 + C\phi_{surface}^{\frac{4}{5}} \left(\frac{n+1}{n^{\frac{1}{3}}} \right) \quad (8.23)$$

where k_e and C are experimentally determined constants and, m and n are ratios of breadth to thickness (thickness of particle) and length to breadth (dimensions of the smallest rectangle that encloses the particle image) respectively. Compactness of a particle shape is also characterized by its shape factor given by [Buffham, 2000],

$$\phi = 3L\bar{\kappa}_m \quad (8.24)$$

where L is the Aris characteristic length given by $L = \frac{Volume}{Area}$ and $\bar{\kappa}_m$ is the area average curvature of the particle. Like before, all analytical relations for shape factors involve only shape specific geometric dimensions that signify particle

properties. Shape factors are also widely used in thermal systems [Incropera, 2007]. Radiation studies are the most common domain where shape factors play characteristic role as *view factors* by incorporating viewing angles and areas exposed to heat flux. They thus affect final solution by attributing effects of geometry that influence flux impinged on a receptor geometry from a radiating body. View factor study and analysis is available abundantly in literature for common interacting geometries [Modest, 2003] and for complex structures [Siegel et al., 2001] where numerical analysis is more rewarding. The common Stefan-Boltzmann's law suggests that body A at temperature T_1 emits to a cooler body B at a rate given by,

$$\dot{Q}_{1-2} = \epsilon_1 \sigma A_1 \phi_{1-2} T_1^4 \quad (8.25)$$

where ϵ_1 is emissivity and A_1 is emitting area of body A . View factor ϕ_{1-2} corrects flux received by body B by discarding the shadow area and using only the heat intercepting portion of body B (see Figure 8.5).

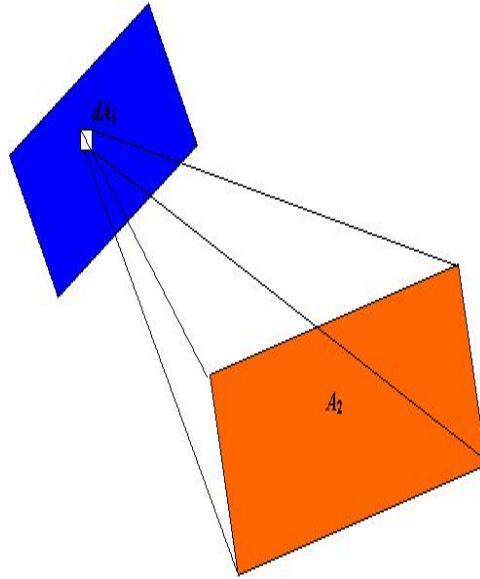


Figure 8.5: View factors in radiative heat transfer

The general estimation of view factor for two interacting surfaces i and j is accomplished using [Incropera, 2007] -

$$\phi_{ij} = \frac{1}{S_i} \int_{S_i} \int_{S_j} \frac{\cos \theta_i \cos \theta_j}{\pi |r_{ij}^2|} dS_i dS_j \quad (8.26)$$

where ϕ is the view factor, S 's are the surface areas, r is the distance between the two surfaces and θ 's are the angles between the respective unit normals. The view factor for two coaxial parallel disks of radii R and r separated by a distance L , for instance, is given by [Biglarbegian, 2005],

$$\phi_{ij} = 0.5 \left[S - \left(S^2 - 4 \left(\frac{R}{r} \right)^2 \right)^{0.5} \right] \quad (8.27)$$

where

$$S = 1 + \frac{1 + \sigma_j^2}{\sigma_i^2} \quad (8.28)$$

and

$$\sigma_i = \frac{r}{L}; \sigma_j = \frac{R}{L} \quad (8.29)$$

Similar to radiation view factors, shape factors are also employed in conduction heat transfer, which is captured using the Langmuir's relation given by [Nickolay et al., 1998],

$$\phi = \int_A \left(\frac{\partial \Theta}{\partial n} \right) dA \quad (8.30)$$

where Θ is dimensionless temperature, A is area and n the normal direction. For instance, the shape factor for a cross-section bounded by two circles of radii r and R is given by [Kołodziej et al., 2001],

$$\phi = \frac{2\pi}{\ln \left(\frac{1}{\rho} \right)} \quad (8.31)$$

where $\rho = \frac{r}{R}$. Use of such shape factors is important in biomedical engineering [Shrivastava et al., 2005] where finite heated tissues have been studied using the Poisson conduction shape factors. Electric arcs have also been studied in convection heat transfer [Cowley, 1974] where the shape factor given by,

$$\phi = \frac{\theta_n}{\theta_\delta} \quad (8.32)$$

denotes the size of the arc. The θ 's respectively represent temperatures required for a condition (n) over the thermal boundary layer (δ). Notice again that all shape factor definitions derive their values from geometric dependence alone and are dimension free. While all of the above relationships represent academic and industrial uses of shape factors, other forms of applications also exist where electronics industries designing computers adopt motherboard *form factors* that determine smallest achievable size and shape of a computer. Further, in a slightly modified sense, correction parameters are always used in engineering equipment like nozzles, venturi and orifice meter. Shapes are also characterized in spectrum studies using shape factors [Shen et al., 1994] and in pollution research [Young et al., 1999]. Based on this initial investigation of shape factors several conclusions can be safely derived as listed below, whose applications in different domains are summarized in the table thereafter (see Table 8.1) -

- Shape factors are dimensionless quantities that define how well a geometry compares with another - usually the standard spherical shape that is symmetric in all principal axes.
- Shape factors are functions of geometry alone and scale a parameter to correct its value specific to the conditions.
- Shape factors signify a measure of effectiveness or efficiency of a particular shape in a given application *i.e.*, qualify and quantify a particular shape.

- Shape factors are domain and application dependent.
- Shape factors are either fixed or variable depending on the type of cross-section.
- Shape factors are functions of characteristic dimensions that define a cross-section.

Table 8.1: Engineering shape factors and their usage

Domain	Application	Significance
Structural	Solids	Optimal material and shape evaluation
Structural	Flexible links	Pressure evaluation
Fluids	Flow	Flow pattern evaluation
Fluids	Flow	Hydraulic conductance and porosity evaluation
Fluids	Drainage	Watershed flow collection evaluation
Fluids	Irrigation	Subsurface infiltration evaluation
Particles	Size Distribution	Flotation and Wetting evaluation
Particles	Size	Permeability and Sedimentation evaluation
Particles	Size	Compactness evaluation
Thermal	Conduction	Conduction Factor evaluation
Thermal	Radiation	View Factor evaluation
Thermal	Convection	Electric Arc evaluation
Other	Electrical	Shape Spectrum evaluation
Other	Electronics	Form Factor evaluation

Note that the table above is only a concise collection of engineering applications of shape factors but is not exhaustive either within or across domains. In the explanation thus far, it has been made quite evident that shape factors are vital to engineering analysis and are extremely useful for a variety of applications. They manifest in different forms in the engineering world as “correction factors” to account for changes in different input, boundary or geometric conditions. They are determined by experimentation [Heywood, 1947], simple geometric methods for regular shapes [Zhangfa et al., 1996], integral methods using vector calculus techniques for curved surfaces [Buffham, 2000],

boundary element methods [Mezrhab et al., 2005] and more often numerically, using methods such as Monte Carlo simulations [Biglarbegian, 2005] for complex shapes. Shape factors are hence integral to analytical understanding of technical features of systems and are insightful in ESM with specific emphasis in specimen selection as is portrayed in the next section.

8.3 Integration of Shape Factors in ESM

Incorporation of shape factors in ESM holds special significance in terms of specimen scaling. Ideally, a single specimen choice should suffice the need for experimental similitude but the choice of such a specimen needs to be done based on justified reasoning and technical argument. Conjuring up a specimen is not a trivial task and hence the need for exploring different specimen geometries that represent the actual system. Hence if C represents shape factor for a particular geometry, then ESM prediction equation is modified to

$$x_p = C_{specimen}(S \times F)x_{ms} \quad (8.33)$$

where $C_{specimen}$ accounts for dissimilarity between the specimen shape and actual geometry. The relation above is specific to sections being scaled and hence will change with varying cross-sections. If a structure comprises multiple cross-sectional shapes, then each shape needs to be scaled using its particular shape factor relation *i.e.*, a specimen needs to be chosen that represents all cross-sections to allow uniform shape factor estimation thereafter. Remember that the objective is to isolate the best available specimen from a chosen set¹ that is practical for scaling. Using the modified ESM equation, the following two examples provide numerical insight into specimen selection using shape factors.

¹The selection process of the set is inductively pursued in the examples presented next.

8.4 Keyboard Spring-Deflection Analysis

A dome keyboard spring is a flexible member made from rubber (see Figure 8.6) that has a gradually increasing central region sandwiched between a circular top and base. This particular design is extremely useful since much of the deflection is transferred to the central region that expands outwards and minimizes downward deflection. Extent of compression is preordained to attain values in a fixed interval *i.e.*, between the two extremes of zero deflection and deflection equalling complete span of the spring. Circular top allows for uniform distribution of input finger pressure and a strong fixture is obtained from the circular bottom (see Figure 8.7). Lateral transfer of motion is required for the spring to return the key to its equilibrium position and also minimize compressive stresses while maintaining fatigue life. Characterizing and quantifying buckling response of the spring is analytically challenging and thus ESM proves to be particularly critical in such circumstances as record of empirical data is available (through experimentation of representative specimen) for further numerical computation. Thus, the key objectives of this experiment are -

- Provide an initial framework for numerically integrating shape factors into ESM.
- Obtain insights into the most important shape factor characteristics affecting performance.
- Apply shape factors of hollow structures, working in linear domains and isolate the best specimen shape.

To understand effect of shape factors in linear ESM, vertical deflection of a point on the edge of the circular top is evaluated for several different forces, mean values of which range in the interval (0 -10 N) [Fagarasanu et al., 2005]. Since the evaluation region is symmetric, choice of location for measurement of deflection values (point of interest) is not critical. The first step in analysis



Figure 8.6: A typical keyboard spring

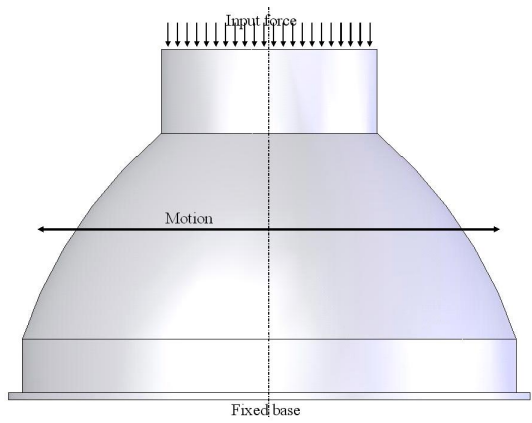


Figure 8.7: Force input and motion in a keyboard spring

is to estimate dimensions of a typical spring which are tabulated below (see Table 8.2 and Figure 8.8) along with those of the model which is of the same scale.

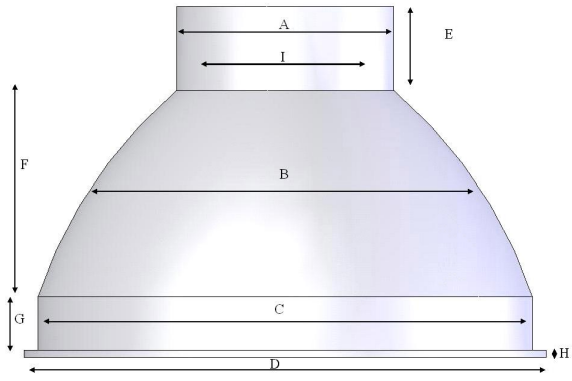


Figure 8.8: Dimensions of a keyboard spring

Table 8.2: Geometric data of a keyboard spring

Dimension	Product	Model
A	2.3390 mm	2.3390 mm
B	3.3585 mm	3.3585 mm
C	5.3340 mm	5.3340 mm
D	5.6360 mm	5.6360 mm
E	0.9030 mm	0.9030 mm
F	2.2130 mm	2.2160 mm
G	0.5760 mm	0.5760 mm
H	0.0800 mm	0.0800 mm
I	2.1060 mm	2.1060 mm

The next step is to choose specimen shapes for ESM evaluation. Three different specimen are chosen including a hollow cylinder of diameters A and I , a hollow ellipse of characteristic dimensions A , B , $A-I$ and $B-I$ and a hollow square of side A and I . All three geometries have length $L = E + F + G + H$ and evaluation for the parameter of interest is done at a point on the edge of the top surface in each geometry (see Figure 8.9). Note that these structures are hollow and shape factors assume complex analytical relations (see Table 8.4) due to greater number of characteristic dimensions, a feature that was alluded to earlier.

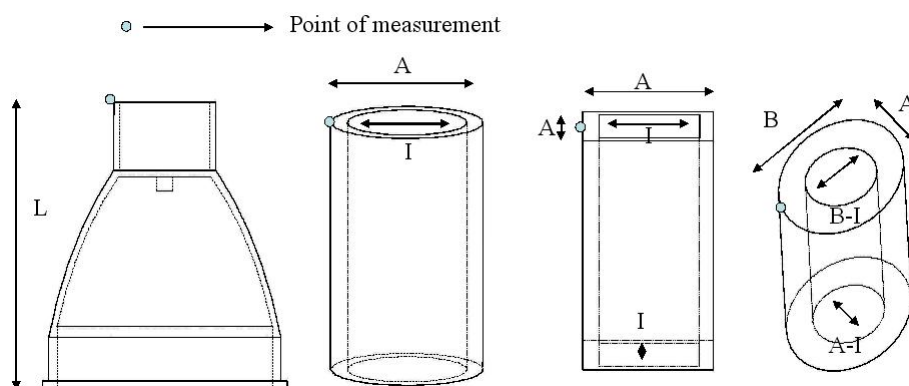


Figure 8.9: Specimen choices for keyboard spring

These three specimen are chosen based on the necessity to maintain consistency in aspect ratio. While many other geometries could have been chosen, cylinder and ellipse are preferred as they offer similar structural features (geometric distortion for ellipse) and the square is selected to test effect of change in boundary shape and number (parametric distortion). The motivation here though is to use specimen shape factors as a guiding tool in selecting the best specimen. Hence, all final values of prediction are scaled using the respective specimen shape factor. Establishing usage in ESM (see Table 8.3) and incorporating shape factors (see Table 8.4) we have [Ashby, 1992],

Table 8.3: ESM representation of the keyboard spring

Geometry	Shape	Material
Product	Complex	Rubber
Product Specimen	Cylinder, Square, Ellipse	Rubber
Model Specimen	Cylinder, Square, Ellipse	Nylon
Model	Complex	Nylon

Table 8.4: Specimen shape factors for keyboard spring experiment

Geometry	Domain	Application	Value
Cylinder	Solids	Buckling	$\frac{A+I}{2(A-I)} = 9.5387$
Square	Solids	Buckling	$\frac{\pi A}{3(A-I)} = 10.5167$
Ellipse	Solids	Buckling	$\frac{2A(1+\frac{3B}{A})}{I(1+\frac{B}{A})^2} = 1.9869$

Notice that the ellipse produces a shape factor closest to 1 implying that its scaled values are closer to the unscaled values unlike the other two shapes. Further, the number of boundaries of the elliptical and cylindrical shapes is consistent with the original design unlike the square shape. In the following analysis, the importance of both these considerations are established *i.e.*, the relevance of a specimen shape factor of 1² and consistency in number of boundaries. Since all required data is obtained, deflection is measured at

²The condition when scaled and unscaled values merge.

the selected location for several different force values (see Tables 8.6 and 8.7). *ABAQUSTM* is once again employed to simulate linear behavior of two distinct polymer forms (rubber and nylon) under compression. Results of simulation are shown below.

Table 8.5: Material data for keyboard spring experiment

Geometry	Scale	Material	Young's modulus	Poisson's ratio
Product	1	Rubber	0.05 GPa	0.50
Product Specimens	1	Rubber	0.05 GPa	0.50
Model	1	Nylon	3.00 GPa	0.35
Model Specimens	1	Nylon	3.00 GPa	0.35

Notice that a flexible polymer (rubber) is being approximated by a more rigid polymer (nylon) despite deviations in ratios of Young's moduli and Poisson's ratio (see Table 8.5). Such representation is valid since both materials are hypothesized to exhibit linear behavior in the range of values (force input) used. This assumption is validated by response values of all concerned geometries as depicted below by the statistical coefficients.

Table 8.6: Measurement data for keyboard spring experiment - Model and Product

Load (N)	$\delta_m(mm)$	$\delta_p(mm)$
0.50	0.000444	0.060390
1.00	0.000888	0.120780
1.50	0.001333	0.181170
2.00	0.001777	0.241560
2.50	0.002221	0.301950
3.00	0.002665	0.362340
3.50	0.003109	0.422730
4.00	0.003554	0.483120
4.50	0.003998	0.543510
5.00	0.004442	0.603900

$$r(X_{ms}, X_{ps})_{Cylinder} = 1 \tag{8.34}$$

Table 8.7: Measurement data for keyboard spring experiment - All specimen

Load (N)	Cylinder	Cylinder	Square	Square	Ellipse	Ellipse
	$\delta_{ms}(mm)$	$\delta_{ps}(mm)$	$\delta_{ms}(mm)$	$\delta_{ps}(mm)$	$\delta_{ms}(mm)$	$\delta_{ps}(mm)$
0.50	0.000278	0.374100	0.000219	0.296700	0.000043	0.057250
1.00	0.000556	0.748200	0.000438	0.593400	0.000086	0.114500
1.50	0.000833	1.122300	0.000657	0.890100	0.000129	0.171750
2.00	0.001111	1.496400	0.000876	1.186800	0.000172	0.229000
2.50	0.001389	1.870500	0.001096	1.483500	0.000215	0.286250
3.00	0.001667	2.244600	0.001315	1.780200	0.000258	0.343500
3.50	0.001945	2.618700	0.001534	2.076900	0.000301	0.400750
4.00	0.002222	2.992800	0.001753	2.373600	0.000343	0.458000
4.50	0.002500	3.366900	0.001972	2.670300	0.000386	0.515250
5.00	0.002778	3.741000	0.002191	2.967000	0.000429	0.572500

$$r(X_{ms}, X_m)_{Cylinder} = 1 \quad (8.35)$$

$$r(X_{ms}, X_{ps})_{Square} = 1 \quad (8.36)$$

$$r(X_{ms}, X_m)_{Square} = 1 \quad (8.37)$$

$$r(X_{ms}, X_{ps})_{Ellipse} = 1 \quad (8.38)$$

$$r(X_{ms}, X_m)_{Ellipse} = 1 \quad (8.39)$$

To provide additional fillip to ESM analysis using conjugate gradient methods, TCG approach is adopted in evaluating the system. The obtained results are shown below (see Table 8.8). All intermediate analysis is summarized in Appendix D. Notice that none of the specimen choices provide accurate results (see Table 8.9). Despite the number of boundaries in the elliptical and circular shapes being consistent with that of the product, errors remain fairly high since the shape factor is not identical to the optimal value of 1. The hollow ellipse, however, can be termed as the “best” specimen choice for this particular problem, since its shape factor value is closest to 1, a feature which translates to the error values as well. This conclusion makes intuitive sense as well since the geometry under stress would be a distorted circle closely

matched by an ellipse. The cylinder specimen provides better results than the square indicating again that the number of boundaries needs to be consistent (see Figure 8.10). Thus, having same number of boundaries corresponds to better accuracy. Other factors and dimensions play pivotal role too but for initial understanding of specimen shapes, it is vital to choose specimens with similar geometric attributes. The objective of this exercise was to demonstrate the use of shape factors in specimen isolation and identify the key features of shape factors that affect end response, which has been accomplished. Bear in mind that the error values, which in this experiment are considerable, can always be reduced to an acceptable level by manipulating the geometry of the ellipse (“best” specimen) such that its shape factor is closer to 1, which is achieved in the next example.

Table 8.8: Predicted values for keyboard spring - scaled

Load (N)	Cylinder	Square	Ellipse
0.50	0.569907	0.632600	0.117426
1.00	1.139237	1.265217	0.234920
1.50	1.713090	1.899245	0.352642
2.00	2.283013	2.531854	0.470096
2.50	2.852917	3.161570	0.587554
3.00	3.422831	3.794179	0.705012
3.50	3.992755	4.426788	0.822470
4.00	4.566007	5.060827	0.942929
4.50	5.135940	5.693425	1.060389
5.00	5.705845	6.326033	1.177843

Having obtained initial insights into the effect of shape factors in specimen selection for ESM, extension into non-linear domains is achieved in the next example where deflection at different geometric distances is evaluated and predicted for a complex structure. Motivation for such expansion is in understanding the differences, if any, in integration between the two domains and how significant the variance is. In the non-linear experiment, however, solid sections are used and, the boundary consistency condition and the necessity

Table 8.9: Error values for keyboard spring - scaled

Error	Cylinder	Square	Ellipse
0.50	843.71%	947.52%	94.45%
1.00	843.73%	947.54%	94.50%
1.50	845.57%	948.32%	94.65%
2.00	845.11%	948.13%	94.61%
2.50	844.83%	947.05%	94.59%
3.00	844.65%	947.13%	94.57%
3.50	844.52%	947.19%	94.56%
4.00	845.11%	947.53%	95.18%
4.50	844.96%	947.53%	95.10%
5.00	844.83%	947.53%	95.04%
RMS Error	844.70%	947.55%	94.72%

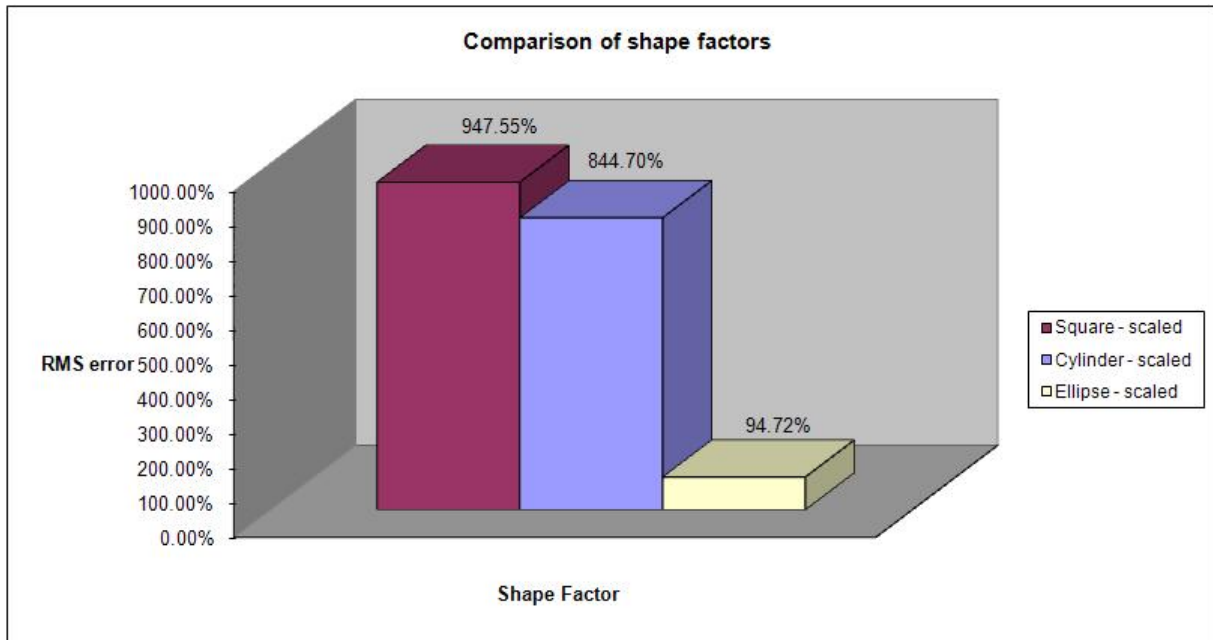


Figure 8.10: Errors due to shape factors for keyboard spring - scaled

of having a shape factor numerically close to a value of 1 is put to test again.

8.5 Interconnect-Deflection Analysis

Inheritance of shape factor effects in non-linear analysis is of particular interest as variations due to geometry might potentially result in large deviations when coupled with non-linear material properties. Thus, the main objectives of this experiment are -

- Apply shape factors of solid structures behaving in non-linear domains and isolate the best specimen shape.
- Identify if the conclusions and the key characteristics of shape factors from the linear experiment hold true in non-linear regimes.
- Reduce error to acceptable margins using the appropriate scale in geometry.

The effect of shape factors in non-linear ESM is presented inductively using an example where vertical deflection of an interconnect is analyzed, a device that mechanically and electrically connects chip packages to the board that they are mounted on [Harper, 2005]. Based on technology developed by IBM, these devices are responsible for fixture between two different geometries and provide very tight tolerances. The traditional design of an interconnect is shown below (see Figure 8.11).

The geometry involves a bottle like structure with a neck region. Compressive forces are applied on top causing stress in the structure. Since neck region is the weakest, fracture occurs at zone ‘*C*’ causing improper electrical and mechanical connectivity. To analyze failure in such problems, several approaches have been used in industry with Finite Element Methods (FEM) [Becket et al, 1981] playing a major role in evaluation.

A typical stress element in the geometry at neck region involves a structure that is subjected to normal compressive stresses and tangential shear stress causing net deformation as shown below. Since normal deformations have numerical precedence, vertical deflection of the element is considered as failure mode for analysis (see Figure 8.12).

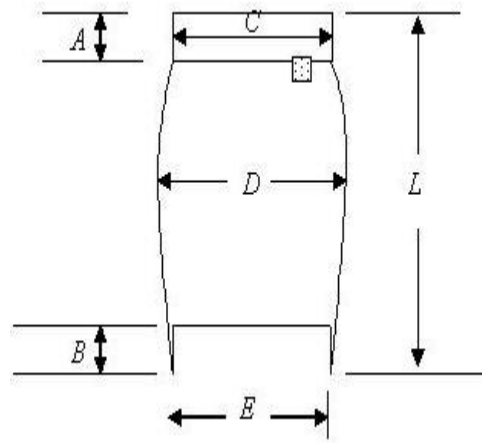


Figure 8.11: A typical interconnect geometry

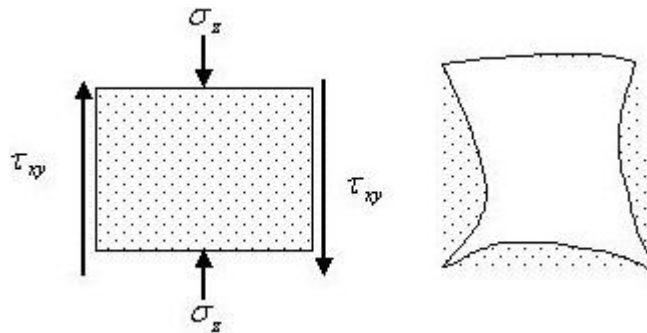


Figure 8.12: Stress element and deformed stress element of the interconnect neck region

This geometry is rather difficult to analyze due to its relative complexity and hence is pertinent to ESM as it involves geometric and parametric distortion while using multiple materials (Pb/Sn alloy) [Jones et al., 1998]. The three specimens that are analyzed are shown below (see Figure 8.13). Geometric distortion arises from the fact that section involving dimension ‘ B ’ is modeled as a continuous structure and cross-section at the neck, ‘ C ’ varies from tapered circle in the product to square, circular and elliptical in specimens. Also, in order to maintain consistency in scaling aspect ratio, the

three structures provide rather simple selection. Further, analysis would need to incorporate scaling in measurement location 'A', which causes parametric distortion. The three specimens selected are hence based on need to maintain length and width consistency while ensuring surface contact between load delivering medium (package) [Pecht et al., 1999] and load bearing surface of interconnect. Since deflection at neck level is analyzed, stress zones are concentrated in this region.

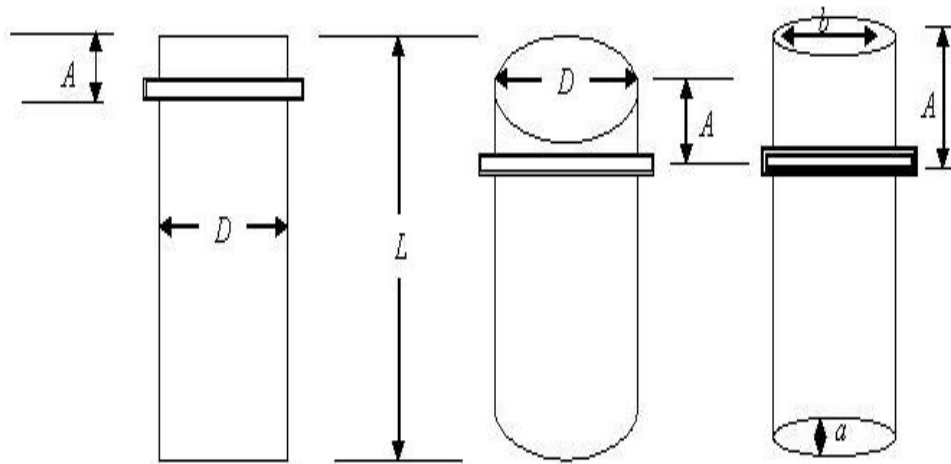


Figure 8.13: Specimen choices for interconnect

The first step is to establish geometric features and dimensions of the product and model. Typical dimensions of product shape is retrieved from [Lau, 1995] and data is compiled below with scale of $\frac{1}{2}$ between the two concerned structures (see Table 8.10).

ESM representation of the problem (see Table 8.11) and the specimen shape factors (see Table 8.12) are tabulated below as the second step in analysis.

The next step is to invoke material data which is summarized below [Jones et al., 1998]. Nylon used for numerical simulation is grade 66 and 60% glass fiber filled different from the material used in earlier examples (see Table 8.13).

Table 8.10: Geometric data of an interconnect

Dimension	Product	Model
<i>A</i>	5.000 μm	2.500 μm
<i>B</i>	3.050 μm	1.525 μm
<i>C</i>	20.000 μm	10.000 μm
<i>D</i>	28.280 μm	14.140 μm
<i>E</i>	10.000 μm	5.000 μm
<i>L</i>	33.230 μm	16.615 μm

Table 8.11: ESM representation of the interconnect

Geometry	Shape	Material
Product	Complex	Pb/Sn alloy
Product Specimen	Cylinder, Square, Ellipse	Pb/Sn Alloy
Model Specimen	Cylinder, Square, Ellipse	Nylon
Model	Complex	Nylon

Table 8.12: Specimen shape factors for interconnect experiment

Geometry	Domain	Application	Fixed	Value
Cylinder	Solids	Buckling	Yes	1.0000
Square	Solids	Buckling	Yes	$\frac{\pi}{3} = 1.0470$
Ellipse	Solids	Buckling	No	$\frac{C}{D} = 0.6944$

Table 8.13: Material data for interconnect experiment

Geometry	Scale	Material	Young's modulus	Poisson's ratio
Product	1.0	37/63 Pb/Sn alloy	37.5 GPa	0.38
Product Specimens	1.0	37/63 Pb/Sn alloy	37.5 GPa	0.38
Model	0.5	Nylon	19.1 GPa	0.35
Model Specimens	0.5	Nylon	19.1 GPa	0.35

Formulation of problem being complete, analysis is performed using *ABAQUSTM* for a compressive load of 10 *N* on all geometries. Values of deflection are estimated at uniform intervals along *x*-direction starting from center and proceeding towards edge in the neck region alone (see Tables 8.14

and 8.15). Non-linear nature of values is confirmed by distribution of numerical values signified by the statistical coefficients.

Table 8.14: Measurement data for interconnect experiment - Model and Product

Measurement	$\delta_m (\mu m)$	$\delta_p (\mu m)$
1	7.384990	7.178020
2	7.253891	7.243170
3	7.322870	7.277724
4	7.297631	7.281089
5	7.184716	7.231078
6	7.243590	7.162704
7	6.967222	7.139768
8	7.078295	7.183193
9	7.067780	7.235070

Table 8.15: Measurement data for interconnect experiment - All specimen

Measurement	Cylinder	Cylinder	Square	Square	Ellipse	Ellipse
	$\delta_{ms} (\mu m)$	$\delta_{ps} (\mu m)$	$\delta_{ms} (\mu m)$	$\delta_{ps} (\mu m)$	$\delta_{ms} (\mu m)$	$\delta_{ps} (\mu m)$
1	8.526560	8.652460	8.612020	8.755550	8.485070	8.581360
2	8.517445	8.639364	8.576720	8.676237	8.470204	8.455087
3	8.511354	8.630395	8.547408	8.626304	8.465454	8.369885
4	8.510312	8.628441	8.524085	8.605752	8.470822	8.325754
5	8.516329	8.636414	8.506750	8.624325	8.487398	8.322928
6	8.528330	8.652756	8.495403	8.690856	8.522386	8.391510
7	8.540235	8.668655	8.490045	8.759358	8.563267	8.502736
8	8.547807	8.677969	8.491265	8.783849	8.592788	8.585087
9	8.553543	8.684317	8.505231	8.773158	8.604695	8.577906

$$r(X_{ms}, X_{ps})_{Cylinder} = 0.9979 \quad (8.40)$$

$$r(X_{ms}, X_m)_{Cylinder} = -0.7415 \quad (8.41)$$

$$r(X_{ms}, X_{ps})_{Square} = -0.1327 \quad (8.42)$$

$$r(X_{ms}, X_m)_{Square} = 0.5828 \quad (8.43)$$

$$r(X_{ms}, X_{ps})_{Ellipse} = 0.6035 \quad (8.44)$$

$$r(X_{ms}, X_m)_{Ellipse} = -0.8142 \quad (8.45)$$

Scale and form transformation matrices are developed using adaptive exponential regression method and prediction estimates are generated for the product. Regression methods are used to analyze the system to further the use of adaptive techniques. Derived parameters of scaling are shown in Appendix E. Obtained intermediate prediction values are scaled by respective shape factors (see Table 8.12) to generate final predicted values as shown below (see Table 8.16).

Table 8.16: Predicted values for interconnect - scaled

Cylinder	Square	Ellipse
7.157360	6.682503	5.759340
6.983910	6.731344	5.068979
6.856570	7.534042	5.779861
6.896240	9.223213	5.686118
7.021030	16.377856	5.312944
7.082580	39.112933	5.288215
6.868450	42.854047	4.904583
7.120450	5.383548	4.907729
7.185820	10.414118	4.924625

Note that the shape factors are used in neck region alone as this is the zone where hypothetical failure occurs. Notice that product is approximated closely by cylinder and not as much by ellipse or square (see Table 8.17). This is a clear and categorical indicator that closer shape resemblance with actual product improves prediction *as long as* the specimen shape factor is close to 1 as well, which is attained by the cylinder in this example. Despite the fact that the square shape has a specimen shape factor close to 1, increase in its error can be attributed to the fact that number of boundaries rises to 4 in comparison with the cylinder (1), a shape that conforms significantly with

the actual system. This increase in boundary count causes edge development resulting in concentrations and non-uniform distribution of stress. Ellipse does perform better than square (see Figure 8.14) due to consistency in number of boundaries but skewness of cross-section (also the shape factor) defined by ratio of its characteristic dimensions makes it a bad choice. Thus, there exists need to maintain close geometric proximity with the actual system for better similarity results.

Table 8.17: Error values for interconnect - scaled

Error	Cylinder	Square	Ellipse
1	0.29%	6.90%	19.76%
2	3.58%	7.07%	30.02%
3	5.79%	3.52%	20.58%
4	5.29%	26.67%	21.91%
5	2.90%	126.49%	26.53%
6	1.12%	446.06%	26.17%
7	3.80%	500.22%	31.31%
8	0.87%	25.05%	31.68%
9	0.68%	43.94%	31.93%
RMS Error	3.33%	228.17%	27.05%

The objectives listed for this experiment are achieved and cylinder specimen is the optimal choice for this particular design. Further, error reduction is achieved by incorporating appropriately scaled specimen geometries. Also, the conclusions arrived at in the linear domain are corroborated by the non-linear results. Hence, it is extremely vital that -

- The number of boundaries remain consistent.
- The specimen shape factor be numerical proximal to a value of 1.

The optimal shape is hence the geometry that meets both criteria. If a geometry of shape factor 1 is not readily feasible, then consistency of boundaries needs to be first ensured and an alternate geometry needs to be chosen

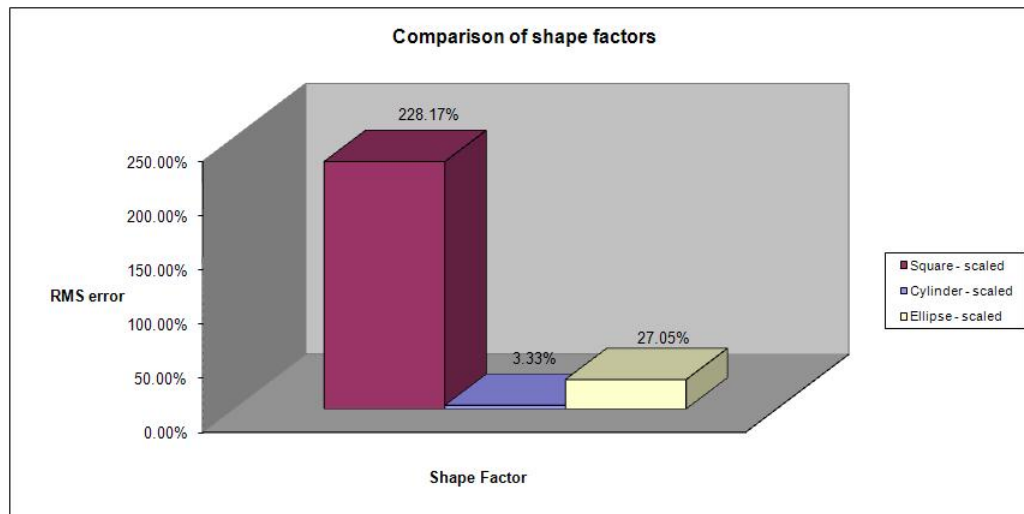


Figure 8.14: Errors due to shape factors for interconnect experiment - scaled

with a specimen shape factor value that is closest to 1 from within the selected set of specimens.

The two examples provided offer primitive integration of shape factors in ESM with special emphasis to mechanical structures. However, applicability of shape factors would be true irrespective of the analysis and systems being investigated. A thermal system with participating radiative bodies would still include prediction equation (8.33) but $C_{specimen}$ would alter to accommodate heat aspects pertinent to the analysis. For combinations of mechanical, thermal and/or other domains, a composite shape factor needs to be generated that incorporates features from all relevant energy mechanisms. This concocted value would replace $C_{specimen}$ in the prediction equation but is left as future exercise. This research though has identified interesting facets of shape factors and their adaptability in ESM. Some of the key aspects and guidelines described are summarized in Table 8.18. Further, a flowchart (see Figure 8.15) offers data flow perspective of shape factor integration in ESM.

Selection of specimen shapes begins with the identification of the product shape itself and its aspect ratio. Determining the complexity of the product shape would then assist in selecting either a finite set of specimen shapes with

Table 8.18: Guidelines for using shape factors in ESM

Attribute	Guideline
Cross-section	Identify shape of the cross-section that is being evaluated
Choice of specimen	Identify set of <i>known</i> specimen shapes (no more than 3) that have same aspect ratio as the product
Similarity of shapes	Maintain geometric proximity with actual shape
Boundary consistency	Maintain number of boundaries if geometric proximity with actual shape is not possible
Shape factor value	Identify shapes that generate a shape factor in the neighborhood of 1
Simplicity of shapes	Always choose simple shapes that have predefined shape factors or have geometric attributes that are easily defined
Shape complexity	Desist from using complex shapes or specimens with varying cross-sections as this is against the principle of simplified representation and is detrimental to shape factor evaluation
Characteristic dimensions	Try to use specimen shapes with one characteristic dimension thus allowing for uniform constant shape factor
Existence of shapes	If a specimen of one characteristic dimension is not viable, then use a shape with no more than 2 characteristic dimensions - remember that complexity rises with increase in dimensions as parameter values assume significance in all directions

basic geometric features or specimen with the same number of boundaries and aspect ratio. Once this task is accomplished, the characteristic dimensions are identified for each specimen choice and shape factor values evaluated. Care needs to be taken to select the shape with a shape factor value close to 1 and has the least number of characteristic dimensions, working upwards gradually to higher number of characteristic dimensions if the previous selection is not possible, thus refining the specimen set. A final selection is then made to isolate the “best” specimen which meets both the boundary consistency and shape factor value requirements. The prediction values of ESM are scaled with the shape factor value of the chosen specimen shape.

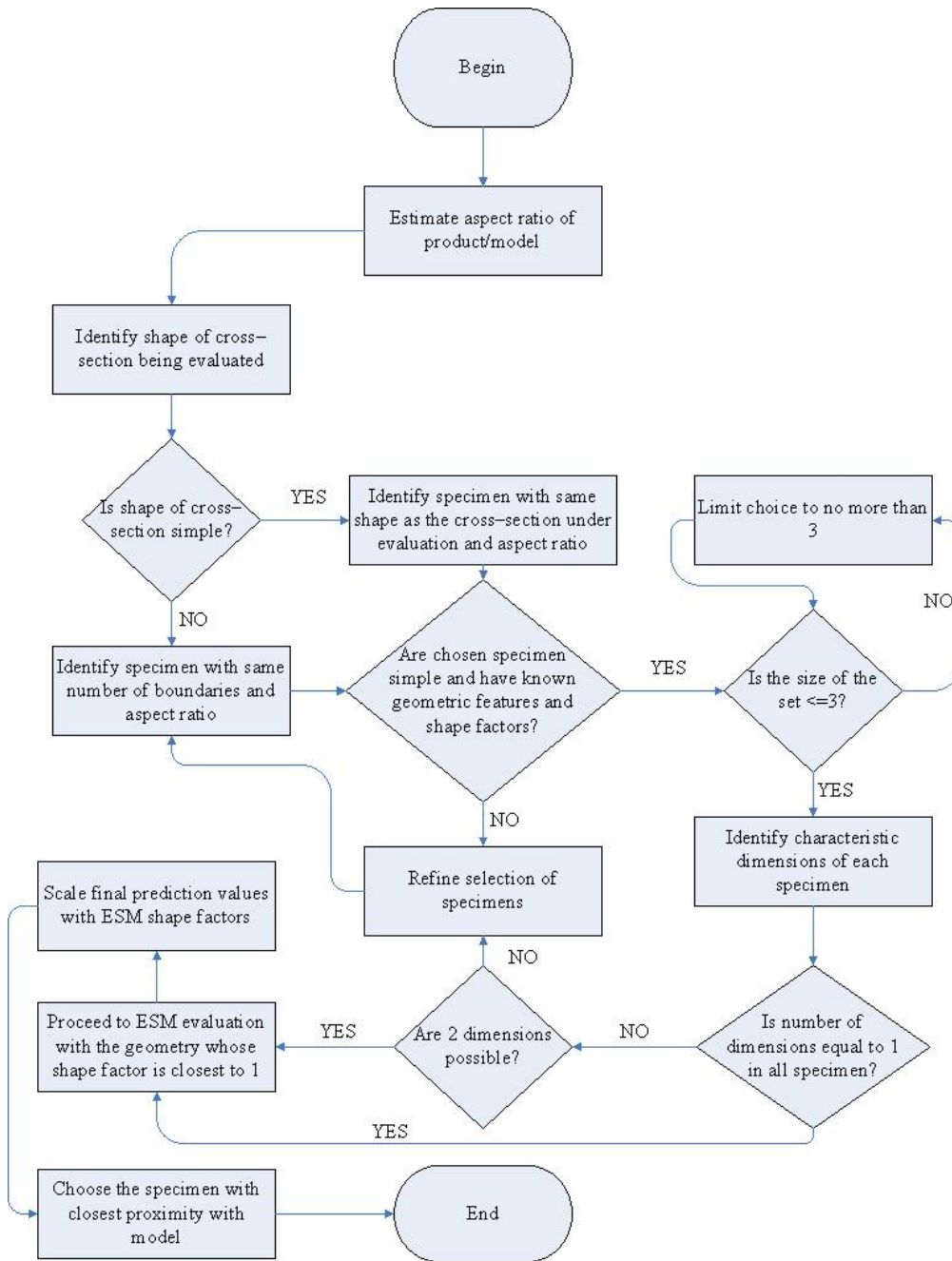


Figure 8.15: Shape factor integration in ESM

8.6 Summary

Complete with numerical examples and applications in simple products, this chapter has introduced and inculcated shape factors in ESM studies. The key motivation of providing initial framework for such analysis has been realized and thus focus of this research has been confined to mechanical systems. Extension into multi-domain and complex systems is possible and needs comprehensive technical investigation. Renewing the necessity to provide experimental evidence to all methods described thus far, the next chapter provides realistic and pragmatic documentation of experimental work undertaken and results achieved.

Chapter 9

Experimental Verification

“All life is an experiment. The more experiments you make the better.” -
Ralph Waldo Emerson

All examples illustrated thus far have been predominantly numerical because the main purpose behind using such designs has been illustration of technical validity of the developed methods. Further, all the products studied are geometrically constrained and/or derived from literature thus having no physical presence for any tangible experimental analysis hence coercing estimation through numerical simulations. Complexity of geometry also necessitates usage of intricate instrumentation for data collection that is not readily available. But since numerical and analytical research findings are fortified by experimental evidence, this chapter provides such justification through the use of a simple example.

9.1 Welding Experiment-Temperature Analysis

In providing experimental evidence for the veracity of linear methods, a gas metal arc welding (GMAW) experiment is conducted on steel and aluminum geometries with apparent geometric distortion (see Figure 9.1). Test

geometries used in this experiment are of rectangular shape with dimensions measured in inches. The focus of this experiment is to estimate peak temperature values ($^{\circ}C$) obtained in all concerned geometries at the locations specified (see Figure 9.2) for a single pass of weld. Thus, the prime objectives of this experiment are -

- Provide experiential validation of the developed linear methods.
- Document the experimental process for usage of linear ESM in engineering parameter evaluation.

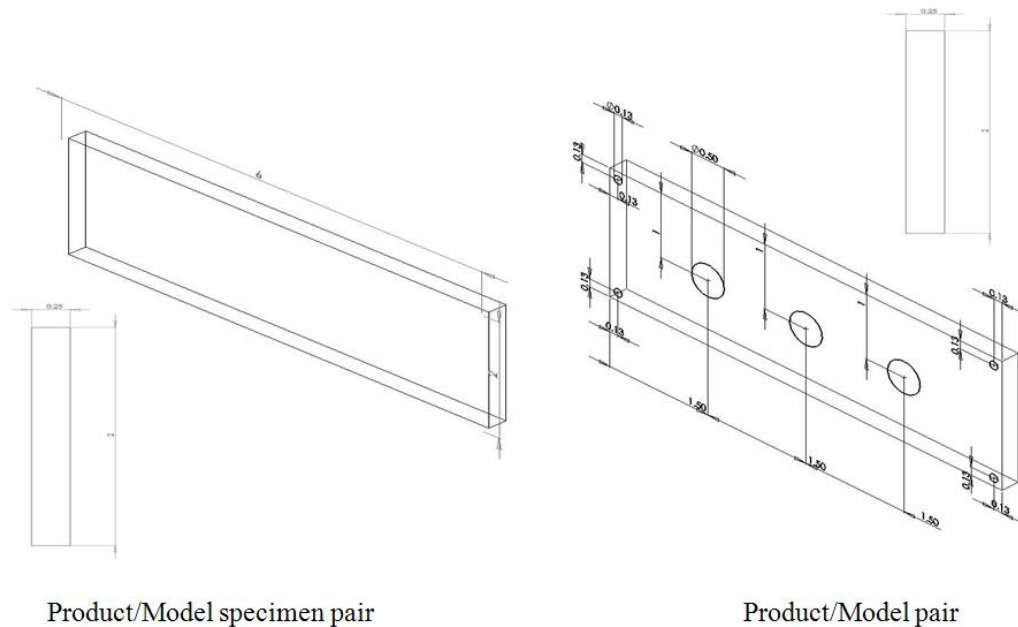


Figure 9.1: Geometries for the weld experiment

As illustrated above, the product/model pair are structures with geometric distortion, captured by four edge holes of diameter 0.125" and three equally distributed central holes of diameter 0.5". The specimen pair does not have any distortion and are of solid shape. Recall that temperature values at discrete locations are being predicted for an alloy (steel) based on the equivalent response of a metal (aluminum). Aluminum is used since it is a isotropic

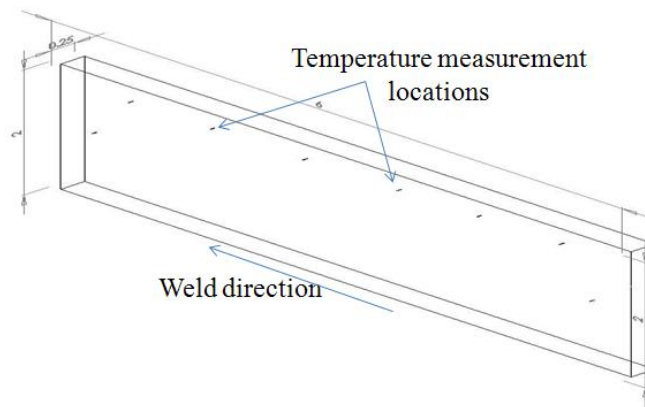


Figure 9.2: Temperature measurement locations in the weld experiment

material that is easily machinable and considerably inexpensive. The ESM representation of the problem is tabulated below (see Table 9.1).

Table 9.1: ESM representation of the welding system

Geometry	Material
Product	Steel with distortions
Product Specimen	Steel without distortions
Model Specimen	Aluminum without distortions
Model	Aluminum with distortions

The GMAW welding parameters used for the experiment include input voltage that determines the current used in the welding process, wire feed rate which is the speed at which the welding wire is fed to the welding gun, and traverse speed, which is the rate of the welding process (see Table 9.2).

Table 9.2: Welding parameters

Voltage (V)	Wire Feed Rate (<i>in/min</i>)	Traverse Speed (<i>in/min</i>)
24	400	20

Note that same input parameters and values have been used across all four geometries (see Figure G.1) to negate parametric distortion. Further, steel

wire is used for steel geometries and aluminum wire for aluminum geometries so as to allow the welding process to successfully fuse the respective materials together (see Figure G.3). Temperature estimation is achieved through the use of thermocouples that are spot welded at the measurement points (see Figure G.2), which record real time data for further analysis. Input source of energy has been obtained through gas combustion by spark ignition caused by the electrode (see Figure G.4). Finally, recorded temperature values have been retrieved through data acquisition (DAQ) sources affixed between thermocouples and the computer (see Figure G.4). The obtained results are tabulated below (see Table 9.3).

Table 9.3: Measurement data for welding experiment

Measurement	T_{ms}	T_{ps}	T_m	T_p
1	176.20	117.74	193.22	141.47
2	136.48	88.71	156.82	108.37
3	141.19	97.63	166.66	113.43
4	149.19	104.45	169.70	110.89
5	154.85	109.44	178.61	113.38
6	163.29	112.54	181.45	116.26
7	168.77	114.19	187.35	115.09
8	208.35	129.22	223.43	132.29

Note that the peak temperature values have been recorded on the far side, away from the weld bead, and points 1 and 8 (points opposite to each other on the longitudinal axis - see Figure 9.2) that are physically closest to the bead record the highest temperature values across all four geometries. Statistical coefficients of correlation shown below indicate a strong linearity trend validating use of linear methods.

$$r(X_{ps}, X_{ms}) = 0.9533 \quad (9.1)$$

$$r(X_m, X_{ms}) = 0.9947 \quad (9.2)$$

Like before, intermediate analysis performed is summarized in Appendix F. Results of analysis are shown below (see Table 9.4) where the TCG technique marginally outperforms all other methods (see Table 9.5) while the HM method is comparable to the rest of the processes (see Figure 9.4).

Table 9.4: Predicted values for welding temperature measurement

Measurement	DM	PI	CM	CpM	HM	TCG
1	129.11	131.66	129.10	126.69	129.54	138.20
2	101.93	99.20	103.65	98.37	102.61	105.17
3	115.25	109.17	113.54	110.71	114.90	117.12
4	118.81	116.80	118.90	115.28	118.81	117.25
5	126.23	122.38	123.12	122.19	125.54	123.37
6	125.06	125.85	125.77	122.25	124.91	121.71
7	126.76	127.70	125.38	123.98	126.40	126.17
8	138.58	144.50	141.43	136.57	138.58	134.60

Table 9.5: Error values for welding temperature measurement

Measurement	DM	PI	CM	CpM	HM	TCG
1	8.74%	6.94%	8.75%	10.45%	8.43%	2.31%
2	5.94%	8.46%	4.35%	9.23%	5.31%	2.95%
3	1.60%	3.75%	0.10%	2.34%	1.30%	3.25%
4	7.14%	5.33%	7.22%	3.96%	7.14%	5.74%
5	11.33%	7.93%	8.59%	7.77%	10.72%	8.81%
6	7.56%	8.25%	8.18%	5.15%	7.44%	4.69%
7	10.14%	10.96%	8.95%	7.73%	9.83%	9.63%
8	4.75%	9.24%	6.91%	3.23%	4.75%	1.75%
RMS Error	7.72%	7.89%	7.21%	6.83%	7.43%	5.62%

Notice from the prediction plot below (see Figure 9.3) that all methods provide near identical values, which can be explained by the fact that peak temperatures used in this experiment are of higher numerical magnitude when compared to earlier examples and hence inversion of matrices would not be issue for non-singular behavior. Also, the TCG technique does not yield any

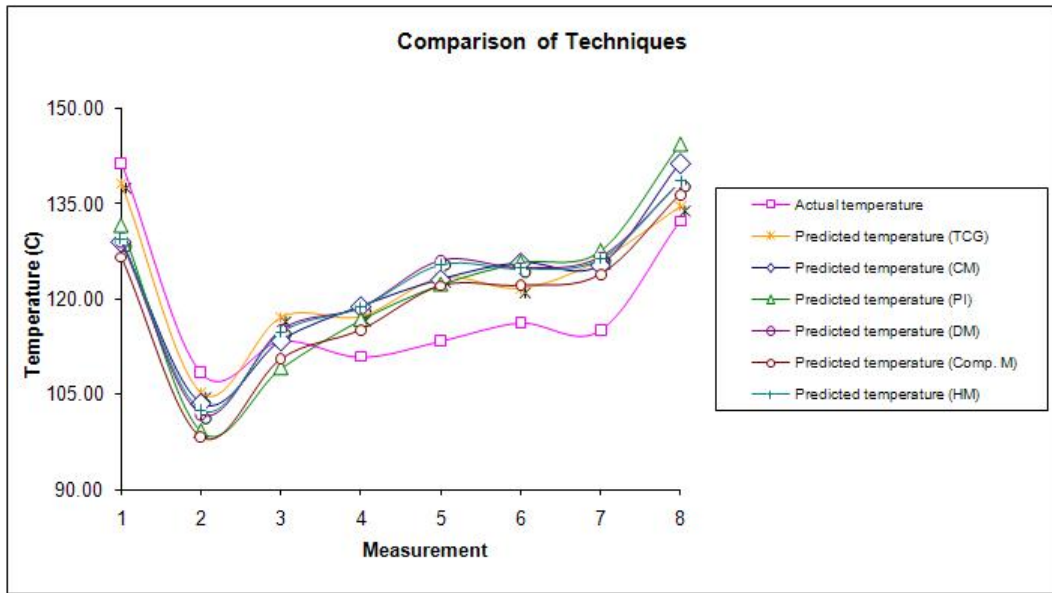


Figure 9.3: Prediction plot for welding temperature measurement

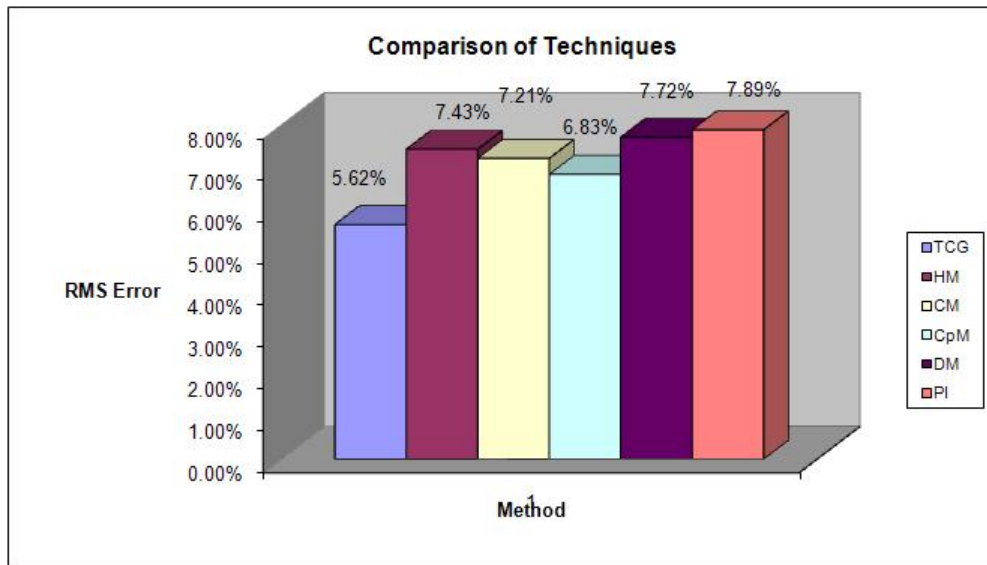


Figure 9.4: Error plot for welding temperature measurement

profound advantage in this experiment but is still better than other methods due to smaller and often time selectable residue margins. The technique thus

imparts significant flexibility and numerical control to the ESM process. Concluding, all objectives listed for this experiment have been successfully realized with illustration of empirical evidence for linear ESM processes.

9.2 Summary

This chapter has realized the most important piece of research by providing a practical example and application for the developed ESM strategies. Thus, applicability and use of these methods in engineering studies, particularly in design, has been demonstrated. Concluding this innovative work, the next chapter summarizes all research highlights by providing glimpses of major milestones attained.

Chapter 10

Results and Conclusions

“Life is the art of drawing sufficient conclusions from insufficient premises.”
- Samuel Butler

Research in potent similarity methods has engulfed numerous modes of analysis much to the benefit of the scientific community. Bettering conventional wisdom acquired through the ages, investigation of technical problems using processes based on dimensions has progressed systematically to include engineering phenomena of academic and industrial value. Several such advancements have been captured in this research effort weaving through many analytical relations and, numerical and experimental examples. Prime objectives set forth in proving hypothesis of research have been conclusively achieved thereby assuring validity of original motivation in experiential similitude. Major achievements and milestones conquered are catalogued below.

10.1 Research Contributions

Beginning with the explanation of techniques of TSM and associated examples and limitations, Buckingham π theorem has been elucidated using a numerical example and its drawbacks have been highlighted. Conventional similarity has been extended to model dynamic systems using modified al-

gorithms and optimization techniques where design of a dynamic system is evaluated using this novel approach. Nodal analysis have been incorporated into dimensional analysis and the first set of rules have been framed for modeling system dynamics where graphs have been developed to offer visualization of data flow in dynamic systems using a common toy example.

Extending into ESM, major means of distortions have been defined and classified. Original principles of ESM have been developed along with statistical measures for problem classification. Hankel matrix based approach and a conjugate gradient based method have been developed for linear analysis using the Toeplitz operator where issues with stiff/large systems have been resolved. Generic estimation in linear domains has been illustrated using two pertinent examples of mechanical deflection and electro-magnetic behavior.

Expanding into non-linear domains, five new adaptive techniques have been innovated with the aim of bettering accuracy in non-linear systems. Robustness has been injected to non-linear analysis by delving into adaptivity features and continuity definitions. Prediction in non-linear domains has been executed using examples from heat transfer and aerodynamics. Rigorous mathematical detail has been supplemented with coherent error arguments.

Shape factors have been integrated into ESM forcing investigation into specimen shape and selection. Applications of shape factors in ESM have been elaborated along with scaling procedure and justification through two deflection examples. Experimentation has also been successfully realized thus corroborating numerical analysis.

Using the above contributions as a basis, a few research extensions are suggested next to better the ESM technique.

10.2 Future Work

Research in all walks of life seeks continuous improvement and enhanced efficiency. While the list summarized above offers technical strength to this current work, it is definitely not complete. ESM offers wide variety of research

avenues that present exciting opportunities for continued investigation. Some of the concerns identified through this research are suggested below.

- **Identification and Classification of Distortions**

Prior research and this exposition have compiled all known distortions that affect similarity methods and means of overcoming such discrepancies. This list is not exhaustive and more focus needs to be attached to extend to a wide array of problems and examples.

- **Optimization**

Optimization is hypothesized to play critical role in future developments of ESM. Since error generation is inherent in numerical analysis, optimization schemes and associated methods offer great potential for error minimization in ESM prediction thus enhancing its analytical credibility.

- **Statistical Investigation**

Statistical techniques have been incorporated into ESM to a fair degree by using regression analysis and correlation tests. However, alternate procedures must be studied including design of experiments and response surface models that are of immense value in generating scale and form transformations since the process is empirical by definition.

- **Gradient and Search Methods**

Both linear and non-linear domains can be successfully extended by probing advanced numerical procedures such as GMRES, PCG and other iterative schemes, and B-splines, Bezier curves and NURBS respectively thus progressing towards complete numerical-experimental control of ESM scaling abilities. Special matrices need to be further explored for possible induction into ESM.

- **Shape Factor Extension**

Integration of shape factors has been demonstrated in mechanical domain alone. Since most products are influenced by multiple inputs, shape

factors from a variety of sources need to be coupled into ESM prediction. Such concoction of values needs to be further studied in terms of mathematical combinations and development of scaling formulae. In conjunction with optimization, specimen selection can be made robust and well-judged for greater prediction accuracy.

- **Greater use of Rapid Prototypes**

Rapid prototypes have offered extreme flexibility in fabrication of test specimen. This leverage has to be furthered by coupling experimentation and instrumentation thus recording real-time data of prescribed parameter of interest. Such in-line measurement offers immediate and accurate numerical values for subsequent analysis.

- **Automation and Software**

As an end product for commercial use, ESM process has to be brought to a level commensurate with its applicability. Automation has to be imbibed so that a software tool or tool box can be generated for engineering use and demonstration. Such programs can be employed in industrial, academic and research organizations for various purposes.

10.3 Summary

The ESM method has greatly enhanced prediction capabilities to incorporate distinct material behavior and complex geometries. Incorporation of such experimental similarity techniques holds unrestricted potential for future designs and design evaluation. Evolution of ESM has progressed from initial polymer based models and simple mathematical techniques to its current state of greater numerical and computational ease using plastics and other alloy materials. This voyage has traversed uncharted research territories seeking rational explanations to couple diverse analytical relations from engineering and mathematical world. While some pebbles have been extracted, lot more excavation is needed in ESM.

Appendix A

Conjugate Gradient Method

Let A be a positive definite matrix¹ and $Ax = b$ be the system of linear equations. The algorithm of CG process iterates for an initial guess x_0 such that end residual is minimized thereby converging to a solution [Shewchuk, 1994] obtained by,

$$r_0 \rightarrow b - Ax_0 \tag{A.1}$$

$$p_0 \rightarrow r_0 \tag{A.2}$$

$$k \rightarrow 0 \tag{A.3}$$

Loop

$$\alpha_k \rightarrow \frac{r_k^T r_k}{p_k^T A p_k} \tag{A.4}$$

$$x_{k+1} \rightarrow x_k + \alpha_k p_k \tag{A.5}$$

$$r_{k+1} \rightarrow r_k - \alpha_k A p_k \tag{A.6}$$

if ($r_{k+1} \leq tol$)

end

¹ $x^T A x > 0 \forall x \in \mathfrak{R}^n$.

else

$$\beta_k \rightarrow \frac{r_{k+1}^T r_{k+1}}{r_k^T r_k} \quad (\text{A.7})$$

$$p_{k+1} \rightarrow r_{k+1} + \beta_k p_k \quad (\text{A.8})$$

$$k \rightarrow k + 1 \quad (\text{A.9})$$

End loop

Appendix B

Transformer-Magnetic Flux Analysis

$$(S \times F)_{DM} =$$

$$\begin{pmatrix} 0.8889 & 0 & 0 & 0 & 0 & 0 & 0 & 0 & 0 & 0 & 0 & 0 \\ 0 & 1.3774 & 0 & 0 & 0 & 0 & 0 & 0 & 0 & 0 & 0 & 0 \\ 0 & 0 & 1.4438 & 0 & 0 & 0 & 0 & 0 & 0 & 0 & 0 & 0 \\ 0 & 0 & 0 & 1.2804 & 0 & 0 & 0 & 0 & 0 & 0 & 0 & 0 \\ 0 & 0 & 0 & 0 & 1.1828 & 0 & 0 & 0 & 0 & 0 & 0 & 0 \\ 0 & 0 & 0 & 0 & 0 & 1.0589 & 0 & 0 & 0 & 0 & 0 & 0 \\ 0 & 0 & 0 & 0 & 0 & 0 & 1.2661 & 0 & 0 & 0 & 0 & 0 \\ 0 & 0 & 0 & 0 & 0 & 0 & 0 & 1.2843 & 0 & 0 & 0 & 0 \\ 0 & 0 & 0 & 0 & 0 & 0 & 0 & 0 & 1.3562 & 0 & 0 & 0 \\ 0 & 0 & 0 & 0 & 0 & 0 & 0 & 0 & 0 & 1.3788 & 0 & 0 \\ 0 & 0 & 0 & 0 & 0 & 0 & 0 & 0 & 0 & 0 & 1.2889 & 0 \\ 0 & 0 & 0 & 0 & 0 & 0 & 0 & 0 & 0 & 0 & 0 & 1.1172 \end{pmatrix}$$

$$(S \times F)_{PI} = \begin{pmatrix} 0.0004 & 0.0011 & 0.0026 & 0.0041 & 0.0051 & 0.0058 & \dots \\ 0.0015 & 0.0041 & 0.0096 & 0.0154 & 0.019 & 0.0216 & \dots \\ 0.0035 & 0.0097 & 0.023 & 0.0369 & 0.0457 & 0.0519 & \dots \\ 0.0058 & 0.0158 & 0.0374 & 0.0599 & 0.0743 & 0.0844 & \dots \\ 0.0073 & 0.02 & 0.0473 & 0.0758 & 0.094 & 0.1067 & \dots \\ 0.0081 & 0.0222 & 0.0524 & 0.084 & 0.1041 & 0.1182 & \dots \\ 0.0088 & 0.0242 & 0.0572 & 0.0917 & 0.1137 & 0.1291 & \dots \\ 0.009 & 0.0249 & 0.0588 & 0.0942 & 0.1168 & 0.1327 & \dots \\ 0.0094 & 0.0258 & 0.061 & 0.0978 & 0.1213 & 0.1377 & \dots \\ 0.0096 & 0.0264 & 0.0623 & 0.0999 & 0.1238 & 0.1406 & \dots \\ 0.0096 & 0.0265 & 0.0626 & 0.1004 & 0.1245 & 0.1413 & \dots \\ 0.0097 & 0.0266 & 0.0629 & 0.1009 & 0.1251 & 0.142 & \dots \end{pmatrix}$$

$$\begin{pmatrix} \dots & 0.0062 & 0.0063 & 0.0064 & 0.0065 & 0.0069 & 0.0075 \\ \dots & 0.0231 & 0.0237 & 0.024 & 0.0245 & 0.0258 & 0.0283 \\ \dots & 0.0555 & 0.0569 & 0.0575 & 0.0587 & 0.0619 & 0.0678 \\ \dots & 0.0901 & 0.0925 & 0.0935 & 0.0954 & 0.1007 & 0.1102 \\ \dots & 0.114 & 0.117 & 0.1182 & 0.1207 & 0.1273 & 0.1395 \\ \dots & 0.1263 & 0.1297 & 0.131 & 0.1337 & 0.1411 & 0.1545 \\ \dots & 0.1379 & 0.1415 & 0.143 & 0.1459 & 0.154 & 0.1687 \\ \dots & 0.1417 & 0.1455 & 0.147 & 0.15 & 0.1583 & 0.1734 \\ \dots & 0.1471 & 0.151 & 0.1526 & 0.1557 & 0.1643 & 0.18 \\ \dots & 0.1502 & 0.1542 & 0.1558 & 0.159 & 0.1678 & 0.1837 \\ \dots & 0.151 & 0.155 & 0.1566 & 0.1598 & 0.1686 & 0.1847 \\ \dots & 0.1517 & 0.1558 & 0.1574 & 0.1606 & 0.1695 & 0.1856 \end{pmatrix}$$

$$(S \times F)_{CM} = \begin{pmatrix} 1.1314 & -0.0206 & -0.022 & 0.0565 & 0.0574 & 0.0834 & \dots \\ 0.1348 & 1.1314 & -0.0206 & -0.022 & 0.0565 & 0.0574 & \dots \\ 0.0647 & 0.1348 & 1.1314 & -0.0206 & -0.022 & 0.0565 & \dots \\ -0.0234 & 0.0647 & 0.1348 & 1.1314 & -0.0206 & -0.022 & \dots \\ -0.0591 & -0.0234 & 0.0647 & 0.1348 & 1.1314 & -0.0206 & \dots \\ -0.0078 & -0.0591 & -0.0234 & 0.0647 & 0.1348 & 1.1314 & \dots \\ -0.1413 & -0.0078 & -0.0591 & -0.0234 & 0.0647 & 0.1348 & \dots \\ 0.0834 & -0.1413 & -0.0078 & -0.0591 & -0.0234 & 0.0647 & \dots \\ 0.0574 & 0.0834 & -0.1413 & -0.0078 & -0.0591 & -0.0234 & \dots \\ 0.0565 & 0.0574 & 0.0834 & -0.1413 & -0.0078 & -0.0591 & \dots \\ -0.022 & 0.0565 & 0.0574 & 0.0834 & -0.1413 & -0.0078 & \dots \\ -0.0206 & -0.022 & 0.0565 & 0.0574 & 0.0834 & -0.1413 & \dots \end{pmatrix}$$

$$\begin{pmatrix} \dots & -0.1413 & -0.0078 & -0.0591 & -0.0234 & 0.0647 & 0.1348 \\ \dots & 0.0834 & -0.1413 & -0.0078 & -0.0591 & -0.0234 & 0.0647 \\ \dots & 0.0574 & 0.0834 & -0.1413 & -0.0078 & -0.0591 & -0.0234 \\ \dots & 0.0565 & 0.0574 & 0.0834 & -0.1413 & -0.0078 & -0.0591 \\ \dots & -0.022 & 0.0565 & 0.0574 & 0.0834 & -0.1413 & -0.0078 \\ \dots & -0.0206 & -0.022 & 0.0565 & 0.0574 & 0.0834 & -0.1413 \\ \dots & 1.1314 & -0.0206 & -0.022 & 0.0565 & 0.0574 & 0.0834 \\ \dots & 0.1348 & 1.1314 & -0.0206 & -0.022 & 0.0565 & 0.0574 \\ \dots & 0.0647 & 0.1348 & 1.1314 & -0.0206 & -0.022 & 0.0565 \\ \dots & -0.0234 & 0.0647 & 0.1348 & 1.1314 & -0.0206 & -0.022 \\ \dots & -0.0591 & -0.0234 & 0.0647 & 0.1348 & 1.1314 & -0.0206 \\ \dots & -0.0078 & -0.0591 & -0.0234 & 0.0647 & 0.1348 & 1.1314 \end{pmatrix}$$

$$\begin{pmatrix} a^* \\ b^* \end{pmatrix}_{CpM} = \begin{pmatrix} -0.0018 \\ 0.9394 \end{pmatrix}, \quad \begin{pmatrix} a_1^* \\ b_1^* \end{pmatrix}_{CpM} = \begin{pmatrix} 0.0267 \\ 1.3026 \end{pmatrix}$$

$$(S \times F)_{HM} = \begin{pmatrix} 1.1172 & 0.1514 & 0.082 & -0.0024 & -0.0515 & -0.0233 & \dots \\ 0 & 1.1172 & 0.1514 & 0.082 & -0.0024 & -0.0515 & \dots \\ 0 & 0 & 1.1172 & 0.1514 & 0.082 & -0.0024 & \dots \\ 0 & 0 & 0 & 1.1172 & 0.1514 & 0.082 & \dots \\ 0 & 0 & 0 & 0 & 1.1172 & 0.1514 & \dots \\ 0 & 0 & 0 & 0 & 0 & 1.1172 & \dots \\ 0 & 0 & 0 & 0 & 0 & 0 & \dots \\ 0 & 0 & 0 & 0 & 0 & 0 & \dots \\ 0 & 0 & 0 & 0 & 0 & 0 & \dots \\ 0 & 0 & 0 & 0 & 0 & 0 & \dots \\ 0 & 0 & 0 & 0 & 0 & 0 & \dots \\ 0 & 0 & 0 & 0 & 0 & 0 & \dots \end{pmatrix}$$

$$\begin{pmatrix} \dots & -0.1583 & 0.0651 & 0.0533 & 0.0581 & -0.0136 & -0.0099 \\ \dots & -0.0233 & -0.1583 & 0.0651 & 0.0533 & 0.0581 & -0.0136 \\ \dots & -0.0515 & -0.0233 & -0.1583 & 0.0651 & 0.0533 & 0.0581 \\ \dots & -0.0024 & -0.0515 & -0.0233 & -0.1583 & 0.0651 & 0.0533 \\ \dots & 0.082 & -0.0024 & -0.0515 & -0.0233 & -0.1583 & 0.0651 \\ \dots & 0.1514 & 0.082 & -0.0024 & -0.0515 & -0.0233 & -0.1583 \\ \dots & 1.1172 & 0.1514 & 0.082 & -0.0024 & -0.0515 & -0.0233 \\ \dots & 0 & 1.1172 & 0.1514 & 0.082 & -0.0024 & -0.0515 \\ \dots & 0 & 0 & 1.1172 & 0.1514 & 0.082 & -0.0024 \\ \dots & 0 & 0 & 0 & 1.1172 & 0.1514 & 0.082 \\ \dots & 0 & 0 & 0 & 0 & 1.1172 & 0.1514 \\ \dots & 0 & 0 & 0 & 0 & 0 & 1.1172 \end{pmatrix}$$

$$(S \times F)_{TCG} = \begin{pmatrix} 0.4837 & -0.2250 & 0.1923 & -0.2895 & 0.2450 & 0.0096 & \dots \\ 0.6802 & 1.5387 & -0.3779 & 0.7185 & -0.8305 & 0.3612 & \dots \\ -0.7956 & 0.4235 & 1.0570 & -0.6351 & 1.0542 & -0.9868 & \dots \\ 0.1033 & -0.9799 & 0.2644 & 0.9593 & -0.3732 & 0.8802 & \dots \\ 0.7480 & 0.5600 & -0.3369 & 0.5924 & 0.3625 & 0.2009 & \dots \\ -0.9921 & 0.4824 & -0.0972 & -0.4565 & 1.0524 & -0.3341 & \dots \\ 0.2794 & -1.0060 & 0.4856 & -0.1129 & -0.4396 & 1.0479 & \dots \\ 0.6985 & 0.3613 & -0.3070 & 0.3978 & -0.3507 & -0.0014 & \dots \\ -0.9978 & 0.7936 & -0.4073 & -0.0120 & 0.4271 & -0.7495 & \dots \\ 0.5492 & -1.0848 & 1.0145 & -0.5560 & 0.0544 & 0.5149 & \dots \\ -0.4046 & 0.3555 & -0.9104 & 0.7631 & -0.3469 & 0.0677 & \dots \\ 0.2933 & 0.0743 & 0.2958 & -0.3821 & 0.1742 & -0.1665 & \dots \end{pmatrix}$$

$$\begin{pmatrix} \dots & -0.1665 & 0.1742 & -0.3821 & 0.2958 & 0.0743 & 0.2933 \\ \dots & 0.0677 & -0.3469 & 0.7631 & -0.9104 & 0.3555 & -0.4046 \\ \dots & 0.5149 & 0.0544 & -0.5560 & 1.0145 & -1.0848 & 0.5492 \\ \dots & -0.7495 & 0.4271 & -0.0120 & -0.4073 & 0.7936 & -0.9978 \\ \dots & -0.0014 & -0.3507 & 0.3978 & -0.3070 & 0.3613 & 0.6985 \\ \dots & 1.0479 & -0.4396 & -0.1129 & 0.4856 & -1.0060 & 0.2794 \\ \dots & -0.1341 & 1.0524 & -0.4565 & -0.0972 & 0.4824 & -0.9921 \\ \dots & 0.2009 & 0.1625 & 0.5924 & -0.3369 & 0.5600 & 0.7480 \\ \dots & 0.8802 & -0.3732 & 0.9593 & 0.2644 & -0.9799 & 0.1033 \\ \dots & -0.9868 & 1.0542 & -0.6351 & 1.1170 & 0.4235 & -0.7956 \\ \dots & 0.3612 & -0.8305 & 0.7185 & -0.3779 & 1.1887 & 0.6802 \\ \dots & 0.0096 & 0.2450 & -0.2895 & 0.1923 & -0.2250 & 0.8337 \end{pmatrix}$$

Appendix C

Airfoil-Coefficient of Drag

Analysis

$$\begin{pmatrix} [u \ u_0 \ v \ v_0]_1 \\ [u \ u_0 \ v \ v_0]_2 \\ [u \ u_0 \ v \ v_0]_3 \\ [u \ u_0 \ v \ v_0]_4 \\ [u \ u_0 \ v \ v_0]_5 \\ [u \ u_0 \ v \ v_0]_6 \\ [u \ u_0 \ v \ v_0]_7 \\ [u \ u_0 \ v \ v_0]_8 \\ [u \ u_0 \ v \ v_0]_9 \\ [u \ u_0 \ v \ v_0]_{10} \\ [u \ u_0 \ v \ v_0]_{11} \\ [u \ u_0 \ v \ v_0]_{12} \\ [u \ u_0 \ v \ v_0]_{13} \end{pmatrix} = \begin{pmatrix} -0.0016 & 0.00002704 & -0.000900 & 0.00001584 \\ 0.0009 & -0.00001548 & -0.000300 & 4.80E - 06 \\ 0.0003 & -0.00000585 & -0.002300 & 0.00003887 \\ 0.0023 & -0.000046 & -0.000500 & 8.60E - 06 \\ 0.0005 & -0.0000093 & 0.001400 & -0.0000273 \\ -0.0014 & 0.00002646 & -0.000300 & 6.00E - 06 \\ 0.0003 & -0.00000612 & -0.001500 & 0.0000279 \\ 0.0015 & -0.0000357 & -0.003400 & 0.00006426 \\ 0.0034 & -0.0000867 & -0.001700 & 0.00003468 \\ 0.0017 & -0.0000459 & -0.001500 & 0.0000357 \\ 0.0015 & -0.00004275 & -0.001500 & 0.00003825 \\ -0.0015 & 0.0000357 & 0.001700 & -0.0000459 \\ -0.0015 & 0.00003825 & 0.001500 & -0.00004275 \end{pmatrix}$$

$$\begin{pmatrix} [u' & u'_0 & v' & v'_0]_1 \\ [u' & u'_0 & v' & v'_0]_2 \\ [u' & u'_0 & v' & v'_0]_3 \\ [u' & u'_0 & v' & v'_0]_4 \\ [u' & u'_0 & v' & v'_0]_5 \\ [u' & u'_0 & v' & v'_0]_6 \\ [u' & u'_0 & v' & v'_0]_7 \\ [u' & u'_0 & v' & v'_0]_8 \\ [u' & u'_0 & v' & v'_0]_9 \\ [u' & u'_0 & v' & v'_0]_{10} \\ [u' & u'_0 & v' & v'_0]_{11} \\ [u' & u'_0 & v' & v'_0]_{12} \\ [u' & u'_0 & v' & v'_0]_{13} \end{pmatrix} = \begin{pmatrix} -0.00025 & 2.98E-06 & -0.00015 & 1.80E-06 \\ 0.00015 & -0.0000018 & -0.0001 & 1.18E-06 \\ 0.0001 & -0.000001235 & -0.00035 & 4.17E-06 \\ 0.00035 & -4.3225E-06 & 0 & 0 \\ 0 & 0 & -0.00015 & 1.85E-06 \\ 0.00015 & -1.9725E-06 & -0.00065 & 8.03E-06 \\ 0.00065 & -9.2625E-06 & -0.0011 & 0.00001375 \\ 0.0011 & -0.000017325 & -0.0015 & 0.000019725 \\ 0.0015 & -0.0000267 & -0.00205 & 2.92125E-05 \\ 0.00205 & -0.000041 & -0.0022 & 0.00003465 \\ 0.0022 & -0.0000473 & -0.0015 & 0.0000267 \\ -0.0022 & 0.00003465 & 0.00205 & -0.000041 \\ -0.0015 & 0.0000267 & 0.0022 & -0.0000473 \end{pmatrix}$$

$$\begin{pmatrix} T_1 \\ T_2 \\ T_3 \\ T_4 \\ T_5 \\ T_6 \\ T_7 \\ T_8 \\ T_9 \\ T_{10} \\ T_{11} \\ T_{12} \\ T_{13} \end{pmatrix} \underset{\text{Bilinear}}{=} \begin{pmatrix} 1.90348 \\ -1.97143 \\ -1.26087 \\ -28.0182 \\ 0.168067 \\ -21.0 \\ -0.0758621 \\ 0.143084 \\ 2.0 \\ -5.5561 \\ -2.09091 \\ -0.225718 \\ -0.375 \end{pmatrix}$$

$$\begin{pmatrix} T_1 \\ T_2 \\ T_3 \\ T_4 \\ T_5 \\ T_6 \\ T_7 \\ T_8 \\ T_9 \\ T_{10} \\ T_{11} \\ T_{12} \\ T_{13} \end{pmatrix} = \begin{pmatrix} -0.0592915 & -2.06301 & -0.916047 & -0.540939 & 1.68984 & 1.9484 & \dots \\ -0.0967012 & -2.3542 & -1.06657 & -0.642676 & 1.9029 & 2.20244 & \dots \\ -0.0737667 & -2.17648 & -0.974621 & -0.580488 & 1.7729 & 2.0474 & \dots \\ -0.0592915 & -2.06301 & -0.916047 & -0.540939 & 1.68984 & 1.9484 & \dots \\ -0.0135529 & -1.69614 & -0.727517 & -0.41405 & 1.42084 & 1.62818 & \dots \\ -0.0135529 & -1.69614 & -0.727517 & -0.41405 & 1.42084 & 1.62818 & \dots \\ 0.00380122 & -1.55269 & -0.654234 & -0.364932 & 1.31548 & 1.50296 & \dots \\ 0.0646661 & -1.01878 & -0.384536 & -0.185616 & 0.922227 & 1.03698 & \dots \\ 0.121848 & -0.393993 & -0.0807578 & 0.0108216 & 0.459287 & 0.493732 & \dots \\ 0.130042 & 0.0368277 & 0.101598 & 0.115892 & 0.138198 & 0.128851 & \dots \\ 0.0638797 & 0.160668 & 0.0925774 & 0.0780542 & 0.0520556 & 0.0577229 & \dots \\ -0.0403567 & 0.0778063 & -0.0374765 & -0.0461835 & 0.138408 & 0.197172 & \dots \\ -0.103077 & 0.0391438 & -0.113434 & -0.120022 & 0.193962 & 0.286232 & \dots \end{pmatrix}$$

Polynomial

$$\begin{pmatrix} \dots & 0.995832 & 1.25768 & 2.08482 & 0.835905 & -0.749676 & -1.81718 & -1.66632 \\ \dots & 1.1058 & 1.40579 & 2.3622 & 0.968341 & -0.837368 & -2.05887 & -1.89109 \\ \dots & 1.03877 & 1.31547 & 2.19289 & 0.887345 & -0.784003 & -1.91147 & -1.75396 \\ \dots & 0.995832 & 1.25768 & 2.08482 & 0.835905 & -0.749676 & -1.81718 & -1.66632 \\ \dots & 0.856117 & 1.07009 & 1.73555 & 0.67131 & -0.637116 & -1.51129 & -1.38243 \\ \dots & 0.856117 & 1.07009 & 1.73555 & 0.67131 & -0.637116 & -1.51129 & -1.38243 \\ \dots & 0.801064 & 0.99639 & 1.5991 & 0.607818 & -0.592354 & -1.39122 & -1.27118 \\ \dots & 0.593254 & 0.719688 & 1.09232 & 0.377586 & -0.420771 & -0.941469 & -0.855551 \\ \dots & 0.33987 & 0.387894 & 0.505202 & 0.131264 & -0.203212 & -0.407426 & -0.36453 \\ \dots & 0.144645 & 0.144232 & 0.119196 & 0.0132931 & -0.0220479 & -0.0312501 & -0.0194775 \\ \dots & 0.0488312 & 0.0485838 & 0.0632851 & 0.0946037 & 0.0837566 & 0.071943 & 0.0840385 \\ \dots & 0.0347972 & 0.0675801 & 0.240636 & 0.292721 & 0.108236 & -0.04117 & 0.00782891 \\ \dots & 0.0272564 & 0.0807206 & 0.353565 & 0.412117 & 0.1122 & -0.125215 & -0.0434483 \end{pmatrix}$$

$$\begin{aligned}
S_{AdaptivePoly.} &= \begin{pmatrix} 0 & 0 & 0 & 0 & \dots \\ 0 & 0 & 0 & 0 & \dots \\ 0 & 0 & 0 & 0 & \dots \\ -24.4493 & 6112.5429 & -6.3549E+05 & 3.5208E+07 & \dots \end{pmatrix} \\
&\begin{pmatrix} \dots & 0.0050595 & 0.6563 & -14.881 \\ \dots & -0.013986 & 2.7093 & -69.6767 \\ \dots & 0.05877 & -4.7023 & 119.0476 \\ \dots & -1.0969E+09 & 1.8233E+10 & 1.26347E+11 \end{pmatrix} \\
F_{AdaptivePoly.} &= \begin{pmatrix} 0 & 0 & 0 & 0 & \dots \\ 0 & 0 & 0 & 0 & \dots \\ 0 & 0 & 0 & 0 & \dots \\ -108.8979 & 27735.2665 & -2.9287E+06 & 1.6417E+08 & \dots \end{pmatrix} \\
&\begin{pmatrix} \dots & 3.2472 & -389.67 & 11746.0317 \\ \dots & 0.05105 & -4.2051 & 128.2051 \\ \dots & 2.19932 & -224.8492 & 5793.6507 \\ \dots & -5.1526E+09 & 8.5855E+10 & -5.9336E+11 \end{pmatrix}
\end{aligned}$$

$$S_{Spline} = \begin{pmatrix} -4.70E+05 & 1.13E+03 & -4.66E-01 & 1.18E-02 \\ -4.70E+05 & -1.43E+02 & 4.18E-01 & 1.19E-02 \\ 1.27E+05 & -5.66E+02 & 2.06E-01 & 1.20E-02 \\ 1.10E+06 & -4.13E+02 & -1.86E-01 & 1.20E-02 \\ -1.09E+07 & 2.88E+03 & 2.28E+00 & 1.25E-02 \\ 4.92E+06 & -6.95E+03 & 1.07E+00 & 1.32E-02 \\ 4.05E+06 & 1.90E+03 & -1.96E+00 & 1.24E-02 \\ -8.83E+06 & 7.97E+03 & 2.97E+00 & 1.24E-02 \\ 3.67E+05 & -2.62E+03 & 5.11E+00 & 1.43E-02 \\ -2.47E+05 & 1.12E+03 & 1.29E-02 & 1.58E-02 \\ -3.59E+03 & -1.39E+02 & 1.68E+00 & 1.78E-02 \\ -3.59E+03 & -1.56E+02 & 1.24E+00 & 2.00E-02 \end{pmatrix}$$

$$F_{Spline} = \begin{pmatrix} 4.37E+07 & -8.89E+04 & 4.14E+01 & 1.95E-02 \\ 4.37E+07 & 2.90E+04 & -1.25E+01 & 1.66E-02 \\ -1.06E+08 & 6.83E+04 & 1.67E+01 & 1.67E-02 \\ 3.21E+07 & -5.87E+04 & 2.06E+01 & 2.75E-02 \\ -8.00E+07 & 3.77E+04 & -4.43E-01 & 2.15E-02 \\ 3.33E+07 & -3.43E+04 & 5.78E-01 & 2.26E-02 \\ -1.70E+07 & 2.57E+04 & -4.58E+00 & 1.78E-02 \\ -3.17E+06 & 1.39E+02 & 8.33E+00 & 1.98E-02 \\ 4.80E+05 & -3.66E+03 & 6.92E+00 & 2.30E-02 \\ -3.08E+05 & 1.24E+03 & -1.35E+00 & 2.30E-02 \\ 1.26E+05 & -3.35E+02 & 1.85E-01 & 2.28E-02 \\ 1.26E+05 & 2.33E+02 & 3.25E-02 & 2.27E-02 \end{pmatrix}$$

$$\begin{pmatrix} a_1 & b_1 \\ a_2 & b_2 \\ a_3 & b_3 \\ a_4 & b_4 \\ a_5 & b_5 \\ a_6 & b_6 \\ a_7 & b_7 \\ a_8 & b_8 \\ a_9 & b_9 \\ a_{10} & b_{10} \\ a_{11} & b_{11} \\ a_{12} & b_{12} \end{pmatrix} \underset{Exp.Reg.}{=} \begin{pmatrix} 0.00951928 & 518337 \\ 0.00937774 & 1.32195E + 06 \\ 0.00742704 & 1.30101E + 12 \\ 0.00967854 & 268269 \\ 0.01235 & 1 \\ 0.0146746 & 0.000179871 \\ 0.000539429 & 2.43108E + 73 \\ 0.00477885 & 1.81722E + 23 \\ 0.00781665 & 6.08174E + 12 \\ 0.00284007 & 1.81341E + 31 \\ 0.00245499 & 5.49535E + 33 \\ 0.00544099 & 8.68913E + 20 \end{pmatrix}$$

$$\begin{pmatrix} c_1 & d_1 \\ c_2 & d_2 \\ c_3 & d_3 \\ c_4 & d_4 \\ c_5 & d_5 \\ c_6 & d_6 \\ c_7 & d_7 \\ c_8 & d_8 \\ c_9 & d_9 \\ c_{10} & d_{10} \\ c_{11} & d_{11} \\ c_{12} & d_{12} \end{pmatrix} \underset{Exp.Reg.}{=} \begin{pmatrix} 0.000626691 & 2.04787E + 93 \\ 0.341329 & 2.01309E - 78 \\ 0.0140129 & 22585.7 \\ 0.0101042 & 4.08509E + 12 \\ 0.000279806 & 3.09297E + 92 \\ 0.0642262 & 2.80327E - 26 \\ 0.000974765 & 1.71106E + 72 \\ 0.0186214 & 28151.4 \\ 0.0227708 & 1.46846 \\ 0.0264552 & 0.00269291 \\ 0.023617 & 0.230659 \\ 0.0104477 & 3.03151E + 12 \end{pmatrix}$$

$$\begin{pmatrix} a_1 & b_1 \\ a_2 & b_2 \\ a_3 & b_3 \\ a_4 & b_4 \\ a_5 & b_5 \\ a_6 & b_6 \\ a_7 & b_7 \\ a_8 & b_8 \\ a_9 & b_9 \\ a_{10} & b_{10} \\ a_{11} & b_{11} \\ a_{12} & b_{12} \end{pmatrix} \underset{\text{PowerReg.}}{=} \begin{pmatrix} 0.0292911 & 0.220894 \\ 0.0306422 & 0.231799 \\ 0.082858 & 0.475583 \\ 0.0304346 & 0.22907 \\ 0.01235 & 0 \\ 0.00644218 & -0.166356 \\ 3797.77 & 3.16825 \\ 0.85483 & 1.05188 \\ 0.178361 & 0.649257 \\ 11.9235 & 1.77349 \\ 31.5606 & 2.03879 \\ 2.50754 & 1.33761 \end{pmatrix}$$

$$\begin{pmatrix} c_1 & d_1 \\ c_2 & d_2 \\ c_3 & d_3 \\ c_4 & d_4 \\ c_5 & d_5 \\ c_6 & d_6 \\ c_7 & d_7 \\ c_8 & d_8 \\ c_9 & d_9 \\ c_{10} & d_{10} \\ c_{11} & d_{11} \\ c_{12} & d_{12} \end{pmatrix} \underset{\text{PowerReg.}}{=} \begin{pmatrix} 58552.1 & 3.60687 \\ 1.01436E-07 & -2.9422 \\ 0.0333429 & 0.170923 \\ 0.144673 & 0.532156 \\ 276896 & 4.20587 \\ 0.000233484 & -1.13504 \\ 5357.38 & 3.11849 \\ 0.0502255 & 0.201223 \\ 0.0237196 & 0.00847441 \\ 0.0133246 & -0.1458 \\ 0.0197535 & -0.0384934 \\ 0.404359 & 0.797343 \end{pmatrix}$$

$$\begin{aligned}
S_{Trig.} &= \begin{pmatrix} -1.7052E+03 & 1.7052E+03 & 6.5625E-01 & \dots \\ -7.8944E+03 & 7.8944E+03 & 2.7093 & \dots \\ 1.3642E+04 & -1.3642E+04 & -4.7024 & \dots \\ -1.8094E+02 & -6.7648E+02 & 5.2562E+06 & \dots \end{pmatrix} \\
&\begin{pmatrix} \dots & 0 & 0 & 0 & 0 \\ \dots & 0 & 0 & 0 & 0 \\ \dots & 0 & 0 & 0 & 0 \\ \dots & -5.2206E+03 & 5.2562E+06 & 6.0780E+03 & -5.2562E+06 \end{pmatrix} \\
F_{Trig.} &= \begin{pmatrix} 1.3460E+06 & -1.3460E+06 & -3.8967E+02 & \dots \\ 1.4691E+04 & -1.4691E+04 & -4.2051 & \dots \\ 6.6390E+05 & -6.6390E+05 & -2.2485E+02 & \dots \\ -2.1558E+03 & -3.4517E+03 & 1.8363E+07 & \dots \end{pmatrix} \\
&\begin{pmatrix} \dots & 0 & 0 & 0 & 0 \\ \dots & 0 & 0 & 0 & 0 \\ \dots & 0 & 0 & 0 & 0 \\ \dots & -1.8020E+04 & 1.8363E+07 & 2.3628E+04 & -1.8363E+07 \end{pmatrix}
\end{aligned}$$

Appendix D

Keyboard Spring-Deflection Analysis

$$(S \times F)_{Cylinder} = \begin{pmatrix} 2151.12 & 10.0983 & -10.1333 & -0.053583 & \dots \\ 1.79415 & 2149.34 & 10.0824 & -10.1171 & \dots \\ -7.38043 & 10.0717 & 2149.3800 & 10.0715 & \dots \\ 1.82096 & -10.1171 & 10.0822 & 2149.34 & \dots \\ 1.87464 & -0.0536891 & -10.1332 & 10.0982 & \dots \\ 1.87464 & 0.00536635 & -0.0699095 & -10.1169 & \dots \\ 1.82096 & 0.0642902 & -0.010588 & -0.0537813 & \dots \\ -7.38043 & 10.1012 & 0.101886 & -0.0213353 & \dots \\ 1.79415 & -10.0877 & 10.1119 & 0.0642634 & \dots \\ 1.90125 & -0.112386 & -10.1038 & 10.1278 & \dots \end{pmatrix}$$

$$\begin{pmatrix} 2.7333 \times 10^{-5} & 0.0590828 & 10.1278 & -10.1038 & -0.112386 & 1.90125 \\ -0.0590 & 2.61111 \times 10^{-5} & 0.0642634 & 10.1119 & -10.0877 & 1.79415 \\ -10.1224 & -0.0591622 & -0.0213353 & 0.101886 & 10.1012 & -7.38043 \\ 10.0929 & -10.1223 & -0.0537813 & -0.010588 & 0.0642902 & 1.82096 \\ 2149.34 & 10.0929 & -10.1169 & -0.0699095 & 0.00536635 & 1.87464 \\ 10.0929 & 2149.34 & 10.0982 & -10.1332 & -0.0536891 & 1.87464 \\ -10.1223 & 10.0929 & 2149.34 & 10.0822 & -10.1171 & 1.82096 \\ -0.0591622 & -10.1224 & 10.0715 & 2149.38 & 10.0717 & -7.38043 \\ 2.61111 \times 10^{-5} & -0.0590294 & -10.1171 & 2149.34 & 1.79415 & \\ 0.0590828 & 2.73332 \times 10^{-5} & -0.053583 & -10.1333 & 10.0983 & 2151.12 \end{pmatrix}$$

$$(S \times F)_{Square} = \begin{pmatrix} 2746.17 & 3.05665 & -3.09888 & -12.5476 & \dots \\ -0.620529 & 2746.79 & 3.05863 & -3.09809 & \dots \\ -3.39221 & 3.05668 & 2746.79 & 3.06576 & \dots \\ -0.576988 & -3.10086 & 3.05869 & 2746.79 & \dots \\ 10.831 & -12.544 & -3.11163 & 3.02671 & \dots \\ -1.70469 & 12.5344 & -12.5401 & -3.10904 & \dots \\ -0.591078 & 0.0275551 & 12.5296 & -12.5263 & \dots \\ -3.42805 & 3.12131 & 0.029511 & 12.5368 & \dots \\ -0.53462 & -3.17971 & 3.12327 & 0.0300245 & \dots \\ -0.581376 & 0.0421971 & -3.17774 & 3.12392 & \dots \end{pmatrix}$$

$$\begin{pmatrix} 12.533 & 0.0254317 & 3.12392 & -3.17774 & 0.0421971 & -0.581376 \\ -12.5525 & 12.5331 & 0.0300245 & 3.12327 & -3.17971 & -0.53462 \\ -3.11621 & -12.5446 & 12.5368 & 0.029511 & 3.12131 & -3.42805 \\ 3.06185 & -3.12406 & -12.5263 & 12.5296 & 0.0275551 & -0.591078 \\ 2746.87 & 3.01501 & -3.10904 & -12.5401 & 12.5344 & -1.70469 \\ 3.01501 & 2746.87 & 3.02671 & -3.11163 & -12.544 & 10.831 \\ -3.12406 & 3.06185 & 2746.79 & 3.05869 & -3.10086 & -0.576988 \\ -12.5446 & -3.11621 & 3.06576 & 2746.79 & 3.05668 & -3.39221 \\ 12.5331 & -12.5525 & -3.09809 & 3.05863 & 2746.79 & -0.620529 \\ 0.0254317 & 12.533 & -12.5476 & -3.09888 & 3.05665 & 2746.17 \end{pmatrix}$$

$$(S \times F)_{\text{Ellipse}} = \begin{pmatrix} 13784.8 & 9.56268 & -16.062 & 0.555385 & \dots \\ 26.0873 & 13759.3 & 8.97998 & -14.9325 & \dots \\ 17.918 & 9.56539 & 13758.7 & 10.1227 & \dots \\ 2.82316 & -15.488 & 15.4548 & 13747.5 & \dots \\ 2.80466 & 0.00171943 & -15.5181 & 15.516 & \dots \\ 2.98473 & -0.180464 & -0.0325923 & -15.4487 & \dots \\ 2.64098 & 0.3598 & -0.21292 & 0.0328275 & \dots \\ -301.964 & 335.114 & 0.0372852 & 0.213832 & \dots \\ 31.756 & -335.1 & 334.713 & 0.82537 & \dots \\ 31.8097 & -0.620623 & -335.58 & 335.651 & \dots \end{pmatrix}$$

$$\begin{pmatrix}
 -0.179852 & 0.360293 & 335.651 & -335.58 & -0.620623 & 31.8097 \\
 0.00230971 & -0.179923 & 0.82537 & 334.713 & -335.1 & 31.756 \\
 -15.4874 & 0.0023089 & 0.213832 & 0.0372852 & 335.114 & -301.964 \\
 15.4813 & -15.4813 & 0.0328275 & -0.21292 & 0.3598 & 2.64098 \\
 13747.4 & 15.4813 & -15.4487 & -0.0325923 & -0.180464 & 2.98473 \\
 15.4813 & 13747.4 & 15.516 & -15.5181 & 0.00171943 & 2.80466 \\
 -15.4813 & 15.4813 & 13747.5 & 15.4548 & -15.488 & 2.82316 \\
 0.0023089 & -15.4874 & 10.1227 & 13758.7 & 9.56539 & 17.918 \\
 -0.179923 & 0.00230971 & -14.9325 & 8.97998 & 13759.3 & 26.0873 \\
 0.360293 & -0.179852 & 0.555385 & -16.062 & 9.56268 & 13784.8
 \end{pmatrix}$$

Appendix E

Interconnect-Deflection Analysis

$$\begin{pmatrix} a_1 & b_1 \\ a_2 & b_2 \\ a_3 & b_3 \\ a_4 & b_4 \\ a_5 & b_5 \\ a_6 & b_6 \\ a_7 & b_7 \\ a_8 & b_8 \end{pmatrix}_{Cylinder} = \begin{pmatrix} 2.09787 & 1.180780 \\ 2.02153 & 1.185930 \\ 1.35758 & 1.242730 \\ 2.33668 & 1.165910 \\ 2.25798 & 1.170610 \\ 2.32 & 1.166730 \\ 2.58 & 1.152370 \\ 2.92 & 1.135970 \end{pmatrix}, \begin{pmatrix} c_1 & d_1 \\ c_2 & d_2 \\ c_3 & d_3 \\ c_4 & d_4 \\ c_5 & d_5 \\ c_6 & d_6 \\ c_7 & d_7 \\ c_8 & d_8 \end{pmatrix}_{Cylinder} = \begin{pmatrix} 3.90524 \times 10^{-7} & 7.135360 \\ 4.05762 \times 10^6 & 0.211439 \\ 4.13954 \times 10^{-12} & 27.4781 \\ 2.76544 \times 10^{10} & 0.0748985 \\ 0.0219423 & 1.97392 \\ 9.17028 \times 10^{12} & 0.0380991 \\ 1.24654 \times 10^{-7} & 8.07531 \\ 64.872 & 0.771687 \end{pmatrix}$$

$$\begin{pmatrix} a_1 & b_1 \\ a_2 & b_2 \\ a_3 & b_3 \\ a_4 & b_4 \\ a_5 & b_5 \\ a_6 & b_6 \\ a_7 & b_7 \\ a_8 & b_8 \end{pmatrix}_{Square} = \begin{pmatrix} 0.95087 & 1.2941 \\ 1.60282 & 1.2176 \\ 3.59895 & 1.1077 \\ 24.842 & 0.8831 \\ 2740.16 & 0.5080 \\ 2.21495 \times 10^6 & 0.2310 \\ 3.19176 \times 10^{-8} & 9.8610 \\ 18.4187 & 0.916492 \end{pmatrix}, \begin{pmatrix} c_1 & d_1 \\ c_2 & d_2 \\ c_3 & d_3 \\ c_4 & d_4 \\ c_5 & d_5 \\ c_6 & d_6 \\ c_7 & d_7 \\ c_8 & d_8 \end{pmatrix}_{Square} = \begin{pmatrix} 0.0934462 & 1.66098 \\ 115.677 & 0.724059 \\ 2.0662 & 1.15955 \\ 0.00341243 & 2.45851 \\ 3262.18 & 0.487134 \\ 1.18373 \times 10^{-26} & 1422.6 \\ 1.09965 \times 10^{-47} & 426910 \\ 17.4772 & 0.899023 \end{pmatrix}$$

$$\begin{pmatrix} a_1 & b_1 \\ a_2 & b_2 \\ a_3 & b_3 \\ a_4 & b_4 \\ a_5 & b_5 \\ a_6 & b_6 \\ a_7 & b_7 \\ a_8 & b_8 \end{pmatrix}_{\text{Ellipse}} = \begin{pmatrix} 0.00181516 & 2.71064 \\ 1.21213 \times 10^{-7} & 8.43371 \\ 34948.6 & 0.373504 \\ 9.90303 & 0.979728 \\ 1.13691 & 1.26434 \\ 0.539136 & 1.38001 \\ 0.519169 & 1.38611 \\ 15.7039 & 0.932135 \end{pmatrix}, \begin{pmatrix} c_1 & d_1 \\ c_2 & d_2 \\ c_3 & d_3 \\ c_4 & d_4 \\ c_5 & d_5 \\ c_6 & d_6 \\ c_7 & d_7 \\ c_8 & d_8 \end{pmatrix}_{\text{Ellipse}} = \begin{pmatrix} 0.00026816 & 3.336310 \\ 1.54903 \times 10^8 & 0.136356 \\ 1695.54 & 0.525622 \\ 21087.4 & 0.390337 \\ 0.992301 & 1.262700 \\ 24091.2 & 0.386142 \\ 0.0708827 & 1.708760 \\ 20.6946 & 0.882626 \end{pmatrix}$$

Appendix F

Welding

Experiment-Temperature

Analysis

$$(S \times F)_{DM} = \begin{pmatrix} 0.7328 & 0 & 0 & 0 & 0 & 0 & 0 & 0 \\ 0 & 0.7469 & 0 & 0 & 0 & 0 & 0 & 0 \\ 0 & 0 & 0.8163 & 0 & 0 & 0 & 0 & 0 \\ 0 & 0 & 0 & 0.7964 & 0 & 0 & 0 & 0 \\ 0 & 0 & 0 & 0 & 0.8152 & 0 & 0 & 0 \\ 0 & 0 & 0 & 0 & 0 & 0.7658 & 0 & 0 \\ 0 & 0 & 0 & 0 & 0 & 0 & 0.7511 & 0 \\ 0 & 0 & 0 & 0 & 0 & 0 & 0 & 0.6651 \end{pmatrix}$$

$$(S \times F)_{PI} = \begin{pmatrix} 0.1082 & 0.0838 & 0.0867 & 0.0916 & 0.0951 & 0.1003 & 0.1036 & 0.1279 \\ 0.0815 & 0.0632 & 0.0653 & 0.0690 & 0.0716 & 0.0756 & 0.0781 & 0.0964 \\ 0.0897 & 0.0695 & 0.0719 & 0.0760 & 0.0789 & 0.0832 & 0.0859 & 0.1061 \\ 0.0960 & 0.0744 & 0.0769 & 0.0813 & 0.0844 & 0.0890 & 0.0919 & 0.1135 \\ 0.1006 & 0.0779 & 0.0806 & 0.0852 & 0.0884 & 0.0932 & 0.0963 & 0.1189 \\ 0.1034 & 0.0801 & 0.0829 & 0.0876 & 0.0909 & 0.0959 & 0.0991 & 0.1223 \\ 0.1049 & 0.0813 & 0.0841 & 0.0889 & 0.0922 & 0.0973 & 0.1005 & 0.1241 \\ 0.1188 & 0.0920 & 0.0952 & 0.1006 & 0.1044 & 0.1101 & 0.1138 & 0.1404 \end{pmatrix}$$

$$(S \times F)_{CM} = \begin{pmatrix} 0.4720 & 0.0941 & -0.1372 & 0.1366 & -0.0312 & 0.1315 & 0.0317 & 0.0581 \\ 0.0581 & 0.4720 & 0.0941 & -0.1372 & 0.1366 & -0.0312 & 0.1315 & 0.0317 \\ 0.0317 & 0.0581 & 0.4720 & 0.0941 & -0.1372 & 0.1366 & -0.0312 & 0.1315 \\ 0.1315 & 0.0317 & 0.0581 & 0.4720 & 0.0941 & -0.1372 & 0.1366 & -0.0312 \\ -0.0312 & 0.1315 & 0.0317 & 0.0581 & 0.4720 & 0.0941 & -0.1372 & 0.1366 \\ 0.1366 & -0.0312 & 0.1315 & 0.0317 & 0.0581 & 0.4720 & 0.0941 & -0.1372 \\ -0.1372 & 0.1366 & -0.0312 & 0.1315 & 0.0317 & 0.0581 & 0.4720 & 0.0941 \\ 0.0941 & -0.1372 & 0.1366 & -0.0312 & 0.1315 & 0.0317 & 0.0581 & 0.4720 \end{pmatrix}$$

$$\begin{pmatrix} a^* \\ b^* \end{pmatrix}_{CpM} = \begin{pmatrix} 25.3741 \\ 0.5168 \end{pmatrix},$$

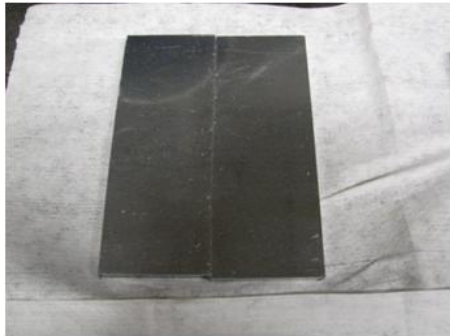
$$\begin{pmatrix} a_1^* \\ b_1^* \end{pmatrix}_{CpM} = \begin{pmatrix} 39.1039 \\ 0.8814 \end{pmatrix}$$

$$(S \times F)_{HM} = \begin{pmatrix} 0.6651 & 0.0679 & 0.0232 & 0.0362 & -0.0040 & 0.0097 & -0.0375 & -0.0012 \\ 0 & 0.6651 & 0.0679 & 0.0232 & 0.0362 & -0.0040 & 0.0097 & -0.0375 \\ 0 & 0 & 0.6651 & 0.0679 & 0.0232 & 0.0362 & -0.0040 & 0.0097 \\ 0 & 0 & 0 & 0.6651 & 0.0679 & 0.0232 & 0.0362 & -0.0040 \\ 0 & 0 & 0 & 0 & 0.6651 & 0.0679 & 0.0232 & 0.0362 \\ 0 & 0 & 0 & 0 & 0 & 0.6651 & 0.0679 & 0.0232 \\ 0 & 0 & 0 & 0 & 0 & 0 & 0.6651 & 0.0679 \\ 0 & 0 & 0 & 0 & 0 & 0 & 0 & 0.6651 \end{pmatrix}$$

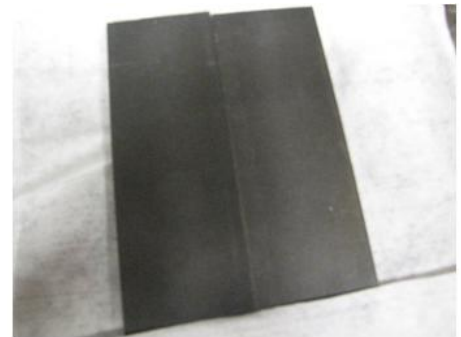
$$(S \times F)_{TCG} = \begin{pmatrix} 0.5360 & -0.1947 & 0.1154 & 0.0879 & 0.2504 & 0.0815 & 0.0912 & -0.1275 \\ 0.0309 & 0.6210 & -0.0284 & 0.1614 & 0.0985 & 0.1261 & -0.0585 & -0.1491 \\ 0.1971 & -0.1533 & 0.5937 & -0.1209 & 0.1678 & 0.0554 & 0.1868 & -0.1392 \\ 0.0936 & 0.1627 & -0.0671 & 0.5878 & -0.1144 & 0.0782 & -0.0053 & 0.0295 \\ 0.0318 & -0.0053 & 0.0782 & -0.1144 & 0.5878 & -0.0671 & 0.1627 & 0.0815 \\ -0.1506 & 0.1868 & 0.0554 & 0.1678 & -0.1209 & 0.5937 & -0.1533 & 0.1802 \\ -0.1639 & -0.0585 & 0.1261 & 0.0985 & 0.1614 & -0.0284 & 0.6210 & 0.0257 \\ -0.1449 & 0.0912 & 0.0815 & 0.2504 & 0.0879 & 0.1154 & -0.1947 & 0.4762 \end{pmatrix}$$

Appendix G

Test Equipment and Process



Aluminum model specimen



Steel product specimen



Aluminum model



Steel product

Figure G.1: Welding experiment - Physical prototypes

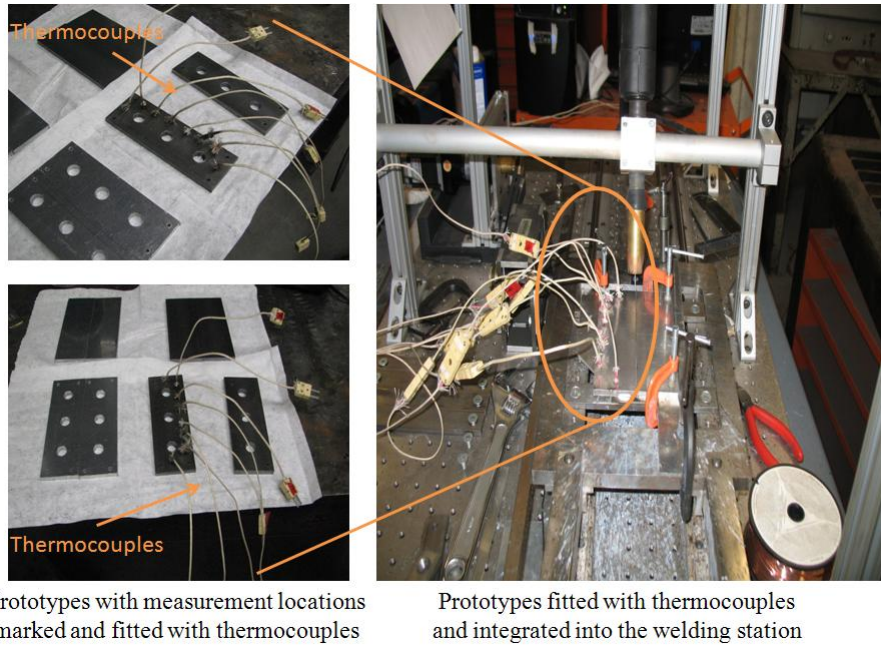


Figure G.2: Welding experiment - Thermocouples affixed and system integrated into the welding station

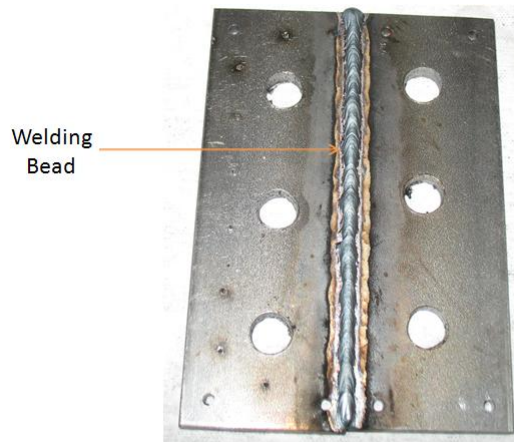


Figure G.3: Welding experiment - Finished weld joint



Gas source and electrical supply



Jig fixtures and rails



Welding station

Computer actuation and DAQ



Weld gun and welding wire



Figure G.4: Welding experiment - Welding station

Bibliography

- [1] Albert, A., 1972, *Regression and the Moore-Penrose Pseudoinverse*, Academic Press.
- [2] Ashby, M. F., 1992, *Materials Selection in Mechanical Design*, Pergamon Press.
- [3] Ashby, M. F., 1991, *Materials and Shape*, *Acta. Metall. Mater.*, 39, 1025-1039.
- [4] Baker, W. E., Westine, P. S., Dodge, F. T., 1991, *Similarity Methods in Engineering Dynamics: Theory and Practice of Scale Modeling*, Elsevier.
- [5] Barr, D. I. H., 1982, *A Survey of Procedures for Dimensional Analysis*, International Journal of Mechanical Engineering Education, Vol. 11, No. 3, 147-159.
- [6] Becker E. B., Carey, G. F., Oden, J.T., 1981, *Finite Elements*, Prentice-Hall, Englewood Cliffs, NJ.
- [7] Bernstein D. S., 2005, *Matrix Mathematics*, Princeton University Press.
- [8] Bethea, R. M., Duran, B. S., Boullion, T. L., 1985, *Statistical Methods for Engineers and Scientists*, Marcel Dekker, Inc., New York.
- [9] Biglarbegian, M., 2005, *An Efficient Monte Carlo Approach for Determining Shape Factors*, The International Journal of Mechanical Engineering Education, Vol. 33, No. 1, January, pp. 39-44.

- [10] Binder, R. C., 1973, *Fluid Mechanics*, 5th Edition, Prentice-Hall, Englewood Cliffs, N.J.
- [11] Bourbaki, N., 1987, *Topological Vector Spaces, Chapters 1-5, Elements of Mathematics*, Springer.
- [12] Bridgman, P. W., 1931, *Dimensional Analysis*, Yale University Press, New Haven.
- [13] Broeren, A. P., Giguère, P., Guglielmo, J. J., Selig, M. S., 1995, *Summary of Low-Speed Airfoil Data*, Vol. 1, SoarTech Publications, Virginia Beach, Virginia.
- [14] Buffham, B. A., 2000, *The Size and Compactness of Particles of Arbitrary Shape: Application to Catalyst Effectiveness Factors*, Chemical Engineering Science, Vol. 55, No. 23, December, pp. 5803-5811.
- [15] Burgess, S. C., 2000, *Shape factors and Material Indices for Dimensionally Constrained Structures-Part 1: Beams*, Proceedings of the Institute of Mechanical Engineers, Vol. 214, Part C, 371-379.
- [16] Burgess, S. C., 2000, *Shape factors and Material Indices for Dimensionally Constrained Structures-Part 2: Shafts*, Proceedings of the Institute of Mechanical Engineers, Vol. 214, Part C, 381-388.
- [17] Burgess, S. C., Kahangamage, U. P., Barr, G., Williams, J. S., 2001, *Shape factors for Beams with Misaligned Loads*, Proceedings of the Institute of Mechanical Engineers, Vol. 215, Part C, 981-993.
- [18] Callister, W. D., 1994, *Materials Science and Engineering: An Introduction*, 3rd Edition, John Wiley & Sons, Inc., New York.
- [19] Cho, U., Wood, K., 1997, *Empirical Similitude Method for the Functional Test with Rapid Prototypes*, Proceedings of the Solid Freeform Fabrication Symposium, Austin TX, September, 1997, pp. 559-567.

- [20] Cho, U., Wood, K. L., Crawford, R. H., 1998b, *Novel Empirical Similarity Method for the Reliable Product Test with Rapid Prototypes*, Proceedings of DETC, Atlanta, GA, September 13-16, 1998.
- [21] Cho, U., Wood, K. L., Crawford, R. H., 1998, *Online Functional Testing with Rapid Prototypes: a Novel Empirical Similarity Method*, Rapid Prototyping Journal, 4, No. 3, pp. 128-138.
- [22] Cho, U., 1999, *Novel Empirical Similarity Method for Rapid Product Testing and Development*, Doctoral dissertation, The University of Texas at Austin.
- [23] Corrsin, S., 1951, *A Simple Geometrical Proof of Buckingham's π -Theorem*, American Journal of Physics, Volume 19, Issue 3, March, 180-181.
- [24] Cowley, M. D., 1974, *Integral Methods of Analysing Electric Arcs: I. Formulation*, Journal of Physics D: Applied Physics, Vol. 7, pp. 2218-2231.
- [25] Daniels, A. R., 1985, *Introduction to Electrical Machines*, Macmillan.
- [26] David, F. W., Nolle, H., 1982, *Experimental Modelling in Engineering*, ButterWorths.
- [27] Davis, P. J., 1979, *Circulant Matrices*, A Wiley-InterScience Publication, John Wiley & Sons.
- [28] Deo N., 1974, *Graph Theory with Applications to Engineering and Computer Science*, Prentice Hall.
- [29] Deb, M. K., Deb, A., 1986, *The Matrix Method: A Powerful Technique in Dimensional Analysis*, Journal of the Franklin Institute, Volume 321, No. 4, April, 233-240.
- [30] Dornfeld, W. H., 1995, *Direct Dynamic Testing of Scaled Stereolithographic Models*, Sound and Vibration, August, 12-17.

- [31] Dunford, N., Schwartz, J. T., 1958, *Linear Operators, Part I: General Theory*, Interscience Publishers, New York.
- [32] Dutson, A. J., 2002, *Functional Prototyping Through Advanced Similitude Techniques*, Doctoral dissertation, The University of Texas at Austin.
- [33] Edwards, A. L., 1976, *An Introduction to Linear Regression and Correlation*, W. H. Freeman, San Francisco, CA.
- [34] Eubank, R. L., 1988, *Spline Smoothing and Nonparametric Regression*, Vol. 90, Marcel Dekker Inc., New York and Basel.
- [35] Fagarasanu, M., Kumar, S., Narayan, Y., 2005, *The Training Effect on Typing on Two Alternative Keyboards*, International Journal of Industrial Ergonomics, Vol. 35, Issue 6, June, 509-516.
- [36] Farrar, C. R., Baker, W. E., Dove, R. C., 1994, *Dynamic Parameter Similitude for Concrete Models*, ACI Structural Journal, Title No. 91-S10, January-February, 90-98.
- [37] Faux, I. D., Pratt, M. J., 1979, *Computational Geometry for Design and Manufacture*, Ellis Horwood Limited, Chichester.
- [38] Finkbeiner II, D. T., 1978, *Introduction to Matrices and Linear Transformations*, 3rd Edition, W.H. Freeman & Company, San Francisco.
- [39] Freedman, D. A., 2005, *Statistical Models: Theory and Practice*, Cambridge University Press.
- [40] Fox, J., 1997, *Applied Regression Analysis, Linear Models and Related Methods*, Sage.
- [41] Gere, J. M., Timoshenko, S. P. , 1985, *Mechanics of Materials*, Wadsworth International, London.
- [42] Gere, J. M., Timoshenko, S. P., 1961, *Theory of Elastic Stability*, McGraw-Hill Koga Kusha Ltd, London.

- [43] Golub, G. H., Van Loan, C. F., 1996, *Matrix Computations*, 3rd Edition, Baltimore, Johns Hopkins.
- [44] Grenander, U., Szegö, G., 1958, *Toeplitz Forms and their Applications*, University of California Press, Berkeley and Los Angeles.
- [45] Grewal, B. S., 1998, *Higher Engineering Mathematics*, Khanna Publishers, Delhi, India.
- [46] Gyselinck, J., Melkebeek, J., 2001, *Two-dimensional Finite Element Modelling of Overlap Joints in Transformer Cores*, COMPEL: The International Journal for Computation and Mathematics in Electrical and Electronic Engineering, Vol. 20, No. 1, pp. 253-268.
- [47] Guo, J. C. Y., 2008, *Application of Kinematic Wave Cascading Plane to Irregular Watershed*, Journal of Hydrologic Engineering.
- [48] Happ, W. W., 1971, *Dimensional Analysis via Directed Graphs*, Journal of the Franklin Institute, 292/1 July, pp. 527-533.
- [49] Happ, W. W., 1967, *Computer-Oriented Procedures for Dimensional Analysis*, Journal of Applied Physics, 38/10, September, pp. 3918-3926.
- [50] Hart, G.W., 1995, *Multidimensional Analysis*, Springer-Verlag.
- [51] Harper, C. A., 2005, *Electronic Packaging and Interconnection Handbook*, 4th Edition, McGraw - Hill.
- [52] Hestenes, M. R., Stiefel, E., 1952, *Methods of Conjugate Gradients for Solving Linear Systems*, Journal of Research of the National Bureau of Standards 49 (6).
- [53] Heywood, H., 1947, *Symposium on Particle Size Analysis*, Supplementary to Transactions of Institution of Chemical Engineers, 25, pp. 14.

- [54] İmrak, C. E., Gerdemeli, İ., 2007, *On the Shape Factor for the Maximum Pressure of the Undercut Groove Form*, International Journal of Mathematical Analysis, Vol. 1, No. 16, 783-790.
- [55] Incropera, F. P., 2007, *Fundamentals of Heat and Mass Transfer*, 6th Edition, John Wiley, Hoboken, NJ.
- [56] Johnson, D. E., Johnson, J. R., 1972, *Graph Theory with Engineering Applications*, The Ronald Press Company, New York.
- [57] Jones, K. W., Liu, Y., Shah, M., Clarke, R., 1998, *Mechanical properties of Pb/Sn Pb/In and Sn-In Solders*, Soldering & Surface Mount Technology, Vol. 10, No. 1, 37-41.
- [58] Juvinall, R. C., Marshek, K. M., 2006, *Fundamentals of Machine Component Design*, 4th Edition, Hoboken, John Wiley & Sons, Hoboken, NJ.
- [59] Karnopp, D. C., Margolis, D. L., Rosenberg, R. C., 2006, *System dynamics: Modeling and Simulation of Mechatronic Systems*, 4th Edition, John Wiley & Sons, Hoboken, NJ.
- [60] Kelly, J. M., Takhirov, S. M., 2004, *Analytical and Numerical Study on Buckling of Elastomeric Bearings with various Shape Factors*, Report No. EERC 2004-03, Earthquake Engineering Research Center.
- [61] Kendell, A. A., 1988, *An Introduction to Numerical Analysis*, 2nd Edition, Section 8.9, John Wiley and Sons.
- [62] Kimothi, S. K., 2002, *The Uncertainty of Measurements: Physical and Chemical Metrology: Impact and Analysis*.
- [63] Edited by Klamkin, M. S., 1987, *Mathematical Modelling: Classroom Notes in Applied Mathematics*, SIAM.
- [64] Kline, S. J., 1965, *Similitude and Approximation Theory*, McGraw-Hill, USA.

- [65] Kołodziej, J. A., Stręk, T., 2001, *Analytical Approximations of the Shape Factors for Conductive Heat Flow in Circular and Regular Polygonal Cross-Sections*, International Journal of Heat and Mass Transfer, Vol. 44, pp. 999-1012.
- [66] Krenk, S., 2001, *Mechanics and Analysis of Beams-Columns and Cables*, 2nd Edition, Springer, Germany.
- [67] Langhaar, H. L., 1951, *Dimensional Analysis and Theory of Models*, John Wiley & Sons, New York.
- [68] Edited by Lau, J. H., 1995, *Ball Grid Array Technology*, McGraw-Hill, Inc.
- [69] Linz, P., 1979, *Theoretical Numerical Analysis: An Introduction to Advanced Techniques*, Wiley, New York.
- [70] Mathias, S. A., Butler, A. P., 2006, *An Improvement on Hvorslev's Shape Factors*, Géotechnique 56, No. 10, 705-706.
- [71] Mezrhab, A., Bouzidi, M., 2005, *Computation of View Factors for Surfaces of Complex Shape Including Screening Effects and using a Boundary Element Approximation*, Engineering Computations: International Journal for Computer-Aided Engineering and Software, Vol. 22, No. 2, pp. 132-148.
- [72] Modest, M. F., 2003, *Radiative Heat Transfer*, 2nd Edition, McGraw-Hill.
- [73] Moon, P., Spencer D.E., 1949, *A Modern Approach to "Dimensions"*, Journal of the Franklin Institute, 248/1483-1488 (July-December), pp. 495-521.
- [74] Mordecai, A., 2003, *Nonlinear Programming: Analysis and Methods*, Dover Publishing.

- [75] Murphy, G., 1950, *Similitude in Engineering*, The Ronald Press Company, New York.
- [76] Ng, M. K., 2004, *Iterative Methods for Toeplitz Systems*, Oxford Science Publications, New York.
- [77] Nickolay, M., Fischer, L., Martin, H., 1998, *Shape Factors for Conductive Heat Flow in Circular and Quadratic Cross-Sections*, International Journal of Heat and Mass Transfer, Vol. 41, No. 11, pp. 1437-1444.
- [78] Otto, K. N., Wood, K.L., 2001, *Product Design-Techniques in Reverse Engineering and New Product Development*, Prentice Hall, Upper Saddle River NJ.
- [79] Parkhouse, J. G., 1984, *Structuring: A Process of Material Dilution*, 3rd International Conference on Space Structures, 367, Elsevier London.
- [80] Parkhouse, J. G., 1987, *Damage Accumulation in Structures*, Reliability Engineering, 17, 97-109.
- [81] Patzek, T. W., Silin, D. B., 2001, *Shape Factor Correlations of Hydraulic Conductance in Noncircular Capillaries I. One-Phase Creeping Flow*, Journal of Colloid and Interface Science, Vol. 236, 295-304.
- [82] Pecht, M. A., Agarwal, R., McCluskey, P., Dishnogh, T., Javadpour, S., Mahajan, R., 1999, *Electronic Packaging: Materials and Their Properties*, CRC Press.
- [83] Peller, V. V., 2003, *Hankel Operators and their Applications*, Springer-Verlag, New York.
- [84] Penrose, R., 1955, *A Generalized Inverse for Matrices*, Proceedings of the Cambridge Philosophical Society 51, 406-413.
- [85] Rayleigh, 1915, *The Principle of Similitude*, Nature, Vol. 95, No. 2368, 66-68.

- [86] Reiss, H., 1997, *Methods of Thermodynamics*, Dover Publications Inc., Mineola, new York.
- [87] Roark, R. J., Young, W. C. , 1976, *Formulas for Stress and Strain*, 5th Edition, McGraw-Hill, London.
- [88] Robinson, E. A., 1981, *Least Squares Regression Analysis in terms of Linear Algebra*, Goose Pond Press, Houston.
- [89] Schnittger, J. R., 1988, *Dimensional Analysis in Design*, Journal of Vibration, Acoustics, Stress and Reliability in Design, Vol. 110, January-February, 401-406.
- [90] Seber, G. A. F, Wild, C. J., 1989, *Nonlinear Regression*, John Wiley and Sons, New York.
- [91] Shanley, F. R., 1960, *Weight-Strength Analysis of Aircraft Structures*, 2nd Edition, Dover Publications, New York.
- [92] Sharp, J.J., 1975, *Application of Dimensional Reasoning to Thermal Systems*, Journal of the Franklin Institute, 299/3, March, pp. 191-197.
- [93] Shen, L., Shen, Y., Rangayyan, R., M., 1994, *Shape Characterization and its Applications*, International Symposium on Speech, Image Processing and Neural Networks, April, pp. 9-12.
- [94] Shewchuk, J. R., 1994, *An Introduction to the Conjugate Gradient Method Without the Agonizing Pain*, Edition 1 $\frac{1}{4}$, School of Computer Science, Carnegie Mellon University Pittsburgh, PA.
- [95] Shrivastava, D., Roemer, R., B., 2005, *An Analytical Study of ‘Poisson Conduction Shape Factors’ for Two Thermally Significant Vessels in a Finite Heated Tissue*, Physics in Medicine and Biology, Vol. 50, pp. 3627-3641.

- [96] Siegel, R., Howell, J. R., 2001, *Thermal Radiation Heat Transfer*, 4th Edition, New York.
- [97] Skoglund, V. J., 1967, *Similitude-Theory and Applications*, International Textbook Company, PA.
- [98] Spiegel, M. R., 1992, *Theory and Problems of Probability and Statistics*, 2nd Edition, McGraw-Hill, New York.
- [99] Stallings, W. T., 1972, *The Pseudoinverse of an r -Circulant Matrix*, Proceedings of the American Mathematical Society 34, 385-388.
- [100] Stevens, S. S., 1946, *On the Theory of Scales of Measurement*, Science, 103, pp. 677-680.
- [101] Szirtes, T., 1998, *Applied Dimensional Analysis and Modeling*, McGraw-Hill, New York.
- [102] Szücs, E., 1980, *Similitude And Modelling*, Elsevier.
- [103] Tayler, A. B., 1986, *Mathematical Models in Applied Mechanics*, Clarendon Press, Oxford.
- [104] Taylor, E. S., 1974, *Dimensional Analysis for Engineers*, Clarendon Press, Oxford.
- [105] Ulusoy, U., 2008, *Fine Particle Technology and Characterization*.
- [106] Valiantzas, J. D., 1997, *Surface Irrigation Advance Equation: Variation of Subsurface Shape Factor*, Journal of Irrigation and Drainage Engineering, July/August, 300-306.
- [107] Van Driest, E. R., 1946, *On Dimensional Analysis and the Presentation of Data in fluid-flow problems*, Journal of applied mechanics, 13, pp. A34-A40.

- [108] Winders, J., 2002, *Power Transformer Principles and Applications*, CRC.
- [109] Wood, J. J., Wood, K. L., 2002b., *Empirical Analysis using Advanced Similarity Methods*, Proceedings of DETC, Montreal, Canada, 2002, pp. 429-438.
- [110] Wood, J. J., 2002, *Design Methodology using Empirical and Virtual Analysis with Application to Compliant Systems*, Doctoral dissertation, Colorado State University.
- [111] Young, H. M., Haddad, A., Rowlands, A.R., Waters, R. T., 1999, *Effect of Shape Factors on the Performance of Polluted Polymeric Insulators*, High Voltage Engineering Symposium, August, No. 467, pp. 4.92.S25-4.95.S25.
- [112] Zhangfa, W., Colbeck, I., 2006, *Studies of the Dynamic Shape Factor of Aerosol Agglomerates*, EuroPhysics Letters, 44 (9), pp. 719-724.
- [113] Zimmerman, R. W., 2005, *Shape Factors for Dual-Porosity Fractured Reservoir Models*, Alain Gringarten Symposium, London, UK.

Vita

Srikanth Tadepalli was born on May 16, 1978 in Hyderabad, India, the son of SitaRama Anjaneya Sastry Tadepalli and Syamala Tadepalli. After completing high school at the St. Mary's Junior College in Hyderabad, India, he attended the Jawaharlal Nehru Technological University (JNTU), Hyderabad, India where he obtained his Bachelor of Technology degree in Mechanical Engineering in June 2001 after successfully completing projects and gaining industry and research related experience in the Indian Space Research Organization (ISRO), Department of Space, Government of India and Defense Research and Development Organization (DRDO), Ministry of Defense, Government of India.

He entered the graduate school of The University of Texas at Austin in the Fall of 2001 to begin graduate study in Manufacturing Systems Engineering with specialization in Design for Manufacturing. He obtained his Master of Science in Engineering degree in December 2003. He subsequently pursued his doctoral studies in Mechanical Engineering at The University of Texas at Austin beginning Spring of 2004.

He has worked as a Teaching Assistant, Research Assistant, Graduate Assistant, Student Consultant and Assistant Instructor for a period of over 7 years at The University of Texas at Austin and was awarded "*The H. Grady*

Rylander Longhorn Mechanical Engineering Club Excellence in Teaching” Fellowship award for the years 2003-2004 and 2007-2008. He has been cited in multiple publications of the “*Who’s Who*” series and has interned at Intel Corporation, Chandler, AZ working on Use Condition Development of chip packages.

He has authored or co-authored 7 technical papers during his graduate and doctoral study. His research interests include Similitude and Scaling Theory, System Dynamics, Non-Linear Dimensional Analysis and Rapid Prototyping with specific emphasis in Selective Laser Sintering and applications in Product Design. He is going to start working in Loughborough University, Leicestershire, UK as a Post-doctoral Research Associate.

Permanent Address: Plot # 82 and 83,
Swaroop Nagar, Uppal,
Hyderabad - 500039
India.

This dissertation was typeset with $\text{\LaTeX} 2_{\epsilon}$ ¹ by the author.

¹ $\text{\LaTeX} 2_{\epsilon}$ is an extension of \LaTeX . \LaTeX is a collection of macros for \TeX . \TeX is a trademark of the American Mathematical Society. The macros used in formatting this dissertation were written by Dinesh Das, Department of Computer Sciences, The University of Texas at Austin, and extended by Bert Kay, James A. Bednar, and Ayman El-Khashab.